

*N*-Glycosyl Aza-Ylides as Intermediates in the Synthesis of Novel *N*-Glycosides

by

Andrew Thomas Murrin

Submitted in Partial Fulfillment of the Requirements

for the Degree of

Master of Science

in the

Chemistry

Program

YOUNGSTOWN STATE UNIVERSITY

May 2020

*N*-Glycosyl Aza-Ylides as Intermediates in the Synthesis of Novel *N*-Glycosides

Andrew Thomas Murrin

I hereby release this thesis to the public. I understand this thesis will be made available from the OhioLINK ETD Center and the Maag Library Circulation Desk for public access. I also authorize the University and other individuals to make copies of this thesis as needed for scholarly research.

Signature:

---

Andrew Thomas Murrin, Student

Date

Approvals:

---

Dr. Peter Norris, Thesis Advisor

Date

---

Dr. John A. Jackson, Committee Member

Date

---

Dr. Nina V. Stourman, Committee Member

Date

---

Dr. Salvatore A. Sanders, Dean of Graduate Studies

Date

### Thesis Abstract

Carbohydrates are ubiquitous biological molecules that facilitate a wide array of cellular processes. Generation of libraries of carbohydrate analogues, as well as developing a complete understanding of their underlying synthetic mechanisms, are therefore imperative in advancing this field of research. This thesis work focused on isolation of the *N*-glycosyl aza-ylide intermediate of the Staudinger reaction between  $\beta$ -D-glucopyranosyl azide and 1,2-bis(diphenylphosphino)ethane (DPPE), and the synthesis of novel glycosylamines from aldehydes via subsequent aza-Wittig chemistry and reductive amination.

*“If you put your mind to it, you can accomplish anything.”*

- Marty McFly, *Back to the Future* (1985)

## Acknowledgements

I would like to express my gratitude to the Chemistry Department at Youngstown State University for accepting me into the graduate program, allowing me to advance my personal study and professional ambitions. The knowledge and encouraging attitude of faculty, as well as hands-on access to the multitude of resources has been instrumental to the successful completion of my Master's degree.

My sincerest appreciation is extended to Dr. Peter Norris, for granting me the opportunity to conduct my Master's research and hone my skills under his guidance. My competency and confidence in carrying out meaningful organic syntheses have grown exponentially as a member of Dr. Norris' laboratory, and for that I am eternally grateful.

I would like to thank Dr. John Jackson, not only for his invaluable contribution to my scholastic abilities, but also for the exposure to various laboratory methods that have become incorporated into my research. To adapt one of his eloquent statements: "I got the goal, but he got the assist." I also appreciate his willingness to be a member of my thesis committee.

I would also like to recognize Dr. Nina Stourman, who demonstrated faith in my capacity as a student while enrolled in her Advanced Biochemistry courses. Her instruction enriched my understanding of cellular processes, and challenged me to more deeply understand their vast interconnectedness. Her acceptance in being a member of my thesis committee is truly an honor.

Among other esteemed faculty, Dr. Doug Genna deserves note, whose erudition and tutelage of Advanced Organic Chemistry have further elucidated the elegance and intricacies of this field. Moreover, his benevolently critical pedagogy has taught me to elevate expectations for myself and helped refine my approach to organic synthesis.

I would also like to acknowledge the advice and support of Dr. Sherri Lovelace-Cameron; the continual chemical supply and management, as well as the safety oversight of Timothy Styranec; the instrumentation experience of Ray Hoff; and the crystallographic assistance of Dr. Matthias Zeller.

To the Norris group, past and present – Matthew Torres, Matt LaLama, Chris Copeland, Emmanuel Buabeng, and Abraham Awuah – thank you for your collaboration and companionship on this amazing journey.

Last, and certainly not least, the ones to whom I owe all of my achievements – my family. Alexander, my little dude, you have been a constant source of motivation and happiness throughout this journey. I hope I make you as proud of me as I am of you. Know that you have all the possibilities, and that you can and will achieve great things. Klotilda, my wife, your sacrifices can never be measured, and I will always remember and cherish those efforts which allowed me the privilege to pursue my Master's degree. You two are my world, and I am truly blessed.

## Table of Contents

Title Page .....	i
Signature Page .....	ii
Abstract .....	iii
Epigraph .....	iv
Acknowledgements .....	v
Table of Contents .....	vii
List of Figures .....	ix
List of Tables .....	xiv
List of Schemes .....	xiv
<b>Introduction</b>	
Organic Azides .....	1
Staudinger Reaction .....	3
Classic Wittig Reaction .....	4
Aza-Wittig Reaction .....	6
Reductive Amination .....	6
Carbohydrates .....	8
Statement of Problem .....	12
<b>Results and Discussion</b>	
Synthesis of $\alpha$ -D-Glucopyranosyl Bromide ( <b>2</b> ) .....	13
Synthesis of $\beta$ -D-Glucopyranosyl Azide ( <b>3</b> ) .....	14
Synthesis and Isolation of 1,2-Bis(Diphenyl-(2,3,4,6)-Tetra- <i>O</i> -Acetyl- $\beta$ -D-Glucopyranosyl-1- <i>N</i> -Iminophosphorane) Ethane ( <b>5</b> ).....	16
Spectral and Crystallographic Analysis of 1,2-Bis(Diphenyl-(2,3,4,6)-Tetra- <i>O</i> -Acetyl- $\beta$ -D-Glucopyranosyl-1- <i>N</i> -Iminophosphorane) Ethane ( <b>5</b> ).....	18
Hydrolysis of 1,2-Bis(Diphenyl-(2,3,4,6)-Tetra- <i>O</i> -Acetyl- $\beta$ -D-Glucopyranosyl-1- <i>N</i> -Iminophosphorane) Ethane ( <b>5</b> ) .....	22

Synthesis of Imines from $\beta$ -D-Glucopyranosyl Azide ( <b>3</b> ) .....	26
Synthesis of Amines from $\beta$ -D-Glucopyranosyl Azide ( <b>3</b> ) .....	33
General Analysis of Product Isolation and Yields .....	36
Unsuccessfully Reacted Aldehydes .....	38
Future Research .....	38
Conclusion .....	39
Experimental	
General Procedures .....	41
References .....	54
Appendix A .....	58
Appendix B .....	112



## List of Figures

<b>Figure 1</b>	Structure of Alkyl Azides .....	1
<b>Figure 2</b>	Azide Reactions .....	2
<b>Figure 3</b>	Azidothymidine (AZT) .....	2
<b>Figure 4</b>	Staudinger Reaction Mechanism .....	3
<b>Figure 5</b>	<i>N</i> -Heterocyclic Compounds in Nature .....	5
<b>Figure 6</b>	Classic Wittig Reaction Mechanism .....	7
<b>Figure 7</b>	Lobry de Bruyn-Alberda van Ekenstein Transformation .....	8
<b>Figure 8</b>	Anomerization of <i>D</i> -Glucose .....	9
<b>Figure 9</b>	Pyranosyl <i>C</i> -, <i>O</i> -, <i>N</i> -, and <i>S</i> -Glycosides .....	10
<b>Figure 10</b>	<i>N</i> -linked Glycan (GlcNAc <sub>2</sub> Man <sub>9</sub> Glc <sub>3</sub> ) .....	11
<b>Figure 11</b>	Biomolecular Probe Attachment via “Click Chemistry” .....	11
<b>Figure 12</b>	<sup>1</sup> H NMR Spectrum Showing $\alpha$ - <i>D</i> -Glucopyranosyl Bromide ( <b>2</b> ) Formation ..	14
<b>Figure 13</b>	<sup>1</sup> H NMR Spectrum Showing $\beta$ - <i>D</i> -Glucopyranosyl Azide ( <b>3</b> ) Formation .....	15
<b>Figure 14</b>	COSY Spectrum for 1,2-Bis(Diphenyl-(2,3,4,6)-Tetra- <i>O</i> -Acetyl- $\beta$ - <i>D</i> -Glucopyranosyl-1- <i>N</i> -Iminophosphorane) Ethane ( <b>5</b> ) .....	19
<b>Figure 15</b>	<sup>1</sup> H and <sup>31</sup> P-Decoupled NMR Spectrum for 1,2-Bis(Diphenyl-(2,3,4,6)-Tetra- <i>O</i> -Acetyl- $\beta$ - <i>D</i> -Glucopyranosyl-1- <i>N</i> -Iminophosphorane) Ethane ( <b>5</b> ) .....	19
<b>Figure 16</b>	<sup>1</sup> H NMR Spectrum (with Inset) for 1,2-Bis(Diphenyl-(2,3,4,6)-Tetra- <i>O</i> -Acetyl- $\beta$ - <i>D</i> -Glucopyranosyl-1- <i>N</i> -Iminophosphorane) Ethane ( <b>5</b> ) .....	20
<b>Figure 17</b>	<sup>31</sup> P NMR Spectrum Showing DPPE and 1,2-Bis(Diphenyl-(2,3,4,6)-Tetra- <i>O</i> -Acetyl- $\beta$ - <i>D</i> -Glucopyranosyl-1- <i>N</i> -Iminophosphorane) Ethane ( <b>5</b> ) .....	21
<b>Figure 18</b>	X-ray Crystal Structure of 1,2-Bis(Diphenyl-(2,3,4,6)-Tetra- <i>O</i> -Acetyl- $\beta$ - <i>D</i> -Glucopyranosyl-1- <i>N</i> -Iminophosphorane) Ethane ( <b>5</b> ) .....	22
<b>Figure 19</b>	<sup>1</sup> H NMR Spectrum (with Inset) for $\beta$ - <i>D</i> -Glucopyranosyl Amine ( <b>6</b> ) .....	24
<b>Figure 20</b>	COSY Spectrum for $\beta$ - <i>D</i> -Glucopyranosyl Amine ( <b>6</b> ) .....	24
<b>Figure 21</b>	<sup>31</sup> P NMR Spectrum of DPPE ( <b>4</b> ) and Oxidized DPPE ( <b>7</b> ) .....	26

<b>Figure 22</b>	$^1\text{H}$ NMR Spectrum Showing ( <i>E</i> )-(2,3,4,6)-Tetra- <i>O</i> -Acetyl- $\beta$ -D-Glucopyranosyl-1- <i>N</i> -3-Nitrobenzaldimine ( <b>9a</b> ) Formation .....	28
<b>Figure 23</b>	COSY Spectrum for ( <i>E</i> )-(2,3,4,6)-Tetra- <i>O</i> -Acetyl- $\beta$ -D-Glucopyranosyl-1- <i>N</i> -3-Nitrobenzaldimine ( <b>9a</b> ) .....	28
<b>Figure 24</b>	X-ray Crystal Structure of ( <i>E</i> )-(2,3,4,6)-Tetra- <i>O</i> -Acetyl- $\beta$ -D-Glucopyranosyl-1- <i>N</i> -3-Nitrobenzaldimine ( <b>9a</b> ) .....	30
<b>Figure 25</b>	Electron Withdrawing Properties of 3-Nitrobenzaldehyde ( <b>8a</b> ) and 4-Nitrobenzaldehyde ( <b>8b</b> ) .....	30
<b>Figure 26</b>	$^1\text{H}$ NMR Spectrum Showing (2,3,4,6)-Tetra- <i>O</i> -Acetyl- $\beta$ -D-Glucopyranosyl-1- <i>N</i> -4-Nitrobenzaldimine ( <b>10b</b> ) Formation .....	35
<b>Figure 27</b>	COSY Spectrum for (2,3,4,6)-Tetra- <i>O</i> -Acetyl- $\beta$ -D-Glucopyranosyl-1- <i>N</i> -4-Nitrobenzaldimine ( <b>10b</b> ) .....	35
<b>Figure 28</b>	400 MHz $^1\text{H}$ NMR Spectrum of $\beta$ -D-Glucopyranosyl Pentaacetate ( <b>1</b> ) .....	59
<b>Figure 29</b>	100 MHz $^{13}\text{C}$ NMR Spectrum of $\beta$ -D-Glucopyranosyl Pentaacetate ( <b>1</b> ) .....	60
<b>Figure 30</b>	400 MHz $^1\text{H}$ NMR Spectrum of $\alpha$ -D-Glucopyranosyl Bromide ( <b>2</b> ) .....	61
<b>Figure 31</b>	100 MHz $^{13}\text{C}$ NMR Spectrum of $\alpha$ -D-Glucopyranosyl Bromide ( <b>2</b> ) .....	62
<b>Figure 32</b>	400 MHz $^1\text{H}$ NMR Spectrum of $\beta$ -D-Glucopyranosyl Azide ( <b>3</b> ) .....	63
<b>Figure 33</b>	100 MHz $^{13}\text{C}$ NMR Spectrum of $\beta$ -D-Glucopyranosyl Azide ( <b>3</b> ) .....	64
<b>Figure 34</b>	400 MHz $^1\text{H}$ NMR Spectrum of 1,2-Bis(Diphenylphosphino)Ethane ( <b>4</b> ) ....	65
<b>Figure 35</b>	100 MHz $^{13}\text{C}$ NMR Spectrum of 1,2-Bis(Diphenylphosphino)Ethane ( <b>4</b> ) ...	66
<b>Figure 36</b>	167 MHz $^{31}\text{P}$ NMR Spectrum of 1,2-Bis(Diphenylphosphino)Ethane ( <b>4</b> ) ....	67
<b>Figure 37</b>	400 MHz $^1\text{H}$ NMR Spectrum of 1,2-Bis(Diphenyl-(2,3,4,6)-Tetra- <i>O</i> -Acetyl- $\beta$ -D-Glucopyranosyl-1- <i>N</i> -Iminophosphorane) Ethane ( <b>5</b> ) in Dichloromethane .....	68
<b>Figure 38</b>	400 MHz $^1\text{H}$ NMR Spectrum of 1,2-Bis(Diphenyl-(2,3,4,6)-Tetra- <i>O</i> -Acetyl- $\beta$ -D-Glucopyranosyl-1- <i>N</i> -Iminophosphorane) Ethane ( <b>5</b> ) Recrystallized from Isopropyl Alcohol .....	69
<b>Figure 39</b>	400 MHz $^{31}\text{P}$ -Decoupled $^1\text{H}$ NMR Spectrum of 1,2-Bis(Diphenyl-(2,3,4,6)-Tetra- <i>O</i> -Acetyl- $\beta$ -D-Glucopyranosyl-1- <i>N</i> -Iminophosphorane) Ethane ( <b>5</b> ) Recrystallized from Isopropyl Alcohol .....	70
<b>Figure 40</b>	100 MHz $^{13}\text{C}$ NMR Spectrum of 1,2-Bis(Diphenyl-(2,3,4,6)-Tetra- <i>O</i> -Acetyl- $\beta$ -D-Glucopyranosyl-1- <i>N</i> -Iminophosphorane) Ethane ( <b>5</b> ) Recrystallized from Isopropyl Alcohol .....	71

<b>Figure 41</b>	167 MHz <sup>31</sup> P NMR Spectrum of 1,2-Bis(Diphenyl-(2,3,4,6)-Tetra- <i>O</i> -Acetyl- $\beta$ -D-Glucopyranosyl-1- <i>N</i> -Iminophosphorane) Ethane ( <b>5</b> ) Recrystallized from Isopropyl Alcohol .....	72
<b>Figure 42</b>	400 MHz <sup>1</sup> H NMR Spectrum of $\beta$ -D-Glucopyranosyl Amine ( <b>6</b> ) .....	73
<b>Figure 43</b>	100 MHz <sup>13</sup> C NMR Spectrum of $\beta$ -D-Glucopyranosyl Amine ( <b>6</b> ). .....	74
<b>Figure 44</b>	400 MHz <sup>1</sup> H NMR Spectrum of 1,2-Ethanediybis(Diphenylphosphine) Dioxide ( <b>7</b> ) .....	75
<b>Figure 45</b>	100 MHz <sup>13</sup> C NMR Spectrum of 1,2-Ethanediybis(Diphenylphosphine) Dioxide ( <b>7</b> ) .....	76
<b>Figure 46</b>	167 MHz <sup>31</sup> P NMR Spectrum of 1,2-Ethanediybis(Diphenylphosphine) Dioxide ( <b>7</b> ) .....	77
<b>Figure 47</b>	400 MHz <sup>1</sup> H NMR Spectrum of 3-Nitrobenzaldehyde ( <b>8a</b> ) .....	78
<b>Figure 48</b>	100 MHz <sup>13</sup> C NMR Spectrum of 3-Nitrobenzaldehyde ( <b>8a</b> ) .....	79
<b>Figure 49</b>	400 MHz <sup>1</sup> H NMR Spectrum of 4-Nitrobenzaldehyde ( <b>8b</b> ) .....	80
<b>Figure 50</b>	100 MHz <sup>13</sup> C NMR Spectrum of 4-Nitrobenzaldehyde ( <b>8b</b> ) .....	81
<b>Figure 51</b>	400 MHz <sup>1</sup> H NMR Spectrum of Benzaldehyde ( <b>8c</b> ) .....	82
<b>Figure 52</b>	100 MHz <sup>13</sup> C NMR Spectrum of Benzaldehyde ( <b>8c</b> ) .....	83
<b>Figure 53</b>	400 MHz <sup>1</sup> H NMR Spectrum of 9-Anthracenecarboxaldehyde ( <b>8d</b> ) .....	84
<b>Figure 54</b>	100 MHz <sup>13</sup> C NMR Spectrum of 9-Anthracenecarboxaldehyde ( <b>8d</b> ) .....	85
<b>Figure 55</b>	400 MHz <sup>1</sup> H NMR Spectrum of 2-Hydroxy-3-Methoxybenzaldehyde ( <b>8e</b> ) .	86
<b>Figure 56</b>	100 MHz <sup>13</sup> C NMR Spectrum of 2-Hydroxy-3-Methoxybenzaldehyde ( <b>8e</b> )	87
<b>Figure 57</b>	400 MHz <sup>1</sup> H NMR Spectrum of 2-Hydroxy-4-Methoxybenzaldehyde ( <b>8f</b> ) ..	88
<b>Figure 58</b>	100 MHz <sup>13</sup> C NMR Spectrum of 2-Hydroxy-4-Methoxybenzaldehyde ( <b>8f</b> ) .	89
<b>Figure 59</b>	400 MHz <sup>1</sup> H NMR Spectrum of 2-Hydroxy-6-Methoxybenzaldehyde ( <b>8g</b> ) .	90
<b>Figure 60</b>	100 MHz <sup>13</sup> C NMR Spectrum of 2-hydroxy-6-Methoxybenzaldehyde ( <b>8g</b> ) .	91
<b>Figure 61</b>	400 MHz <sup>1</sup> H NMR Spectrum of ( <i>E</i> )-(2,3,4,6)-Tetra- <i>O</i> - Acetyl- $\beta$ -D-Glucopyranosyl-1- <i>N</i> -3-Nitrobenzaldimine ( <b>9a</b> ) .....	92
<b>Figure 62</b>	100 MHz <sup>13</sup> C NMR Spectrum of ( <i>E</i> )-(2,3,4,6)-Tetra- <i>O</i> - Acetyl- $\beta$ -D-Glucopyranosyl-1- <i>N</i> -3-Nitrobenzaldimine ( <b>9a</b> ) .....	93

<b>Figure 63</b>	400 MHz <sup>1</sup> H NMR Spectrum of ( <i>E</i> )-(2,3,4,6)-Tetra- <i>O</i> -Acetyl-β-D-Glucopyranosyl-1- <i>N</i> -4-Nitrobenzaldimine ( <b>9b</b> ) .....	94
<b>Figure 64</b>	100 MHz <sup>13</sup> C NMR Spectrum of ( <i>E</i> )-(2,3,4,6)-Tetra- <i>O</i> -Acetyl-β-D-Glucopyranosyl-1- <i>N</i> -4-Nitrobenzaldimine ( <b>9b</b> ) .....	95
<b>Figure 65</b>	400 MHz <sup>1</sup> H NMR Spectrum of ( <i>E</i> )-(2,3,4,6)-Tetra- <i>O</i> -Acetyl-β-D-Glucopyranosyl-1- <i>N</i> -Benzaldimine ( <b>9c</b> ) .....	96
<b>Figure 66</b>	100 MHz <sup>13</sup> C NMR Spectrum of ( <i>E</i> )-(2,3,4,6)-Tetra- <i>O</i> -Acetyl-β-D-Glucopyranosyl-1- <i>N</i> -Benzaldimine ( <b>9c</b> ) .....	97
<b>Figure 67</b>	400 MHz <sup>1</sup> H NMR Spectrum of ( <i>E</i> )-(2,3,4,6)-Tetra- <i>O</i> -Acetyl-β-D-Glucopyranosyl-1- <i>N</i> -9-Anthracenecarboxaldimine ( <b>9d</b> ) .....	98
<b>Figure 68</b>	100 MHz <sup>13</sup> C NMR Spectrum of ( <i>E</i> )-(2,3,4,6)-Tetra- <i>O</i> -Acetyl-β-D-Glucopyranosyl-1- <i>N</i> -9-Anthracenecarboxaldimine ( <b>9d</b> ) .....	99
<b>Figure 69</b>	400 MHz <sup>1</sup> H NMR Spectrum of ( <i>E</i> )-(2,3,4,6)-Tetra- <i>O</i> -Acetyl-β-D-Glucopyranosyl-1- <i>N</i> -2-Hydroxy-3-Methoxybenzaldimine ( <b>9e</b> ) .	100
<b>Figure 70</b>	100 MHz <sup>13</sup> C NMR Spectrum of ( <i>E</i> )-(2,3,4,6)-Tetra- <i>O</i> -Acetyl-β-D-Glucopyranosyl-1- <i>N</i> -2-Hydroxy-3-Methoxybenzaldimine ( <b>9e</b> ) .	101
<b>Figure 71</b>	400 MHz <sup>1</sup> H NMR Spectrum of ( <i>E</i> )-(2,3,4,6)-Tetra- <i>O</i> -Acetyl-β-D-Glucopyranosyl-1- <i>N</i> -2-Hydroxy-4-Methoxybenzaldimine ( <b>9f</b> ) .	102
<b>Figure 72</b>	100 MHz <sup>13</sup> C NMR Spectrum of ( <i>E</i> )-(2,3,4,6)-Tetra- <i>O</i> -Acetyl-β-D-Glucopyranosyl-1- <i>N</i> -2-Hydroxy-4-Methoxybenzaldimine ( <b>9f</b> ) .	103
<b>Figure 73</b>	400 MHz <sup>1</sup> H NMR Spectrum of ( <i>E</i> )-(2,3,4,6)-Tetra- <i>O</i> -Acetyl-β-D-Glucopyranosyl-1- <i>N</i> -2-Hydroxy-6-Methoxybenzaldimine ( <b>9g</b> ) .	104
<b>Figure 74</b>	100 MHz <sup>13</sup> C NMR Spectrum of ( <i>E</i> )-(2,3,4,6)-Tetra- <i>O</i> -Acetyl-β-D-Glucopyranosyl-1- <i>N</i> -2-Hydroxy-6-Methoxybenzaldimine ( <b>9g</b> ) .	105
<b>Figure 75</b>	400 MHz <sup>1</sup> H NMR Spectrum of (2,3,4,6)-Tetra- <i>O</i> -Acetyl-β-D-Glucopyranosyl-1- <i>N</i> -4-Nitrobenzaldimine ( <b>10b</b> ) .....	106
<b>Figure 76</b>	100 MHz <sup>13</sup> C NMR Spectrum of (2,3,4,6)-Tetra- <i>O</i> -Acetyl-β-D-Glucopyranosyl-1- <i>N</i> -4-Nitrobenzaldimine ( <b>10b</b> ) .....	107
<b>Figure 77</b>	400 MHz <sup>1</sup> H NMR Spectrum of 1,2-Bis(Diphenyl-(2,3,4,6)-Tetra- <i>O</i> -Acetyl-β-D-Galactopyranosyl-1- <i>N</i> -Iminophosphorane) Ethane ( <b>11</b> ) in Isopropyl Alcohol .....	108
<b>Figure 78</b>	400 MHz <sup>31</sup> P-Decoupled <sup>1</sup> H NMR Spectrum of 1,2-Bis(Diphenyl-(2,3,4,6)-Tetra- <i>O</i> -Acetyl-β-D-Galactopyranosyl-1- <i>N</i> -Iminophosphorane) Ethane ( <b>11</b> ) in Isopropyl Alcohol .....	109

<b>Figure 79</b>	100 MHz $^{13}\text{C}$ NMR Spectrum of 1,2-Bis(Diphenyl-(2,3,4,6)-Tetra- <i>O</i> -Acetyl- $\beta$ -D-Galactopyranosyl-1- <i>N</i> -Iminophosphorane) Ethane ( <b>11</b> ) in Isopropyl Alcohol .....	110
<b>Figure 80</b>	167 MHz $^{31}\text{P}$ NMR Spectrum of 1,2-Bis(Diphenyl-(2,3,4,6)-Tetra- <i>O</i> -Acetyl- $\beta$ -D-Galactopyranosyl-1- <i>N</i> -Iminophosphorane) Ethane ( <b>11</b> ) in Isopropyl Alcohol .....	111
<b>Figure 81</b>	X-ray Crystal Structure of Iminophosphorane <b>5</b> with 50% Probability Ellipsoids.....	113
<b>Figure 82</b>	X-ray Crystal Structure of ( <i>E</i> )-(2,3,4,6)-Tetra- <i>O</i> -Acetyl- $\beta$ -D-Glucopyranosyl-1- <i>N</i> -3-Nitrobenzaldimine ( <b>9a</b> ) with 50% Probability Ellipsoids .....	125

**List of Tables**

<b>Table 1</b>	Synthesized Glucopyranosyl Imines <b>9</b> .....	32
<b>Table 2</b>	Synthesized Glucopyranosyl Amines <b>10</b> .....	34

**List of Schemes**

<b>Scheme 1</b>	The Aza-Wittig Reaction .....	6
<b>Scheme 2</b>	Reductive Amination .....	7
<b>Scheme 3</b>	Synthesis of $\alpha$ -D-Glucopyranosyl Bromide ( <b>2</b> ) .....	13
<b>Scheme 4</b>	Synthesis of $\beta$ -D-Glucopyranosyl Azide ( <b>3</b> ) .....	14
<b>Scheme 5</b>	Synthesis of 1,2-Bis(Diphenyl-(2,3,4,6)-Tetra- <i>O</i> -Acetyl- $\beta$ -D-Glucopyranosyl-1- <i>N</i> -Iminophosphorane) Ethane ( <b>5</b> ) .....	16
<b>Scheme 6</b>	Hydrolysis of 1,2-Bis(Diphenyl-(2,3,4,6)-Tetra- <i>O</i> -Acetyl- $\beta$ -D-Glucopyranosyl-1- <i>N</i> -Iminophosphorane) Ethane ( <b>5</b> ) .....	23
<b>Scheme 7</b>	Synthesis of Glucopyranosyl Imines <b>9</b> .....	26
<b>Scheme 8</b>	Synthesis of Glucopyranosyl Amines <b>10</b> .....	33
<b>Scheme 9</b>	Alternate Synthesis of Glucopyranosyl Amines <b>10</b> .....	34
<b>Scheme 10</b>	Proposed Synthesis of Glycopolymers .....	39

## Introduction

### Organic Azides

Organic azides were first discovered by Peter Grieb in 1864 by reacting arenediazonium perbromides and ammonia to yield a phenyl azide, and comprise a functional group consisting of a linear arrangement of three resonance-stabilized nitrogen atoms (**Figure 1**).<sup>1-3</sup>

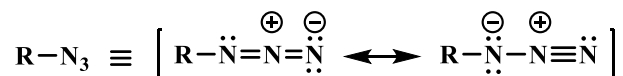


**Figure 1.** Resonance structures of an alkyl azide.

In the time since, there has been considerable development in the application and utility of azides in organic syntheses of amines (hydrogenation), amides (acyl chlorides), isocyanates (Curtius rearrangement), and triazoles (Huisgen reaction) to name a few (**Figure 2**).<sup>3</sup> Azido compounds are therefore favorable in pharmaceutical development, with one of the more notable examples being the HIV inhibitor azidothymidine, more commonly known as AZT (**Figure 3**).<sup>4</sup>

The potential for hazards with azido compounds underlies their versatility due to their potentially explosive nature. Azides, in general, are extremely sensitive to thermal and mechanical perturbations, and thus are susceptible to rapid decomposition with concomitant release of nitrogen gas. This reactivity can be attributed to the polarizability of the  $\pi$ -bond system within the azide; additionally, synthetic incorporation of an azide functional group can increase the potential energy of the compound by 290-355 kJ/mol.<sup>2</sup> Overall, then, azide reactions are strongly favored both entropically and enthalpically. Consequently, azides are categorized as high-energy density materials (HEDM), which has led to their use as primary detonators (e.g., lead or silver azides) or propellants (e.g., air bags and hypergolic fuels).<sup>5</sup>

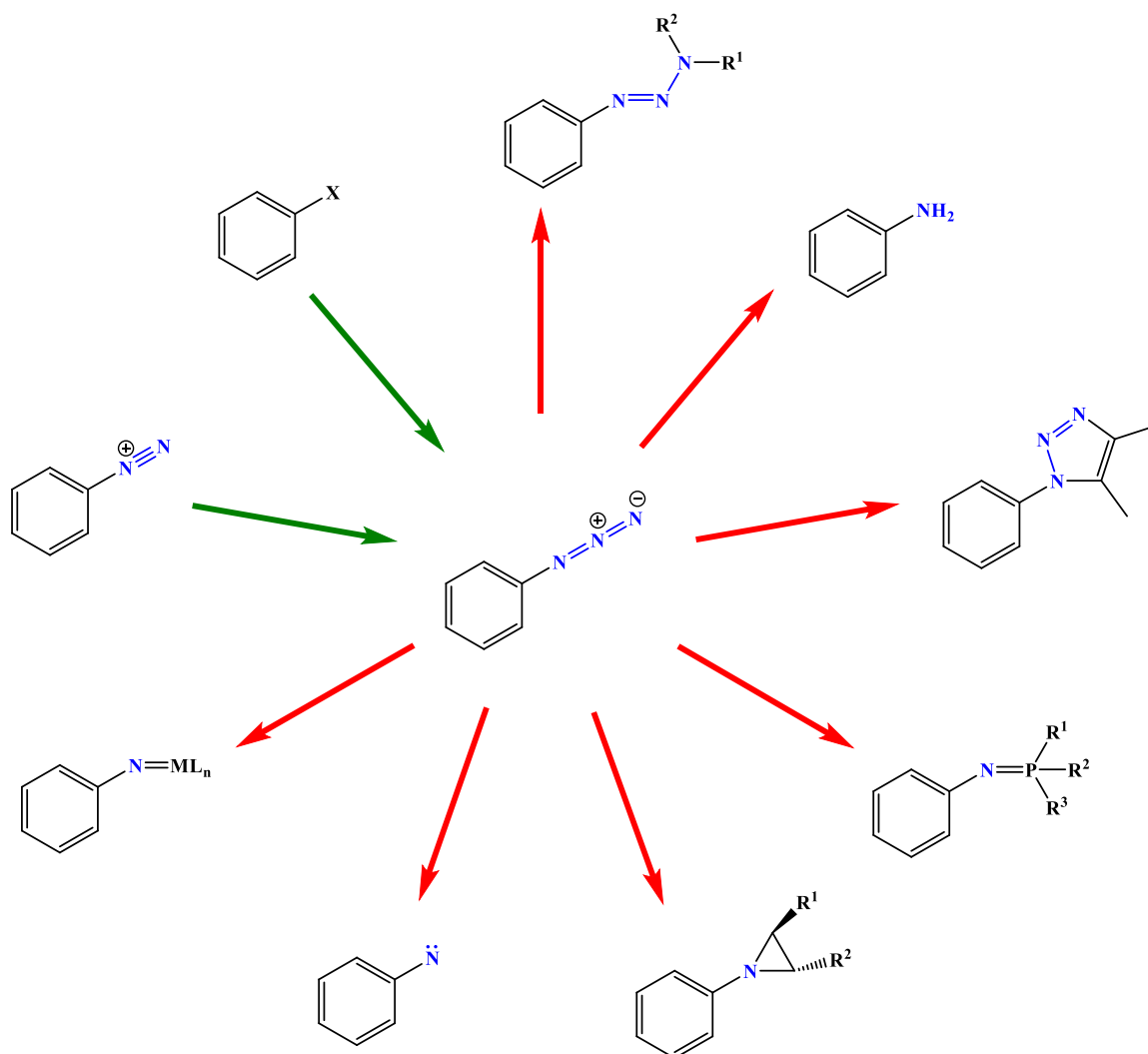


**Figure 2.** Versatility in the synthesis and reaction of organic azides.

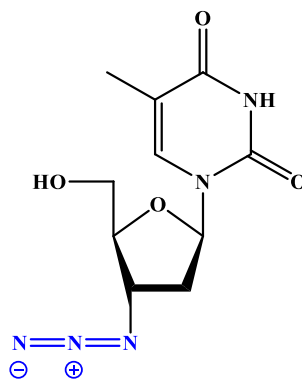


**Figure 3.** HIV inhibitor azidothymidine (AZT).



## Staudinger Reaction

First discovered by Hermann Staudinger and Jules Meyer in 1919, the Staudinger reaction involves the reaction of an azide with a trialkyl-substituted phosphine (**Figure 4**). Mechanistically, the phosphine serves as a reducing agent, undergoing nucleophilic addition to the terminal azido nitrogen forming a zwitterionic intermediate. The alkyl-linked nitrogen (bearing a formal negative charge) then attacks the positively-charged phosphorous, thereby forming a 4-membered ring which collapses, generating nitrogen gas and the iminophosphorane (aza-ylide) product.<sup>6</sup>

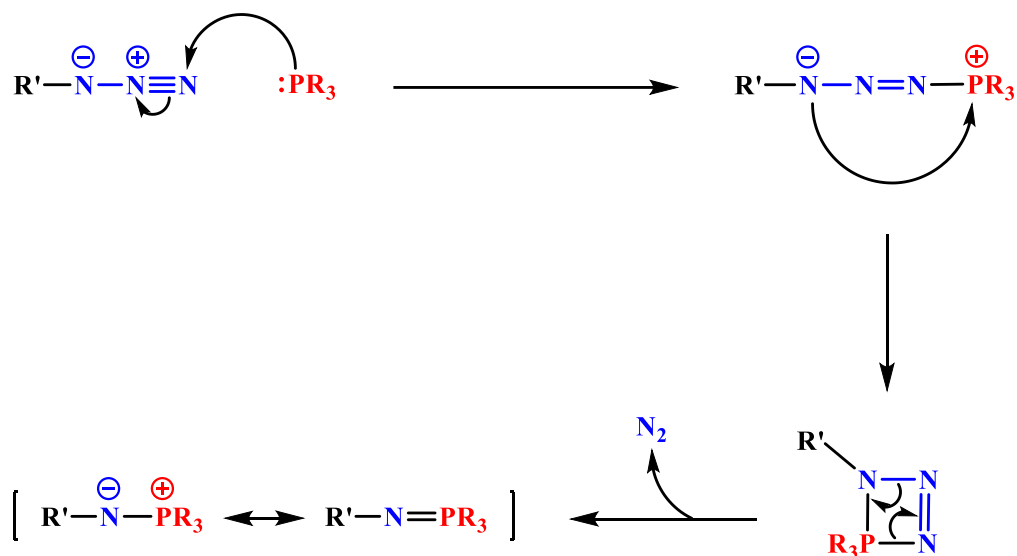


**Figure 4.** Reaction pathway for the Staudinger reaction between an alkyl azide and a trialkyl phosphine.

Classically, triarylphosphines have been utilized to carry out the reaction; the drawback, however, is that the phosphine oxide byproducts from sequential reactions can be difficult to separate, on account of streaking and propensity for coelution with the compounds of interest. The addition of basic moieties on the phosphines to counter this effect has been used; this approach is not practical, though, for acid-sensitive compounds. Availability of polymer-bound triarylphosphine columns present a remedy, albeit limited because of the decreased reactivity compared to the free reagent, coupled with the cost-prohibitive facet large-scale reactions would

entail. Recently, 1,2-bis(diphenylphosphino)ethane (henceforth referred to as DPPE), has been discovered to be a suitable replacement in the Staudinger (as well as Mitsunobu) reactions, avoiding many of the aforementioned resolution issues.<sup>7-9</sup>

Despite the availability of the Staudinger reaction for nearly a century, a complete mechanistic characterization of the ligation (coupling the iminophosphorane with a carboxylic acid derivative to yield an amide) was not undertaken until 2005, by Carolyn Bertozzi and collaborators.<sup>10</sup> Bertozzi's pioneering research involving the Staudinger ligation has also become influential in the burgeoning field of "bioorthogonal chemistry," which utilizes non-naturally occurring compounds that react in parallel to physiological pathways in order to selectively tag relevant cellular motifs.<sup>11</sup> One particular modification, known as the "traceless" Staudinger ligation functionalizes one of the phenyl groups with an acyl group which is then subject to intramolecular nucleophilic acyl substitution, which, following hydrolysis will yield a peptide.<sup>12</sup>

### **Classic Wittig Reaction**

The classic Wittig reaction (**Figure 5**) was discovered by Georg Wittig in 1954, whereby the negative charge-bearing carbon of a carbon-phosphorus ylide attacks the carbonyl of either a ketone or aldehyde, resulting in formation of a betaine intermediate, which subsequently forms a 4-member cyclic (oxaphosphetane) intermediate, ultimately collapsing to produce an olefin and triarylphosphine oxide.<sup>13</sup>

The Wittig reaction found immediate application for both natural product synthesis (vitamin D) and industrial synthesis (vitamin A),<sup>14</sup> due to its exact "positional selectivity," whereby a carbonyl is exclusively replaced by an alkene.<sup>15</sup> Since that time, there has been an increase in the understanding of fundamental aspects governing the reaction, thus permitting researchers to impart greater stereochemical control over the formation of *E*- and *Z*-isomers. Several adaptations of the Wittig reaction – so-called "non-classical" reactions – have been developed in this regard, including the Horner-Wadsworth-Emmons reaction (for predominantly *E*-isomers) and the Still-Gennari

reaction (for predominantly *Z*-isomers).<sup>15,16</sup> Furthermore, the substrate scope of the Wittig reaction has been expanded from traditional aldehydes and ketones to esters, lactones, and amides, for example.<sup>16</sup>

As previously noted, the oxidized triarylphosphines which are generated as byproducts of the Wittig reaction can pose a nuisance during purification and isolation steps, but can be mitigated by substitution with DPPE. “Non-classical” Wittig reactions, such as the Horner-Wadsworth-Emmons and Horner-Wittig, circumvent this problem by employing organophosphorus reagents whose oxidized forms are water-soluble, which lend themselves to facile removal.<sup>15</sup> In the modern era of “green chemistry,” the triphenylphosphine oxide byproduct of the classic Wittig reaction also represents a gross inefficiency of roughly 80% in terms of “atom economy”<sup>\*</sup> owing largely to the readily unusable generation of said byproduct.<sup>17,18</sup>

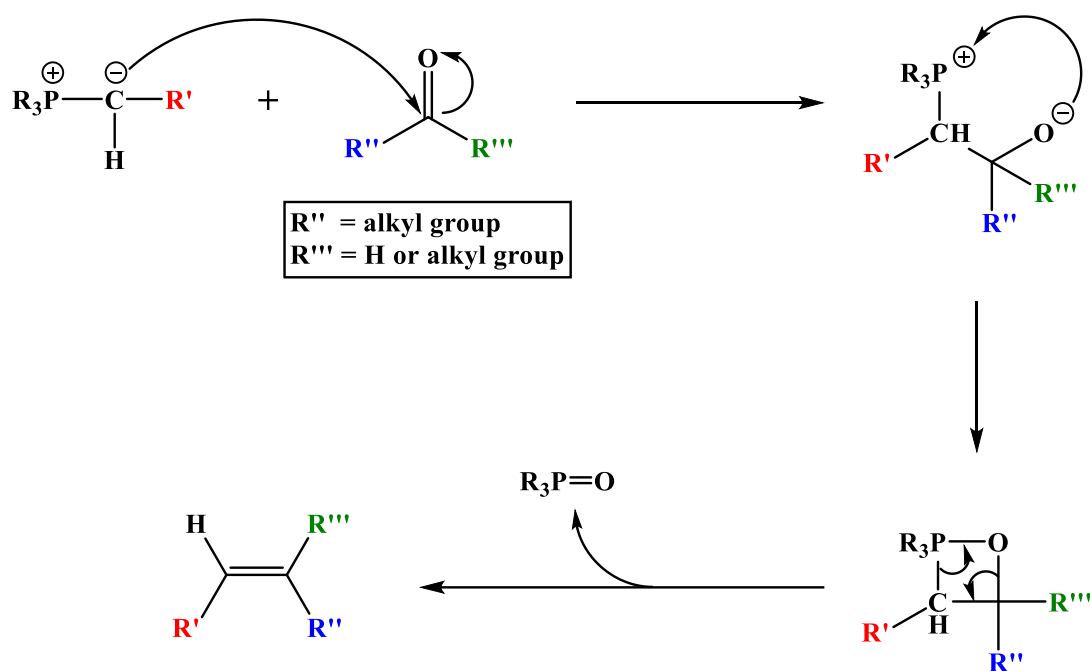


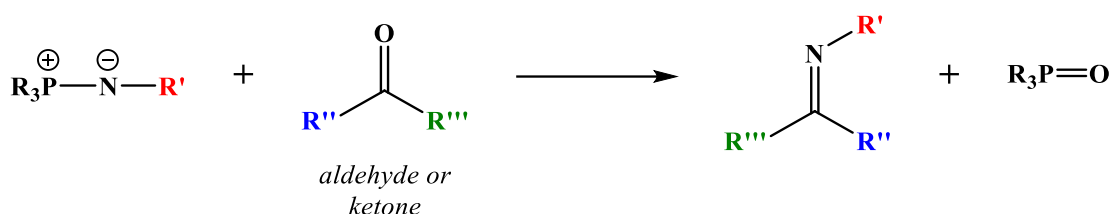
**Figure 5.** Mechanism of the classic Wittig reaction.

<sup>\*</sup> Atom efficiency can be defined in several ways; the calculation in this manuscript follows the equation:  

$$\text{atom economy} = \frac{\text{molecular mass of target compound}}{\text{molecular mass of starting materials}} \times 100\%.$$

## The aza-Wittig Reaction

Among the “non-classical” Wittig reaction variants is the aza-Wittig reaction, which is an amalgamation of the Staudinger and Wittig reactions. The reaction, which proceeds mechanistically by its principal namesake, is initiated by the formation of a Staudinger aza-ylide (iminophosphorane), which can then react with aldehydes or ketones to synthesize carbon-nitrogen double bonds (**Scheme 1**). In contrast to classic imine formation from 1° amines and aldehydes or ketones, water is not produced in the aza-Wittig reaction, thereby negating reversibility.



**Scheme 1.** The aza-Wittig reaction.

Synthesis of such imines is of great consequence in natural product synthesis, undergoing both intra- and intermolecular reactions.<sup>19,20</sup> Among intramolecular reactions in particular, the formation of *N*-heterocyclic compounds and their respective analogues is desirable due to their prevalence in biological systems – purines and pyrimidines which are major components of nucleotides, as well as alkaloids, which effect a multitude of physiological responses (**Figure 7**).<sup>21-23</sup> Alternatively, the imines could simply be reduced to the amine products.

## Reductive Amination

The process of converting an imine to an amine facilitated by a reducing agent is called reductive amination. Sodium borohydride (NaBH<sub>4</sub>) or lithium aluminum hydride (LiAlH<sub>4</sub>) are common reducing agents. However, issues with selectivity and termination may arise with either of those compounds. Sodium cyanoborohydride (NaBH<sub>3</sub>CN) was investigated by Borch, and found to selectively reduce aldehydes and ketones to alcohols optimally at pH 3-4, while imines are reduced at pH 6-8 (necessitated by the formation of an iminium species). It is therefore possible to

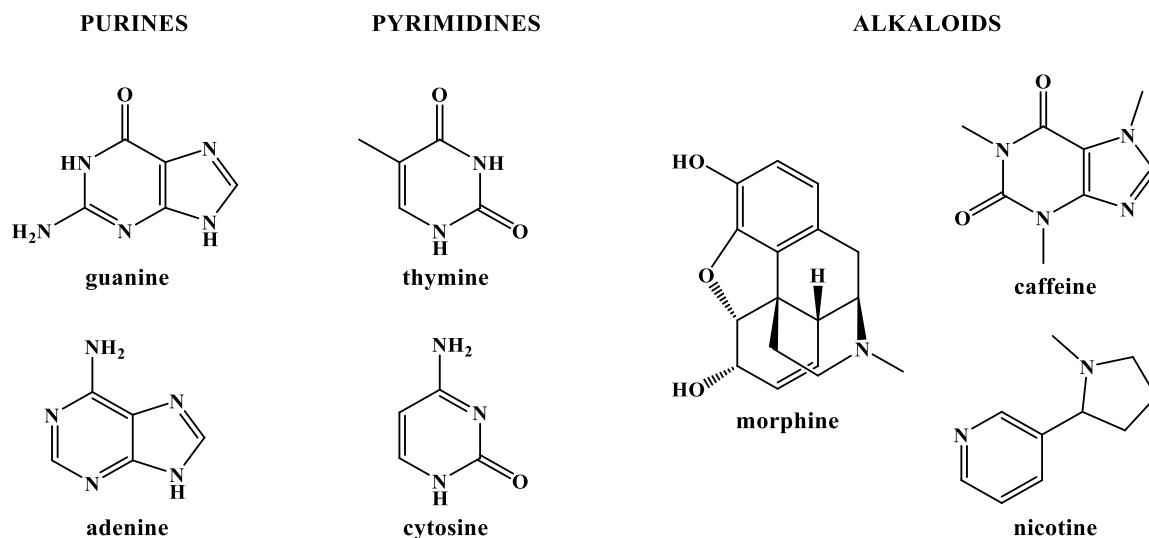
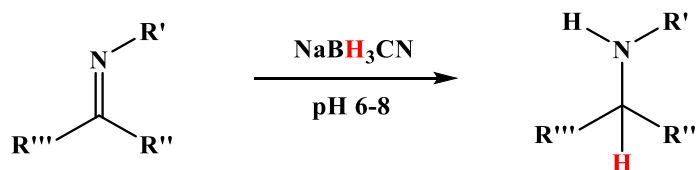


**Figure 6.** Naturally occurring *N*-heterocyclic compounds.

introduce the  $\text{NaBH}_3\text{CN}$  to the reaction mixture containing both the initial amine and aldehyde or ketone with little probability for side reductions.<sup>24</sup>

One caveat with using  $\text{NaBH}_3\text{CN}$  as the reducing agent, is the production of toxic hydrogen cyanide (HCN) and sodium cyanide (NaCN) byproducts during workup.<sup>25</sup> To this end, alternative reducing agents like sodium triacetoxyborohydride ( $\text{NaBH}(\text{OAc})_3$ )<sup>26</sup> and  $\alpha$ -picoline borane<sup>27</sup> that maintain high selectivity have been developed. Of these two,  $\text{NaBH}(\text{OAc})_3$  suffers from water-instability and non-selective reduction in methanol, which can pose problems when working with certain carbonyl-containing reagents such as formaldehyde that are typically available in aqueous solution.<sup>26</sup>



**Scheme 2.** Reductive amination of an aldehyde- or keto-based imine.

## Carbohydrates

Carbohydrates are ubiquitous molecules within biological organisms, and exhibit a diverse functionality – structural support (cellulose, collagen); extracellular interactions via integral membrane glycoproteins (surface and cellular adhesion, hormone receptors); cellular energy (nucleoside triphosphates); and nucleic acid backbones (DNA and RNA).<sup>28</sup> Carbohydrates, therefore, are favorable targets for pharmacological developments.<sup>29</sup>

Carbohydrates are composed of monomeric subunits known as monosaccharides, which can form dimeric structures called *disaccharides*, short (3-10 subunit) chains known as *oligosaccharides*, as well as more complex, branched structures referred to as *polysaccharides*.<sup>30,31</sup> Carbohydrates can further be classified based on the number of atoms present in the ring form: furanoses (5-membered cycles) and pyranoses (6-membered cycles). Interconversion of these forms can occur through ring-opening and ring-closing mechanisms accompanied by Lobry de Bruyn-Alberda van Ekenstein transformations and epimerizations (**Figure 7**).<sup>32</sup>

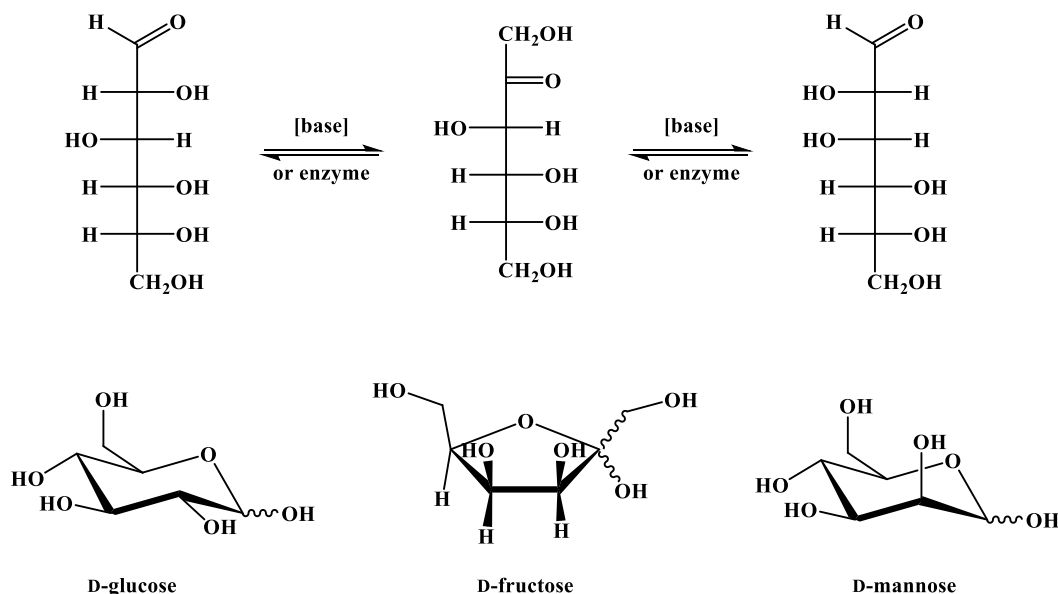


**Figure 7.** Lobry de Bruyn-Alberda van Ekenstein transformation of D-glucose to D-mannose. The cyclic structures are below the corresponding Fischer projections.

A central feature of carbohydrates is the *anomeric carbon*, which is denoted as the carbonyl carbon that is present when the monosaccharide is in the open-chain form. As there is free bond rotation along the carbon backbone in the acyclic state, upon ring-closing, the hydroxyl group may be aligned either above the plane of the sugar or below. These two possible conformations are nominally distinguished as the  $\alpha$ -position (if the hydroxyl group is positioned on the *same side* as  $\text{CH}_2\text{OH}$  on the bottom-most chiral center of the Fischer projection) and the  $\beta$ -position (if the hydroxyl group is positioned on the *opposite side* as  $\text{CH}_2\text{OH}$  on the bottom-most chiral center of the Fischer projection). Collectively, these isomers are termed *anomers* (**Figure 8**), and the preference for the  $\alpha$ - or  $\beta$ -orientation in carbohydrate heterocycles is dictated by the *anomeric effect*.<sup>30,33</sup>

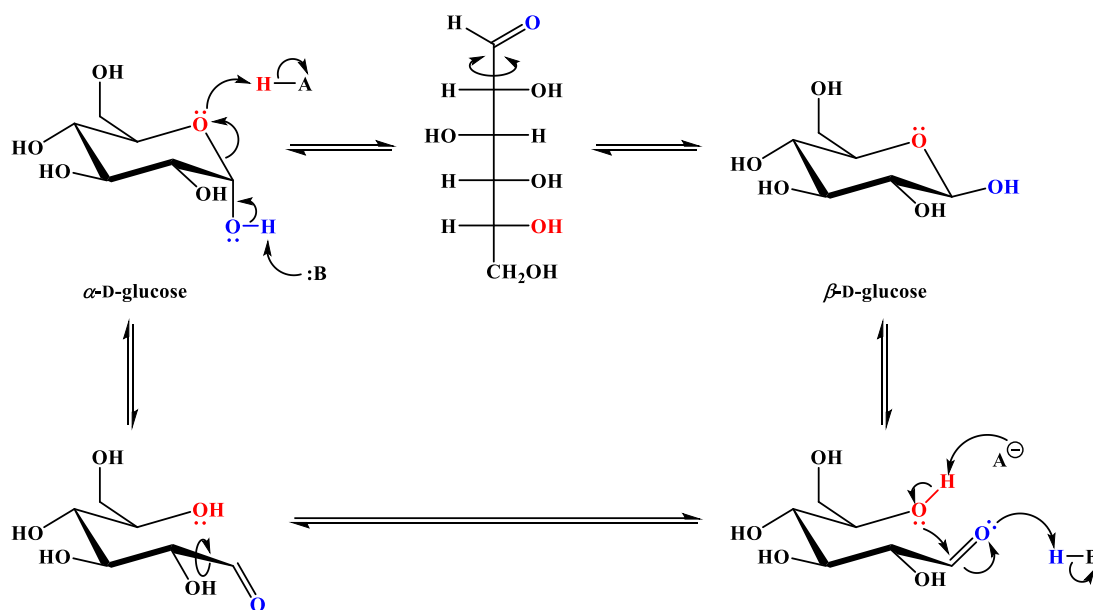


**Figure 8.** Anomerization of D-glucose.

It is through the anomeric carbon that glycosidic linkages are generated among carbohydrates or with other molecules. The linkages can be characterized by the atom bonded to the anomeric site: “C-linked glycosides” (carbon), “N-linked glycosides” (nitrogen), “O-linked glycosides” (oxygen), and “S-linked glycosides” (sulfur) (**Figure 9**).<sup>34</sup> Furanosyl *N*-glycosidic linkages have prominence in nucleotide bases, but pyranosyl *N*-glycosides have significance in *N*-

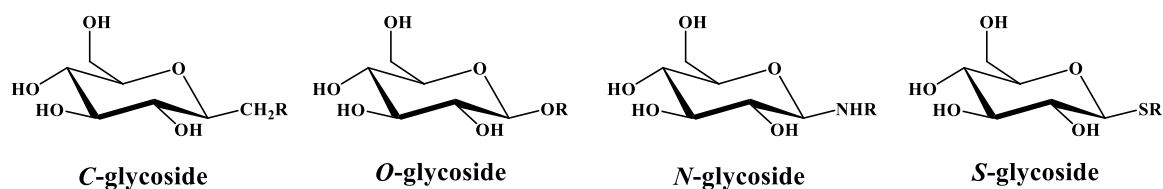


**Figure 9.** C-, O-, N-, and S-glycosidic pyranoses.

glycans – carbohydrate portions of glycoconjugates that are anchored within the membranes of certain eukaryotic organelles, and some prokaryotes and archaea, mediated by anomeric linkages to asparagine residues (**Figure 10**).<sup>34-37</sup> Glycans are implicated as protein-stabilizing scaffolds that also act as points of recognition for glycan-binding proteins (GBPs). Abnormal glycosylation is associated with cancer cells, which makes glycans an auspicious target for therapeutic research.<sup>35</sup> Work by Danishefsky<sup>38</sup> and Andreana<sup>39</sup> have built off of this concept in the development of “tumor-associated carbohydrate antigens” (TACAs).

The emergence of “click chemistry” – the formation of 1,2,3-triazoles by the [4+2] cycloaddition reaction of azides and alkynes, or through Staudinger ligation – has also held promise with regard to carbohydrate chemistry by being able to append fluorescent or biotin tags for visualization and purification of biomolecules (**Figure 11**). Furthermore, this *in vivo* bioorthogonal approach provides a possible way of identifying interacting biochemical pathway constituents by establishing covalent linkages between the complementary molecules.<sup>40</sup>



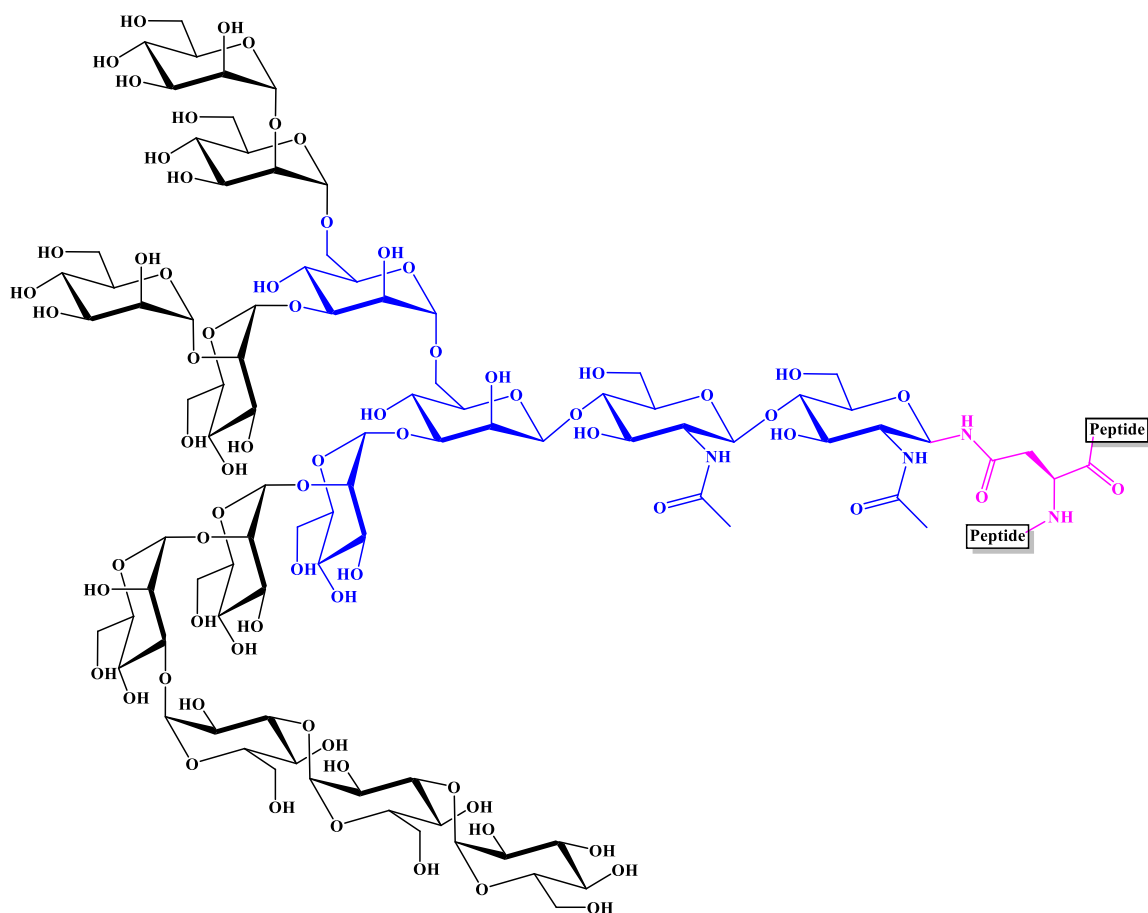


**Figure 10.** *N*-glycan showing conserved pentameric core (blue) and asparagine linkage (purple).<sup>36</sup>

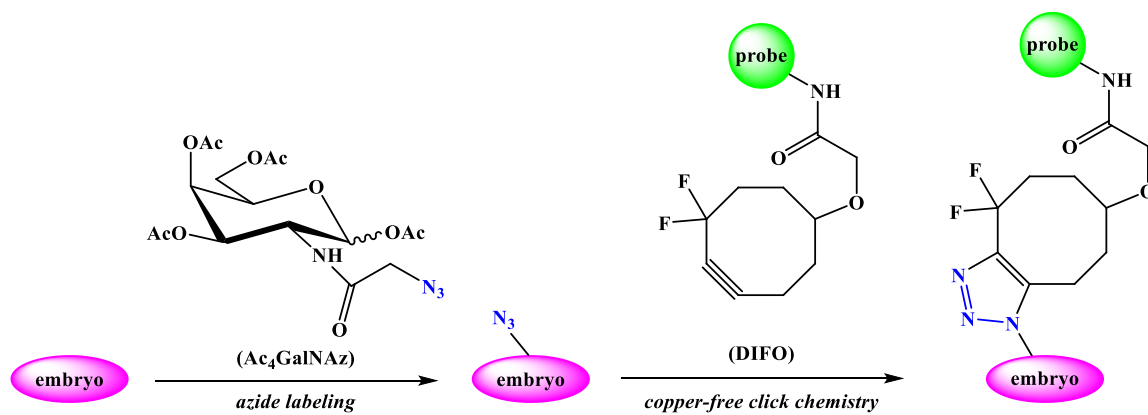


**Figure 11.** Incorporation of biomarkers via “click chemistry.”<sup>40</sup>

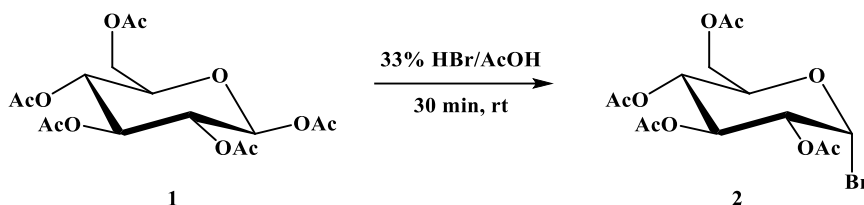
### Statement of Problem

The evolution of orthogonal approaches to the study of biochemical pathways, as well as recognition of the promotion of carbohydrates as targets of interest for pharmaceutical advancement have reinforced the need to develop a complete mechanistic understanding of the reactions involved in their syntheses. The Staudinger ligation has been highlighted for its applicability in such designs, and the generated nitrogen-phosphorus ylide serves as an intermediate in the aza-Wittig reaction. While 1,2-bis(diphenylphosphino)ethane (DPPE) has recently become a favorable substitute for traditional triphenylphosphine (PPh<sub>3</sub>) in these reactions, the observed ylide from its reaction with glucopyranosyl azides has not been isolated.

The intent of this research, therefore, is two-fold: first, to isolate and characterize the aza-ylide intermediate formed from  $\beta$ -D-glucopyranosyl azide and DPPE to confirm the putative mechanism of the Staudinger ligation through which the reaction proceeds; second, to then apply the ylide in novel aza-Wittig reactions with aldehydes, followed by subsequent selective reductive amination using NaBH<sub>3</sub>CN to synthesize glucopyranosyl amines for the purpose of further developing libraries of compounds with potential as therapeutic glycomimetics.

## Results and Discussion

### Synthesis $\alpha$ -D-Glucopyranosyl Bromide (2)



**Scheme 3.** Synthesis of  $\alpha$ -D-glucopyranosyl bromide (2).

Addition of 33% hydrobromic acid (HBr) in acetic acid (AcOH) to  $\beta$ -D-glucose pentaacetate (**1**) quantitatively yielded the  $\alpha$ -D-glucopyranosyl bromide (**2**) after approximately 30 minutes, as monitored by thin-layer chromatography (TLC). Exposure of a burned spot by the sulfuric acid stain possessing an  $R_f$  lower than the glucopyranosyl precursor **1** was representative of a compound endowed with the greater degree of polarity imparted by bromine having replaced an acetyl group. The reaction itself proceeds through an  $S_N1$  pathway, albeit with the bromide solely assuming the axial position as predicated by the anomeric effect.

Spectroscopically, the formation of bromide product **2** was confirmed through  $^1\text{H}$  NMR data, whereby the anomeric hydrogen (H-1, distinguished as the only “doublet” in the spectra, being coupled to only one other proton, H-2) was inverted from the axial to the equatorial position, effecting a change in the vicinal coupling constant from 8.28 Hz (5.70 ppm) for **1** to 4.04 Hz (6.61 ppm) for **2** as dictated by the Karplus curve, also accompanied by an appreciable downfield shift resulting from the presence of a larger, highly electronegative bromine atom (**Figure 12**). The totality of the inversion is also borne out by the proton NMR spectra, where it exists as a solitary “doublet” with the requisite coupling constant designated by the  $\alpha$ -anomer.

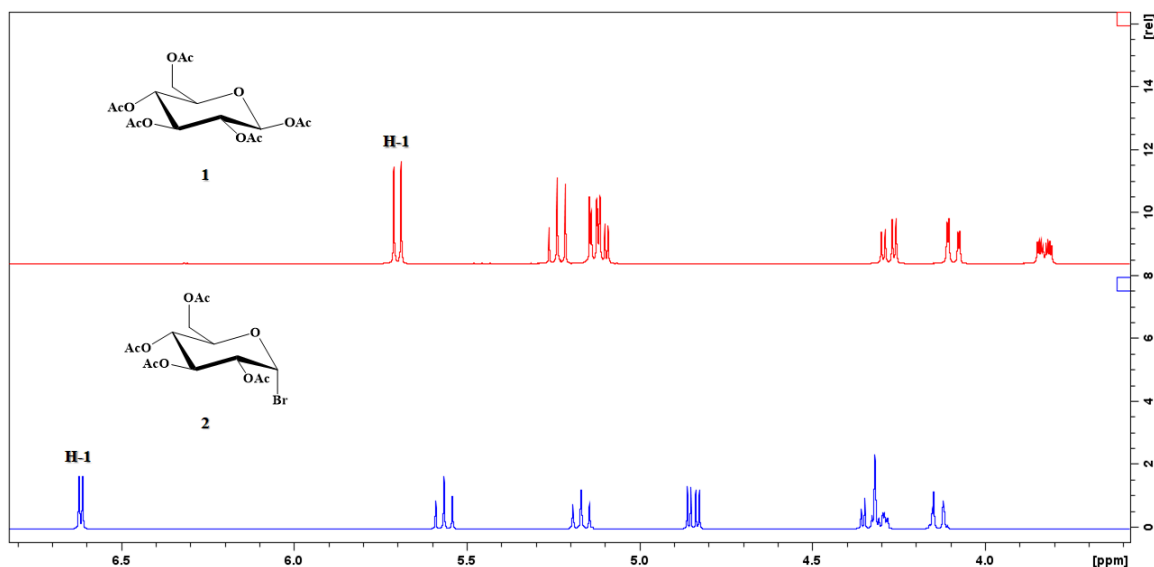
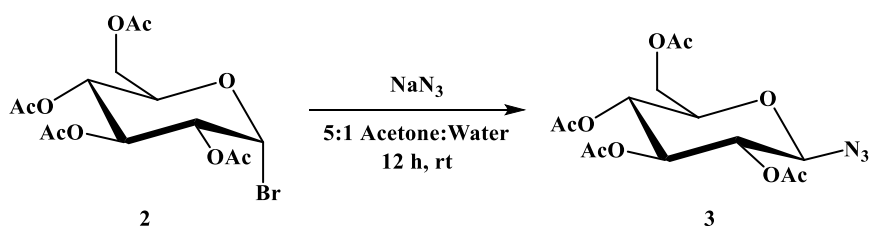


**Figure 12.** Stacked partial view of the  $^1\text{H}$  NMR spectra for  $\beta$ -D-glucose pentaacetate (**1**, top, red spectrum) and  $\alpha$ -D-glucopyranosyl bromide (**2**, bottom, blue spectrum).

#### Synthesis of $\beta$ -D-Glucopyranosyl Azide (**3**)



**Scheme 4.** Synthesis of  $\beta$ -D-glucopyranosyl azide (**3**).

The glucopyranosyl bromide **2** and sodium azide ( $\text{NaN}_3$ ) were reacted in a 5:1 acetone:water solvent mixture, with the water component being necessary to enable dissolution of the  $\text{NaN}_3$ .<sup>41</sup> The reaction mixed overnight, and its completion was demonstrated through TLC as before. The crude glucopyranosyl azide **3** was isolated, dissolved in hot isopropyl alcohol, and allowed to recrystallize before collecting the pure azide **3** (76.8% yield) via vacuum filtration.

Spectroscopic data again point to a single inversion event at the anomeric carbon (**Figure 13**), attributable to the corresponding reversion of the H-1 and H-2 vicinal coupling

constant to that of an equatorial position as predicted by the Karplus curve ( $J = 8.88$  Hz, 4.65 ppm). This is approximately equal to that of the equatorial  $\beta$ -D-glucose pentaacetate (**1**,  $J = 8.28$  Hz, 5.70 ppm), with the slight differences being justified by the different steric and electronic environments created by the anomeric substituents in each compound **1**, **3**.

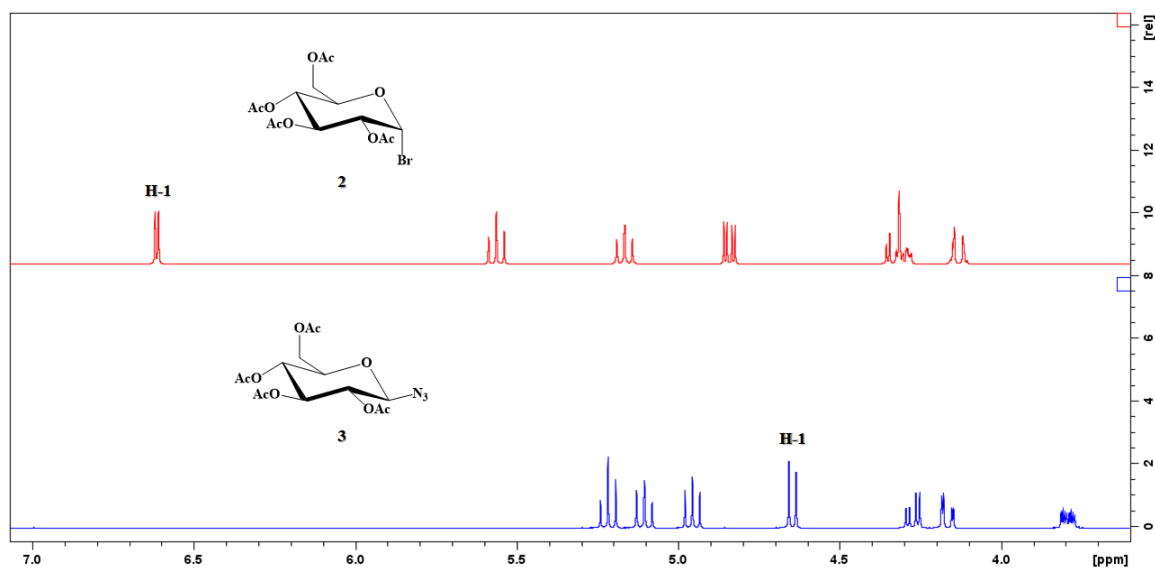
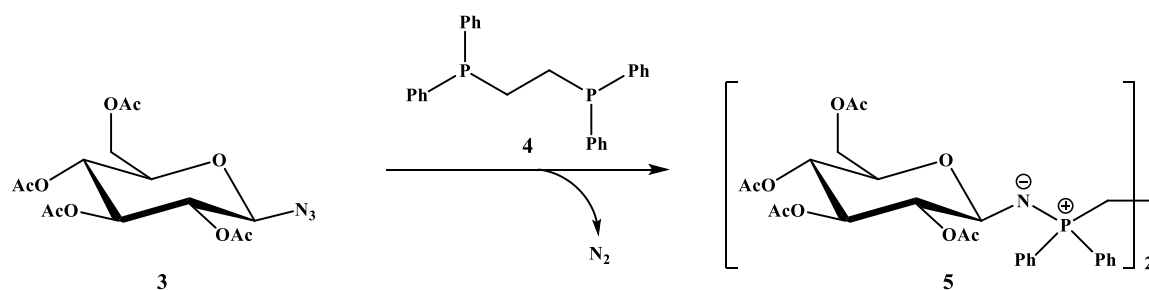


**Figure 13.** Stacked partial view of the  $^1\text{H}$  NMR spectra for  $\alpha$ -D-glucopyranosyl bromide (**2**, top, red spectrum) and  $\beta$ -D-glucopyranosyl azide (**3**, bottom, blue spectrum).

### Synthesis and Isolation of 1,2-Bis(Diphenyl-(2,3,4,6)-Tetra-*O*-Acetyl- $\beta$ -D-Glucopyranosyl-1-*N*-Iminophosphorane) Ethane (**5**)



**Scheme 5.** Synthesis of 1,2-bis(diphenyl-(2,3,4,6)-tetra-*O*-acetyl- $\beta$ -D-glucopyranosyl-1-*N*-iminophosphorane) ethane (**5**).

The glucopyranosyl azide **3** was reacted with DPPE (**4**) in solution to effect the Staudinger reaction, which yielded the bis-aza-ylide **5** (Scheme 5). A vigorous evolution of nitrogen gas was observed (as predicted), lasting approximately 3-5 minutes as evidenced by the effervescence at the surface of the reaction mixture.

Since DPPE has two phosphorus atoms capable of reacting with the azide functional groups, only a half-molar equivalent was used relative to the glucopyranosyl azide **3**. The intention was to: 1.) ensure complete formation of iminophosphorane **5** while minimizing the presence of unreacted starting materials, and 2.) preclude the formation of single-ylide iminophosphorane products which could occur if excess DPPE were to be used. (Note that this eventuality would not hinder the ability of such an iminophosphorane from further reaction with the aldehydes.)

Initial efforts to synthesize the iminophosphorane **5** centered on proper solvent selection. Based on its traditional usage in the literature, tetrahydrofuran (THF) was chosen for the solvent given that it is polar, aprotic, and has a reasonably low boiling point (66 °C). However, removal of the solvent *in vacuo* left a clear syrup rather than the desired solid which could ideally be crystallized for X-ray structure determination.

Chloroform-d (b.p. 61.2 °C) was the next solvent candidate, as it served the dual purpose of being both the reaction facilitator and means by which to monitor reaction progression through NMR. Despite these advantageous characteristics, chloroform-d succumbed to the same fate as THF – formation of a clear syrup.

Dichloromethane (b.p. 39.6 °C) was yet another medium postulated to reliably synthesize the glucopyranosyl bis-ylide **5**. The significantly lower boiling point still could not effectively contribute to the full removal of the solvent by evaporation under reduced pressure, again leaving only a clear syrup.

In all trials, testing the clear syrup by TLC (100:7 dichloromethane:methanol,  $R_f = 0.30$ ) with visualization through 5%  $H_2SO_4$  in ethanol stain indicated formation of the iminophosphorane **5**. The glucopyranosyl azide **3** was susceptible to charring using sulfuric acid

stain visualization, but is not visible under UV light; conversely, DPPE (**4**) is visible by UV light (attributed to the presence of four highly-conjugated phenyl groups), but not by sulfuric acid stain. It was posited that the iminophosphorane **5** – as an amalgamation of these compounds – would exhibit susceptibility to the sulfuric acid stain in addition to visualization by UV light, which indeed was displayed by a single TLC spot (with parallel disappearance of the starting material spots). Moreover, the suspected iminophosphorane **5** spot demonstrated a high degree of polarity, only departing from the baseline when a methanolic solvent system was employed. This would be expected in part based on the polarity of the bis-ylide species, as well as its large inherent mass. (For reference, the glucopyranosyl azide **3** appears in the upper-middle region of the TLC plate, and the nonpolar DPPE (**4**) appearing towards the top.)

Bolstering this assertion that the iminophosphorane **5** had been synthesized, the clear syrup did show NMR spectra that were consistent with the formation of the iminophosphorane, particularly the  $^1\text{H}$  and  $^{31}\text{P}$  acquisitions. Unfortunately, these spectra contained poor signal-to-noise ratios due to the respective solvents still present in the samples (data not shown).

Considering the prospect that a more rapid removal of the solvent might enable formation of a solid product, and given the short timeframe required for completion of the reaction, it was surmised that performing the reaction on a rotary evaporator could simultaneously create these optimal conditions. Thus, stoichiometric quantities of glucopyranosyl azide **3** and DPPE (**4**) were added to a round bottom flask, followed by addition of dichloromethane (4 mL) and immediate placement upon the rotary evaporator at a temperature conducive to rapid evaporation of the solvent. The solvent began to quickly boil off, fortuitously leaving a solid white foam after several minutes. The reaction vessel remained for approximately one hour under vacuum and heat following this in order to ensure a maximal amount of solvent was removed.

The white foam product was analyzed via NMR, through which it was concluded that the iminophosphorane product **5** had successfully formed with only trace levels of impurities. Dissolution in hot isopropyl alcohol proved to be effective among various attempts at

recrystallization. Methanol (60 °C) and ethanol (70 °C) as recrystallization solvents resulted in suspected solvolysis of the iminophosphorane **5**.

### **Spectral and Crystallographic Analysis of 1,2-Bis(Diphenyl-(2,3,4,6)-Tetra-*O*-Acetyl- $\beta$ -D-Glucopyranosyl-1-*N*-Iminophosphorane) Ethane (**5**)**

The H-5 proton was uniquely distinguished as the lone “doublet of doublet of doublets” peak, and thus used as a starting point of reference in mapping the spectra (**Figure 14**). Given that three of the proton peaks had aggregated, and the spectrum was devoid of the erstwhile H-1 doublet, two assumptions were made in assigning NMR peaks: 1.) a lack of stereochemical rearrangement might not drastically alter the order of glucopyranosyl peaks from the antecedent azide **3**, and 2.) heteronuclear coupling of  $^1\text{H}$  and  $^{31}\text{P}$  atoms with respect to the H-1 glucosyl proton and the phosphorus of the ligated DPPE (**4**) would occur, thereby forming a “doublet of doublets” for the H-1 atom in the  $^1\text{H}$  NMR spectra. Taking an iterative approach, both the H-2 and H-4 protons were readily identified. Final assignment of the H-1 and H-3 protons was settled through the  $^{31}\text{P}$ -decoupled proton NMR spectra of the iminophosphorane **5**, wherein the cluster peaks persisted and the insular “doublet of doublets” reverted to a doublet (**Figure 15**), thereby validating the previous assumptions. The acetyl group, ethane linker, and phenyl protons were determined based on known chemical shifts and integration values.

Reinforcing the identity of the iminophosphorane **5**, integration of the  $^1\text{H}$  NMR peaks revealed a 1:2 ratio between the purported protons associated with the DPPE linker and the *N*-linked glucopyranosyl pendant groups, respectively (**Figure 16**).



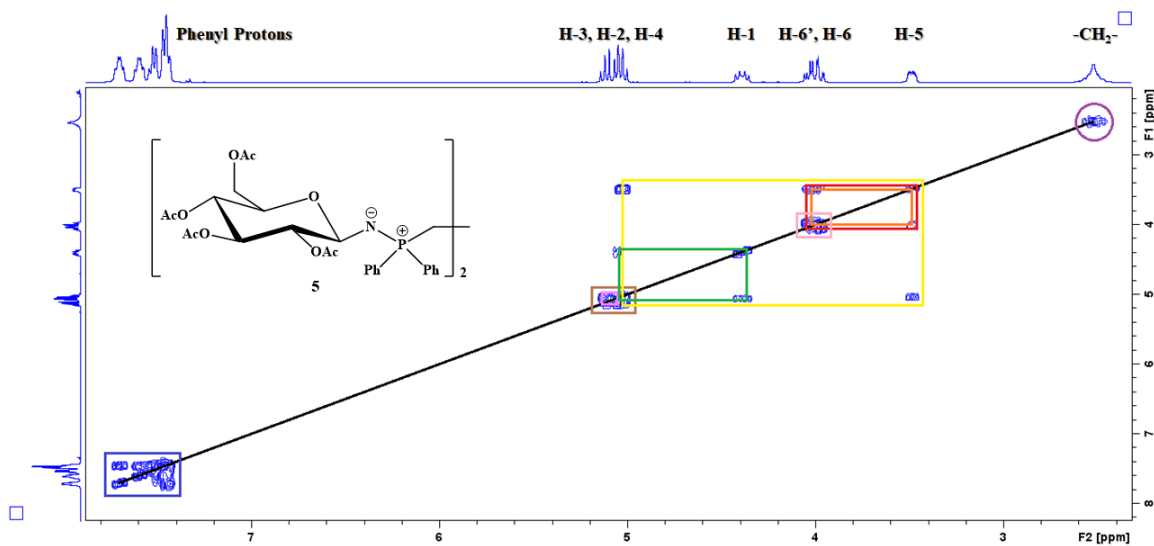


**Figure 14.** COSY spectrum for iminophosphorane **5**.

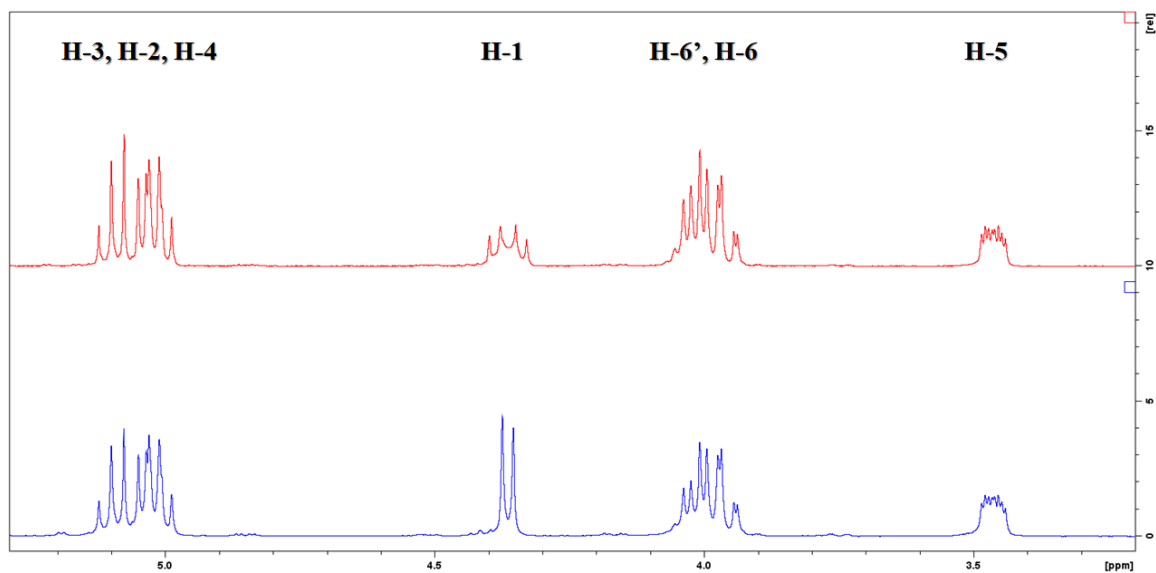


**Figure 15.** Stacked partial view of the  $^1\text{H}$  NMR spectra for iminophosphorane **5** (standard  $^1\text{H}$  spectra, top, red spectrum) and  $\beta$ -D-glucopyranosyl azide (**3**) ( $^1\text{H}$  spectra with  $^{31}\text{P}$  decoupling, bottom, blue spectrum).

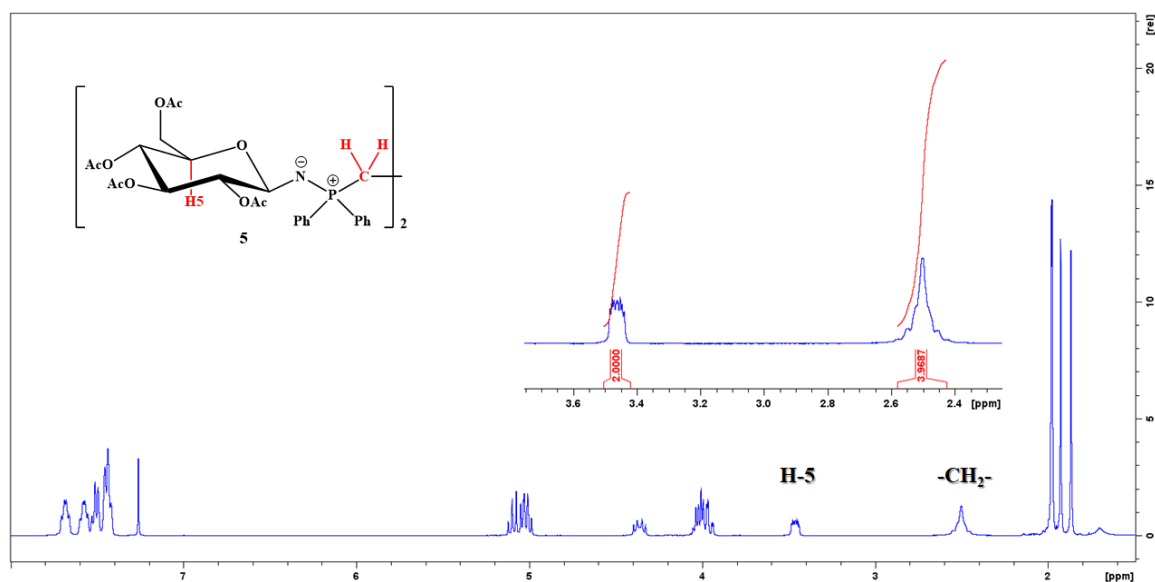


**Figure 16.**  $^1\text{H}$  NMR spectrum of iminophosphorane **5**. Inset shows 1:2 ratio between the H-5 glucopyranosyl proton peak and the ethyl  $-\text{CH}_2-$  proton peak.

In order to confirm that the proton spectra did not simply reflect the presence of both the glucopyranosyl azide **3** and DPPE (**4**), the  $^{31}\text{P}$  NMR was acquired for both DPPE and the hypothesized iminophosphorane **5** (**Figure 17**). Whereas the DPPE (**4**) standard displayed a single peak at  $-12.69$  ppm, the iminophosphorane **5** peak presented itself at  $20.23$  ppm. The downfield shift of the phosphorus peak corroborates the proximity of the phosphorus atom to a more highly electronegative atom – in this case, nitrogen. Furthermore, the manifestation of only a single  $^{31}\text{P}$  NMR peak for the iminophosphorane **5** suggests that only the bis-ylide species was formed. Presumably, any singly-reacted DPPE (**4**) would display a combination of peaks accounting for deshielding of only one phosphorus atom.

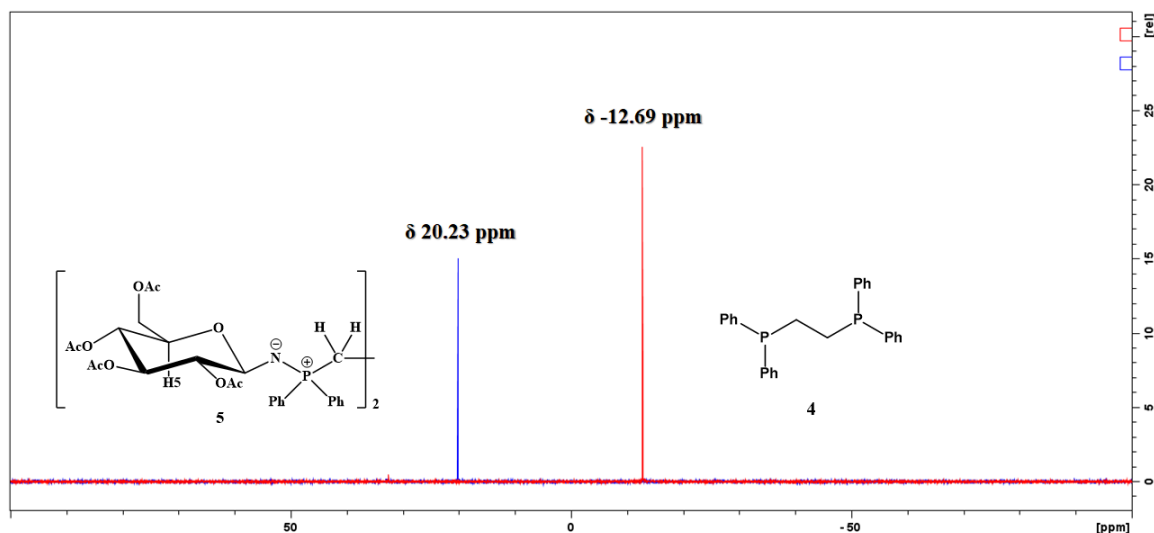


**Figure 17.**  $^{31}\text{P}$  NMR spectra showing DPPE (**4**, red) and iminophosphorane (**5**, blue).

Examination of the crystal structure (**Figure 18**) clearly illustrates the formation of the predicted iminophosphorane **5**: *N*-linked glucopyranosyl moieties joined by a central DPPE (**4**) linker. The crystal structure also shows that both glucopyranosyl sugars were in the thermodynamically favored chair conformation, with their anomeric nitrogens retaining the beta configuration from the glucopyranosyl azide **3** progenitors. Their conjunction with the DPPE (**4**) imbues the iminophosphorane **5** molecule with a  $C_2$  spatial symmetry.

Sundry attempts at complete removal of the isopropyl alcohol (e.g., extended periods on a rotary evaporator, pumping down overnight, Abderhalden drying pistol) proved unsuccessful, and its spectral signature produced  $^1\text{H}$  NMR chemical shifts at 1.23 ppm ( $-\text{CH}_3$ ), 1.30 ppm ( $-\text{OH}$ ), and in conglomeration with the H-6 and H-6' near 4.00 ppm ( $-\text{CH}-$ ). Integration of the former's peaks revealed a 2:1 ratio of isopropyl alcohol to the iminophosphorane **5** (not shown) – yet another detail illuminated by the solved crystal structure. More than occupying space within the crystal structure, each of the two isopropyl alcohol molecules – despite minor disorder being noted – form hydrogen bonds of length 1.99-2.06 Å with the ylide nitrogens. These coordinate with the iminophosphorane **5** in a way that appears to stereochemically stabilize the molecule fostering crystal formation. Such favorability might be lacking in the galactopyranosyl

iminophosphorane **11** due to steric complications encountered by its axially-oriented C-4 acetyl group impeding access to the isopropyl alcohol molecule. This proposition is superficially buttressed by spectroscopic data of the crude galactopyranosyl iminophosphorane **11** (included in the Appendix) showing a less than 1:1 ratio with isopropyl alcohol. It could also be speculated that the slightly higher pKa of isopropyl alcohol might attenuate the chance for solvolysis or hydrolysis.

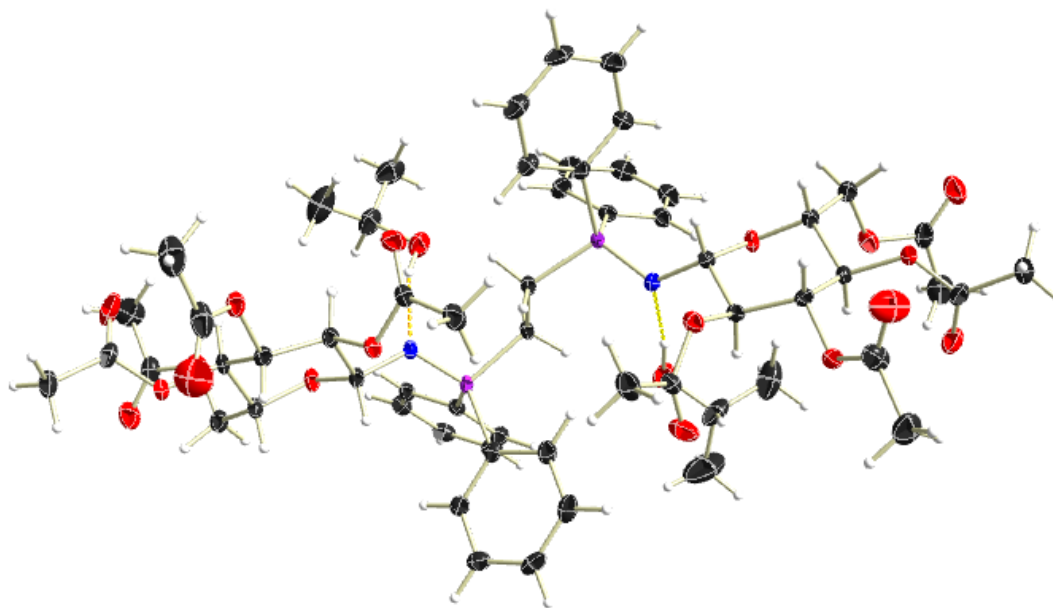
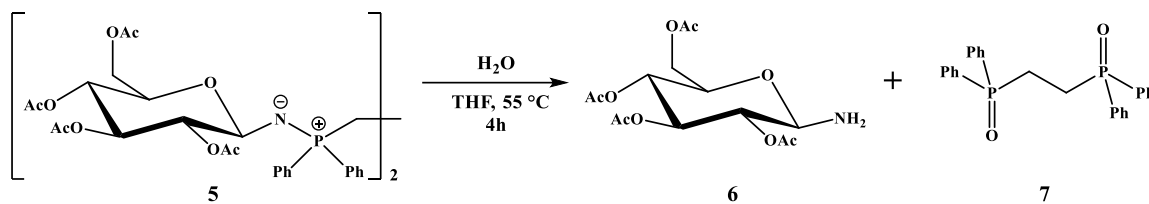


**Figure 18.** X-ray crystal structure of iminophosphorane **5** with 50% probability ellipsoids. Hydrogen bonds are represented by dashed yellow lines.

### Hydrolysis of 1,2-Bis(Diphenyl-(2,3,4,6)-Tetra-*O*-Acetyl- $\beta$ -D-Glucopyranosyl-1-*N*-Iminophosphorane) Ethane (**5**)

Further, indirect testing aimed to establish the identity of iminophosphorane **5** by hydrolyzing it, which was anticipated to produce a glucopyranosyl amine **6** and bis-oxidized DPPE (**7**) as outlined in **Scheme 6**.



**Scheme 6.** Hydrolysis of 1,2-bis(diphenyl-(2,3,4,6)-tetra-*O*-acetyl- $\beta$ -D-glucopyranosyl-1-*N*-iminophosphorane) ethane (**5**).

After conducting the hydrolysis, the  $\beta$ -D-glucopyranosyl amine (**6**) was isolated in 21.7% yield via flash column chromatography, and spectroscopically evaluated. A cursory examination of the <sup>1</sup>H NMR spectra (**Figure 19**) appeared to leave two protons unaccounted for; upon closer inspection, though, two peaks were located upfield adjacent to the acetyl peaks. Originally ascribed to a potential contaminant, each peak individually integrated to one proton (alternatively perceived as a broad singlet integrating to two protons). The COSY spectrum (**Figure 20**) cleanly revealed a homonuclear coupling between the alleged amino protons (a “doublet” at 1.98 ppm) and the H-1 proton (4.19 ppm), whose signal was embedded within the H-6 and H-6’ peaks. Fully deducing all topological connectivities, and giving deference to the Karplus curve and the intrinsic  $J = 8.82$  Hz splitting in the H-1 proton, the glucopyranosyl amine **6** was structurally recreated and plausibly envisioned to preserve the  $\beta$ -configuration. The accuracy of this conjecture was later confirmed by X-ray crystallography, although that data could not be included in this work. Primary literature<sup>42</sup> was later found to substantiate these values, although some discrepancies were noted: only a “broad singlet” chemical shift (2.02-2.10 ppm) was specified for the amino protons as opposed to the clearly resolved “doublet” in this work; also, the H-1 proton was labeled as a “doublet” in the literature, whereas a “doublet of doublets” coupling was observable in the current study. The latter finding also more convincingly offers support for H-1 interaction with the amino protons.

Literature values for the melting point of  $\beta$ -D-glucopyranosyl amine (**6**) were variably reported as 115-116 °C (Esteves, et al.)<sup>42</sup> and 138-140 °C (Kondratenko, et al.)<sup>43</sup>, with the determined range of 121-125 °C in closer agreement with the former.

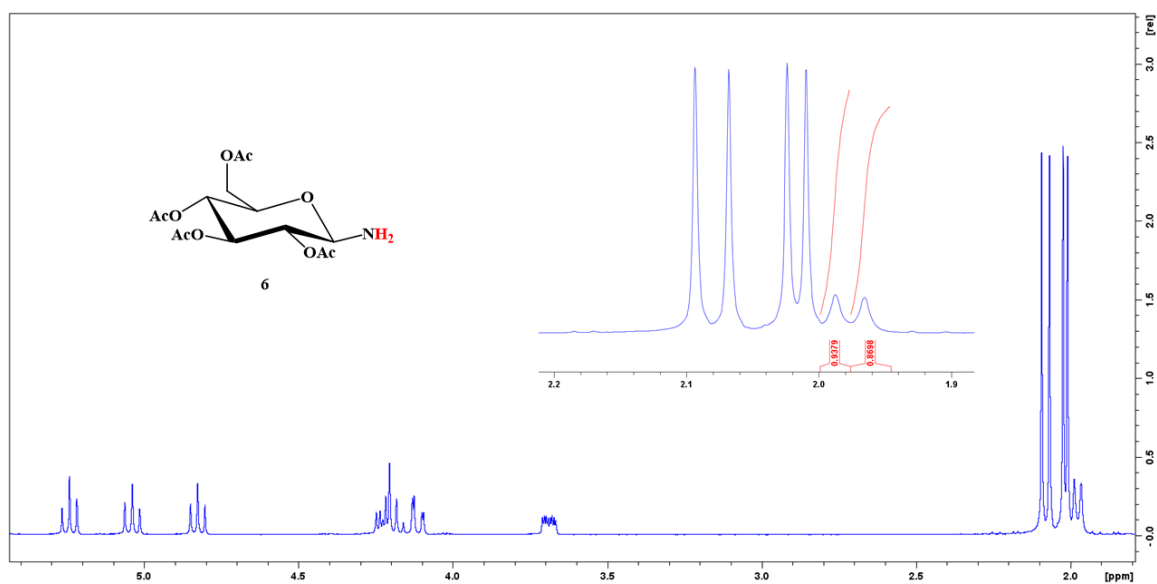


**Figure 19.**  $^1\text{H}$  NMR spectrum for  $\beta$ -D-glucopyranosyl amine (6). Inset shows integration of distinct amine proton peaks.

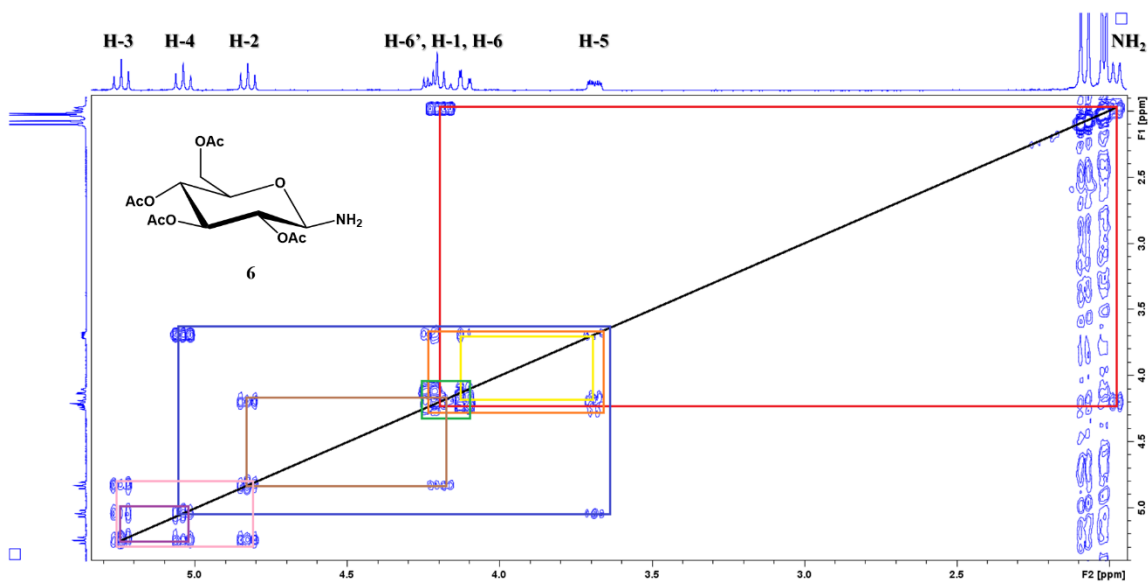


**Figure 20.** COSY spectrum for  $\beta$ -D-glucopyranosyl amine (6).

While the oxidized DPPE product (**7**) was typically noted to have precipitated out in successive imine synthesis reactions, its physical manifestation was absent under these hydrolysis conditions, with the reaction mixture remaining homogeneous. Coincident with the attempted purification of  $\beta$ -D-glucopyranosyl amine (**6**) via flash column chromatography, the oxidized DPPE (**7**) was observed through TLC (100:7 dichloromethane:methanol; UV visualization) to have eluted, and withal being detected by both  $^1\text{H}$  and  $^{31}\text{P}$  NMR. Nevertheless, it was not efficaciously isolated and quantified.

Chromatographically, installation of the oxygen atoms constructed a more polar species, reflected in the translocation of DPPE standard spot toward the baseline from  $R_f = 1.00$  to  $R_f = 0.55$  for the oxidized form (100:7 dichloromethane:methanol). The spectroscopic data gave the clearest support for the generation of the oxidized DPPE (**7**) – a downfield shift of the methylene protons from 2.09 ppm in the DPPE standard\* to 2.52 ppm, as well as phenyl protons of a nearly equal distance. Most telling, though, was the pronounced downfield shift in the  $^{31}\text{P}$  spectra – from a single peak at -12.69 ppm in the DPPE standard to 32.43 ppm upon oxidation (**Figure 21**). The strongly electronegative oxygens confer a deshielding effect, responsible for the downfield shifts in each spectrum.

The isolation and characterization of the  $\beta$ -D-glucopyranosyl amine (**6**) hydrolysis product, combined with the detection and observation of the oxidized DPPE (**7**) products – respectively, both directly and indirectly – strengthened the conclusion that the intermediate iminophosphorane **5** had been synthesized.

---

\* Delost<sup>44</sup> reported a value of 1.5 ppm, while Horn and Sommer<sup>45</sup> supported the value in this work with a chemical shift of 2.1 ppm.

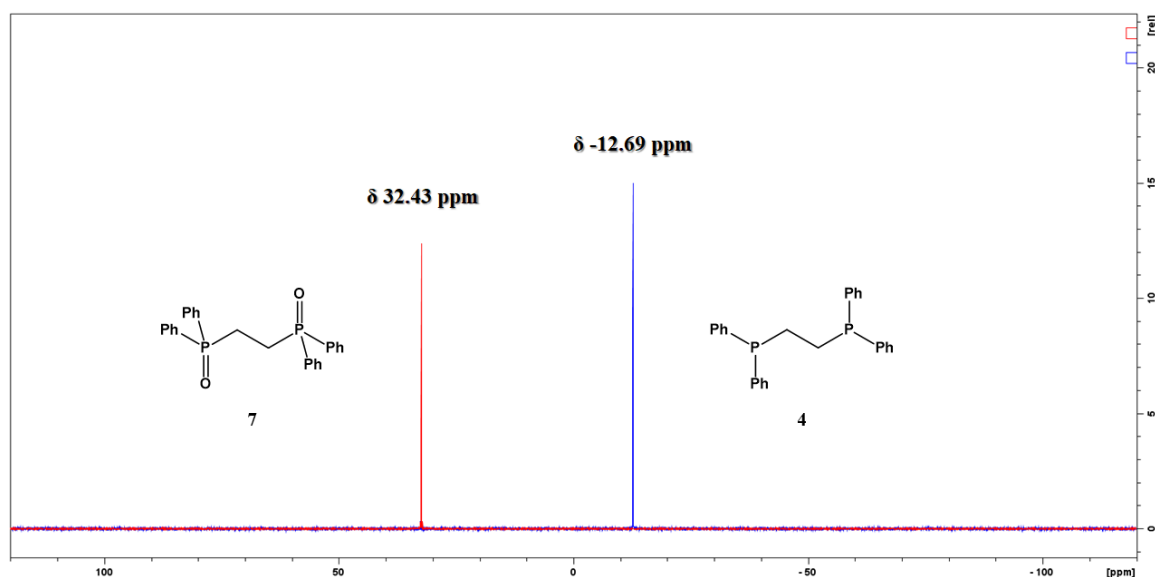
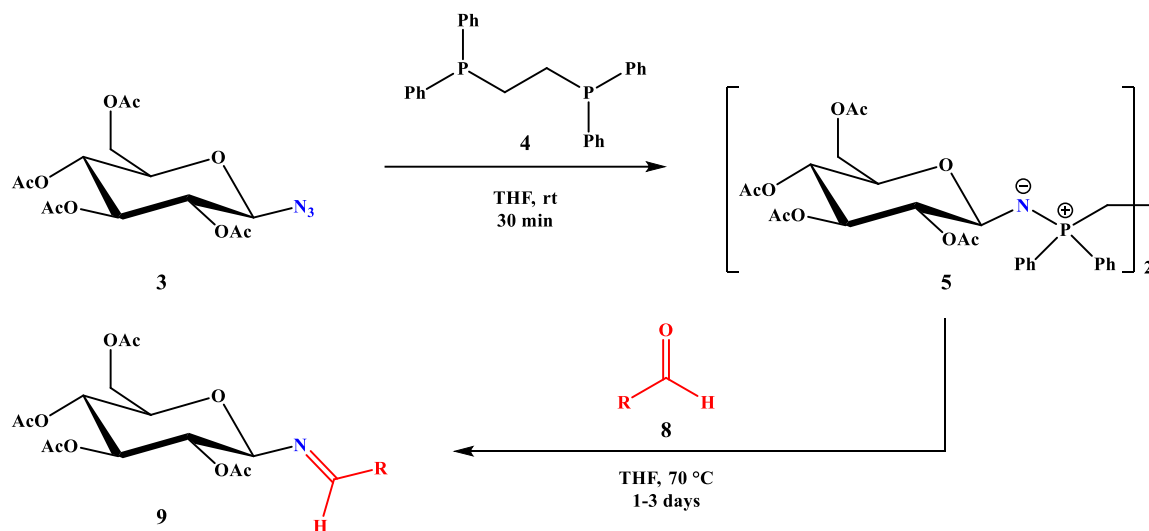


**Figure 21.**  $^{31}\text{P}$  NMR spectra of DPPE (**4**, blue) and oxidized DPPE (**7**, red).

### Synthesis of Imines from $\beta$ -D-Glucopyranosyl Azide (**3**)



**Scheme 7.** Synthesis of glucopyranosyl imines **9**.

The penultimate step in the synthesis of glucopyranosyl amines involved the intermediate formation of their analogous imines. To comprehensively validate the proposed synthetic pathway, it was deemed imperative to isolate the glucopyranosyl imine products. Having previously



synthesized the iminophosphorane **5** via Staudinger reaction of the glucopyranosyl azide **3** with DPPE (**4**), assorted aldehydes were subsequently introduced to the reaction mixture to attain these imine compounds (**Table 1**). Reflux conditions were determined essential to promote the ensuing aza-Wittig reactions.

Relying on the melding of UV-activity by the conjugated aryl substituents and charring from the sulfuric acid stain, TLC provided a crude primary assessment of reaction progress based on the singular presentation of such a spot. Unable to directly recrystallize the glucopyranosyl imines **9** from the crude reaction mixture remaining after evaporation of the THF solvent, flash column chromatography became the conventional recourse for their purification. Difficulties arose at the outset, as only the aldehydes **8** were recovered in small, yet quantifiable amounts. Investigation of this occurrence revealed that the acidity of the silica gel accounted for decomposition of the imines to their principal aldehydes **8** and glucopyranosyl amine **6**. Deactivation of the silica gel by triethylamine in the solvent system obviated this complication, permitting isolation of the intended glucopyranosyl imines **9**.

More definitive authentication was afforded by NMR spectral analysis – specifically, targeting the  $^1\text{H}$  shift of the aldehydic proton from  $\delta$  9.48-11.49 ppm in the aldehydes to  $\delta$  8.44-9.95 ppm in the imines. This justifiably correlates with the substitution of the more electronegative oxygen atom ( $\chi = 3.5$ ) in the former for the moderately less electronegative nitrogen atom ( $\chi = 3.0$ ) in the latter (**Figure 22**). Comparably diminished deshielding effects were seen in the  $^{13}\text{C}$  NMR spectra as well. The COSY and NOESY spectra extended the stereochemical insight by showing correlation between the iminylic proton and the H-1 proton of the glucose subunit (**Figure 23**). For this to occur, the glucopyranosyl imine **9** must adopt the *E*-configuration about the imine C=N bond. This isomer would also be anticipated, as the bulky glucosyl and aryl groups are positioned diametrically opposite to each other, thereby minimizing any steric influences.  $^{31}\text{P}$  NMR exhibited no spectral peaks, denoting that residual DPPE (**4**), iminophosphorane **5**, or oxidized DPPE (**7**) were not present.

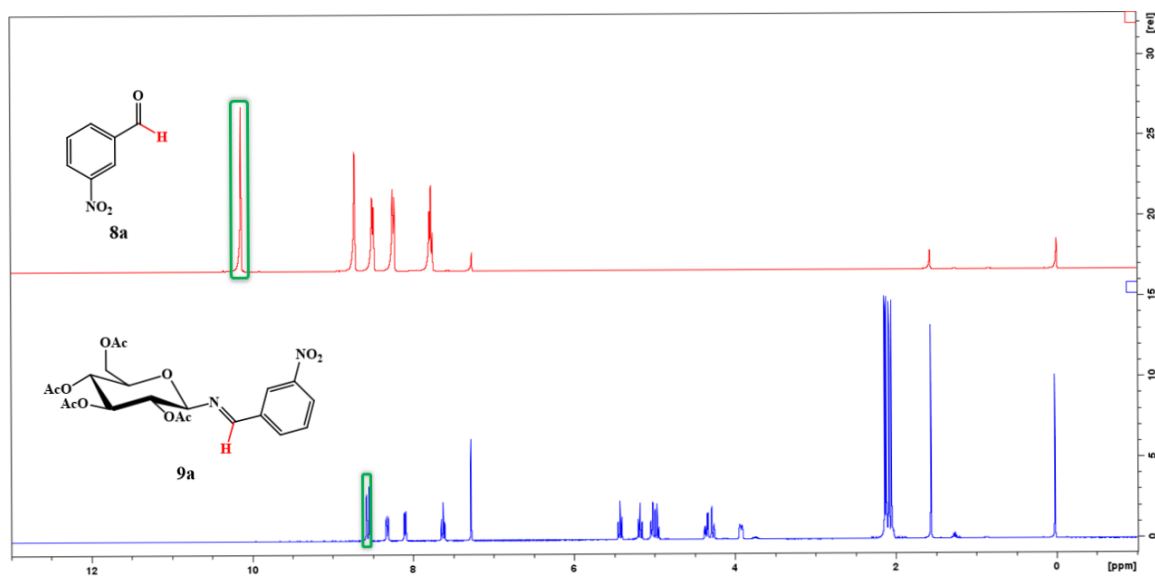


**Figure 22.** Stacked partial view of the <sup>1</sup>H NMR spectra for 3-nitrobenzaldehyde (**8a**, top, red spectrum) and *(E)*-(2,3,4,6)-tetra-*O*-acetyl-β-*D*-glucopyranosyl-1-*N*-3-nitrobenzaldehyde (**9a**, bottom, blue spectrum). The respective aldehydic and iminylic proton peaks are highlighted with green boxes.

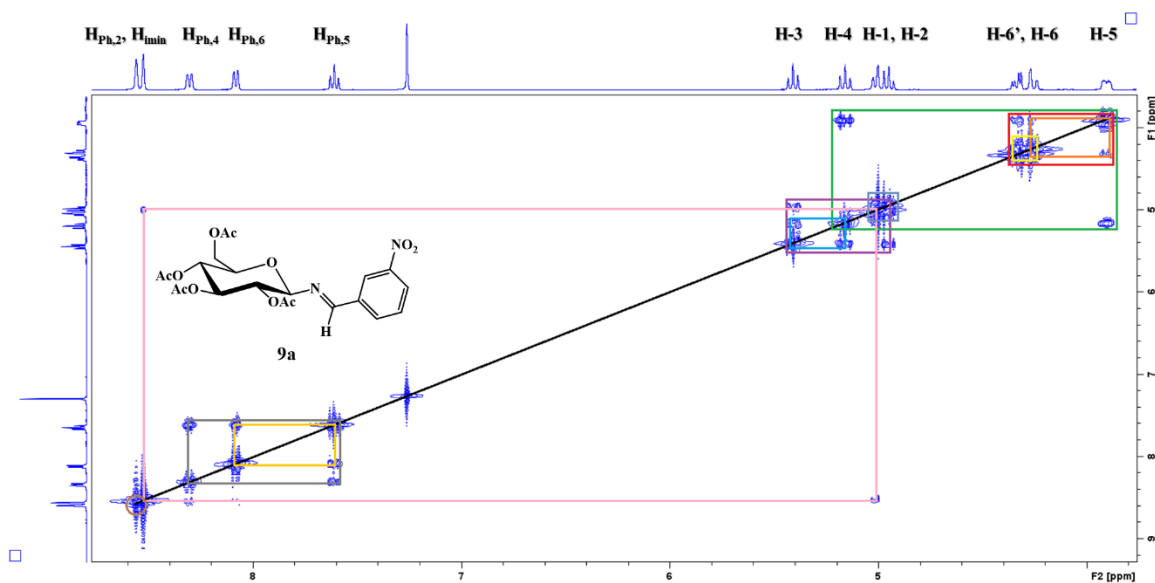
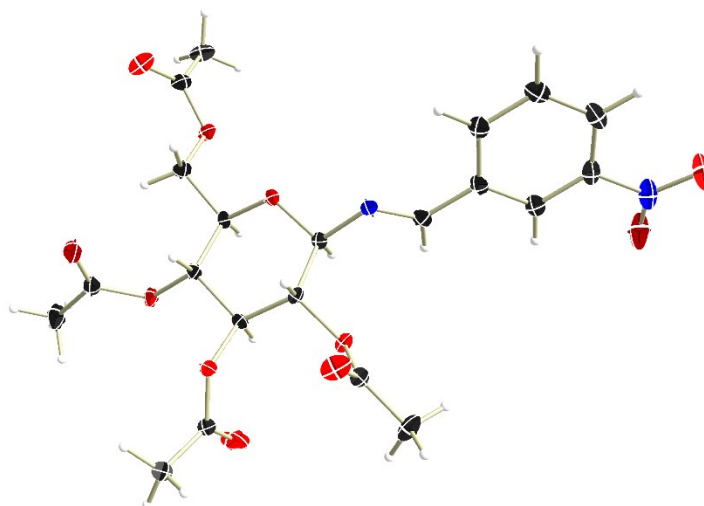


**Figure 23.** COSY spectrum for *(E)*-(2,3,4,6)-tetra-*O*-acetyl-β-*D*-glucopyranosyl-1-*N*-3-nitrobenzaldehyde (**9a**). The pink rectangle indicates the correlation between the H-1 and iminylic protons.

Imine synthesis and exact stereochemistry were only able to be conclusively affirmed by X-ray crystallography for glucopyranosyl imine **9a** (Figure 24); however, based on aforementioned empirical data, it is likely that this stereochemistry is preserved for thermodynamic stability.

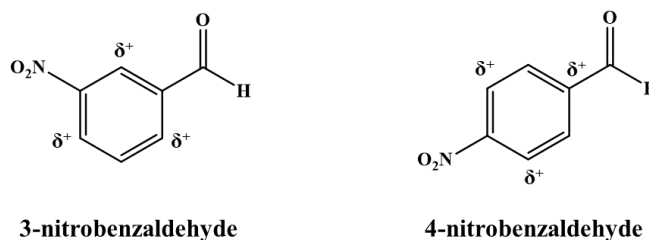
Topologically, the imine is evident from the 1.267 Å carbon-nitrogen bond concatenating the glucopyranosyl and aldehydic constituents, which differs from the 1.451 Å carbon-nitrogen bond emanating from the anomeric position of glucopyranosyl segment. These values are compatible with the literature value of 1.279 Å for C=N bonds and 1.465 Å for C–N bonds, respectively.<sup>46</sup> As with the iminophosphorane intermediate **5**, there is retention of the  $\beta$ -anomeric configuration in the glucopyranosyl moiety. Globally, the imine assumes the *E*-isomer (characterized by a 176.29° torsion angle), with the aryl group adopting an orthogonal orientation relative to the glucopyranose, obviating steric interactions. The anomeric hydrogen is situated proximally to the iminylic proton (2.137 Å), visible as a prominent cross-peak in the COSY and NOESY spectra. Alignment of the nitro group – directed toward the glucosyl plane, rather than away – might be a consequence of crystal packing, but could possibly represent stabilizing dipole minimization within the molecule.

To the extent that the limited sample size of pure glucopyranosyl imines allows, there are preliminary indications – based on percent yields – that aryl substituents actively influence imine formation through their electron withdrawing or donating properties. As a relative standard, unsubstituted benzaldehyde resulted in the lowest yield of its corresponding glucopyranosyl imine **9c** (5.0% yield), marginally improving when the bulkier (three conjoined benzene rings), yet more reactive 9-anthracenecarboxaldehyde was used (24.4% yield). Presence of nitro (-NO<sub>2</sub>) substituents on the benzaldehyde resulted in significantly higher net imine yields, with notable quantitative bias toward 4-nitrobenzaldehyde (57.1% yield) over the 3-nitrobenzaldehyde (43.6% yield) in synthesizing the glucopyranosyl imine derivatives.



**Figure 24.** X-ray crystal structure of glucopyranosyl imine **9a** with 50% probability ellipsoids.

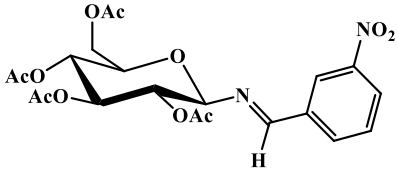
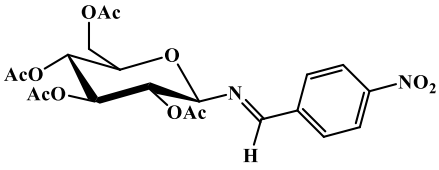
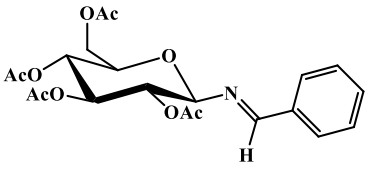
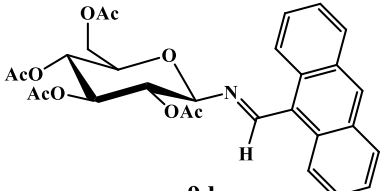
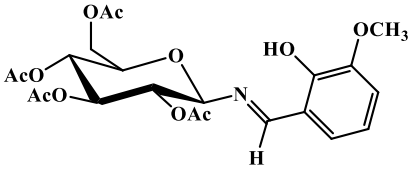
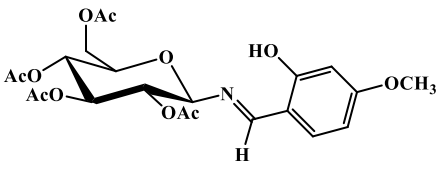
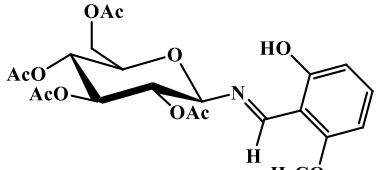
As an electron withdrawing substituent, the location of the nitro functional group engenders a partial positive charge at the *ortho*- and *para*-positions; equivalently, less of a partial positive charge in the *meta*-positions (**Figure 25**). A tenable electronics argument can be advanced then, that, in the case of 3-nitrobenzaldehyde, this drives electron density toward the iminylic carbonyl, thereby reducing the electrophilicity of the carbon and retarding the likelihood of nucleophilic attack by the nitrogen atom of the iminophosphorane **5**; in contrast, 4-nitrobenzaldehyde induces a partial positive charge adjacent to the carbonyl carbon, augmenting its potential as a site for nucleophilic attack.



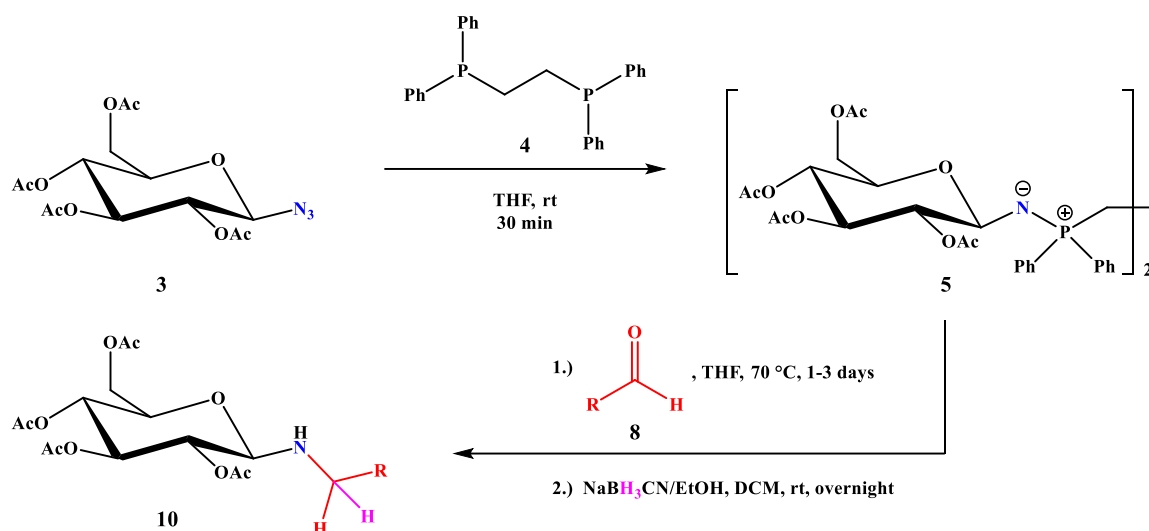
**Figure 25.** Structures of 3-nitrobenzaldehyde and 4-nitrobenzaldehyde showing partial charges due to electron-withdrawing ability of the nitro group.

The viability of this hypothesis is sustained when applied to electron donating groups, such as the hydroxy (-OH) and methoxy (-OCH<sub>3</sub>) dual substituents of the vanillin isomers. For all three molecules, the hydroxy group remains fixed at the 2-position, contributing to the localization of a partial negative charge next to the carbonyl carbon of the aldehyde. When the methoxy group is in the 3-position on the benzene ring, a reduction in partial negative charge develops at that same  $\alpha$ -carbon such that the electron density contributions counteract. (Hydroxy groups are considered stronger activators than methoxy groups, and therefore its partial negative charge may not be fully offset.<sup>47</sup>) The methoxy group in the 4-position and the 6-position each cooperatively concentrate partial negative charges at the  $\alpha$ -carbon, amplifying the electron density and eroding the electrophilicity of the carbonyl carbon. Among this isomeric aldehyde subset, the highest glucopyranosyl imine yield was indeed observed with 2-hydroxy-3-methoxybenzaldehyde (52.2% yield), followed by 2-hydroxy-4-methoxybenzaldehyde (23.5% yield) and 2-hydroxy-6-methoxybenzaldehyde (10.4% yield). *A posteriori* interpretation suggests that the *ortho*-position of the 6-methoxy group relative to the aldehyde substituent is more effective at intensifying the negative charge build-up versus the farther-removed *para*-position of the 4-methoxy group. Additionally, the 6-methoxy group might sterically impede nucleophilic access to the reactive carbonyl carbon, contributing to the lower yield.

**Table 1.** Synthesized glucopyranosyl imines **9** with respective characterizations.

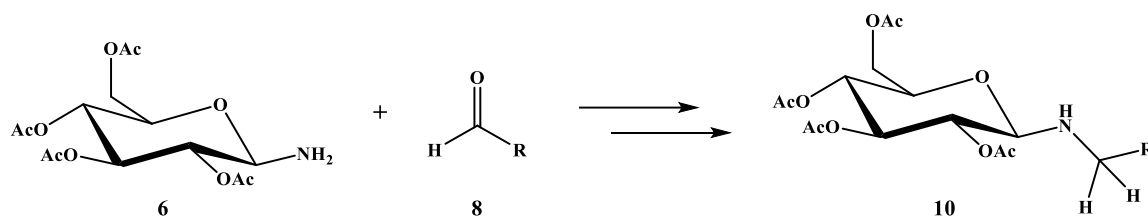
Imine Product	Yield (%)	Melting Point (°C)	Description
 <p><b>9a</b></p>	43.6	145-148	off-white crystals
 <p><b>9b</b></p>	57.1	155-159	yellow-white crystals
 <p><b>9c</b></p>	5.0	166-170	white crystals
 <p><b>9d</b></p>	24.4	163-166	yellow crystals
 <p><b>9e</b></p>	52.2	146-150	yellow-white crystals
 <p><b>9f</b></p>	23.5	145-149	yellow-white crystals
 <p><b>9g</b></p>	10.4	118-120	yellow crystals

### Synthesis of Amines from $\beta$ -D-Glucopyranosyl Azide (3)



**Scheme 8.** Synthesis of glucopyranosyl amines **10**.

Direct synthesis of the amine derivatives was hampered by the overall dearth of glucopyranosyl imine product, although several attempts were conducted. Initially envisioning a “one-pot” synthetic approach, incorporation of an alcohol solvent when using  $\text{NaBH}_3\text{CN}$  under heat risked losing the iminophosphorane **5** through solvolysis or hydrolysis (as previously encountered in crystallization endeavors), and thus was eschewed. (**Scheme 9** outlines how the glucopyranosyl amine **6** hydrolysis product might nevertheless lead to the aldehydic glucosyl amine derivatives **10** without proceeding through the intended aza-Wittig pathway.) Ultimately, the chosen recourse involved first synthesizing the glucopyranosyl imine, collecting the crude product, and finally carrying out the reductive amination. Due to time constraints, however, an optimal synthesis protocol was unable to be defined, and only a single pure glucopyranosyl amine was isolated (**Table 2**).



**Scheme 9.** Alternative synthesis of glucopyranosyl amines **10**.

The 4-nitrobenzaldehyde-derived  $\beta$ -D-glucopyranosyl amine (**10b**) was successfully synthesized and isolated. Despite the paucity of product recovered (6.8% yield), it was still able to be rigorously examined by NMR to conclude its identity. The most salient feature of the  $^1\text{H}$  NMR was the loss of the downfield iminylic proton peak, accounted for by the conversion of the imine carbon to a methylene and loss of its associated electron density (**Figure 26**). As similarly encountered with the hydrolysis product  $\beta$ -D-glucopyranosyl amine (**6**), the amine proton shifted upfield beside those of the acetyl groups. Absent a suitable crystal to analyze absolute stereochemistry, COSY NMR capacitated topological reconstruction of the synthesized amine (**Figure 27**).

**Table 2.** Synthesized glucopyranosyl amines **10** with respective characterizations.

Amine Product	Yield (%)	Melting Point (°C)	Description
<p style="text-align: center;"><b>10b</b></p>	<b>6.8</b>	<b>124-127</b>	<b>white crystals</b>



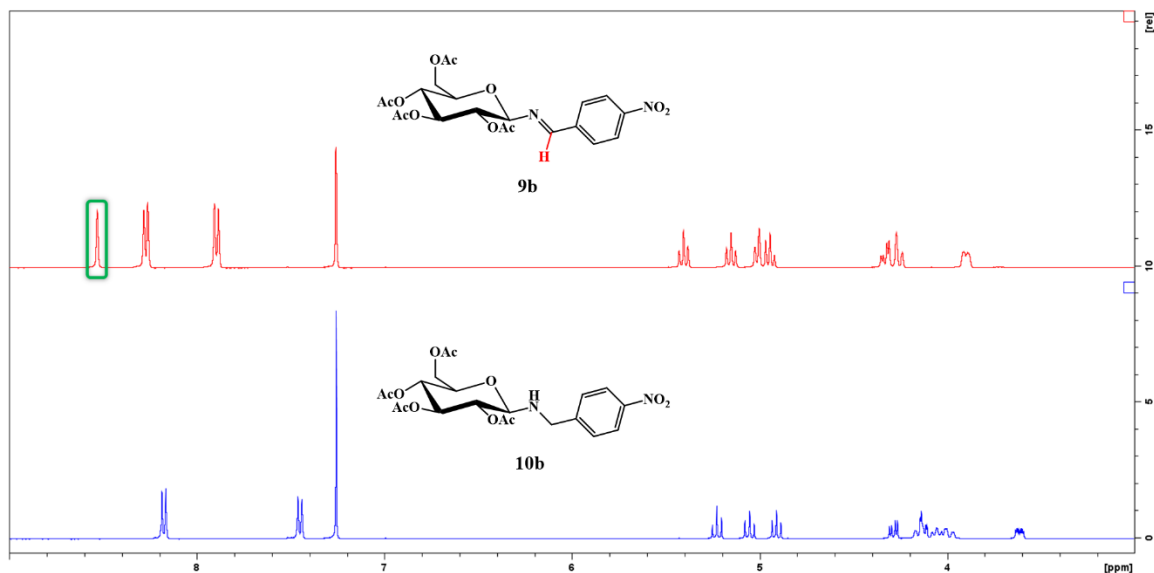


**Figure 26.** Stacked partial view of the <sup>1</sup>H NMR spectra for (*E*)-(2,3,4,6)-tetra-*O*-acetyl-β-D-glucopyranosyl-1-*N*-4-nitrobenzaldimine (**9b**, top, red spectrum) and (2,3,4,6)-tetra-*O*-acetyl-β-D-glucopyranosyl-1-*N*-4-nitrobenzaldamine (**10b**, bottom, blue spectrum). The respective iminylic peak is highlighted with a green box.

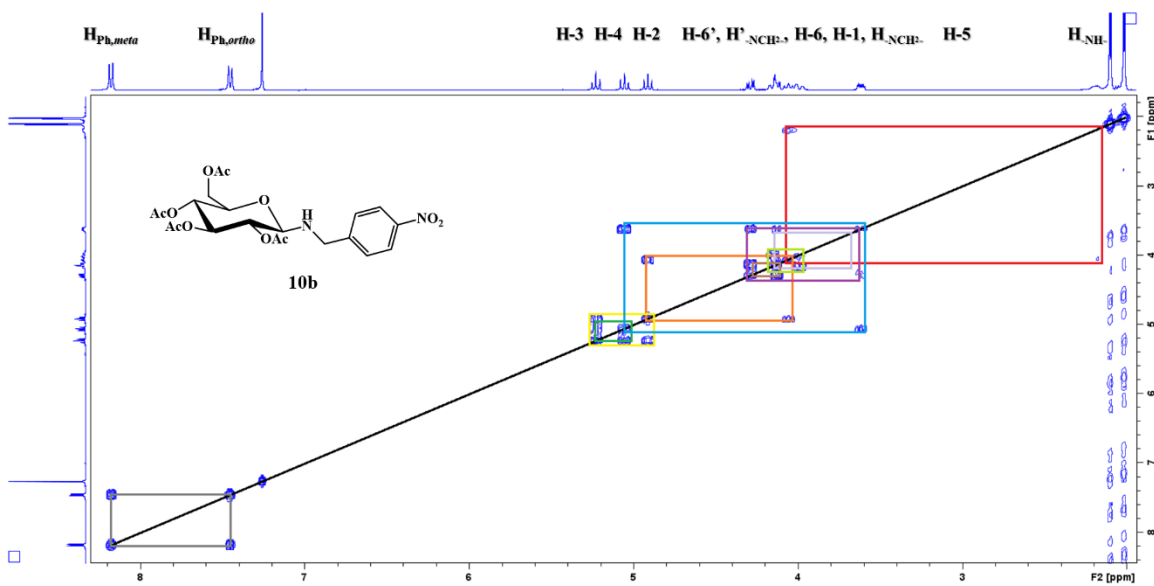


**Figure 27.** COSY spectrum for (2,3,4,6)-tetra-*O*-acetyl-β-D-glucopyranosyl-1-*N*-4-nitrobenzaldamine (**10b**).

### General Analysis of Product Isolation and Yields

One of the major obstacles confronted in this work was the efficient purification and isolation of the glucopyranosyl imines **9**. The acidic silica gel matrix used in flash column chromatography renders imines vulnerable to hydrolysis, decomposing into their component aldehydes and amines. Ergo, prophylactic deactivation of the silica gel and preparation of solvent systems using triethylamine (Et<sub>3</sub>N) became instituted practices. While a broad, qualitative improvement in recovery of glucopyranosyl imine products **9** stemmed from these modifications, the extent of hydrolytic exacerbation by the silica was not definitively established. Two-dimensional TLC of (*E*)-(2,3,4,6)-tetra-*O*-acetyl- $\beta$ -D-glucopyranosyl-1-*N*-3-nitrobenzaldimine (**9a**) on a non-deactivated plate developed with solvent systems free of triethylamine showed no apparent imine decomposition or ancillary spotting. Thus, the effect of silica acid hydrolysis may simply be a secondary effect.

Due to the persistence of aldehydes evidenced by TLC and NMR, recovery of aldehyde precursors was undertaken to ascertain if a significant amount had remained unreacted, detracting from the yields of glucopyranosyl imines **9**. Less than 10% of the starting aldehyde was ever recovered, though, which – although still an appreciable quantity – could not exclusively implicate lack of reactivity as the primary source of restricted yields. Moreover, this finding can neither categorically affirm nor eliminate the complementary prospect that reversion via silica acid hydrolysis noticeably contributed to the aldehyde levels.

As previously alluded to, bis-oxidized DPPE (**7**) – as confirmed by TLC and NMR – precipitated out of the reaction mixture as an off-white solid when attempting to synthesize glucopyranosyl derivatives. This would either settle on top of the sand layer when running a flash column (hexanes:ethyl acetate), or could be removed by gravity filtration prior to concentration of the reaction mixture. Principally, the appearance of this expected by-product objectively sustained the espoused aza-Wittig pathway. Peripherally, quantification of the bis-oxidized DPPE (**7**) offered a rudimentary measure of the reaction progress, with recovered yields greater than 80% relative to

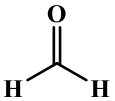
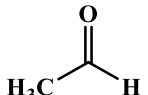
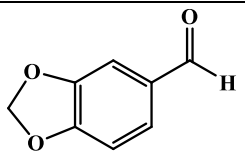
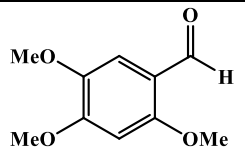
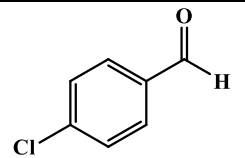
theoretical consumption (over 60% relative to total DPPE (**4**) present in the reaction mixture). Allowing the reaction to continue post-filtration often resulted in further, yet modest formation of the bis-oxidized DPPE (**7**), providing some accord with Le Chatelier's principle. No resolution to the benefit of the filtration was formally enumerated, nor does this distinguish lack of reactivity between iminophosphorane **5** with the aldehyde substrates versus hydrolytic decomposition of the iminophosphorane **5**.

Spectral elements of glucopyranosyl amine **6** are discernable in  $^1\text{H}$  NMR data of the crude reaction mixture, yet exhibit non-detectable levels via TLC or flash column chromatography. This observation does furnish some distinction that hydrolysis is taking place, without directly ascribing it to the acidity of the silica gel. Tentatively, the root of deficient yields seems to reside largely with technique.

### Unsuccessfully Reacted Aldehydes

Other aldehydes (**Table 3**) were utilized when attempting to convert the  $\beta$ -D-glucopyranosyl azide (**4**) into the analogous glucopyranosyl imines, which culminated with no recovered product yields. While NMR spectroscopy demonstrated some small degree of reactivity with each of the aldehydes **8h-l**, none was able to be isolated, even in trace amounts. Formaldehyde (**8h**) – the simplest aldehyde – was available as a 37% solution in water, with 10-15% methanol as a stabilizer to prevent polymerization. In order to avoid unwanted imine product hydrolysis or methanolysis of the iminophosphorane **5** intermediate, this reagent selection was thenceforth abandoned. Acetaldehyde (**8i**) was similarly dispensed with, since its boiling point (20.2 °C) was not amenable to the elevated temperatures generally used to promote the aza-Wittig reaction. Piperonaldehyde (**8j**), 2,4,5-trimethoxybenzaldehyde (**8k**), and 4-chlorobenzaldehyde (**8l**) were also ineffective as aldehyde sources, though the precise basis is unclear.

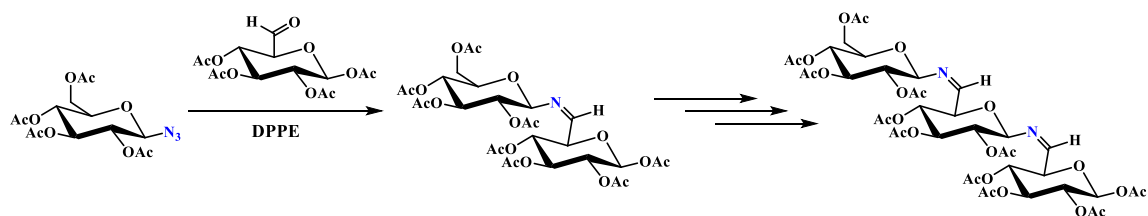
**Table 3.** Aldehydes **8** unsuccessfully reacted to form glucopyranosyl imines **9**.

Aldehyde	Yield (%)
 <b>8h</b>	<b>0.0</b>
 <b>8i</b>	<b>0.0</b>
 <b>8j</b>	<b>0.0</b>
 <b>8k</b>	<b>0.0</b>
 <b>8l</b>	<b>0.0</b>

### Future Work

Future efforts will focus on generating a larger library of compounds – both imines and amines – while concurrently improving product yields. A greater emphasis on the role of electron-withdrawing and electron-donating substituents to augment these reactions would be investigated as well. Of particular interest would be the feasibility of synthesizing glycosidic dimers, trimers,

and polymers effectuated by glucuronic aldehydes (**Scheme 10**). To the end of increasing yields, refinement of technical adroitness would be paramount. Modifications such as including molecular sieves to the reaction mixture might reduce any hydrolytic effects; it might also be worthwhile (in spite of the greater cost) to attempt reverse-phase chromatography for purification to avoid potential acid hydrolysis that can be encountered with standard silica gel. Determining compound structures through X-ray crystallography – possibly of other glycosidic bis-aza-ylide intermediates – will continue to prove crucial for validation and interpretation of synthetic pathways and product purity.



**Scheme 10.** Proposed synthetic pathway of glycosidic polymers.

Regarding the preparation of glucopyranosyl amines, a standardized protocol will be essential for reproducibility and optimization. Ideally, such a paradigm would tolerate “one-pot synthesis” conditions, exploiting the selective reductive amination property of  $\text{NaBH}_3\text{CN}$ .

## Conclusion

The previously observed glucopyranosyl iminophosphorane **5** intermediate of the Staudinger reaction between  $\beta$ -D-glucopyranosyl azide (**3**) and DPPE (**4**) was successfully isolated and characterized by NMR and X-ray crystallography, with preliminary insight gained into its  $\beta$ -D-galactopyranosyl iminophosphorane **11** counterpart.

Several glucopyranosyl imines were subsequently synthesized via aza-Wittig reaction in low to moderate yields utilizing various aldehydes as precursors, with stereochemical confirmation

provided by X-ray crystallography. Provisionally, substituted benzaldehydes have been found to produce greater imine yields when the net effect of the electron-withdrawing or electron-donating groups localized a positive charge adjacent to the aldehydic carbonyl.

Progress has been made in the synthesis of glucopyranosyl amines by way of selective reductive amination using  $\text{NaBH}_3\text{CN}$ , although an accepted protocol was not fully developed.

## Experimental

### General Procedures

All glassware was dried at 100 °C in a Fisher Scientific isotemp oven prior to use. Reactions were monitored on aluminum-backed TLC plates, with ultraviolet (UV) light and 5% (v/v) H<sub>2</sub>SO<sub>4</sub> in ethanol, *p*-anisaldehyde, or ninhydrin stains utilized for visualization of compounds. Purification of compounds was achieved either via flash column chromatography with 32-63 Å silica powder in combination with various solvent systems or through recrystallization. Deactivation of the silica matrix for isolation of the glucopyranosyl imines and amines entailed preparing the wet-packed slurry using a 5% (v/v) triethylamine solvent system solution, followed by flushing the column with 200 mL of the basified solvent system prior to addition of the crude product.

### Instrumentation

NMR spectra were obtained using a Bruker Ultrashield 400 spectrometer in the Chemistry Department at Youngstown State University. Signal peaks are defined as follows: s (singlet), d (doublet), t (triplet), q (quartet), dd (doublet of doublets), ddd (doublet of doublets of doublets), br s (broad singlet), app t (apparent triplet), and m (multiplet). All chemical shifts are reported in parts per million (ppm).

X-ray crystallography data were obtained using either the Bruker AXS X8 Prospector with copper microsource, or the Bruker AXS D8 Quest with molybdenum microsource. These in-house diffractometers are hosted in the X-ray Diffraction Lab at Youngstown State University.

### Materials

All chemical reagents were obtained from Sigma-Aldrich, Alfa Aesar, and Fisher Scientific.

*$\beta$ -D-Glucose pentaacetate (1)*: white powder;  $^1\text{H}$  NMR (400 MHz,  $\text{CDCl}_3$ )  $\delta$  2.00 (s, 3H,  $-\text{C}(\text{O})\text{CH}_3$ ), 2.02 (s, 3H,  $-\text{C}(\text{O})\text{CH}_3$ ), 2.02 (s, 3H,  $-\text{C}(\text{O})\text{CH}_3$ ), 2.08 (s, 3H,  $-\text{C}(\text{O})\text{CH}_3$ ), 2.10 (s, 3H,  $-\text{C}(\text{O})\text{CH}_3$ ), 3.83 (ddd,  $J = 10.02, 4.46, 2.20$  Hz, 1H, H-5), 4.09 (dd,  $J = 12.50, 2.18$  Hz, 1H, H-6'), 4.28 (dd,  $J = 12.52, 4.52$  Hz, 1H, H-6), 5.11 (dd,  $J = 9.70, 9.70$  Hz, 1H, H-4), 5.12 (dd,  $J = 9.44, 8.36$  Hz, 1H, H-2), 5.24 (dd,  $J = 9.40, 9.40$  Hz, 1H, H-3), 5.70 (d,  $J = 8.28$  Hz, 1H, H-1);  $^{13}\text{C}$  NMR (100 MHz,  $\text{CDCl}_3$ )  $\delta$  20.57, 20.72, 20.83, 61.40, 67.68, 70.17, 72.68, 72.75, 91.66, 168.97, 169.25, 169.39, 170.10, 170.61.

*1,2-Bis(diphenylphosphino)ethane (4)*: white powder;  $^1\text{H}$  NMR (400 MHz,  $\text{CDCl}_3$ )  $\delta$  2.09 (t,  $J = 4.00$  Hz, 4H,  $-\text{CH}_2-$ ), 7.27-7.35 (m, 20H, 4 x phenyl protons);  $^{13}\text{C}$  NMR (100 MHz,  $\text{CDCl}_3$ )  $\delta$  23.78 (d,  $J = 3.04$  Hz), 128.44 (t,  $J = 3.37$  Hz), 128.65, 128.51, 132.72 (t,  $J = 9.54$  Hz), 138.03 (dd,  $J = 7.33, 5.85$  Hz);  $^{31}\text{P}$  NMR (161 MHz,  $\text{CDCl}_3$ )  $\delta$  -12.69.

*3-Nitrobenzaldehyde (8a)*: yellow powder;  $^1\text{H}$  NMR (400 MHz,  $\text{CDCl}_3$ )  $\delta$  7.77 (t,  $J = 7.86$  Hz, 1H,  $\text{H}_{\text{Ph-5}}$ ), 8.24 (d,  $J = 7.56$  Hz, 1H,  $\text{H}_{\text{Ph-6}}$ ), 8.50 (d,  $J = 8.08$  Hz, 1H,  $\text{H}_{\text{Ph-4}}$ ), 8.72 (s, 1H,  $\text{H}_{\text{Ph-2}}$ ), 10.13 (s, 1H,  $\text{H}_{\text{ald}}$ );  $^{13}\text{C}$  NMR (100 MHz,  $\text{CDCl}_3$ )  $\delta$  124.47, 128.56, 130.37, 134.57, 137.44, 148.84, 189.64.

*4-Nitrobenzaldehyde (8b)*: yellow powder;  $^1\text{H}$  NMR (400 MHz,  $\text{CDCl}_3$ )  $\delta$  8.07 (d,  $J = 8.64$  Hz, 1H,  $\text{H}_{\text{Ph-2}}$  and  $\text{H}_{\text{Ph-6}}$ ), 8.40 (d,  $J = 8.64$  Hz, 1H,  $\text{H}_{\text{Ph-3}}$  and  $\text{H}_{\text{Ph-5}}$ ), 10.16 (s, 1H,  $\text{H}_{\text{ald}}$ );  $^{13}\text{C}$  NMR (100 MHz,  $\text{CDCl}_3$ )  $\delta$  124.31 (double intensity), 130.46 (double intensity), 140.08, 151.17, 190.19.

*Benzaldehyde (8c)*: clear liquid;  $^1\text{H}$  NMR (400 MHz,  $\text{CDCl}_3$ )  $\delta$  7.43-7.51 (m, 2H, *meta*-CH-), 7.54-7.61 (m, 1H, *para*-CH-), 7.80-7.85 (m, 2H, *ortho*-CH-), 9.97 (s, 1H,  $\text{H}_{\text{ald}}$ );  $^{13}\text{C}$  NMR (100 MHz,  $\text{CDCl}_3$ )  $\delta$  128.99 (double intensity), 129.71 (double intensity), 134.46, 136.37, 192.40.

*9-Anthracenecarboxaldehyde (8d)*: yellow-brown powder;  $^1\text{H}$  NMR (400 MHz,  $\text{CDCl}_3$ )  $\delta$  7.52 (t,  $J = 7.40$  Hz, 2H,  $\text{H}_{\text{anthr-3}}$  and  $\text{H}_{\text{anthr-6}}$ ), 7.66 (t,  $J = 7.60$  Hz, 2H,  $\text{H}_{\text{anthr-2}}$  and  $\text{H}_{\text{anthr-7}}$ ), 8.02 (d,  $J = 8.39$  Hz, 2H,  $\text{H}_{\text{anthr-4}}$  and  $\text{H}_{\text{anthr-5}}$ ), 8.63 (s, 1H,  $\text{H}_{\text{anthr-10}}$ ), 8.95 (d,  $J = 8.92$  Hz, 2H,  $\text{H}_{\text{anthr-1}}$  and  $\text{H}_{\text{anthr-8}}$ ), 11.48 (s, 1H,  $\text{H}_{\text{ald}}$ );  $^{13}\text{C}$  NMR (100 MHz,  $\text{CDCl}_3$ )  $\delta$  123.54 (double intensity), 124.74,



125.67 (double intensity), 129.09 (double intensity), 129.27 (double intensity), 131.08 (double intensity), 132.11 (double intensity), 135.16, 192.93.

*2-Hydroxy-3-methoxybenzaldehyde (8e)*: yellow crystals;  $^1\text{H}$  NMR (400 MHz,  $\text{CDCl}_3$ )  $\delta$  3.91 (s, 3H,  $-\text{OCH}_3$ ), 6.96 (t,  $J = 7.90$  Hz, 1H,  $\text{H}_{\text{Ph-5}}$ ), 7.11 (d,  $J = 7.88$  Hz, 1H,  $\text{H}_{\text{Ph-4}}$ ), 7.18 (d,  $J = 7.84$  Hz, 1H,  $\text{H}_{\text{Ph-6}}$ ), 9.91 (s, 1H  $\text{H}_{\text{ald}}$ ), 11.08 (s, 1H,  $-\text{OH}$ );  $^{13}\text{C}$  NMR (100 MHz,  $\text{CDCl}_3$ )  $\delta$  56.28, 118.01, 119.56, 120.80, 124.52, 148.28, 151.63, 196.58.

*2-Hydroxy-4-methoxybenzaldehyde (8f)*: off-white crystals;  $^1\text{H}$  NMR (400 MHz,  $\text{CDCl}_3$ )  $\delta$  3.86 (s, 3H,  $-\text{OCH}_3$ ), 6.43 (d,  $J = 2.12$  Hz, 1H,  $\text{H}_{\text{Ph-3}}$ ), 6.54 (dd,  $J = 8.64, 2.24$  Hz, 1H,  $\text{H}_{\text{Ph-5}}$ ), 7.42 (d,  $J = 8.64$  Hz, 1H,  $\text{H}_{\text{Ph-6}}$ ), 9.71 (s, 1H,  $\text{H}_{\text{ald}}$ ), 11.47 (s, 1H,  $-\text{OH}$ );  $^{13}\text{C}$  NMR (100 MHz,  $\text{CDCl}_3$ )  $\delta$  55.69, 100.68, 108.37, 115.21, 135.22, 164.55, 166.85, 194.34.

*2-Hydroxy-6-methoxybenzaldehyde (8g)*: yellow crystals;  $^1\text{H}$  NMR (400 MHz,  $\text{CDCl}_3$ )  $\delta$  3.89 (s, 3H,  $-\text{OCH}_3$ ), 6.37 (d,  $J = 8.28$  Hz, 1H,  $\text{H}_{\text{Ph-3}}$ ), 6.52 (d,  $J = 8.48$  Hz, 1H,  $\text{H}_{\text{Ph-5}}$ ), 7.40 (t,  $J = 8.38$  Hz, 1H,  $\text{H}_{\text{Ph-4}}$ ), 10.34 (s, 1H,  $\text{H}_{\text{ald}}$ ), 11.96 (s, 1H,  $-\text{OH}$ );  $^{13}\text{C}$  NMR (100 MHz,  $\text{CDCl}_3$ )  $\delta$  55.81, 100.96, 109.89, 110.88, 138.36, 162.51, 163.67, 194.31.

**$\alpha$ -D-Glucopyranosyl Bromide (2)**. Hydrobromic acid (20 mL, 116 mmol, 33% HBr in AcOH) was added to  $\beta$ -D-glucose pentaacetate (2.50 g, 6.41 mmol) and allowed to react for 30 minutes in an oven-dried 250 mL round-bottom flask fitted with a rubber septum and syringe needle for ventilation. The reaction was monitored for completion using TLC (1:3 hexanes:ethyl acetate,  $R_f = 0.78$ ), with the plate subsequently immersed in 5% (v/v)  $\text{H}_2\text{SO}_4$  in EtOH solution and placed on a hot plate for visualization.

The reaction mixture was then diluted with ethyl acetate (25 mL) and the flask placed in an ice bath where it was allowed to cool to 0 °C before being transferred to a separatory funnel, then carefully neutralized using 10% (w/v) NaOH (70 mL, added in two equal portions) and saturated  $\text{NaHCO}_3$  (7 mL); additionally, periodic venting of evolved carbon dioxide was performed. The organic layer was collected, and the aqueous layer extracted with ethyl acetate

(3 x 25 mL). The organic layers were then combined, dried over anhydrous MgSO<sub>4</sub>, and filtered into a pre-weighed 250 mL round-bottom flask.

The organic solution was placed on a rotary evaporator, where the solvent was removed *in vacuo*, leaving the bromide product **2** as an amber syrup (2.64 g, 100% yield).

The solid  $\alpha$ -D-glucopyranosyl bromide (**2**) can be isolated through placement of the syrup in a freezer overnight to allow the glucosyl bromide **2** to solidify out. Recrystallization with hot (80 °C) ethanol – exercising care to maintain a temperature below the melting point of the pure bromide product **2** (86-89 °C) to avoid decomposition – and subsequent collection via vacuum filtration afforded pure  $\alpha$ -D-glucopyranosyl bromide (**2**) in 85.0% yield. Substitution of dichloromethane for ethyl acetate during extraction markedly enhanced this process.

*$\alpha$ -D-Glucopyranosyl bromide (2)*: white solid; <sup>1</sup>H NMR (400 MHz, CDCl<sub>3</sub>)  $\delta$  2.04 (s, 3H, -C(O)CH<sub>3</sub>), 2.06 (s, 3H, -C(O)CH<sub>3</sub>), 2.10 (s, 3H, -C(O)CH<sub>3</sub>), 2.11 (s, 3H, -C(O)CH<sub>3</sub>), 4.12 (dd,  $J = 12.42, 1.78$  Hz, 1H, H-6'), 4.26-4.36 (m, 2H, H-5 and H-6), 4.84 (dd,  $J = 10.00, 4.04$  Hz, 1H, H-2), 5.16 (dd,  $J = 9.78, 9.78$  Hz, 1H, H-4), 5.55 (dd,  $J = 9.72, 9.72$  Hz, 1H, H-3), 6.61 (d,  $J = 4.04$  Hz, 1H, H-1); <sup>13</sup>C NMR (100 MHz, CDCl<sub>3</sub>)  $\delta$  20.58, 20.65, 20.68, 20.70, 60.93, 67.14, 70.14, 70.59, 72.12, 86.55, 169.49, 169.82, 169.88, 170.54.

**$\beta$ -D-Glucopyranosyl Azide (3)**. NaN<sub>3</sub> (1.95 g, 30.0 mmol) and 70 mL 5:1 acetone:water were added to  $\alpha$ -D-glucopyranosyl bromide (**2**) and allowed to mix with a magnetic stirbar overnight in a round-bottom flask fitted with a rubber septum and aerated via syringe needle. TLC (1:2 hexanes:ethyl acetate, R<sub>f</sub> = 0.69) was used to monitor conversion of compound **2** into the desired azide compound **3**.

Following completion of the reaction, the acetone was removed *in vacuo*, leaving water and a white solid. This was partitioned between water (50 mL) and ethyl acetate (75 mL), ensuring that the white solid was completely dissolved. The organic layer was separated, and the aqueous layer extracted with ethyl acetate (2 x 50 mL). The organic layers were then combined, dried over anhydrous MgSO<sub>4</sub>, and filtered into a pre-weighed 250 mL round-bottom flask.

The ethyl acetate was evaporated under vacuum, leaving a white solid – crude  $\beta$ -D-glucopyranosyl azide. The crude product was then dissolved in a minimal amount of isopropyl alcohol at 90 °C, allowing sufficient time to recrystallize. The pure crystals were finally collected by vacuum filtration (1.84 g, 76.8% yield).

*$\beta$ -D-Glucopyranosyl azide (3)*: clear, white crystals;  $^1\text{H}$  NMR (400 MHz,  $\text{CDCl}_3$ )  $\delta$  2.01 (s, 3H, -C(O)CH<sub>3</sub>), 2.03 (s, 3H, -C(O)CH<sub>3</sub>), 2.08 (s, 3H, -C(O)CH<sub>3</sub>), 2.10 (s, 3H, -C(O)CH<sub>3</sub>), 3.79 (ddd,  $J$  = 10.02, 4.76, 2.30 Hz, 1H, H-5), 4.17 (dd,  $J$  = 12.44, 2.28 Hz, 1H, H-6), 4.27 (dd,  $J$  = 12.48, 4.80 Hz, 1H, H-6'), 4.65 (d,  $J$  = 8.88 Hz, 1H, H-1), 4.96 (dd,  $J$  = 9.22, 9.22 Hz, 1H, H-2), 5.11 (dd,  $J$  = 9.74, 9.74 Hz, 1H, H-4), 5.22 (dd,  $J$  = 9.44, 9.00 Hz, 1H, H-3);  $^{13}\text{C}$  NMR (100 MHz,  $\text{CDCl}_3$ )  $\delta$  20.57 (double intensity), 20.60, 20.73, 61.64, 67.84, 70.60, 72.58, 74.01, 87.92, 169.23, 169.33, 170.15, 170.64.

**1,2-Bis(diphenyl-(2,3,4,6)-Tetra-*O*-Acetyl- $\beta$ -D-Glucopyranosyl-1-*N*-**

**Iminophosphorane) Ethane (5).** *Method 1*:  $\text{CH}_2\text{Cl}_2$  (4 mL) was added to  $\beta$ -D-glucopyranosyl azide (**3**; 0.373g, 1.00 mmol) and DPPE (**4**; 0.199 g, 0.500 mmol) in a 100 mL round-bottom flask under agitation on a rotary evaporator with hot water bath at 40 °C. The crude iminophosphorane **5** was subsequently dissolved in a minimal amount of hot (90 °C) isopropyl alcohol and allowed to recrystallize overnight. The pure crystals were collected via vacuum filtration (0.556 g, 0.511 mmol; 102.2% yield). *Method 2*:  $\beta$ -D-glucopyranosyl azide (**3**; 0.373 g, 1.00 mmol) and DPPE (**4**; 0.199 g, 0.500 mmol) were added to a 100 mL round-bottom flask, to which approximately 4 mL of hot (90 °C) isopropyl alcohol was added until both starting compounds were dissolved. The pure iminophosphorane product **5** crystallized out overnight, and was collected by vacuum filtration (0.573 g, 0.526 mmol; 105.4% yield). The appearance of a spot via TLC (100:7 dichloromethane:methanol,  $R_f$  = 0.30) indicated formation of compound **5**.

**$\beta$ -D-Glucopyranosyl Amine (6).**  $\beta$ -D-glucopyranosyl azide (**3**; 0.373 g, 1.00 mmol) and DPPE (**4**; 0.199 g, 0.500 mmol) dissolved in THF (5 mL) were reacted in a 100 mL round-bottom flask equipped with a magnetic stirbar and rubber septum to generate

iminophosphorane **5** over a 30 minute time period. Deionized water (2 mL) was subsequently added, and the reaction allowed to proceed for 4-5 hours at 55 °C. The reaction mixture was partitioned between dichloromethane (40 mL) and water (40 mL), and the aqueous layer removed. The organic layer was subsequently extracted with water (2 x 40 mL), dried over anhydrous MgSO<sub>4</sub>, and filtered into a pre-weighed 100 mL round-bottom flask before being concentrated under reduced pressure.

Formation of the glucopyranosyl amine **6** was observed by TLC (100:7 dichloromethane:methanol, R<sub>f</sub> = 0.45), and isolation was facilitated via flash column (100:7 dichloromethane:methanol). After removal of the solvent *in vacuo*, the amine product was recrystallized in hot (90 °C) isopropyl alcohol and collected through vacuum filtration (0.075 g, 21.7% yield).

*β-D-Glucopyranosyl amine (6)*: white crystals; <sup>1</sup>H NMR (400 MHz, CDCl<sub>3</sub>) δ 1.98 (d, *J* = 8.80 Hz, 2H, -NH<sub>2</sub>), 2.01 (s, 3H, -C(O)CH<sub>3</sub>), 2.02 (s, 3H, -C(O)CH<sub>3</sub>), 2.07 (s, 3H, -C(O)CH<sub>3</sub>), 2.09 (s, 3H, -C(O)CH<sub>3</sub>), 3.69 (ddd, *J* = 10.04, 4.80, 2.32 Hz, 1H, H-5), 4.11 (dd, *J* = 12.26, 2.26 Hz, 1H, H-6), 4.19 (q, *J* = 8.96 Hz, H-1), 4.23 (dd, *J* = 12.36, 4.92 Hz, H-6'), 4.83 (dd, *J* = 9.38, 9.38 Hz, 1H, H-4), 5.04 (dd, *J* = 9.70, 9.70 Hz, 1H, H-2), 5.24 (dd, *J* = 9.52, 9.52 Hz, 1H, H-3); <sup>13</sup>C NMR (100 MHz, CDCl<sub>3</sub>) δ 20.64, 20.66, 20.81, 20.83, 62.29, 68.77, 72.04, 72.74, 73.16, 85.02, 169.59, 170.20, 170.22, 170.72. Melting point: 121-125 °C. (lit. 115-116 °C<sup>42</sup>; 138-140 °C<sup>43</sup>)

**1,2-Ethanediybis(diphenylphosphine) dioxide (7)**. This compound is a predicted hydrolysis product, which, although unable to isolate via flash column chromatography, was able to be synthesized as a solvolysis product of glucopyranosyl iminophosphorane **5** from hot (70-80 °C) ethanol (38.7% yield) or methanol (34.7% yield). The oxidized DPPE was also found to form as a precipitate in the reaction vessels, which could be removed through gravity filtration (81.0% yield based on stoichiometric calculations; 61.5% yield based on total quantity of DPPE added), or would settle on top of the sand layer when performing flash column chromatography.

Detection of its formation during reactions was also noted via TLC (1:1 hexanes:ethyl acetate,  $R_f = 0.14$ ).

**(E)-(2,3,4,6)-Tetra-O-Acetyl- $\beta$ -D-Glucopyranosyl-1-N-3-Nitrobenzaldimine (9a).** To a 100 mL round-bottom flask equipped with magnetic stirbar and reflux condenser,  $\beta$ -D-glucopyranosyl azide (**3**; 0.373 g, 1.00 mmol) and DPPE (**4**; 0.259 g, 0.650 mmol) were reacted in THF (5 mL) at ambient temperature for 30 minutes to first generate the iminophosphorane **5**. 3-Nitrobenzaldehyde (**8a**; 0.151 g, 1.00 mmol), having been dissolved in THF (3 mL), was subsequently added dropwise to the reaction mixture, at which time the reaction mixture was heated to 70 °C and allowed to proceed overnight. Formation of the imine **9a** was observed via TLC (1:1 hexanes:ethyl acetate,  $R_f = 0.51$ ). The crude reaction mixture was concentrated under vacuum, and purified by flash column chromatography (1:1 hexanes:ethyl acetate, 3% triethylamine). The isolated product was recrystallized in hot (80 °C) ethanol, and the pure crystals collected via vacuum filtration (0.136 g, 43.6% yield).

**(E)-(2,3,4,6)-Tetra-O-acetyl- $\beta$ -D-glucopyranosyl-1-N-3-nitrobenzaldimine (9a):** off-white crystals;  $^1\text{H}$  NMR (400 MHz,  $\text{CDCl}_3$ )  $\delta$  2.03 (s, 3H,  $-\text{C}(\text{O})\text{CH}_3$ ), 2.06 (s, 3H,  $-\text{C}(\text{O})\text{CH}_3$ ), 2.09 (s, 3H,  $-\text{C}(\text{O})\text{CH}_3$ ), 2.11 (s, 3H,  $-\text{C}(\text{O})\text{CH}_3$ ), 3.90 (ddd,  $J = 10.03, 4.59, 2.21$  Hz, 1H, H-5), 4.25 (dd,  $J = 12.38, 2.02$  Hz, 1H, H-6), 4.33 (dd,  $J = 12.42, 4.78$  Hz, 1H, H-6'), 4.95 (dd,  $J = 9.22, 9.22$  Hz, 1H, H-2), 5.01 (dd,  $J = 9.10, 1.46$  Hz, 1H, H-1), 5.16 (dd,  $J = 9.74, 9.74$  Hz, 1H, H-4), 5.41 (dd,  $J = 9.38, 9.38$  Hz, 1H, H-3), 7.61 (dd,  $J = 7.92, 7.92$  Hz, 1H,  $\text{H}_{\text{Ph-5}}$ ), 8.08 (d,  $J = 7.68$  Hz, 1H,  $\text{H}_{\text{Ph-6}}$ ), 8.30 (d,  $J = 8.45$  Hz, 1H,  $\text{H}_{\text{Ph-4}}$ ), 8.52 (d,  $J = 1.36$  Hz, 1H,  $\text{H}_{\text{imin}}$ ), 8.56 (s, 1H,  $\text{H}_{\text{Ph-2}}$ );  $^{13}\text{C}$  NMR (100 MHz,  $\text{CDCl}_3$ )  $\delta$  20.59, 20.63, 20.71, 20.77, 62.03, 68.51, 72.09, 73.32, 73.97, 91.29, 123.53, 125.83, 129.75, 133.97, 137.06, 148.63, 157.97, 169.37, 169.43, 170.26, 170.65. Melting point: 145-148 °C.

**(E)-(2,3,4,6)-Tetra-O-Acetyl- $\beta$ -D-Glucopyranosyl-1-N-4-Nitrobenzaldimine (9b).** To a 100 mL round-bottom flask equipped with magnetic stirbar and reflux condenser,  $\beta$ -D-glucopyranosyl azide (**3**; 0.373 g, 1.00 mmol) and DPPE (**4**; 0.259 g, 0.650 mmol) were reacted in

THF (5 mL) at ambient temperature for 30 minutes to first generate the iminophosphorane **5**. 4-Nitrobenzaldehyde (**8b**; 0.151 g, 1.00 mmol), having been dissolved in THF (3 mL), was subsequently added dropwise to the reaction mixture, at which time the reaction mixture was heated to 70 °C and allowed to proceed overnight. Formation of the imine **9b** was observed via TLC (1:1 hexanes:ethyl acetate,  $R_f$ = 0.41). The crude reaction mixture was concentrated under vacuum, and purified by flash column chromatography (2:1 hexanes:ethyl acetate, 3% triethylamine). The isolated product was recrystallized in hot (80 °C) ethanol, and the pure crystals collected via vacuum filtration (0.275 g, 57.1% yield).

*(E)*-(2,3,4,6)-Tetra-*O*-acetyl- $\beta$ -D-glucopyranosyl-1-*N*-4-nitrobenzaldimine (**9b**): yellow-white crystals;  $^1\text{H}$  NMR (400 MHz,  $\text{CDCl}_3$ )  $\delta$  2.03 (s, 3H, -C(O)CH<sub>3</sub>), 2.06 (s, 3H, -C(O)CH<sub>3</sub>), 2.08 (s, 3H, -C(O)CH<sub>3</sub>), 2.11 (s, 3H, -C(O)CH<sub>3</sub>), 3.90 (ddd,  $J$  = 10.04, 4.60, 2.30 Hz, 1H, H-5), 4.26 (dd,  $J$  = 12.38, 2.14 Hz, 1H, H-6), 4.33 (dd,  $J$  = 12.40, 4.72 Hz, 1H, H-6'), 4.95 (dd,  $J$  = 9.26, 9.26 Hz, 1H, H-2), 5.02 (dd,  $J$  = 9.08, 1.64 Hz, 1H, H-1), 5.15 (dd,  $J$  = 9.74, 9.74 Hz, 1H, H-4), 5.41 (dd,  $J$  = 9.40, 9.40 Hz, 1H, H-3), 7.89 (d,  $J$  = 8.64 Hz, 2H, H<sub>Ph</sub>-2 and H<sub>Ph</sub>-6), 8.27 (d,  $J$  = 8.64 Hz, 2H, H<sub>Ph</sub>-3 and H<sub>Ph</sub>-5), 8.53 (d,  $J$  = 1.44 Hz, 1H, H<sub>imin</sub>);  $^{13}\text{C}$  NMR (100 MHz,  $\text{CDCl}_3$ )  $\delta$  20.59, 20.62, 20.70, 20.76, 62.01, 68.49, 72.05, 73.31, 73.97, 91.35, 123.91 (double intensity), 129.39 (double intensity), 140.74, 149.58, 158.24, 169.28, 169.42, 170.25, 170.63. Melting point: 155-159 °C.

*(E)*-(2,3,4,6)-Tetra-*O*-Acetyl- $\beta$ -D-Glucopyranosyl-1-*N*-Benzaldimine (**9c**). To a 100 mL round-bottom flask equipped with magnetic stirbar and reflux condenser,  $\beta$ -D-glucopyranosyl azide (**3**; 0.373 g, 1.00 mmol) and DPPE (**4**; 0.259 g, 0.650 mmol) were reacted in THF (5 mL) at ambient temperature for 30 minutes to first generate the iminophosphorane **5**. Benzaldehyde (**8c**; 0.10 mL, 0.98 mmol), having been dissolved in THF (3 mL), was subsequently added dropwise to the reaction mixture, at which time the reaction mixture was heated to 70 °C and allowed to proceed overnight. Formation of the imine **9c** was observed via TLC (1:1 hexanes:ethyl acetate,  $R_f$ = 0.46). The crude reaction mixture was concentrated under vacuum, and purified by flash column

chromatography (1:1 hexanes:ethyl acetate, 3% triethylamine). The isolated product was recrystallized in hot (80 °C) ethanol, and the pure crystals collected via vacuum filtration (0.0213 g, 5.0% yield).

*(E)*-(2,3,4,6)-Tetra-*O*-acetyl- $\beta$ -D-glucopyranosyl-1-*N*-benzaldimine (**9c**): white crystals;  $^1\text{H}$  NMR (400 MHz,  $\text{CDCl}_3$ )  $\delta$  2.01 (s, 3H, -C(O)CH<sub>3</sub>), 2.02 (s, 3H, -C(O)CH<sub>3</sub>), 2.05 (s, 3H, -C(O)CH<sub>3</sub>), 2.10 (s, 3H, -C(O)CH<sub>3</sub>), 3.89 (ddd,  $J = 10.01, 4.72, 2.33$  Hz, 1H, H-5), 4.23 (dd,  $J = 12.32, 2.20$  Hz, 1H, H-6), 4.32 (dd,  $J = 12.32, 4.84$  Hz, 1H, H-6'), 4.85 (dd,  $J = 8.88, 1.12$  Hz, 1H, H-1), 5.02 (dd,  $J = 9.24, 9.24$  Hz, 1H, H-2), 5.18 (dd,  $J = 9.72, 9.72$  Hz, 1H, H-4), 5.37 (t,  $J = 9.50, 9.50$  Hz, 1H, H-3), 7.38-7.49 (m, 3H, H<sub>Ph</sub>-3, H<sub>Ph</sub>-4, and H<sub>Ph</sub>-5), 7.74 (dd,  $J = 8.12, 1.32$  Hz, 2H, H<sub>Ph</sub>-2 and H<sub>Ph</sub>-6), 8.42 (d,  $J = 1.08$  Hz, 1H, H<sub>imin</sub>);  $^{13}\text{C}$  NMR (100 MHz,  $\text{CDCl}_3$ )  $\delta$  20.61, 20.63, 20.65, 20.77, 62.20, 68.62, 72.08, 73.50, 73.82, 93.21, 128.66 (double intensity), 128.84 (double intensity), 131.68, 135.22, 161.80, 169.14, 169.42, 170.37, 170.73. Melting point: 166-170 °C (lit. 162-163 °C<sup>48</sup> and 164-165 °C<sup>49</sup>).

***(E)*-(2,3,4,6)-Tetra-*O*-Acetyl- $\beta$ -D-Glucopyranosyl-1-*N*-9-Anthracenecarboxaldimine (**9d**)**. To a 100 mL round-bottom flask equipped with magnetic stirbar and reflux condenser,  $\beta$ -D-glucopyranosyl azide (**3**; 0.373 g, 1.00 mmol) and DPPE (**4**; 0.259 g, 0.650 mmol) were reacted in THF (5 mL) at ambient temperature for 30 minutes to first generate the iminophosphorane **5**. 9-Anthracenecarboxaldehyde (**8d**; 0.206 g, 1.00 mmol), having been dissolved in THF (3 mL), was subsequently added dropwise to the reaction mixture, at which time the reaction mixture was heated to 70 °C and allowed to proceed overnight. Formation of the imine **9d** was observed via TLC (1:1 hexanes:ethyl acetate,  $R_f = 0.41$ ). The crude reaction mixture was concentrated under vacuum, and purified by flash column chromatography (2:1 hexanes:ethyl acetate, 3% triethylamine). The isolated product was recrystallized in hot (80 °C) ethanol, and the pure crystals collected via vacuum filtration (0.131 g, 24.4% yield).

*(E)*-(2,3,4,6)-Tetra-*O*-acetyl- $\beta$ -D-glucopyranosyl-1-*N*-9-anthracenecarboxaldimine (**9d**): yellow crystals;  $^1\text{H}$  NMR (400 MHz,  $\text{CDCl}_3$ )  $\delta$  2.02 (s, 3H, -C(O)CH<sub>3</sub>), 2.06 (s, 3H, -C(O)CH<sub>3</sub>),

2.09 (s, 3H, -C(O)CH<sub>3</sub>), 2.13 (s, 3H, -C(O)CH<sub>3</sub>), 4.02 (ddd,  $J = 10.05, 4.69$  Hz, 2.47, 1H, H-5), 4.33 (dd,  $J = 12.36, 2.40$  Hz, 1H, H-6), 4.42 (dd,  $J = 12.38, 4.78$  Hz, 1H, H-6'), 5.18 (dd,  $J = 9.00, 1.56$  Hz, 1H, H-1), 5.30 (dd,  $J = 9.26, 9.26$  Hz, 1H, H-2), 5.32 (dd,  $J = 9.12, 9.12$  Hz, 1H, H-4), 5.47 (dd,  $J = 9.42, 9.42$  Hz, 1H, H-3), 7.46-7.52 (m, 2H, H<sub>anthr-3</sub> and H<sub>anthr-6</sub>), 7.52-7.59 (m, 2H, H<sub>anthr-2</sub> and H<sub>anthr-7</sub>), 8.02 (d,  $J = 8.28$  Hz, 2H, H<sub>anthr-4</sub> and H<sub>anthr-5</sub>), 8.53 (s, 1H, H<sub>anthr-10</sub>), 8.57 (d,  $J = 8.92$  Hz, 2H, H<sub>anthr-1</sub> and H<sub>anthr-8</sub>), 9.69 (d,  $J = 1.48$  Hz, 1H, H<sub>imin</sub>); <sup>13</sup>C NMR (100 MHz, CDCl<sub>3</sub>)  $\delta$  20.65, 20.67, 20.70, 20.79, 62.18, 68.67, 72.45, 73.86, 73.95, 93.36, 124.60 (double intensity), 125.37 (double intensity), 126.29, 127.14 (double intensity), 128.96 (double intensity), 130.46 (double intensity), 130.81, 131.23 (double intensity), 161.41, 169.43, 169.45, 170.43, 170.75. Melting point: 163-166 °C.

**(E)-(2,3,4,6)-Tetra-O-Acetyl- $\beta$ -D-Glucopyranosyl-1-N-2-Hydroxy-3-**

**Methoxybenzaldimine (9e).** To a 100 mL round-bottom flask equipped with magnetic stirbar and reflux condenser,  $\beta$ -D-glucopyranosyl azide (**3**; 0.373 g, 1.00 mmol) and DPPE (**4**; 0.259 g, 0.650 mmol) were reacted in THF (5 mL) at ambient temperature for 30 minutes to first generate the iminophosphorane **5**. 2-Hydroxy-3-methoxybenzaldehyde (**8e**; 0.152 g, 1.00 mmol), having been dissolved in THF (3 mL), was subsequently added dropwise to the reaction mixture, at which time the reaction mixture was heated to 70 °C and allowed to proceed overnight. Formation of the imine **9e** was observed via TLC (1:1 hexanes:ethyl acetate,  $R_f = 0.29$ ). The crude reaction mixture was concentrated under vacuum, and purified by flash column chromatography (1:1 hexanes:ethyl acetate, 3% triethylamine). The isolated product was recrystallized in hot (80 °C) ethanol, and the pure crystals collected via vacuum filtration (0.251 g, 52.2% yield).

*(E)-(2,3,4,6)-Tetra-O-acetyl- $\beta$ -D-glucopyranosyl-1-N-2-hydroxy-3-methoxybenzaldimine (9e):* yellow-white crystals; <sup>1</sup>H NMR (400 MHz, CDCl<sub>3</sub>)  $\delta$  2.02 (s, 3H, -C(O)CH<sub>3</sub>), 2.06 (s, 3H, -C(O)CH<sub>3</sub>), 2.08 (s, 3H, -C(O)CH<sub>3</sub>), 2.11 (s, 3H, -C(O)CH<sub>3</sub>), 3.89 (ddd,  $J = 10.31, 4.66, 2.38$  Hz, 1H, H-5), 3.92 (s, 3H, -OCH<sub>3</sub>), 4.25 (dd,  $J = 12.38, 2.18$  Hz, 1H, H-6), 4.33 (dd,  $J = 12.40, 4.72$  Hz, 1H, H-6'), 4.98 (dd,  $J = 9.12, 9.12$  Hz, 1H, H-2), 5.01 (dd,  $J = 8.90, 1.38$  Hz, 1H, H-1),



5.16 (dd,  $J = 9.74, 9.74$  Hz, 1H, H-4), 5.37 (dd,  $J = 9.24, 9.24$  Hz, 1H, H-3), 6.85 (dd,  $J = 7.88, 7.88$  Hz, 1H, H<sub>Ph</sub>-5), 6.96 (d,  $J = 3.08$ , 1H H<sub>Ph</sub>-4), 6.98 (dd,  $J = 4.16, 1.12$  Hz, 1H, H<sub>Ph</sub>-6), 8.57 (br s, 1H, H<sub>imin</sub>), 12.45 (s, 1H, -OH); <sup>13</sup>C NMR (100 MHz, CDCl<sub>3</sub>)  $\delta$  20.58, 20.69 (double intensity), 20.75, 56.16, 61.92, 68.37, 72.42, 73.40, 74.20, 89.20, 115.05, 118.36, 118.56, 124.10, 148.35, 150.92, 164.88, 169.28, 169.37, 170.27, 170.63. Melting point: 146-150 °C.

**(E)-(2,3,4,6)-Tetra-O-Acetyl- $\beta$ -D-Glucopyranosyl-1-N-2-Hydroxy-4-**

**Methoxybenzaldimine (9f).** To a 100 mL round-bottom flask equipped with magnetic stirbar and reflux condenser,  $\beta$ -D-glucopyranosyl azide (**3**; 0.373 g, 1.00 mmol) and DPPE (**4**; 0.259 g, 0.650 mmol) were reacted in THF (5 mL) at ambient temperature for 30 minutes to first generate the iminophosphorane **5**. 2-Hydroxy-4-methoxybenzaldehyde (**8f**; 0.152 g, 1.00 mmol), having been dissolved in THF (3 mL), was subsequently added dropwise to the reaction mixture, at which time the reaction mixture was heated to 70 °C and allowed to proceed overnight. Formation of the imine **9f** was observed via TLC (1:1 hexanes:ethyl acetate,  $R_f = 0.40$ ). The crude reaction mixture was concentrated under vacuum, and purified by flash column chromatography (1:1 hexanes:ethyl acetate, 3% triethylamine). The isolated product was recrystallized in hot (80 °C) ethanol, and the pure crystals collected via vacuum filtration (0.112 g, 23.5% yield).

*(E)-(2,3,4,6)-Tetra-O-acetyl- $\beta$ -D-glucopyranosyl-1-N-2-hydroxy-4-methoxybenzaldimine (9f):* yellow-white crystals; <sup>1</sup>H NMR (400 MHz, CDCl<sub>3</sub>)  $\delta$  2.02 (s, 3H, -C(O)CH<sub>3</sub>), 2.05 (s, 3H, -C(O)CH<sub>3</sub>), 2.05 (s, 3H, -C(O)CH<sub>3</sub>), 2.11 (s, 3H, -C(O)CH<sub>3</sub>), 3.81 (s, 3H, -OCH<sub>3</sub>), 3.87 (ddd,  $J = 10.00, 4.56, 2.24$  Hz, 1H, H-5), 4.23 (dd,  $J = 12.36, 2.12$  Hz, 1H, H-6), 4.31 (dd,  $J = 12.40, 4.68$  Hz, 1H, H-6'), 4.84 (dd,  $J = 8.90, 1.19$  Hz, 1H, H-1), 5.02 (dd,  $J = 9.28, 9.28$  Hz, 1H, H-2), 5.16 (dd,  $J = 9.72, 9.72$  Hz, 1H, H-4), 5.35 (dd,  $J = 9.50, 9.50$  Hz, 1H, H-3), 6.44 (d,  $J = 2.28$  Hz, 1H, H<sub>Ph</sub>-3), 6.46 (d,  $J = 2.56$  Hz, 1H, H<sub>Ph</sub>-5), 7.20 (dd,  $J = 6.23, 3.00$  Hz, 1H, H<sub>Ph</sub>-6), 8.44 (d,  $J = 0.92$  Hz, 1H, H<sub>imin</sub>), 12.61 (s, 1H, -OH); <sup>13</sup>C NMR (100 MHz, CDCl<sub>3</sub>)  $\delta$  20.53, 20.58, 20.62, 20.75, 55.42, 61.98, 68.44, 72.46, 73.26, 74.11, 90.43, 101.09, 107.03, 112.15, 133.73, 163.31, 164.12, 164.58, 169.27, 169.38, 170.30, 170.66. Melting point: 145-149 °C.

**(E)-(2,3,4,6)-Tetra-O-Acetyl- $\beta$ -D-Glucopyranosyl-1-N-2-Hydroxy-6-**

**Methoxybenzaldimine (9g).** To a 100 mL round-bottom flask equipped with magnetic stirbar and reflux condenser,  $\beta$ -D-glucopyranosyl azide (**3**; 0.373 g, 1.00 mmol) and DPPE (**4**; 0.259 g, 0.650 mmol) were reacted in THF (5 mL) at ambient temperature for 30 minutes to first generate the iminophosphorane **5**. 2-Hydroxy-6-methoxybenzaldehyde (**8g**; 0.152 g, 1.00 mmol), having been dissolved in THF (3 mL), was subsequently added dropwise to the reaction mixture, at which time the reaction mixture was heated to 70 °C and allowed to proceed overnight. Formation of the imine **9g** was observed via TLC (1:1 hexanes:ethyl acetate,  $R_f = 0.40$ ). The crude reaction mixture was concentrated under vacuum, and purified by flash column chromatography (1:1 hexanes:ethyl acetate, 3% triethylamine). The isolated product was recrystallized in hot (80 °C) ethanol, and the pure crystals collected via vacuum filtration (0.0506 g, 10.4% yield).

*(E)-(2,3,4,6)-Tetra-O-acetyl- $\beta$ -D-glucopyranosyl-1-N-2-hydroxy-6-methoxybenzaldimine (9g):* yellow crystals;  $^1\text{H}$  NMR (400 MHz,  $\text{CDCl}_3$ )  $\delta$  2.02 (s, 3H, -C(O)CH<sub>3</sub>), 2.03 (s, 3H, -C(O)CH<sub>3</sub>), 2.05 (s, 3H, -C(O)CH<sub>3</sub>), 2.11 (s, 3H, -C(O)CH<sub>3</sub>), 3.85 (s, 3H, -OCH<sub>3</sub>), 3.87 (ddd,  $J = 10.03, 4.70, 2.34$  Hz, 1H, H-5), 4.23 (dd,  $J = 12.32, 2.24$  Hz, 1H, H-6), 4.32 (dd,  $J = 12.38, 4.74$  Hz, 1H, H-6'), 4.83 (dd,  $J = 9.34, 1.13$  Hz, 1H, H-1), 5.05 (dd,  $J = 9.26, 9.26$  Hz, 1H, H-2), 5.17 (dd,  $J = 9.72, 9.72$  Hz, 1H, H-4), 5.34 (dd,  $J = 9.50, 9.50$  Hz, 1H, H-3), 6.33 (d,  $J = 8.24$  Hz, 1H, H<sub>Ph</sub>-3), 6.53 (d,  $J = 9.52$  Hz, 1H H<sub>Ph</sub>-5), 7.26 (dd,  $J = 8.32, 8.32$  Hz, 1H, H<sub>Ph</sub>-4), 9.00 (d,  $J = 0.99$  Hz, 1H, H<sub>imin</sub>), 12.99 (s 1H, -OH);  $^{13}\text{C}$  NMR (100 MHz,  $\text{CDCl}_3$ )  $\delta$  20.51, 20.58, 20.62, 20.73, 55.69, 62.05, 68.52, 72.37, 73.30, 74.05, 91.25, 100.37, 107.94, 110.15, 134.54, 160.20, 162.20, 162.79, 169.23, 169.38, 170.32, 170.67. Melting point: 118-122 °C.

**(E)-(2,3,4,6)-Tetra-O-Acetyl- $\beta$ -D-Glucopyranosyl-1-N-4-Nitrobenzaldimine (10b).**

To a 100 mL round-bottom flask equipped with magnetic stirbar and reflux condenser,  $\beta$ -D-glucopyranosyl azide (**3**; 0.373g, 1.00 mmol) and DPPE (**4**; 0.259 g, 0.650 mmol) were reacted in THF (5 mL) at ambient temperature for 30 minutes to first generate the iminophosphorane **5**. 4-Nitrobenzaldehyde (**8b**; 0.151 g, 1.00 mmol), having been dissolved in THF (3 mL), was

subsequently added dropwise to the reaction mixture, at which time the reaction mixture was heated to 70 °C and allowed to proceed overnight. Precipitated DPPE dioxide (**7**) was removed by gravity filtration, allowing to further react overnight again under heat. The reaction mixture was concentrated under vacuum, and NaBH<sub>3</sub>CN (0.251 g, 4.00 mmol) dissolved in ethanol (5 mL) was added. Dichloromethane (3 mL) was also added to ensure that all compounds present were dissolved, allowing the reaction to proceed overnight with no applied heat.

The reaction mixture was then partitioned between dichloromethane (25 mL) and water (25 mL), mixing with 10% (v/v) HCl in water (2 mL). Saturated NaHCO<sub>3</sub> (10 mL) was used to neutralize the solution after vigorous mixing, and the organic layer was isolated before extracting it with water (1 x 20 mL) and brine (2 x 20 mL). The organic layer was dried over anhydrous MgSO<sub>4</sub> and filtered, followed by removal of the solvent *in vacuo*. The remaining crude syrup was purified by flash column chromatography (1:1 hexanes:ethyl acetate, 3% triethylamine), with the isolated product recrystallized in hot (80 °C) ethanol and collected via vacuum filtration (0.0328 g, 6.8% yield).

*(E)*-(2,3,4,6)-Tetra-*O*-Acetyl- $\beta$ -*D*-Glucopyranosyl-1-*N*-4-Nitrobenzaldamine (**10b**): white crystals; <sup>1</sup>H NMR (400 MHz, CDCl<sub>3</sub>)  $\delta$  2.01 (s, 3H, -C(O)CH<sub>3</sub>), 2.02 (s, 3H, -C(O)CH<sub>3</sub>), 2.09 (s, 3H, -C(O)CH<sub>3</sub>), 2.10 (s, 3H, -C(O)CH<sub>3</sub>), 2.15-2.25 (m, 1H, -NH-), 3.61 (ddd,  $J = 10.00, 4.64, 2.40$  Hz, 1H, H-5), 3.99 (dd,  $J = 15.01, 3.24$  Hz, 1H, H<sub>-NCH<sub>2</sub>-</sub>), 4.05 (app t,  $J = 10.08$  Hz, 1H, H-1), 4.13 (dd,  $J = 12.16, 2.36$  Hz, 1H, H-6), 4.15 (dd,  $J = 15.45, 1.48$  Hz, 1H, H'<sub>-NCH<sub>2</sub>-</sub>), 4.29 (dd,  $J = 12.28, 4.68$  Hz, 1H, H-6'), 4.91 (dd,  $J = 9.38, 9.38$  Hz, 1H, H-2), 5.05 (dd,  $J = 9.70, 9.70$  Hz, 1H, H-4), 5.23 (dd,  $J = 9.52, 9.52$  Hz, 1H, H-3), 7.45 (d,  $J = 8.68$  Hz, 2H, H<sub>Ph-2</sub> and H<sub>Ph-6</sub>), 8.18 (d,  $J = 8.72$  Hz, 2H, H<sub>Ph-3</sub> and H<sub>Ph-5</sub>); <sup>13</sup>C NMR (100 MHz, CDCl<sub>3</sub>)  $\delta$  20.58, 20.60, 20.74, 20.78, 48.05, 62.13, 68.82, 70.96, 72.85, 73.07, 88.41, 123.65, 128.34, 129.29, 147.21, 155.77, 162.91, 169.53, 170.14, 170.59, 170.88. Melting point: 124-127 °C.

## References

1. Grieb, P. On a New Class of Compounds in Which Nitrogen is Substituted for Hydrogen. *Proceedings of the Royal Society of London* **1864**, *13*, 375-384.
2. Keicher, T.; Löbbecke, S. Lab-scale Synthesis of Azido Compounds: Safety Measures and Analysis. In *Organic Azides: Syntheses and Applications*; Bräse, S.; Banert, K., Eds.; John Wiley & Sons, Ltd., 2010; Chapter 1, pp 3-27.
3. Bräse, S.; Gil, C.; Knepper, K.; Zimmermann, V. Organic Azides: An Exploding Diversity of a Unique Class of Compounds. *Angew. Chem. Int. Ed.* **2005**, *44*, 5188-5240.
4. Lin, T. S.; Prusoff, W. H. Synthesis and Biological Activity of Several Amino Analogues of Thymidine. *J. Med. Chem.* **1978**, *21*(1), 109-112.
5. Mellor, B. A Preliminary Technical Review of DMAZ: A Low-Toxicity Hypergolic Fuel. *Proceedings of the 2<sup>nd</sup> International Conference on Green Propellants for Space Propulsion*, Sardinia, Italy, June 7-8, 2004.
6. Staudinger, H.; Meyer, J. Über neue organische Phosphorverbindungen III. Phosphinmethylenderivate und Phosphinimine. *Helv. Chim. Acta* **1919**, *2*(1), 635-646.
7. Temelkoff, D. P.; Smith, C. R.; Kibler, D. A.; McKee, S.; Duncan, S. J.; Zeller, M.; Hunsen, M.; Norris, P. Application of bis(diphenylphosphino)ethane (DPPE) in Staudinger-type *N*-glycopyranosyl Amide Synthesis. *Carbohydrate Research* **2006**, *341*, 1645-1656.
8. O'Neil, I. A.; Thompson, S.; Murray, C. L.; Kalindjian, S. B. DPPE: A Convenient Replacement for Triphenylphosphine in the Staudinger and Mitsunobu Reactions. *Tetrahedron Letters* **1998**, *39*, 7787-7790.
9. Schwabacher, A. W.; Lane, J. W.; Schlesher, M. W.; Leigh, K. M.; Johnson, C. W. Desymmetrization Reactions: Efficient Preparation of Unsymmetrically Substituted Linker Molecules. *J. Org. Chem.* **1998**, *63*, 1727-1729.
10. Lin, F. L.; Hoyt, H. M.; van Halbeek, H.; Bergman, R. G.; Bertozzi, C. R. Mechanistic Investigation of the Staudinger Ligation. *J. Am. Chem. Soc.* **2005**, *127*, 2686-2695.
11. Saxon, E.; Bertozzi, C. R. Cell Surface Engineering by a Modified Staudinger Reaction. *Science* **2000**, *287*(5460), 2007-2010.
12. Saxon, E.; Armstrong, J. I.; Bertozzi, C. R. A "Traceless" Staudinger ligation for the Chemoselective Synthesis of Amide Bonds. *Organic Letters* **2000**, *2*(14), 2141-2143.
13. Wittig, G.; Schöllkopf, U. Über Triphenyl-Phosphin-Methylene als Olefinbildende Reagenzien I. *Chemische Berichte* **1954**, *87*(9), 1318-1330.
14. Hoffmann, R. W. Wittig and His Accomplishments: Still Relevant Beyond His 100<sup>th</sup> Birthday. *Angew. Chem. Int. Ed.* **2001**, *40*(8), 1411-1416.
15. Edmonds, M.; Abell, A. The Wittig Reaction. In *Modern Carbonyl Olefination*. Takeda, T., Ed.; Wiley-VCH Verlag GmbH & Co. KGaA: Weinheim, FRG, 2004; Chapter 1.

16. Murphy, P. J.; Lee, S. E. Recent Synthetic Applications of the Non-Classical Wittig Reaction. *J. Chem. Soc., Perkin Trans. 1*, **1999**, 3049-3066.
17. Trost, B. M. The Atom Economy: A Search for Synthetic Efficiency. *Science* **1991**, *254*(5037), 1471-1477.
18. Siau, W-Y.; Zhang, Y.; Zhao, Y. Stereoselective Synthesis of Z-Alkenes. *Top Curr. Chem.* **2012**, *327*, 33-58.
19. Palacios, F.; Alonso, C.; Aparicio, D.; Rubiales, G.; de los Santos, J. M. The Aza-Wittig Reaction: An Efficient Tool for the Construction of Carbon-Nitrogen Double Bonds. *Tetrahedron* **2007**, *63*, 523-575.
20. Palacios, F.; Alonso, C.; Aparicio, D.; Rubiales, G.; de los Santos, J. M. Aza-Wittig Reaction in Natural Product Syntheses. In *Organic Azides: Syntheses and Applications*; Bräse, S.; Banert, K., Eds.; John Wiley & Sons, Ltd., 2010; Chapter 15, pp 439-467.
21. Martin, S. F. Recent Applications of Imines as Key Intermediates in the Synthesis of Alkaloids and Novel Nitrogen Heterocycles. *Pure Appl. Chem.* **2009**, *81*(2), 195-204.
22. Fresneda, P. M.; Molina, P. Application of Iminophosphorane-Based Methodologies for the Synthesis of Natural Products. *Synlett* **2004**, *1*, 1-17.
23. Bleda, J. A.; Fresneda, P. M.; Orenes, R.; Molina, P. Preparation of Fused Tetracyclic Quinazolinones by Combinations of Aza-Wittig Methodologies and Cu(I)-Catalysed Heteroarylation Processes. *Eur. J. Org. Chem.* **2009**, *2009*(15), 2490-2504.
24. Borch, R. F.; Bernstein, M. D.; Durst, H. D. The Cyanohydridoborate Anion as a Selective Reducing Agent. *JACS* **1971**, *93*(12), 2897-2904.
25. Cosenza, V. A.; Navarro, D. A.; Stortz, C. A. Usage of  $\alpha$ -Picoline Borane for the Reductive Amination of Carbohydrates. *Org. Chem. in Argentina (ARKIVOC)* **2011**, *2011*(vii), 182-194.
26. Abdel-Magid, A. F.; Carson, K. G.; Harris, B. D.; Maryanoff, C. A.; Shah, R. D. Reductive Amination of Aldehydes and Ketones with Sodium Triacetoxyborohydride. Studies on Direct and Indirect Reductive Amination Procedures. *J. Org. Chem.* **1996**, *61*, 3849-3862.
27. Sato, S.; Sakamoto, T.; Miyazawa, E.; Kikugawa, Y. One-Pot Reductive Amination of Aldehydes and Ketones with  $\alpha$ -Picoline Borane in Methanol, in Water, and in Neat Conditions. *Tetrahedron* **2004**, *60*(36), 7899-7906.
28. Murray, R. K.; Granner, D. K.; Mayes, P. A.; Rodwell, V. W. Glycoproteins. In *Harper's Illustrated Biochemistry, 26<sup>th</sup> edition*; Foltin, J.; Ransom, J.; Oransky, J. M., Eds.; McGraw-Hill Publishing Company, 2003; Chapter 47.
29. Shi, M.; Kleski, K. A.; Trabbic, K. R.; Bourgault, J. P.; Andreana, P. R. STn-PS A1 as an Entirely Carbohydrate Immunogen: Synthesis and Immunological Evaluation. *J. Am. Chem. Soc.* **2016**, *138*, 14264-14272.

30. Voet, D.; Voet, J. G. Sugars and Polysaccharides. In *Biochemistry*, 4<sup>th</sup> edition; Recta, P.; Kalkut, J., Eds.; JohnWiley & Sons, Inc., 2011; Chapter 11, 259-385.
31. U.S. National Library of Medicine. Oligosaccharides. <https://meshb.nlm.nih.gov/#/record/ui?name=Oligosaccharides> (Accessed March 3, 2017).
32. Miljković, M. Isomerization of Sugars. In *Carbohydrates: Synthesis, Mechanisms, and Stereoelectronic Effects*; Springer, 2010; Chapter 4, pp 95-111.
33. Juaristi, E.; Cuevas, G. Recent Studies in the Anomeric Effect. *Tetrahedron* **1992**, 48(24), 5019-5087.
34. Norris, P. Pyranose *N*-Glycosyl Amines: Emerging Targets with Diverse Biological Potential. *Curr. Top. Med. Chem.* **2008**, 8(2), 101-113.
35. Dalziel, M.; Crispin, M.; Scanlan, C. N.; Zitzmann, N.; Dwek, R. A. Emerging Principles for the Therapeutic Exploitation of Glycosylation. *Science* **2014**, 343(6166), 1235681.
36. Imperiali, B.; O'Connor, S. E. Effect of *N*-Linked Glycosylation on Glycopeptide and Glycoprotein Structure. *Curr. Opin. Chem. Biol.* **1999**, 3, 643-649.
37. Larkin, A.; Imperiali, B. The Expanding Horizons of Asparagine-Linked Glycosylation. *Biochemistry* **2011**, 50(21), 4411-4426.
38. Ouerfelli, O.; Warren, J. D.; Wilson, R. M.; Danishefsky, S. J. Synthetic Carbohydrate-Based Antitumor Vaccines: Challenges and Opportunities. *Expert Rev. Vaccines*, **2005**, 4(5), 677-685.
39. Shi, M.; Kleski, K. A.; Trabbic, K. R.; Bourgault, J-P.; Andreana, P. R. Sialyl-Tn Polysaccharide A1 as an Entirely Carbohydrate Immunogen: Synthesis and Immunological Evaluation. *JACS*, **2016**, 138, 14264-14272.
40. Nwe, K.; Brechbiel, M. W. Growing Applications of "Click Chemistry" for Bioconjugation in Contemporary Biomedical Research. *Cancer Biotherapy and Radiopharmaceuticals* **2009**, 24(3), 289-302.
41. Ibatullin, F. M.; Shabalin, K. A. A Simple and Convenient Synthesis of Glycosyl Azides. *Syn. Comm.* **2000**, 30(15), 2819-2823.
42. Esteves, A. P.; Rodrigues, L. M.; Silva, M. E.; Gupta, S.; Oliveira-Campos, A. M. F., Machalicky, O.; Mendonça, A. J. Synthesis and Characterization of Novel Fluorescent *N*-Glycoconjugates. *Tetrahedron* **2005**, 61, 8625-8632.
43. Kondratenko, R. M.; Baltina, L. A.; Mustafina, S. R.; Vasiléva, E. V.; Pompei, R.; Deidda, D.; Plyasunova, O. A.; Pokrowvskii, A. G.; Tolstikov, A. The Synthesis and Antiviral Activity of Glycyrrhizic Acid Conjugates with  $\alpha$ -D-Glucosamine and Some Glycosylamines. *Russ. J. Bioorg. Chem.* **2004**, 30(3), 308-315.
44. Delost, M. D. Synthesis of Amine Derivatives from a "One-Pot" Synthesis of Biphenyl-4-Methylazide. Master's Thesis, Youngstown State University, Youngstown, OH, 2015.

45. Horn, H. G.; Sommer, K.  $^1\text{H}$ -,  $^{31}\text{P}$ -NMR and IR-Spectra of Some Ditertiary Phosphines. *Spect. Acta* **1971**, *27A*, 1049-1054.
46. Allen, F. H.; Kennard, O.; Watson, D. G.; Brammer, L.; Orpen, A. G.; Taylor, R. Tables of Bond Lengths Determined by X-ray and Neutron Diffraction. Part I: Bond Lengths in Organic Compounds. *J. Chem. Soc., Perkin Trans. 2* **1987**, *0*, S1-S19.
47. Hunt, I. University of Calgary. Substituent Effects.  
<http://www.chem.ucalgary.ca/courses/350/Carey5th/useful/subeff.html> (Accessed October 2, 2017).
48. Helferich, B.; Mitrowsky, A. Über *N*-Glykoside. *Chem. Berichte* **1952**, *85*(1), 1-8.
49. Kovács, L.; Ósz, E.; Domokos, V.; Holzer, W.; Györgydeák, Z. An Easy Access to Anomeric Glycosyl Amides and Imines (Schiff Bases) via Transformation of Glycopyranosyl Trimethylphosphinimides. *Tetrahedron* **2001**, *57*, 4609-4621.
50. Hübschle, C. B.; Sheldrick, G. M.; Dittrich, B. ShelXle: A Qt Graphical User Interface for SHELXL. *J. Appl. Cryst.* **2011**, *44*, 1281-1284.

# Appendix A

NMR Spectra



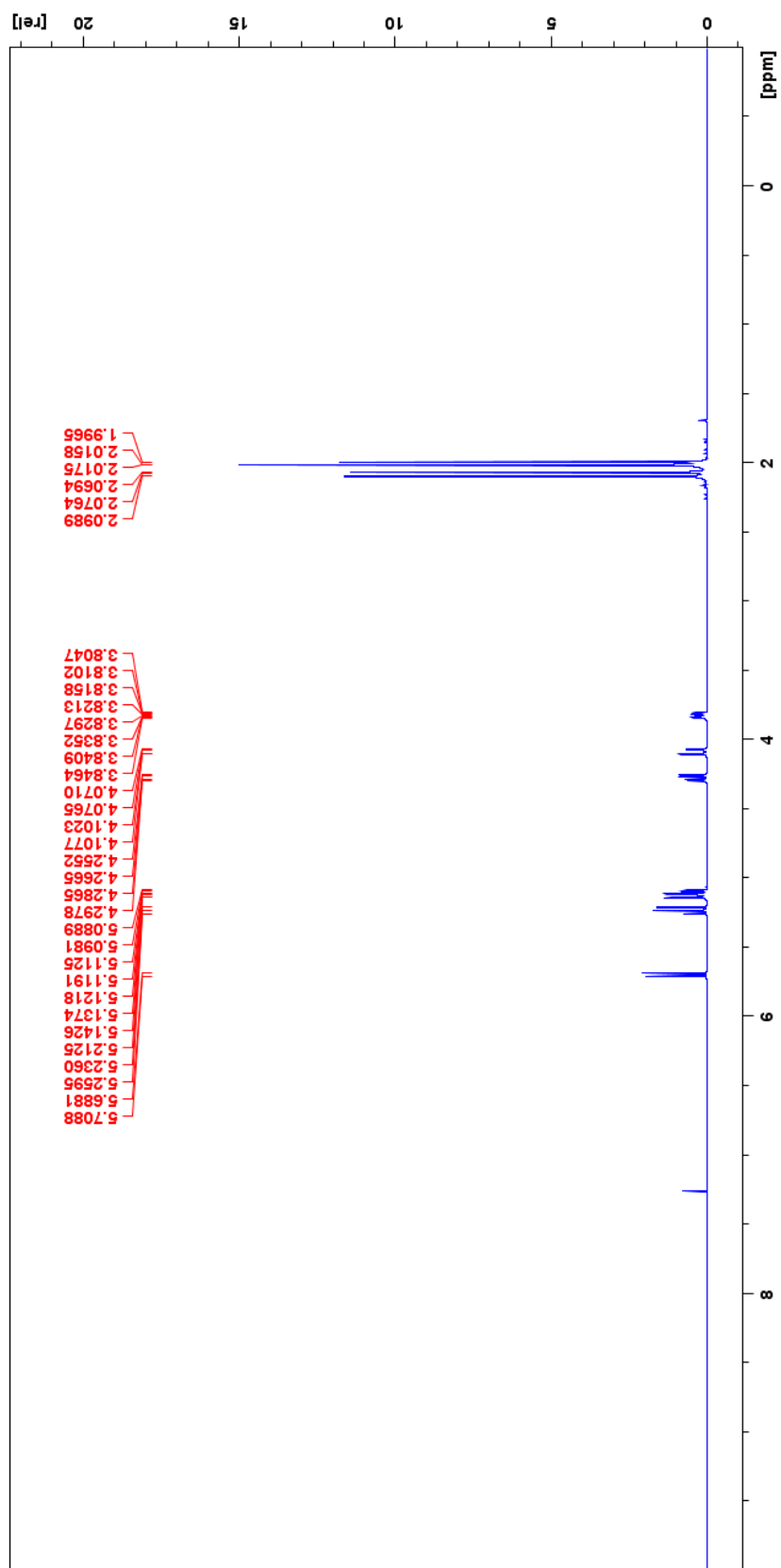


Figure 28. 400 MHz  $^1\text{H}$  NMR spectrum of  $\beta$ -D-glucopyranosyl pentaacetate (1).

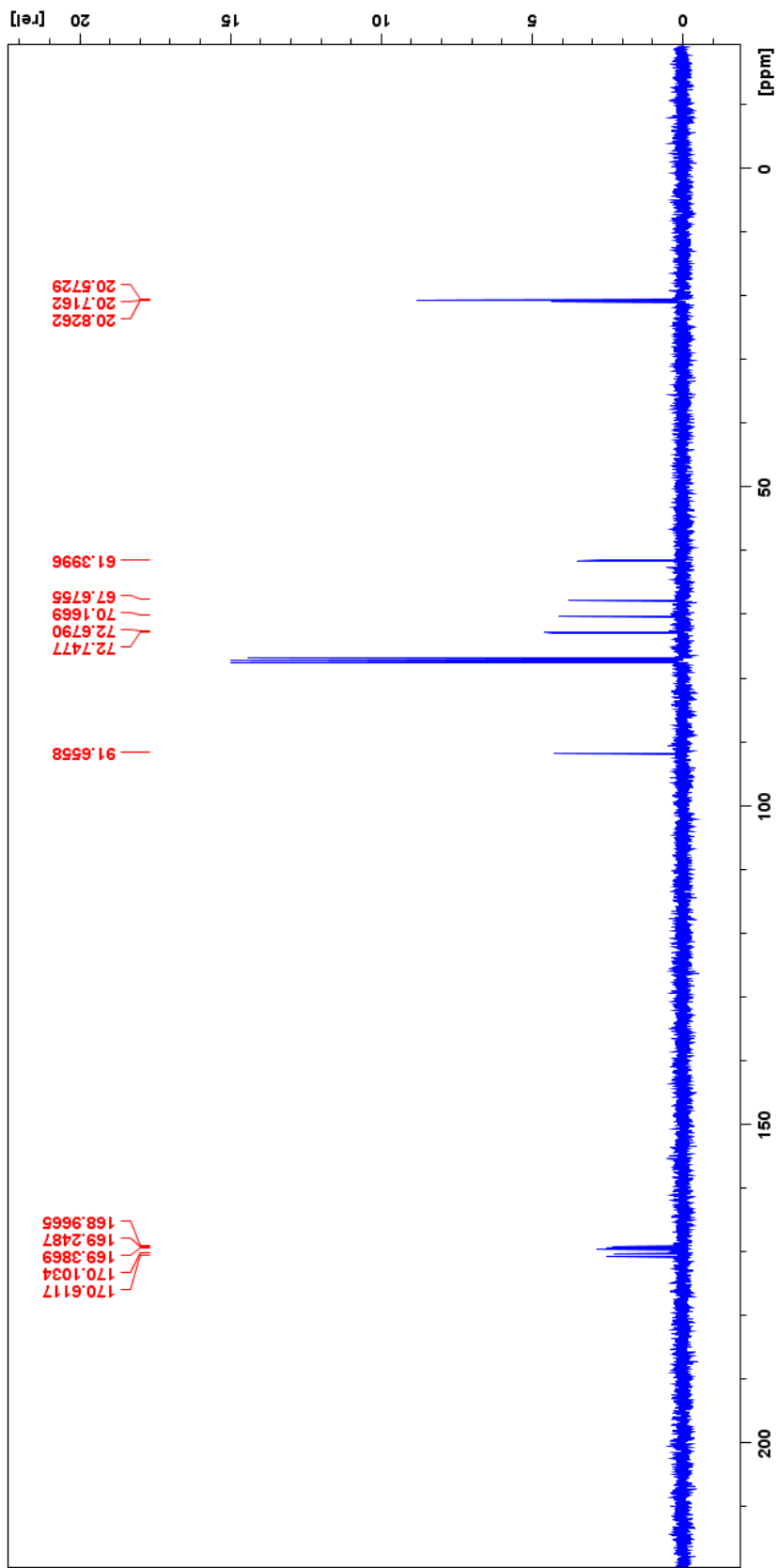
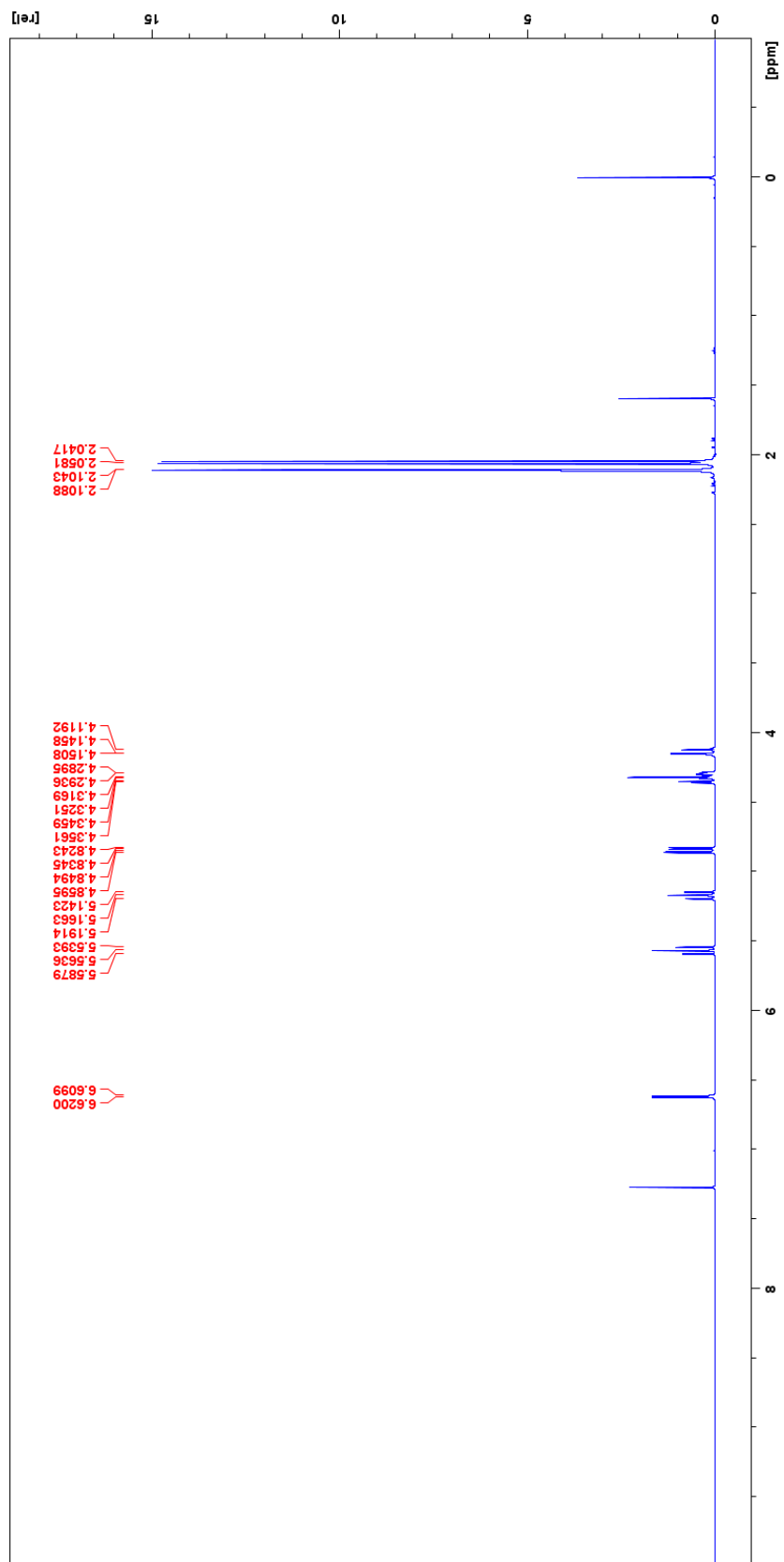
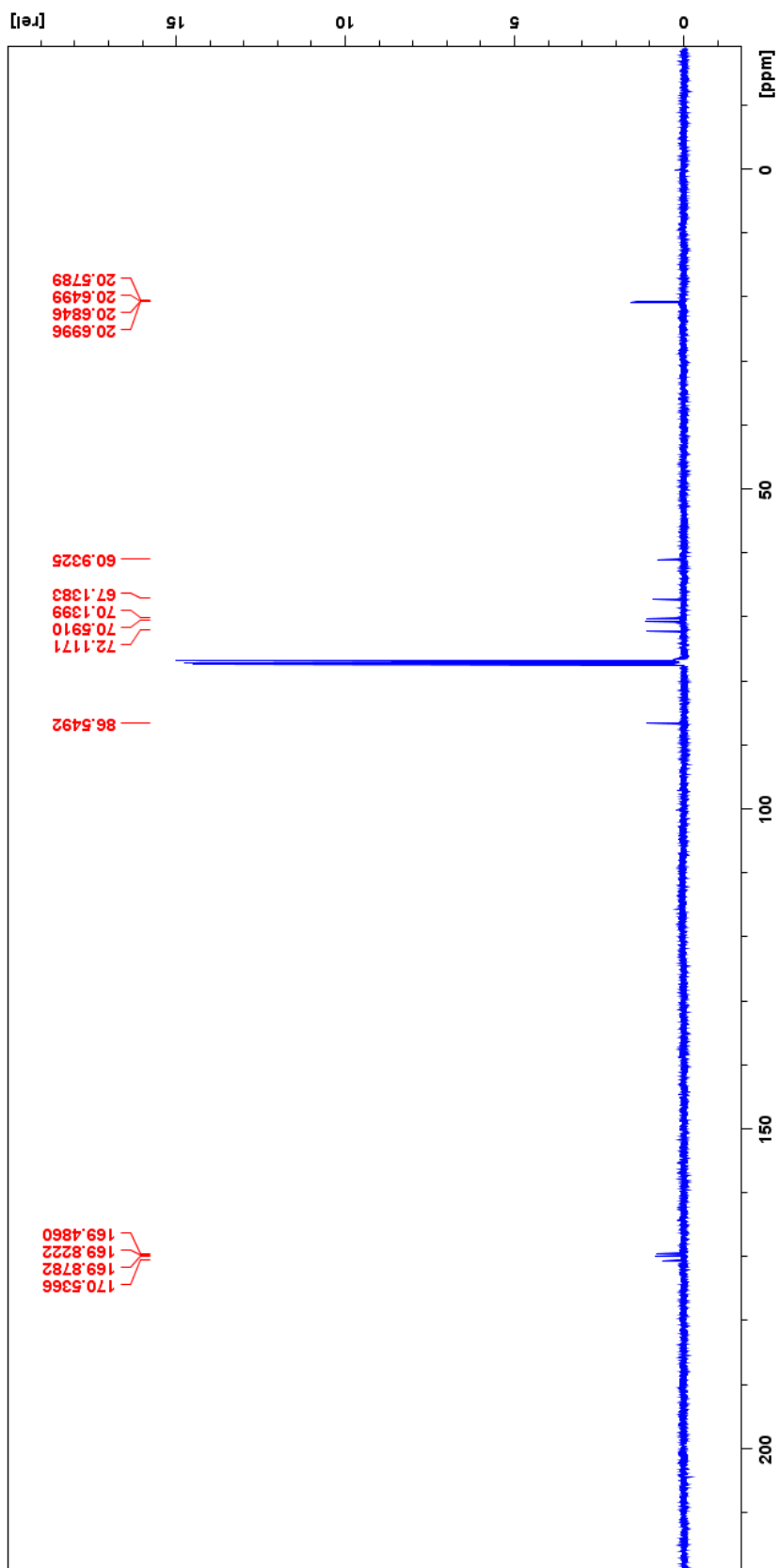


Figure 29. 100 MHz <sup>13</sup>C NMR spectrum of β-D-glucopyranosyl pentaacetate (1).



**Figure 30.** 400 MHz <sup>1</sup>H NMR spectrum of α-D-glucopyranosyl bromide (2).



**Figure 31.** 100 MHz  $^{13}\text{C}$  NMR spectrum of  $\alpha$ -D-glucopyranosyl bromide (2).

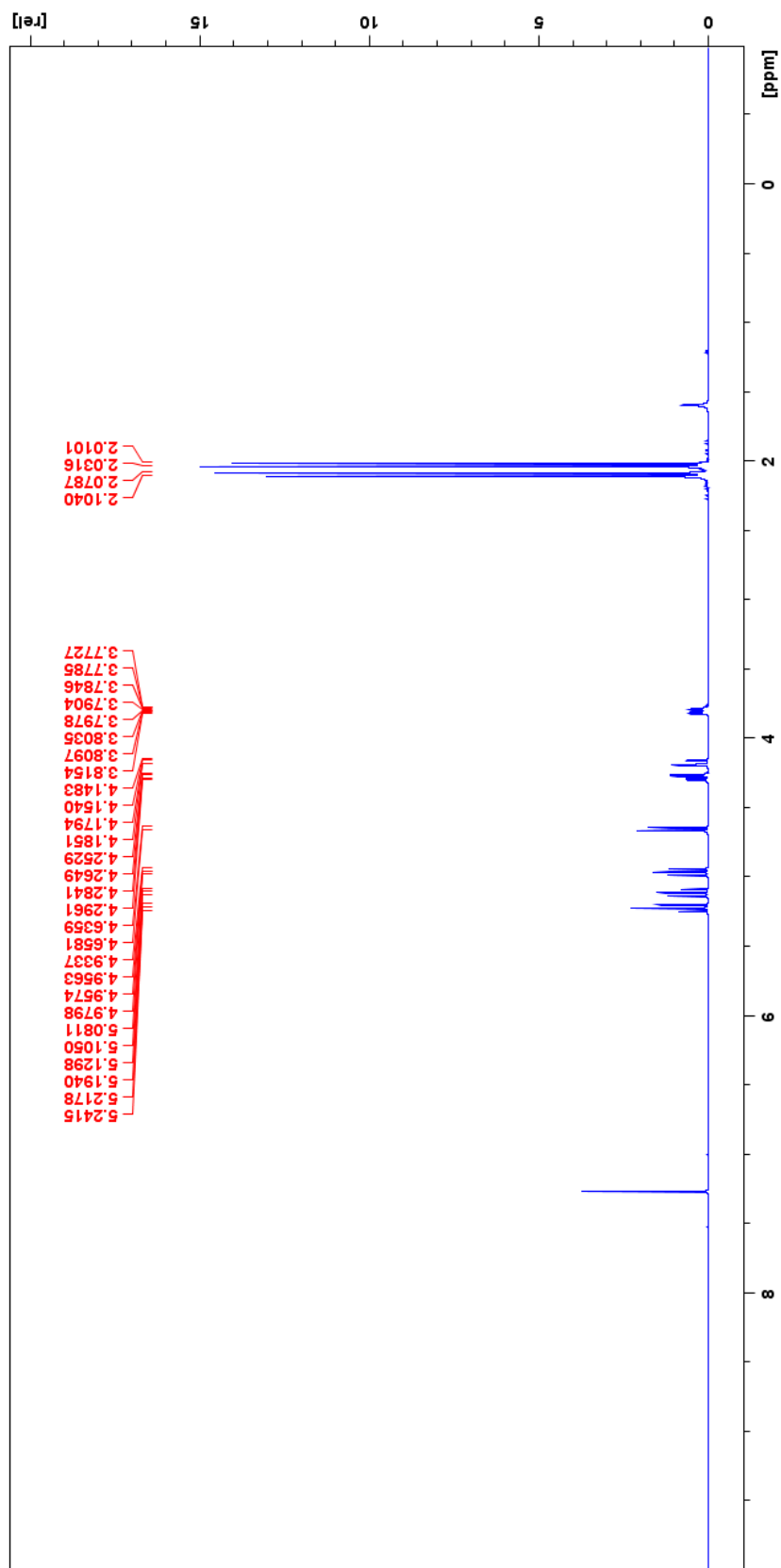
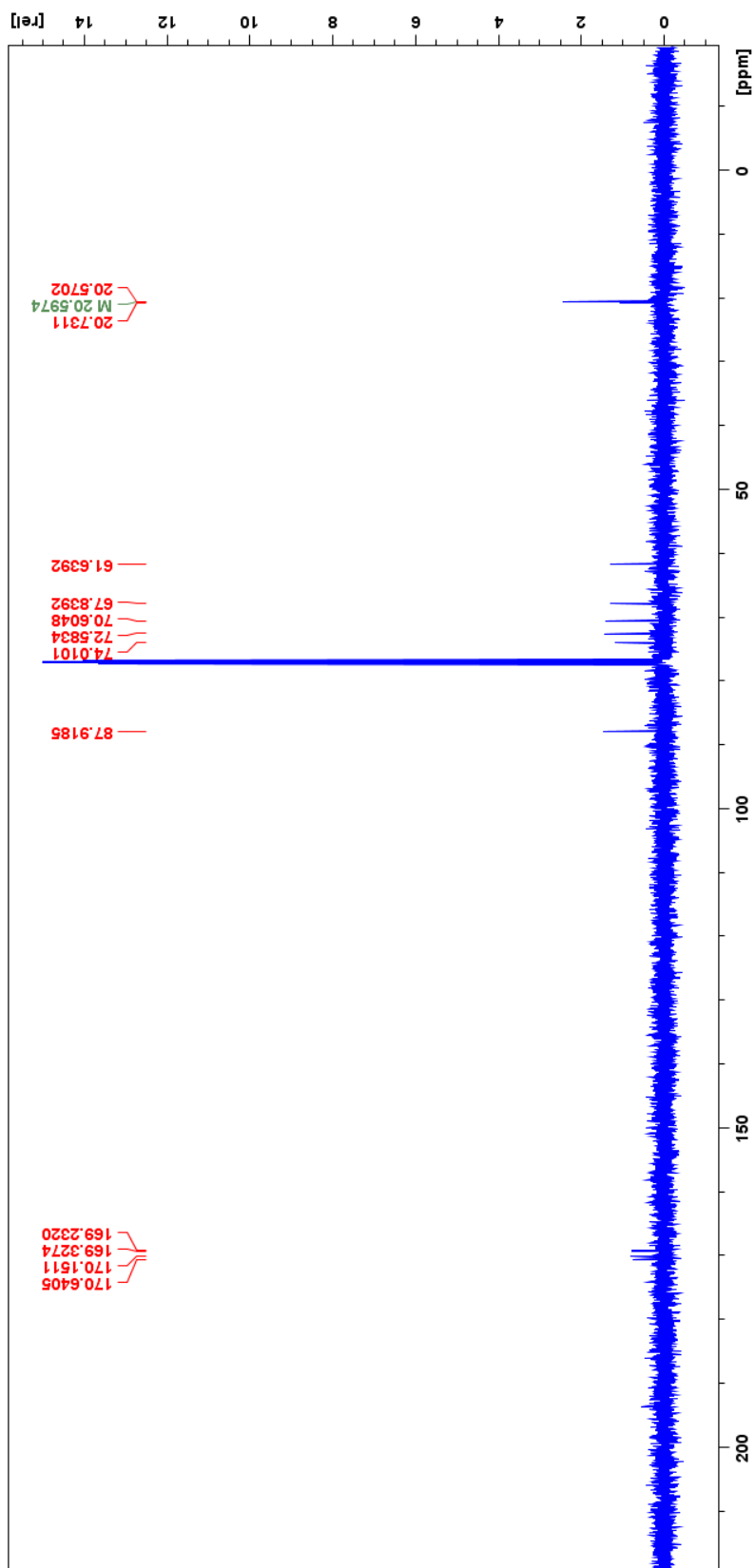
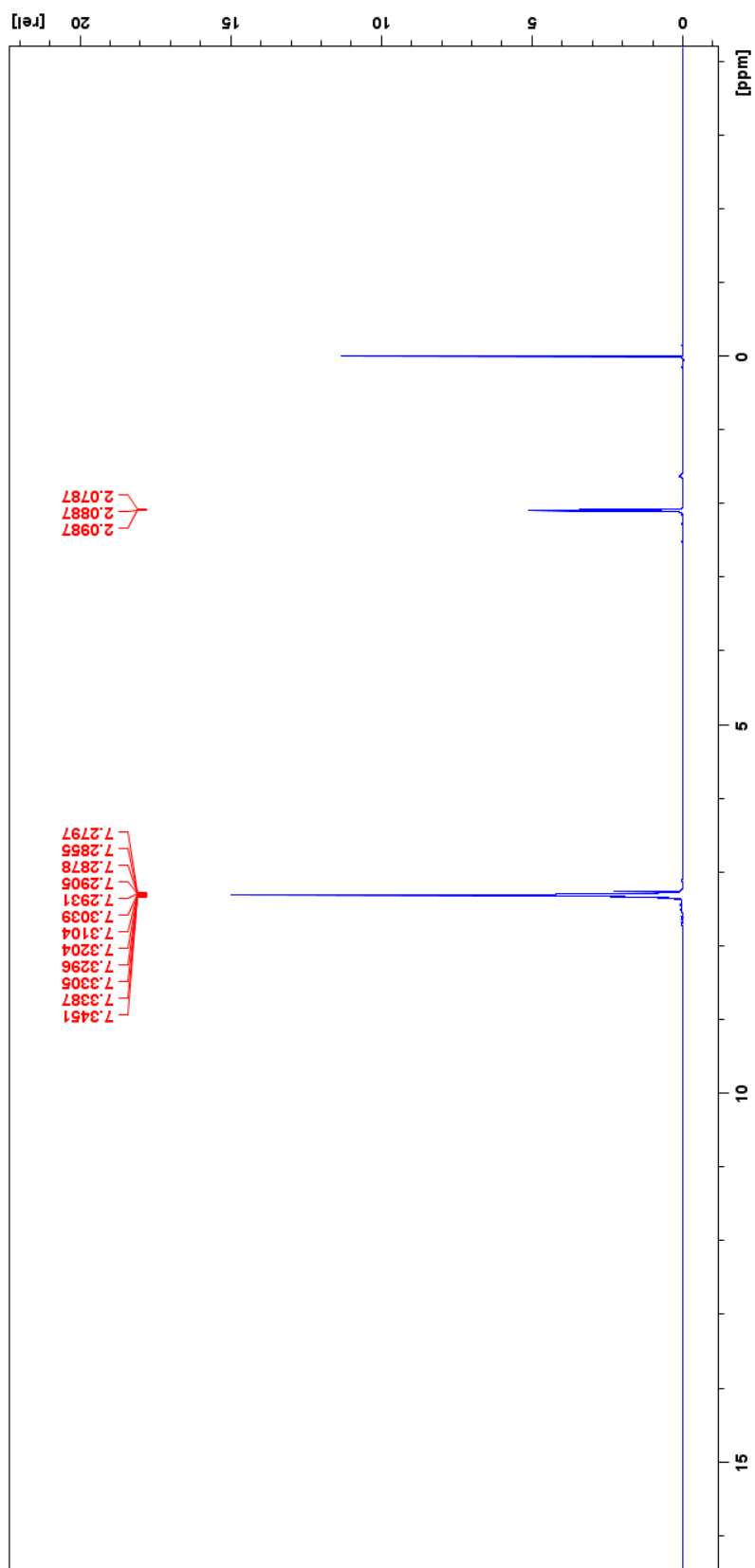


Figure 32. 400 MHz <sup>1</sup>H NMR spectrum of β-D-glucopyranosyl azide (3).



**Figure 33.** 100 MHz  $^{13}\text{C}$  NMR spectrum of  $\beta$ -D-glucopyranosyl azide (3).



**Figure 34.** 400 MHz <sup>1</sup>H NMR spectrum of 1,2-bis(diphenylphosphino)ethane (**4**).

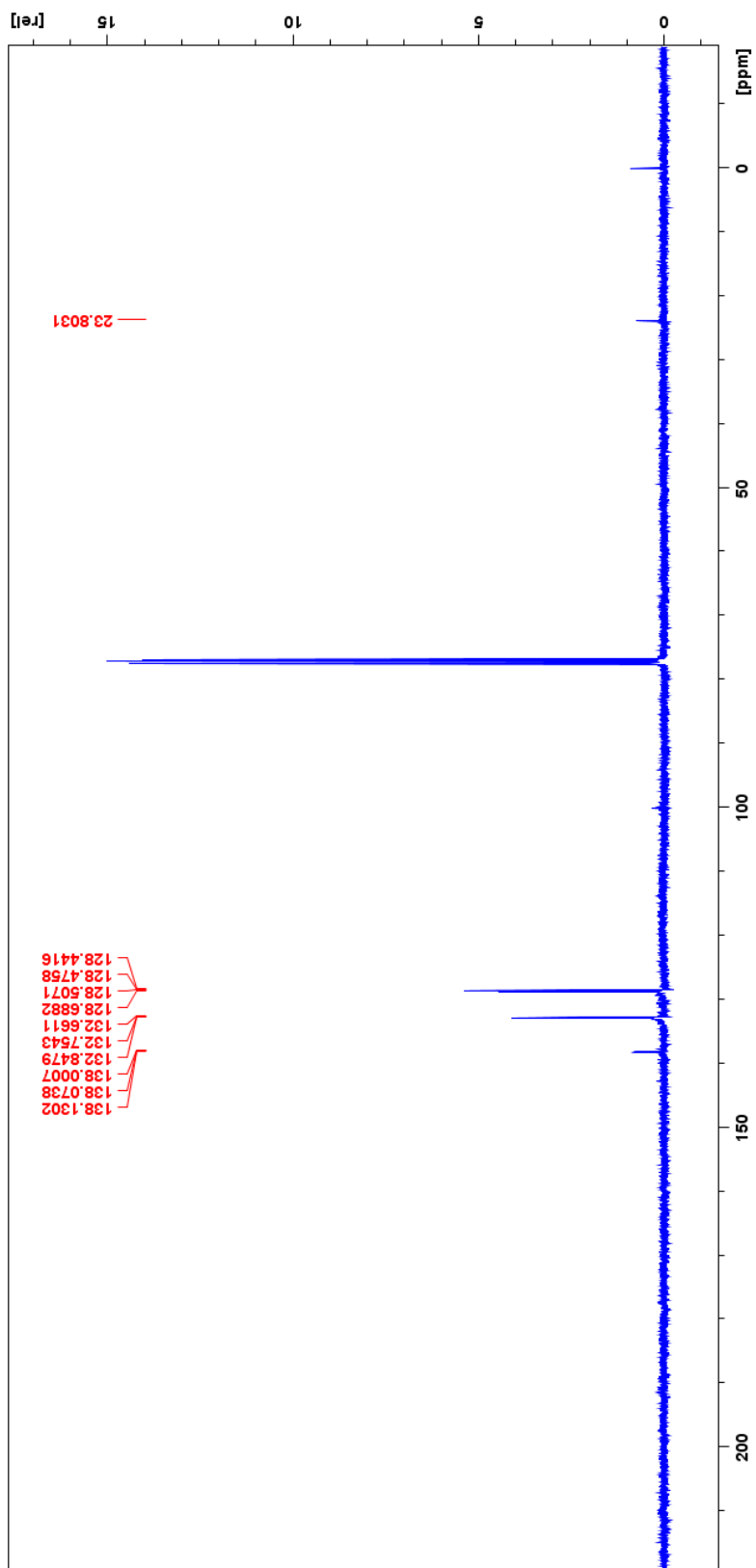


**Figure 35.** 100 MHz  $^{13}\text{C}$  NMR spectrum of 1,2-bis(diphenylphosphino)ethane (4).



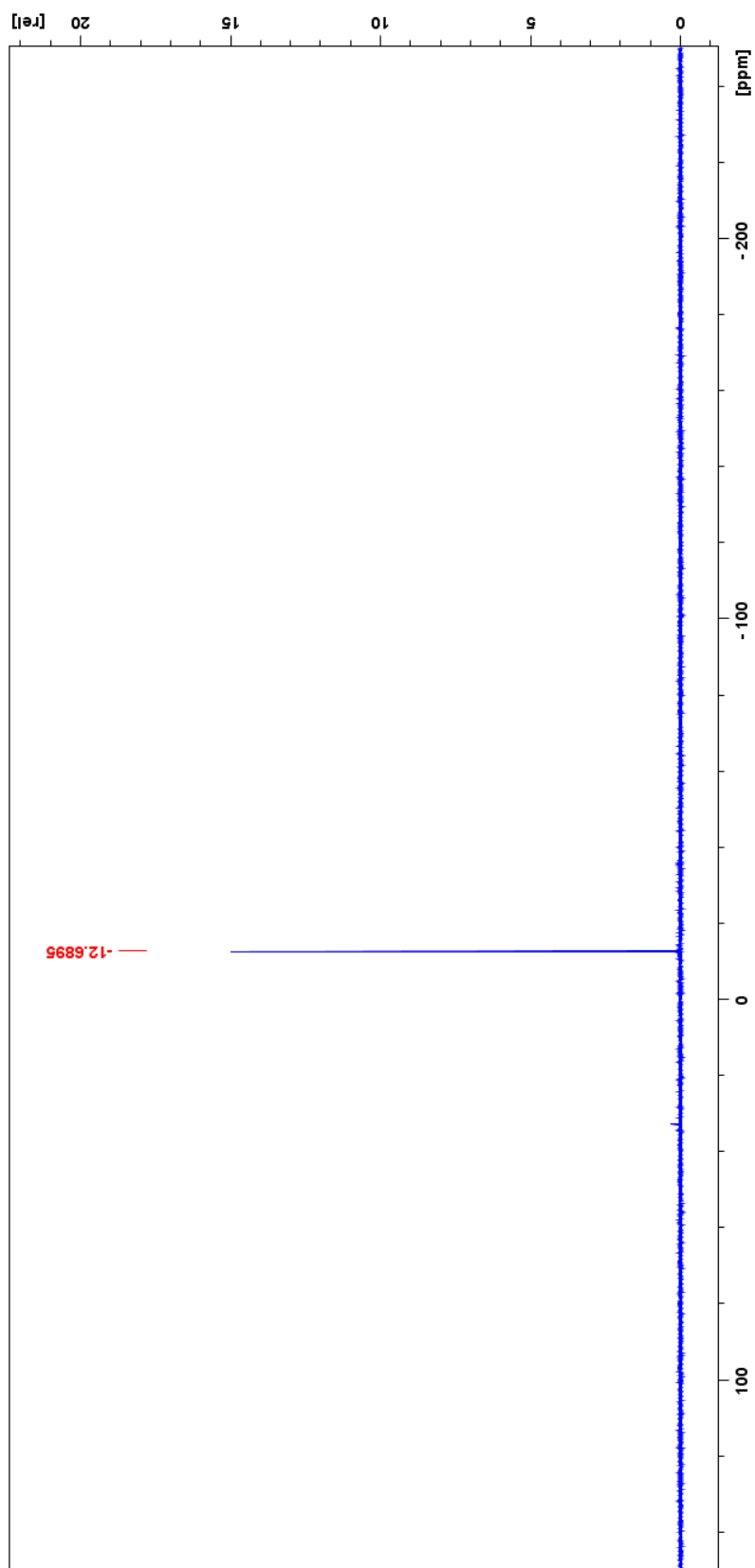


**Figure 36.** 167 MHz  $^{31}\text{P}$  NMR spectrum of 1,2-bis(diphenylphosphino)ethane (**4**).

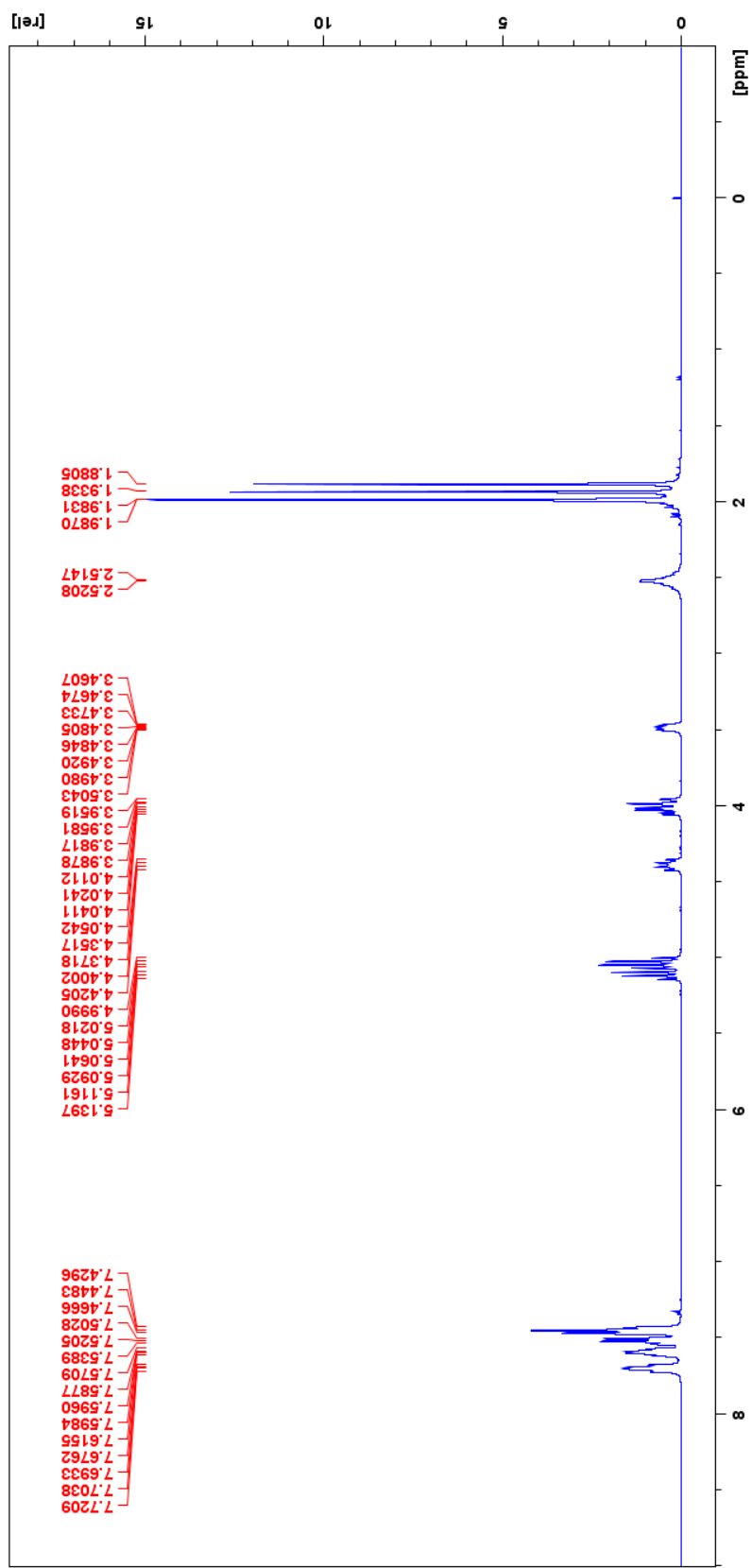


**Figure 37.** 400 MHz <sup>1</sup>H NMR spectrum of 1,2-bis(diphenyl-(2,3,4,6)-tetra-*O*-acetyl- $\beta$ -D-glucopyranosyl)-1-*N*-iminophosphorane ethane (5) in dichloromethane.

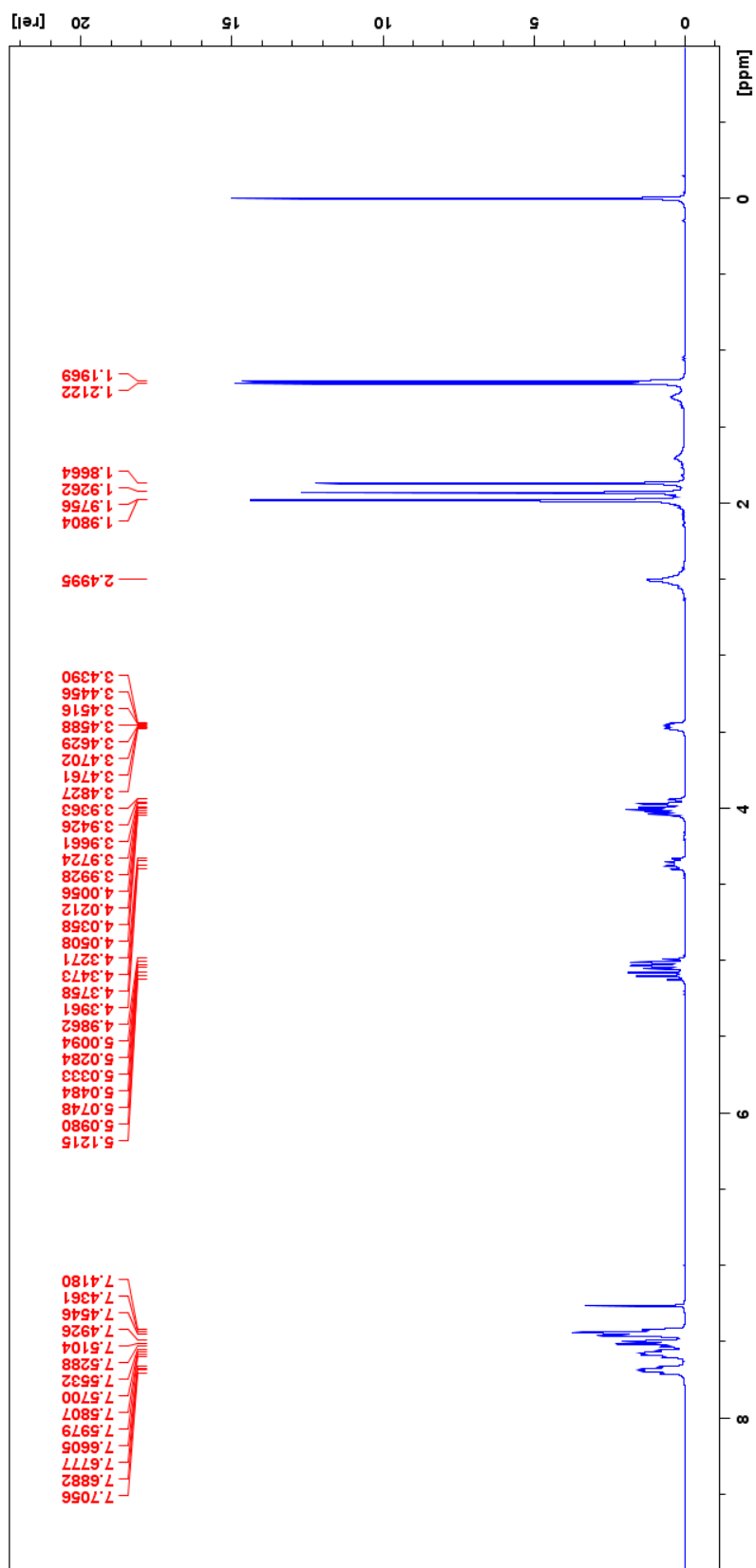


**Figure 38.** 400 MHz  $^1\text{H}$  NMR spectrum of 1,2-bis(diphenyl-(2,3,4,6)-tetra-*O*-acetyl- $\beta$ -D-glucopyranosyl)-1-*N*-iminophosphorane ethane (5) recrystallized in isopropyl alcohol.

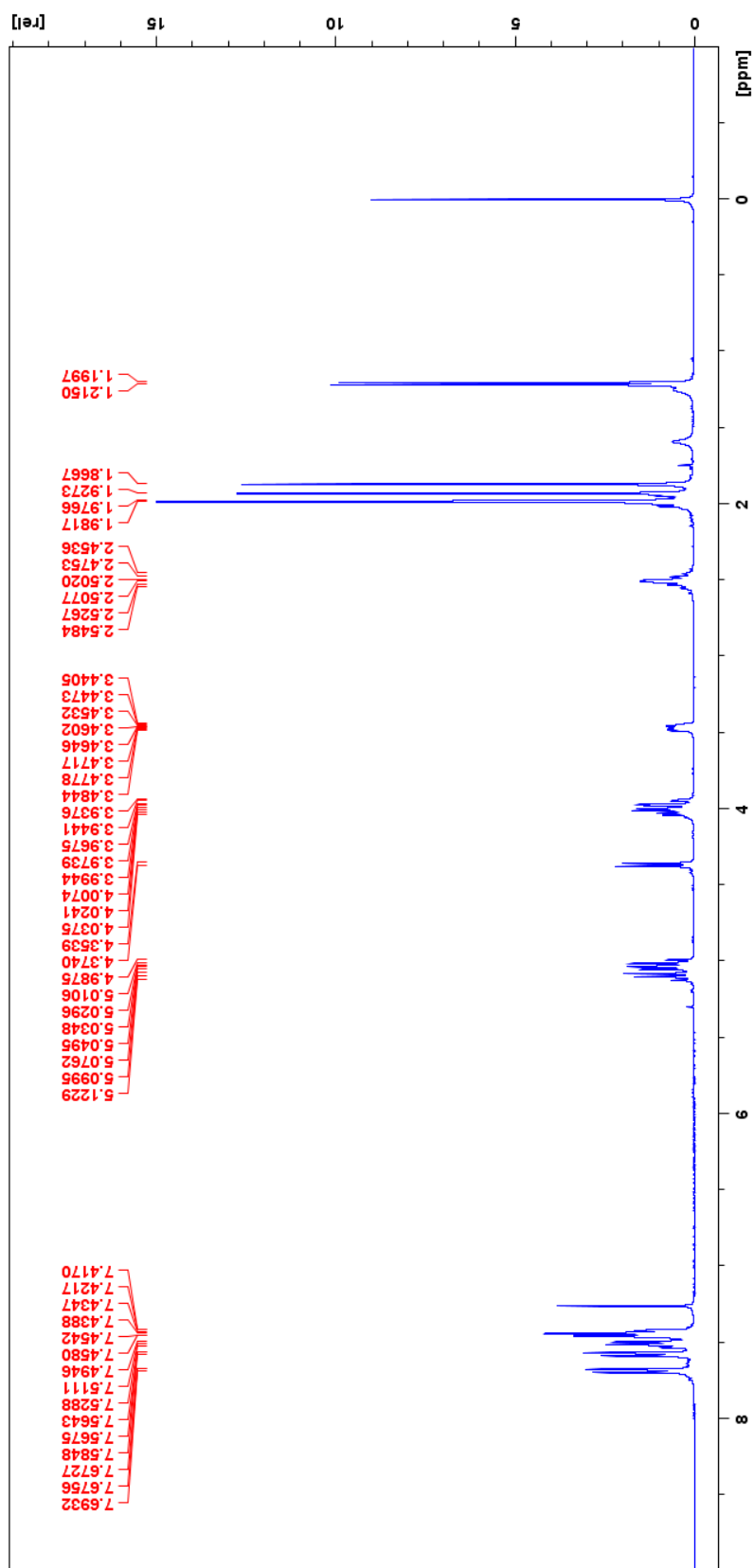


**Figure 39.** 400 MHz <sup>31</sup>P-decoupled <sup>1</sup>H NMR spectrum of 1,2-bis(diphenyl-(2,3,4,6)-tetra-O-acetyl-β-D-glucopyranosyl)-1-N-iminophosphorane ethane (**5**) recrystallized in isopropyl alcohol.

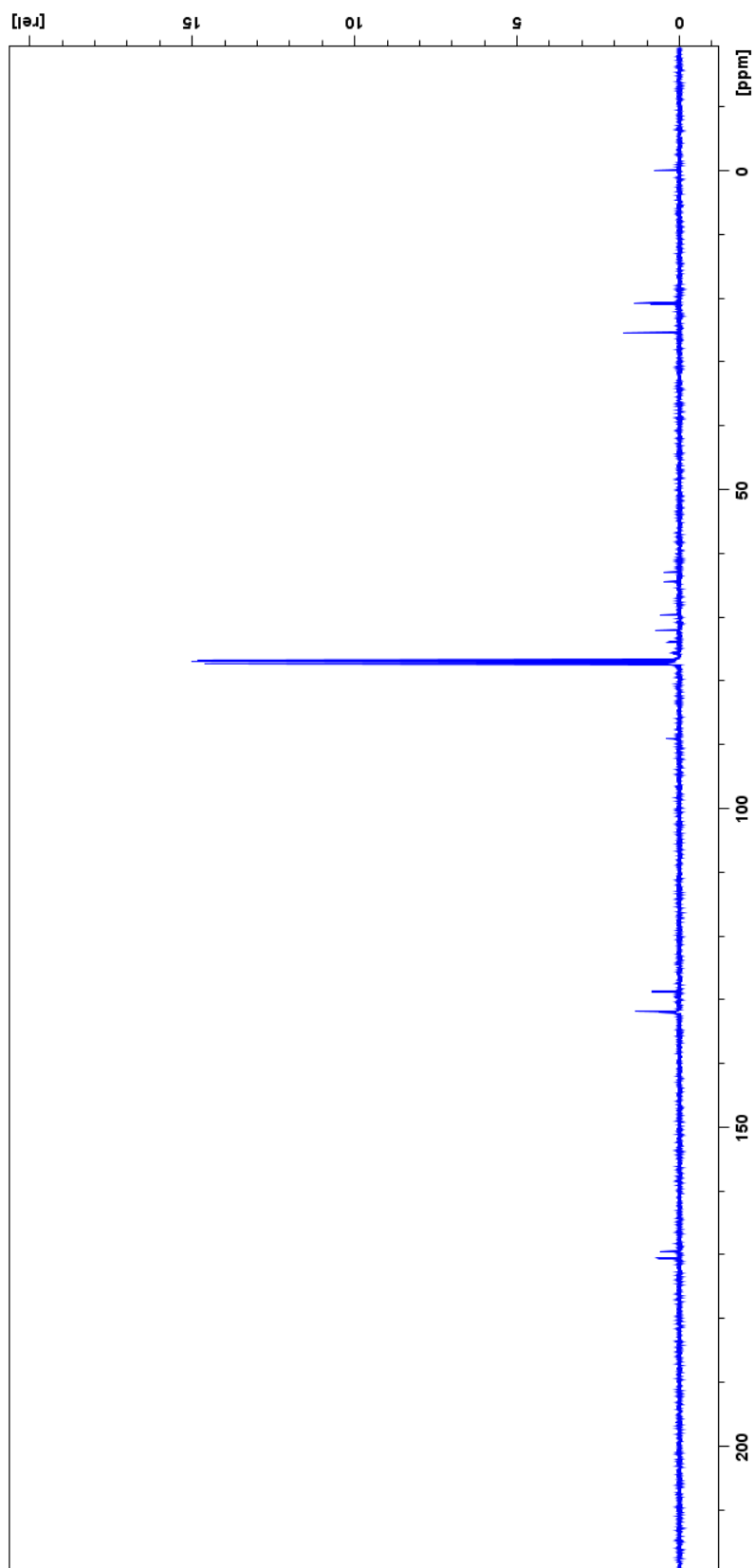


**Figure 40.** 100 MHz  $^{13}\text{C}$  NMR spectrum of 1,2-bis(diphenyl(2,3,4,6)-tetra-*O*-acetyl- $\beta$ -D-glucopyranosyl-1-*N*-iminophosphorane) ethane (**5**) recrystallized in isopropyl alcohol.

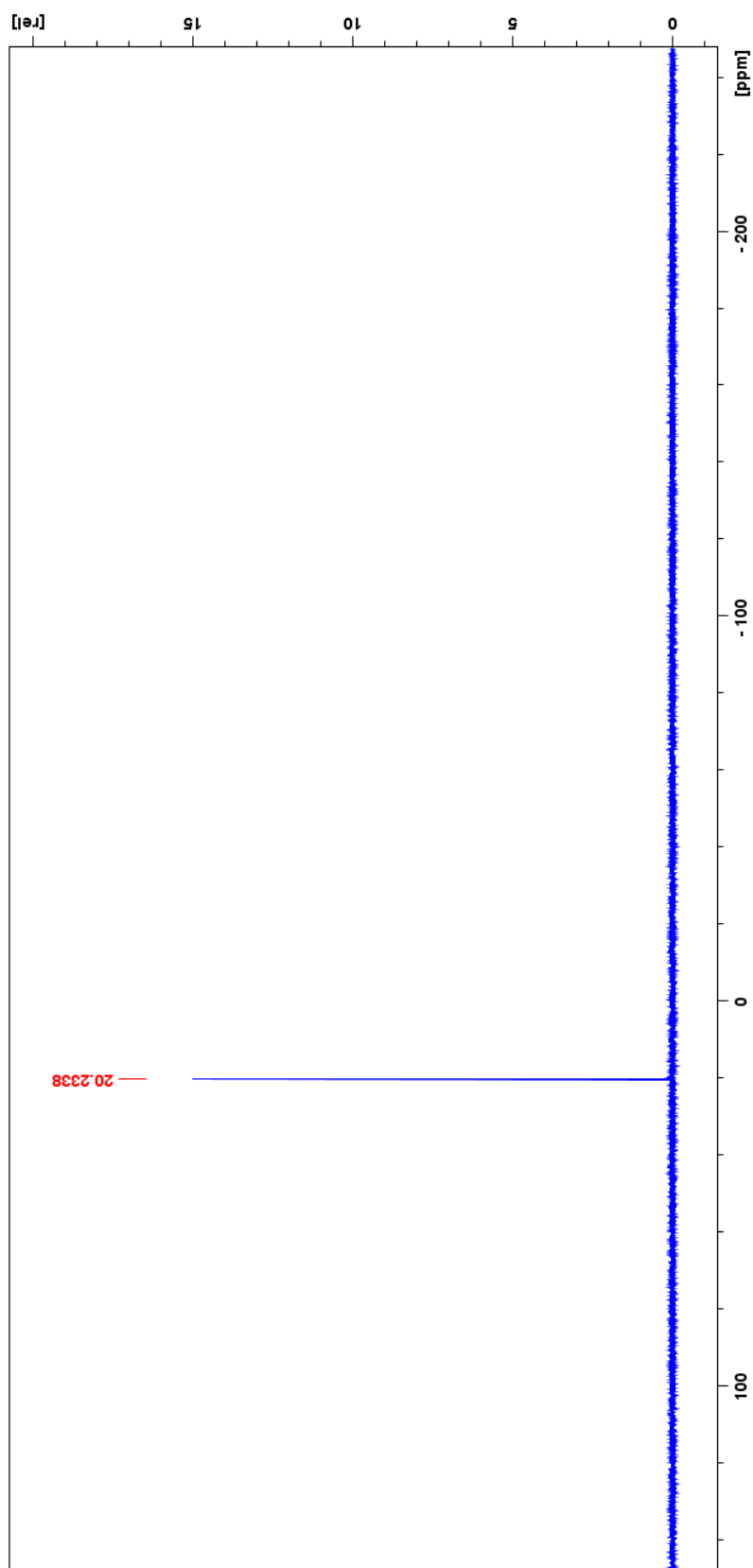


**Figure 41.** 167 MHz  $^{31}\text{P}$  NMR spectrum of 1,2-bis(diphenyl-(2,3,4,6)-tetra-*O*-acetyl- $\beta$ -D-glucopyranosyl)-1-*N*-iminophosphorane) ethane (**5**) recrystallized in isopropyl alcohol.

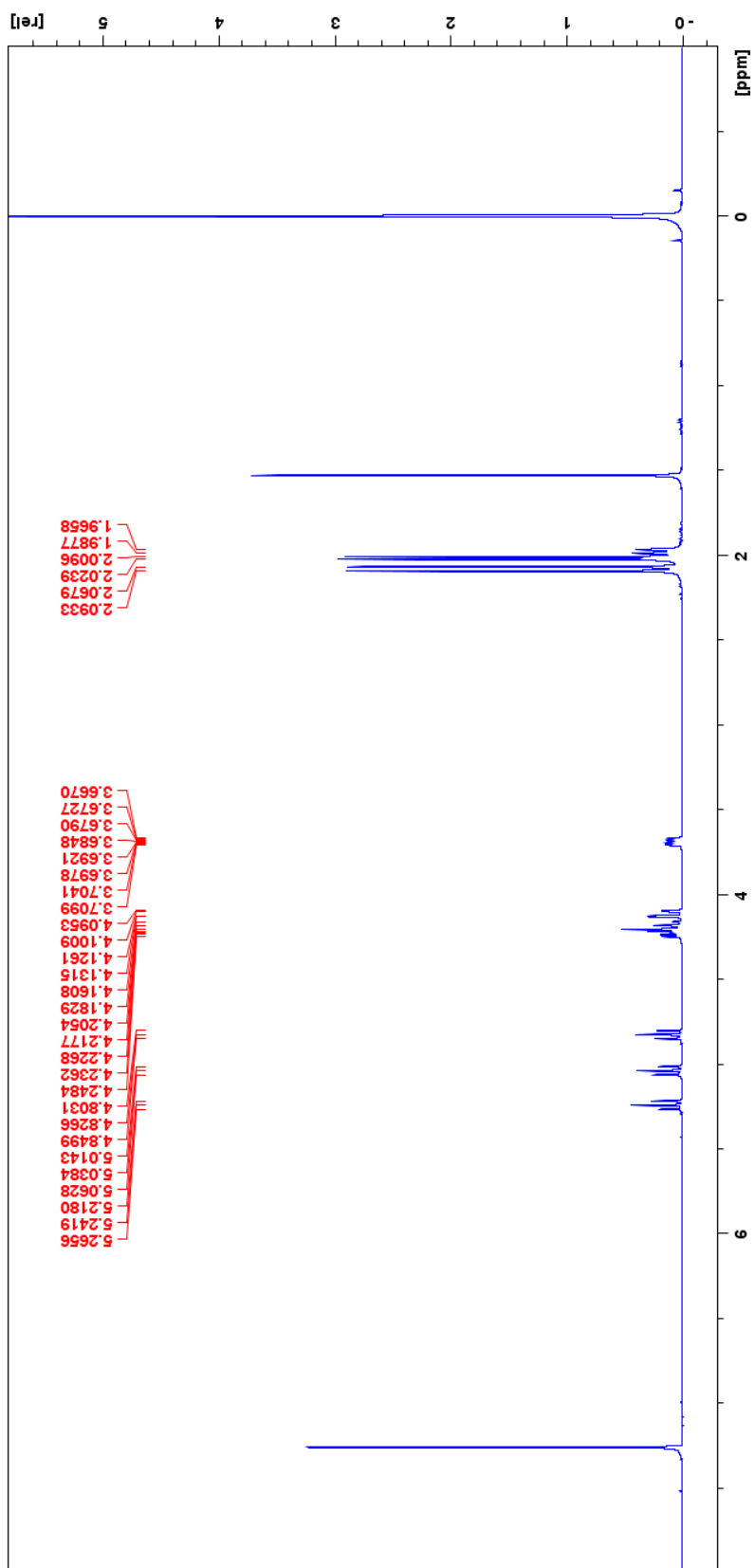
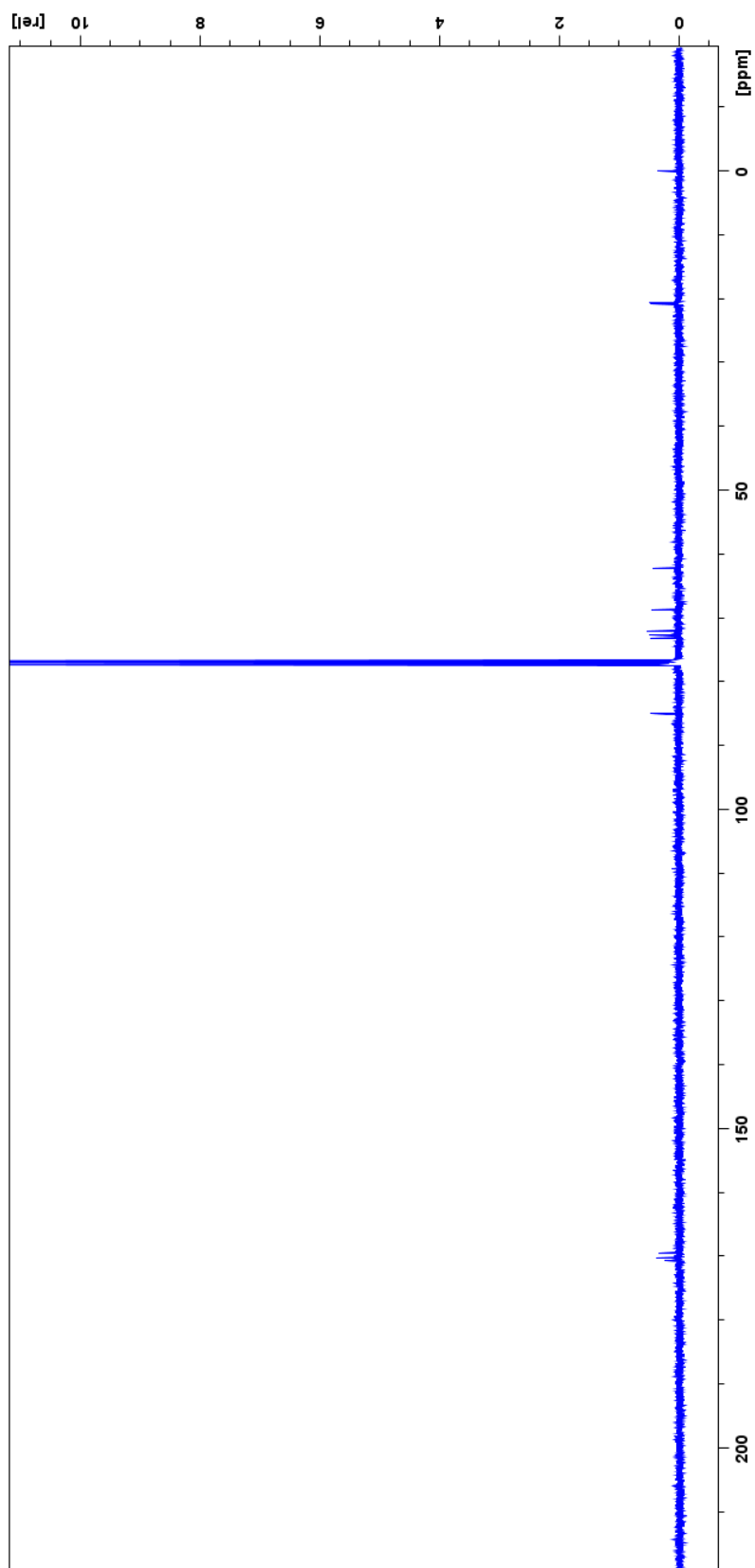


Figure 42. 400 MHz <sup>1</sup>H NMR spectrum of β-D-glucopyranosyl amine (6).



**Figure 43.** 100 MHz  $^{13}\text{C}$  NMR spectrum of  $\beta$ -D-glucopyranosyl amine (6).



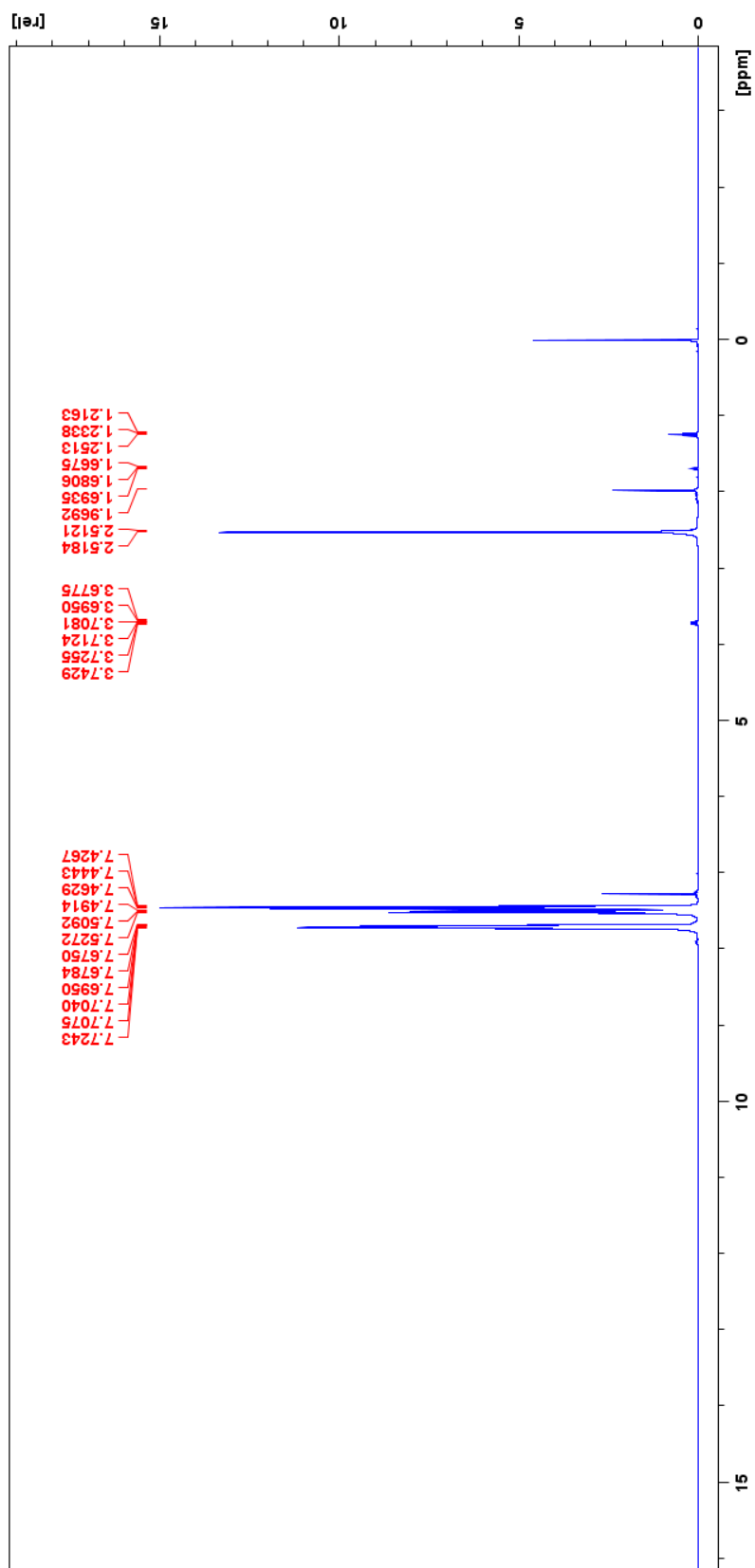
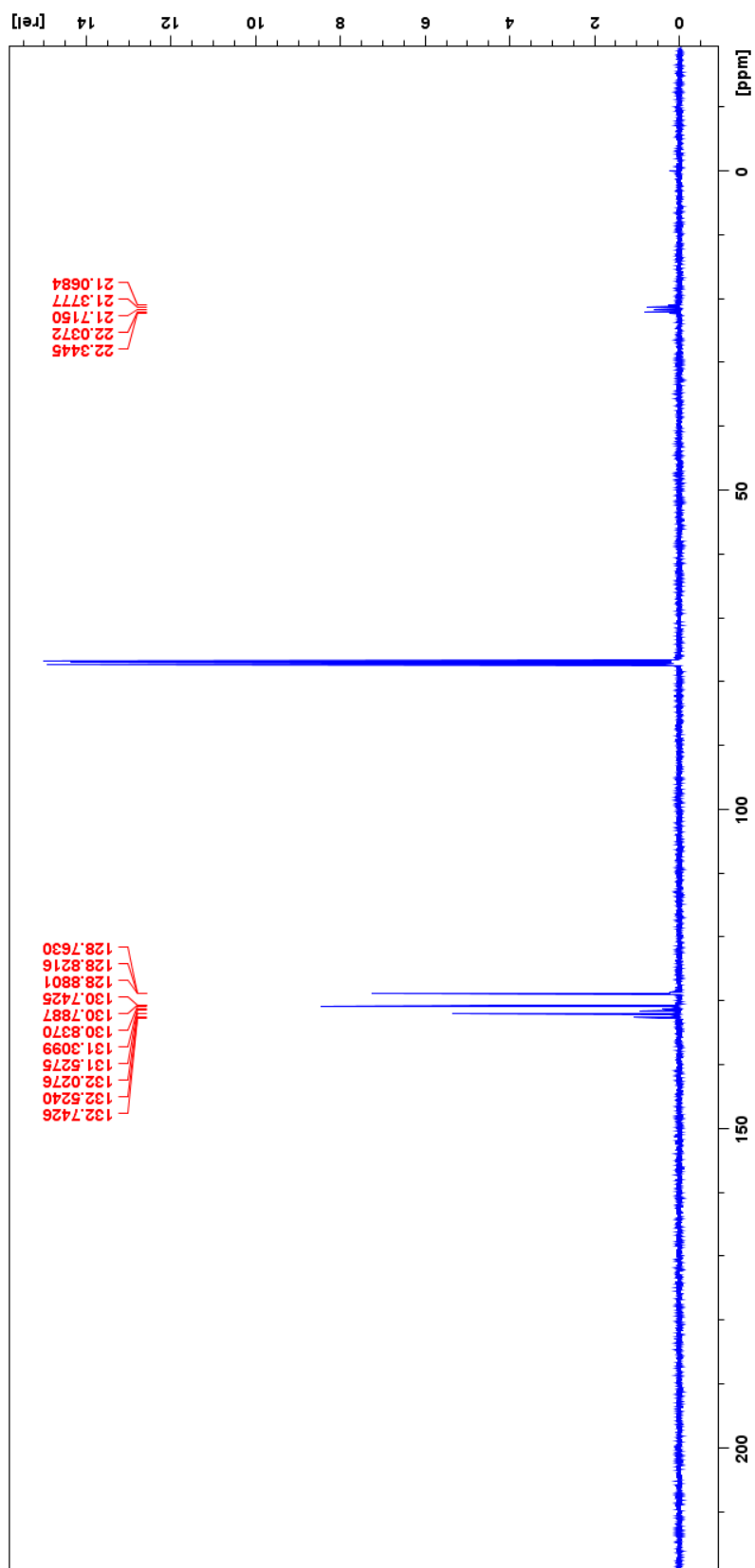
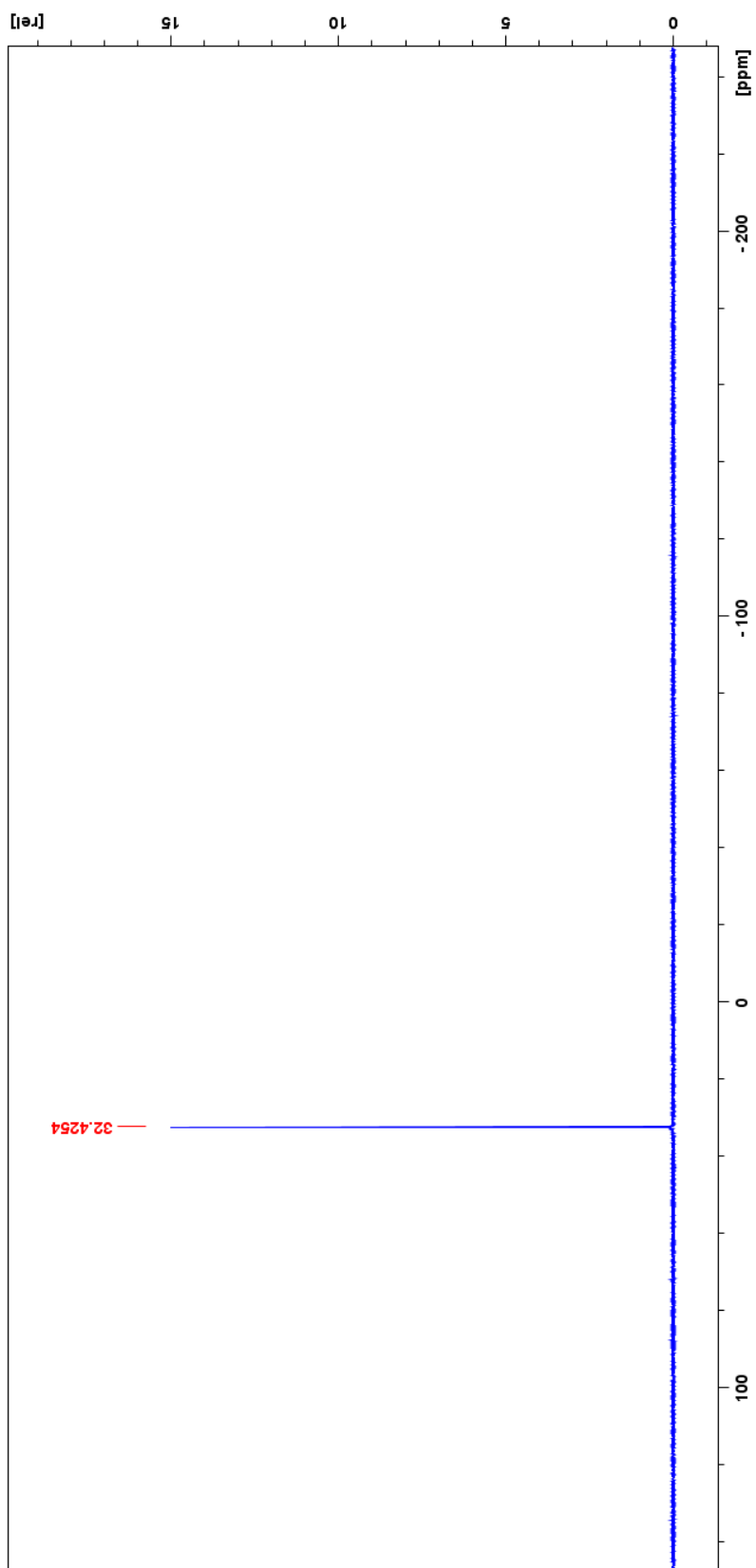


Figure 44. 400 MHz <sup>1</sup>H NMR spectrum of 1,2-ethanediybis(diphenylphosphine) dioxide (7).



**Figure 45.** 100 MHz  $^{13}\text{C}$  NMR spectrum of 1,2-ethanediybis(diphenylphosphine) dioxide (7).



**Figure 46.** 167 MHz  $^{31}\text{P}$  NMR spectrum of 1,2-ethanediyldis(diphenylphosphine) dioxide (7).

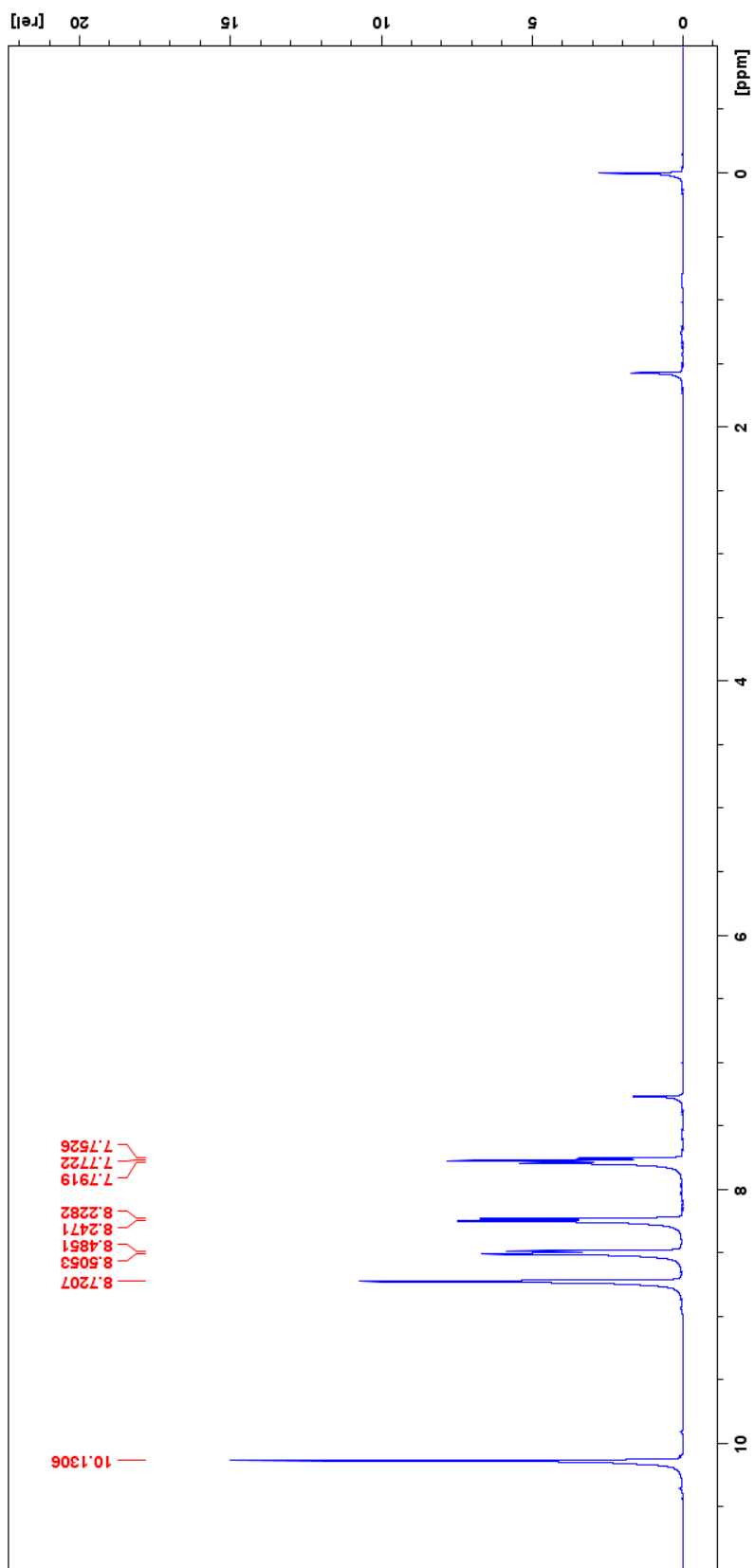


Figure 47. 400 MHz <sup>1</sup>H NMR spectrum of 3-nitrobenzaldehyde (**8a**).

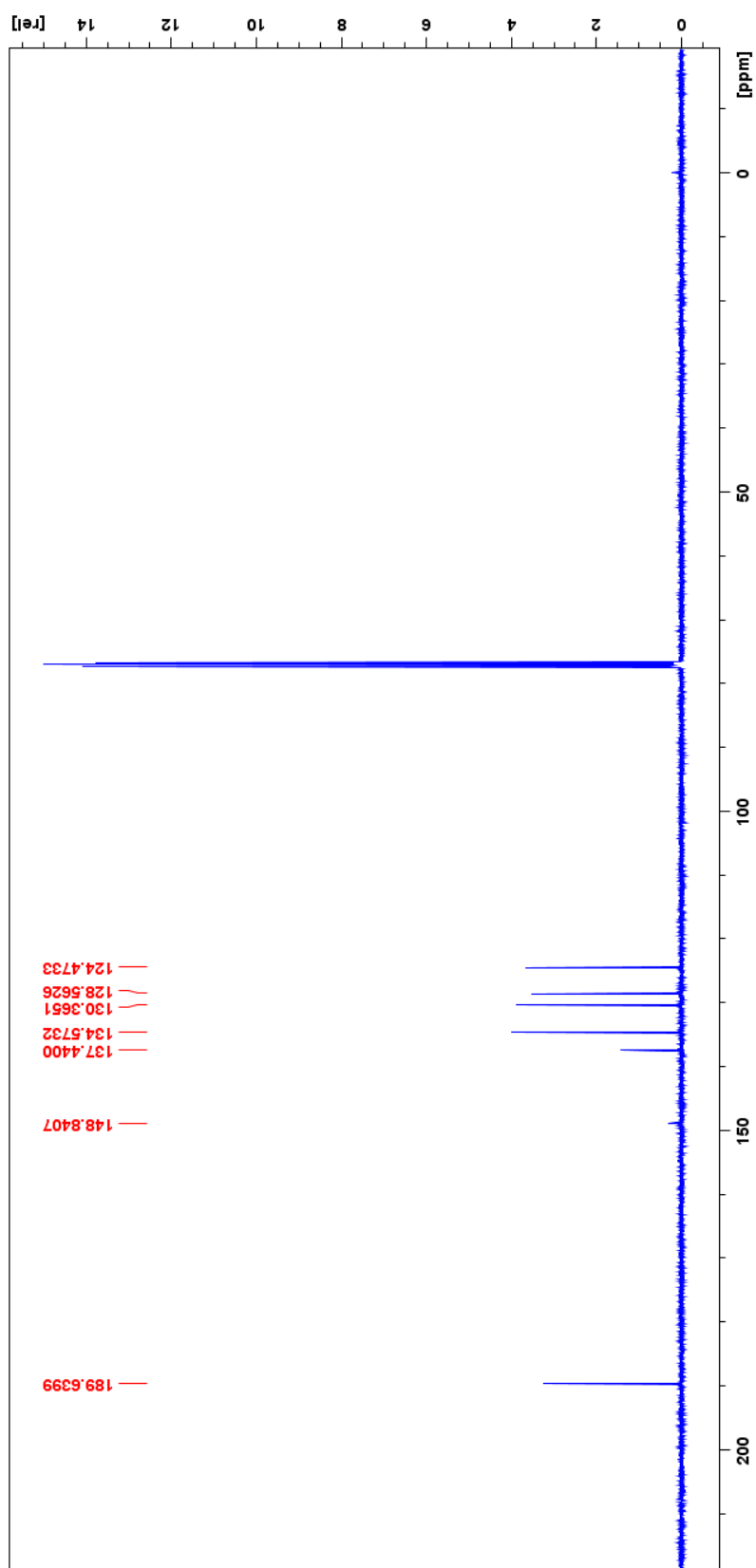


Figure 48. 100 MHz  $^{13}\text{C}$  NMR spectrum of 3-nitrobenzaldehyde (**8a**).

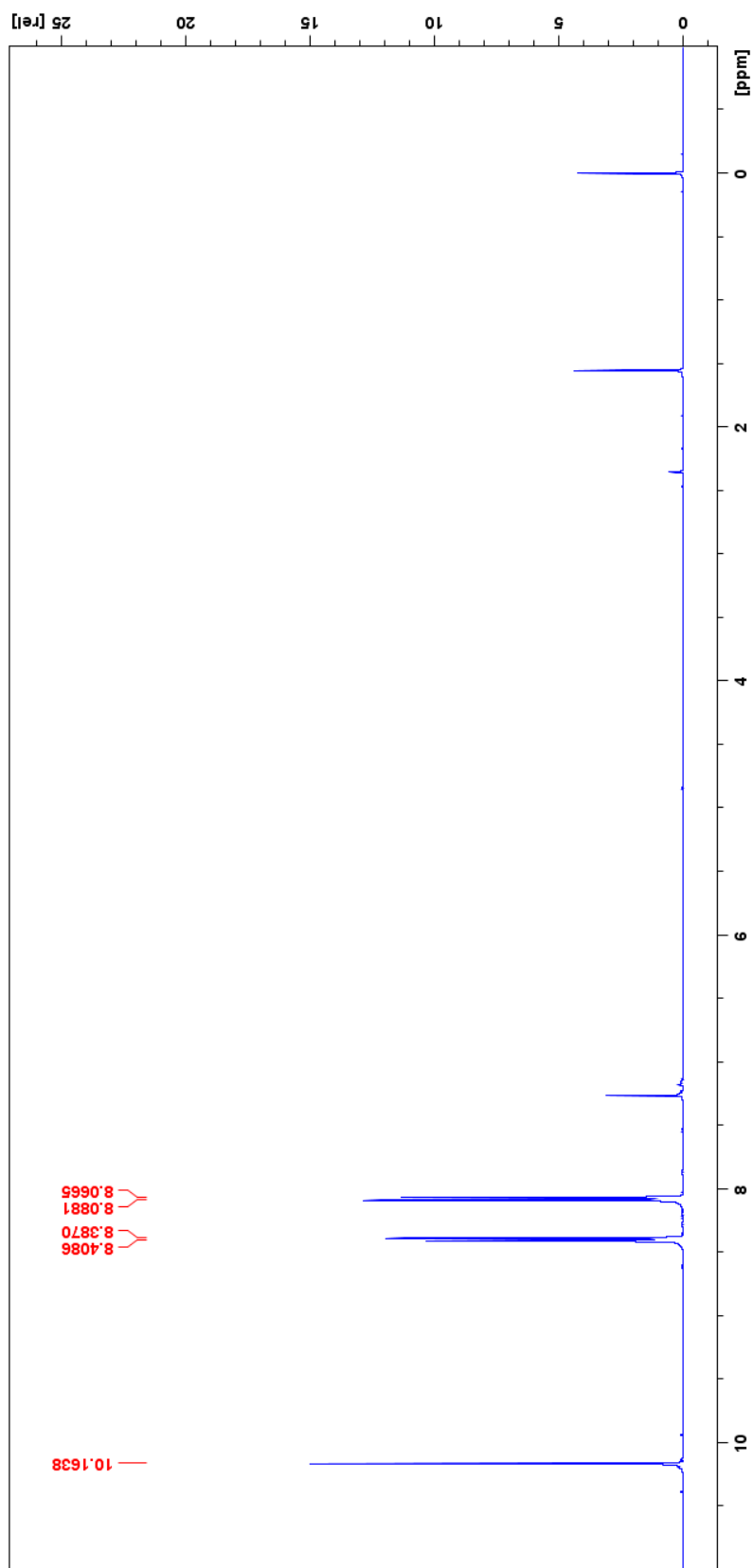
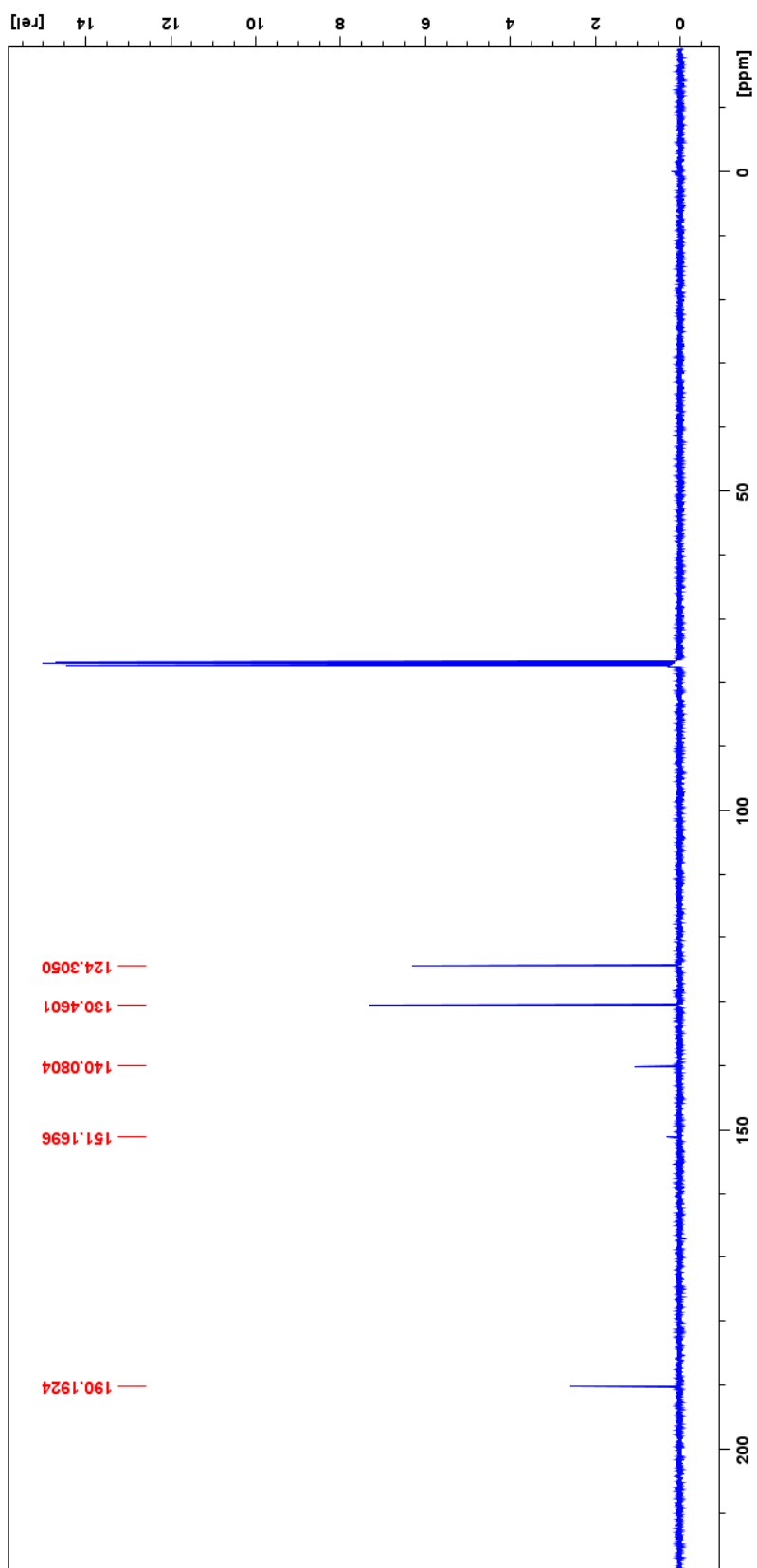


Figure 49. 400 MHz <sup>1</sup>H NMR spectrum of 4-nitrobenzaldehyde (8b).



**Figure 50.** 100 MHz  $^{13}\text{C}$  NMR spectrum of 4-nitrobenzaldehyde (**8b**).

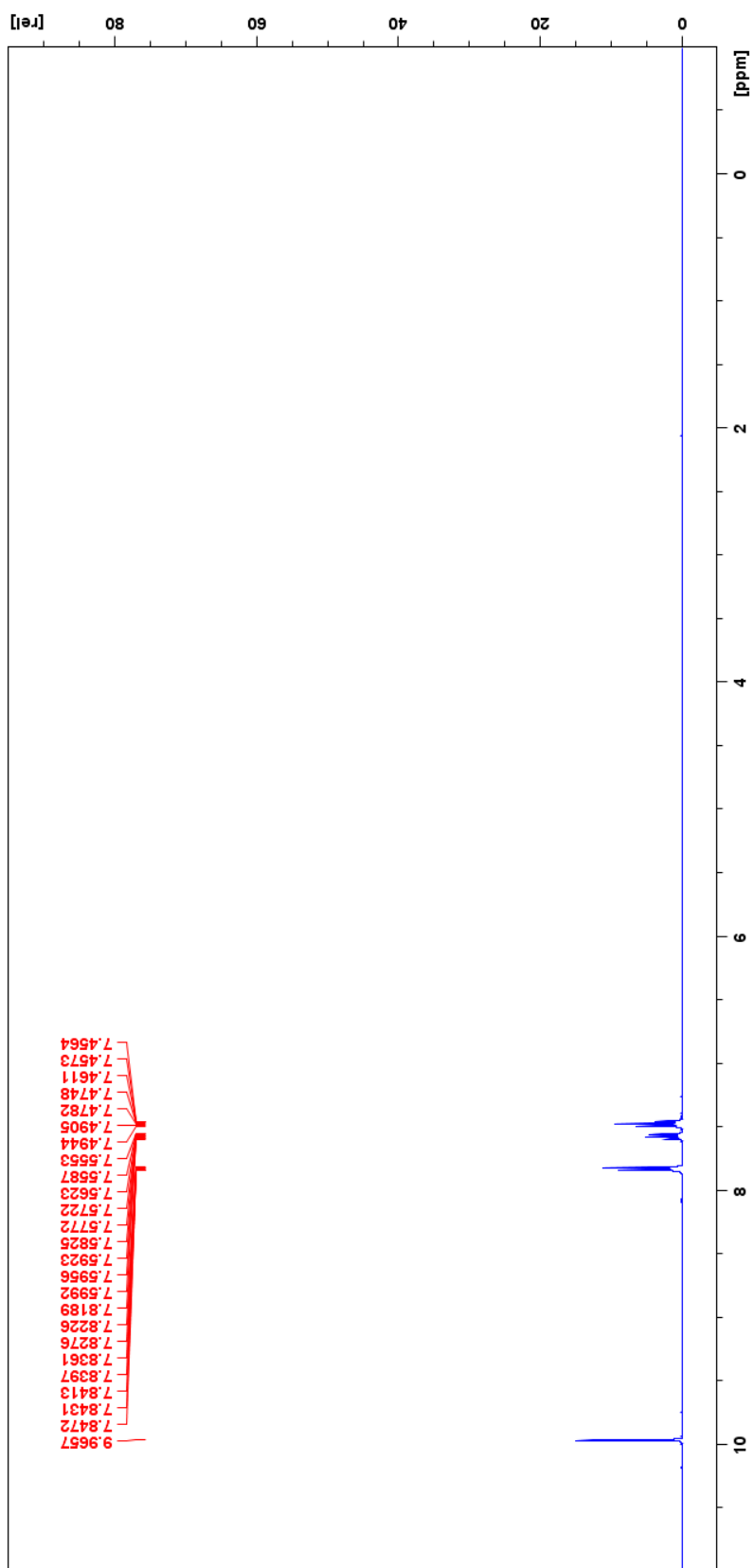


Figure 51. 400 MHz <sup>1</sup>H NMR spectrum of benzaldehyde (8c).



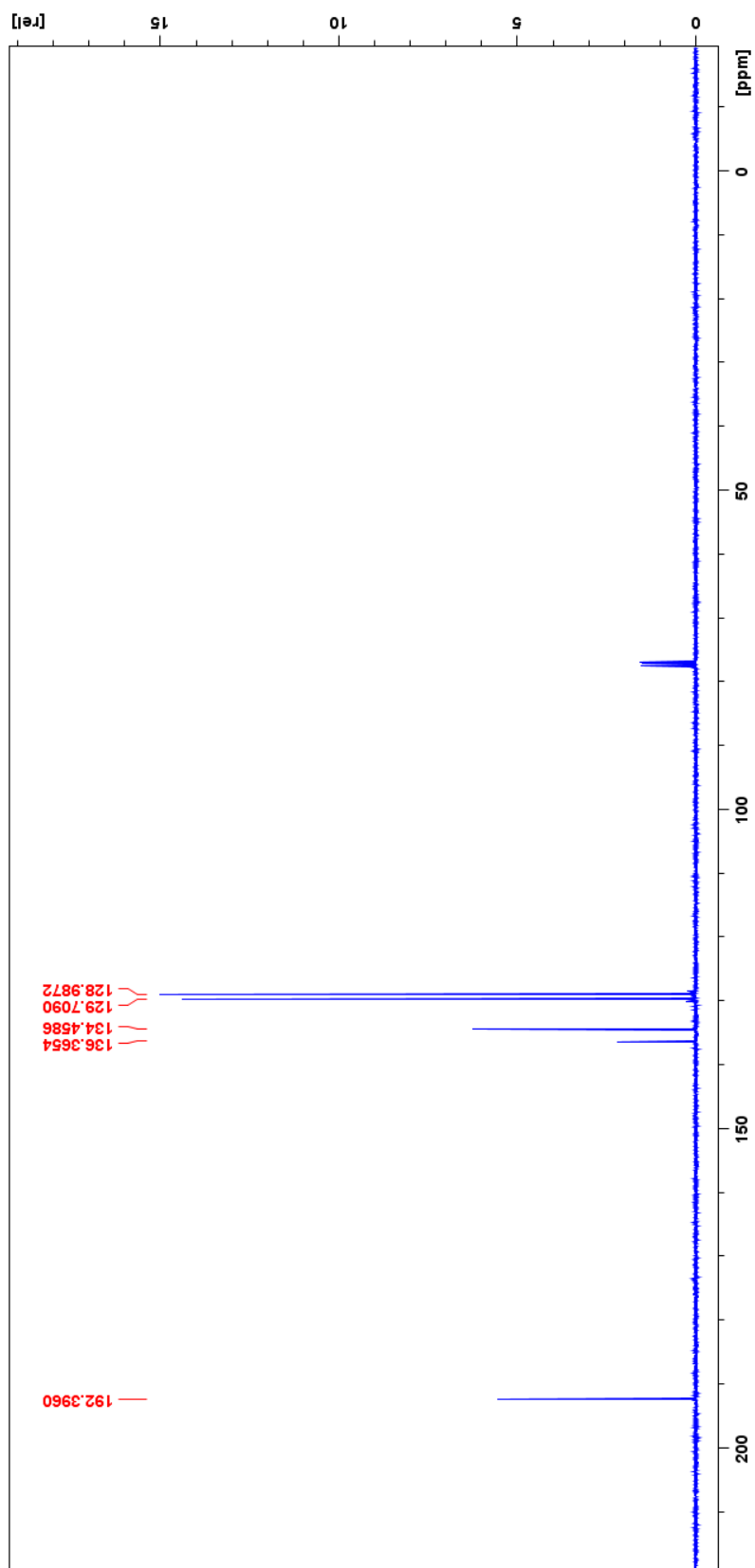


Figure S2. 100 MHz  $^{13}\text{C}$  NMR spectrum of benzaldehyde (8c).

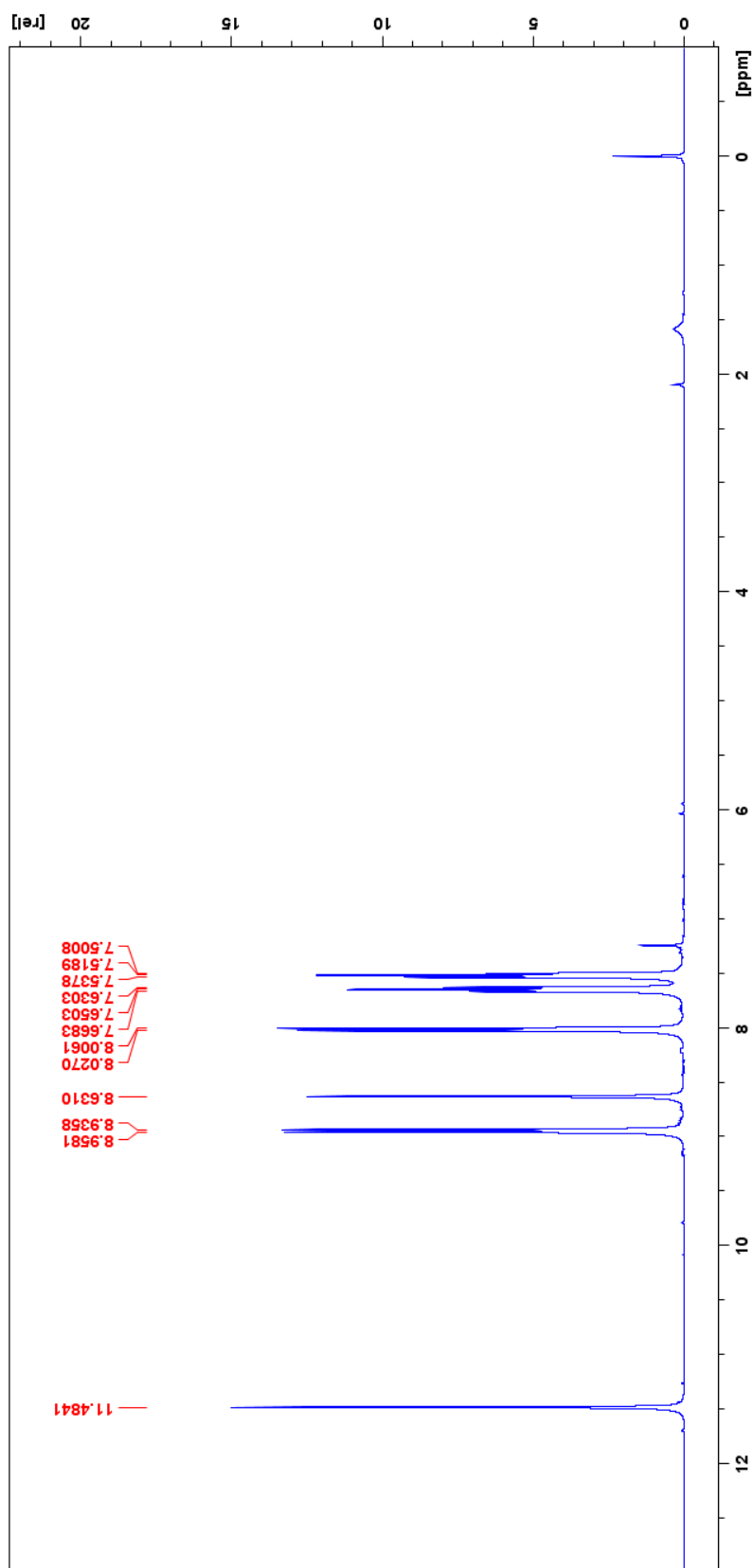


Figure 53. 400 MHz <sup>1</sup>H NMR spectrum of 9-anthracenecarboxaldehyde (8d).

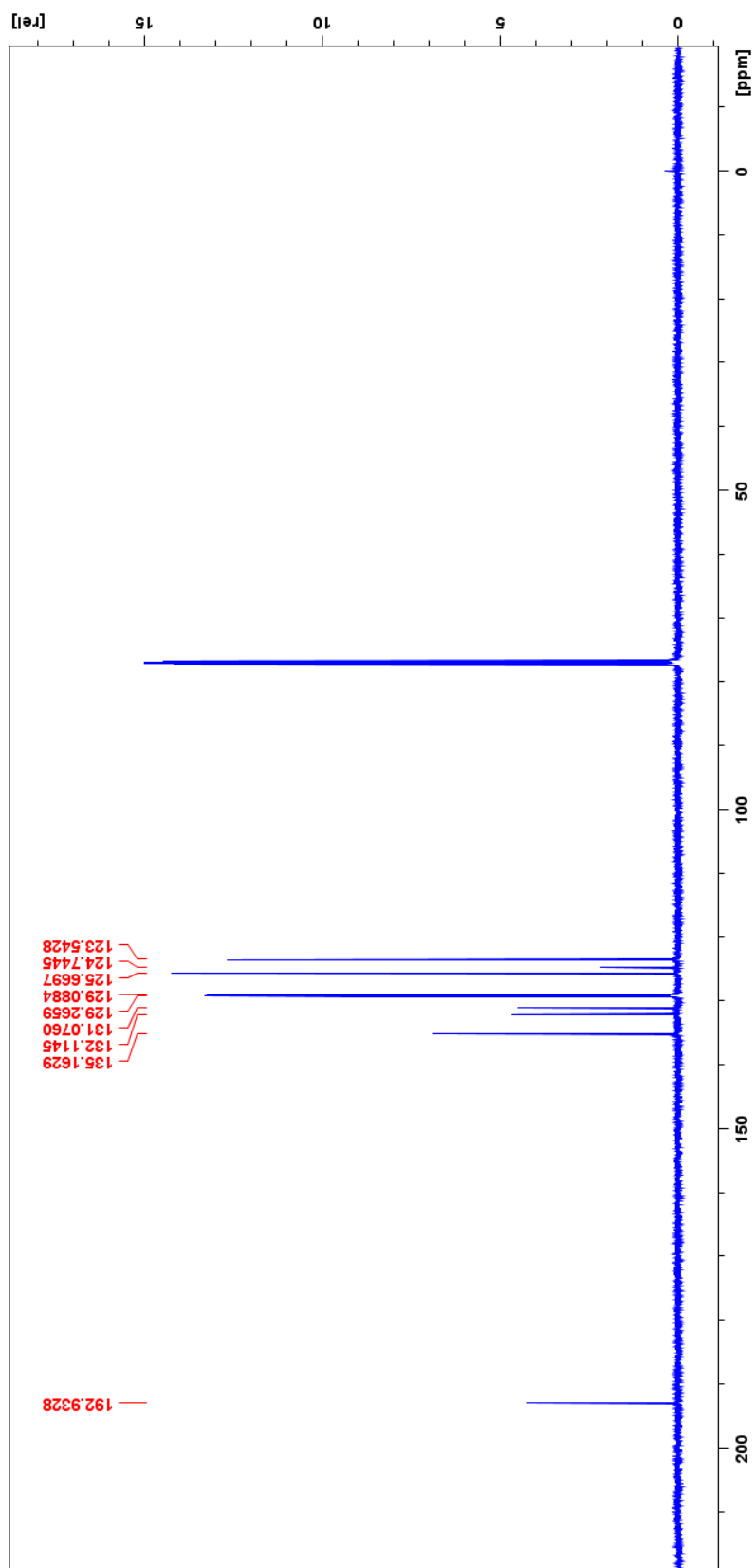


Figure 54. 100 MHz  $^{13}\text{C}$  NMR spectrum of 9-anthracenecarboxaldehyde (8d).

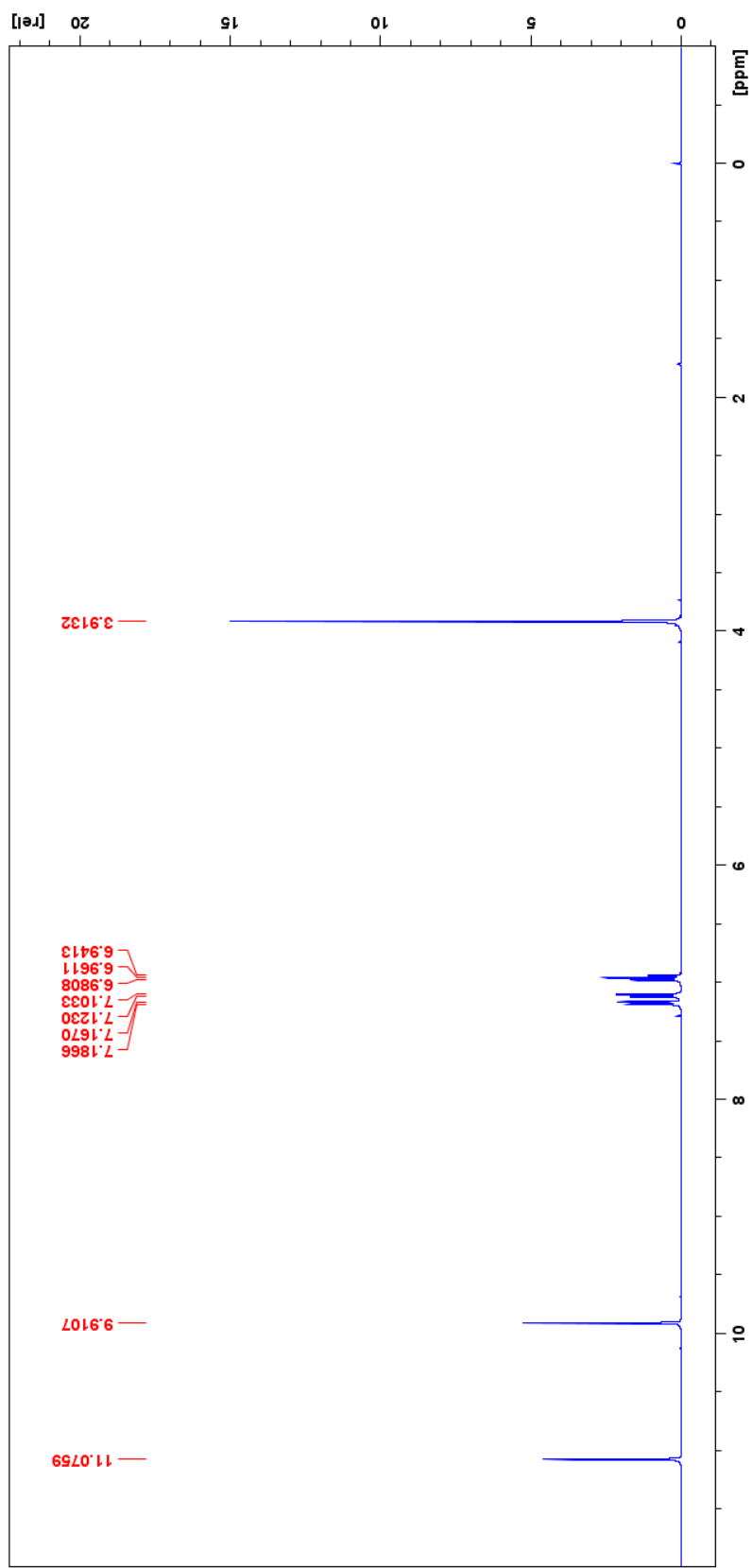
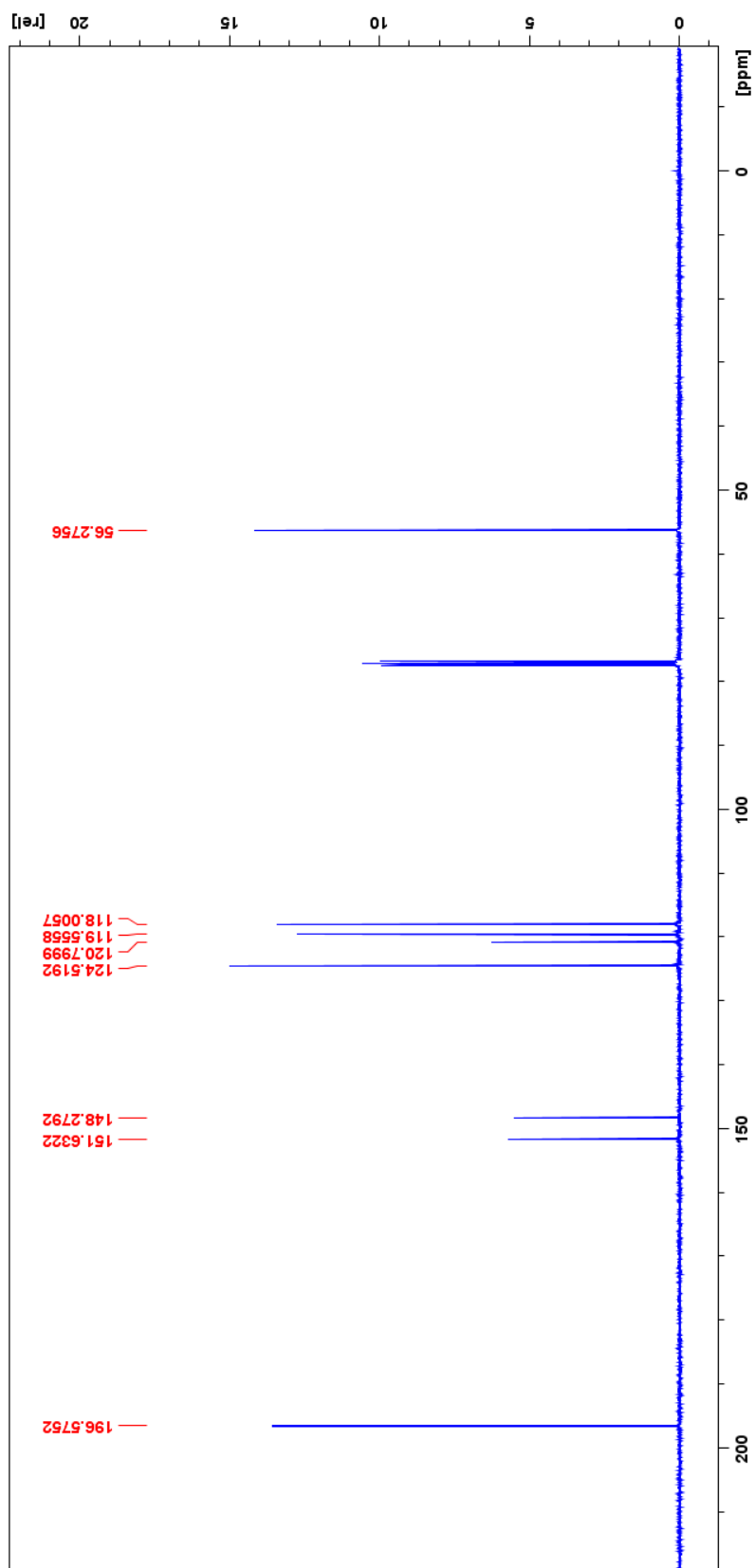


Figure S5. 400 MHz <sup>1</sup>H NMR spectrum of 2-hydroxy-3-methoxybenzaldehyde (8e).



**Figure 56.** 100 MHz  $^{13}\text{C}$  NMR spectrum of 2-hydroxy-3-methoxybenzaldehyde (**8e**).

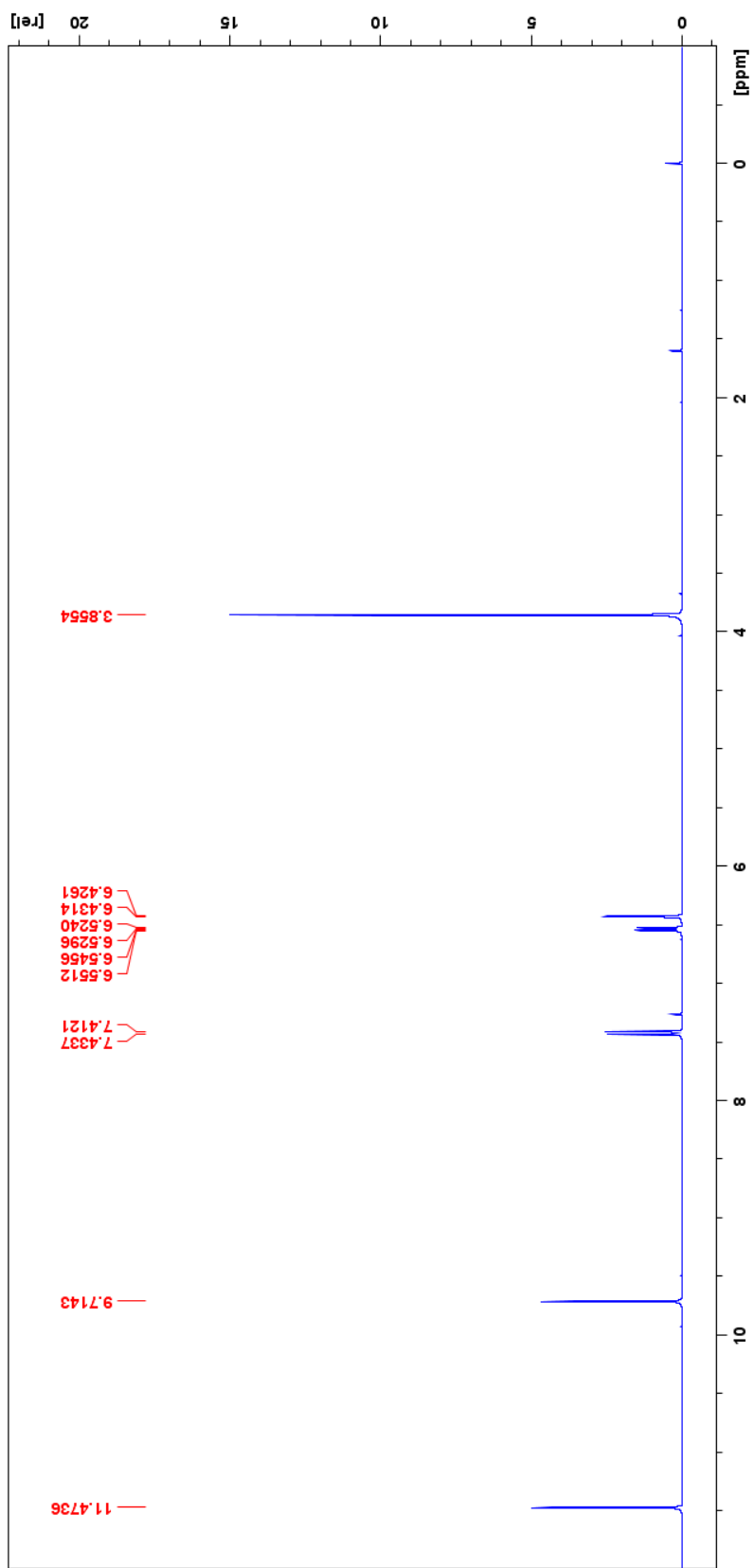


Figure S7. 400 MHz <sup>1</sup>H NMR spectrum of 2-hydroxy-4-methoxybenzaldehyde (8f).

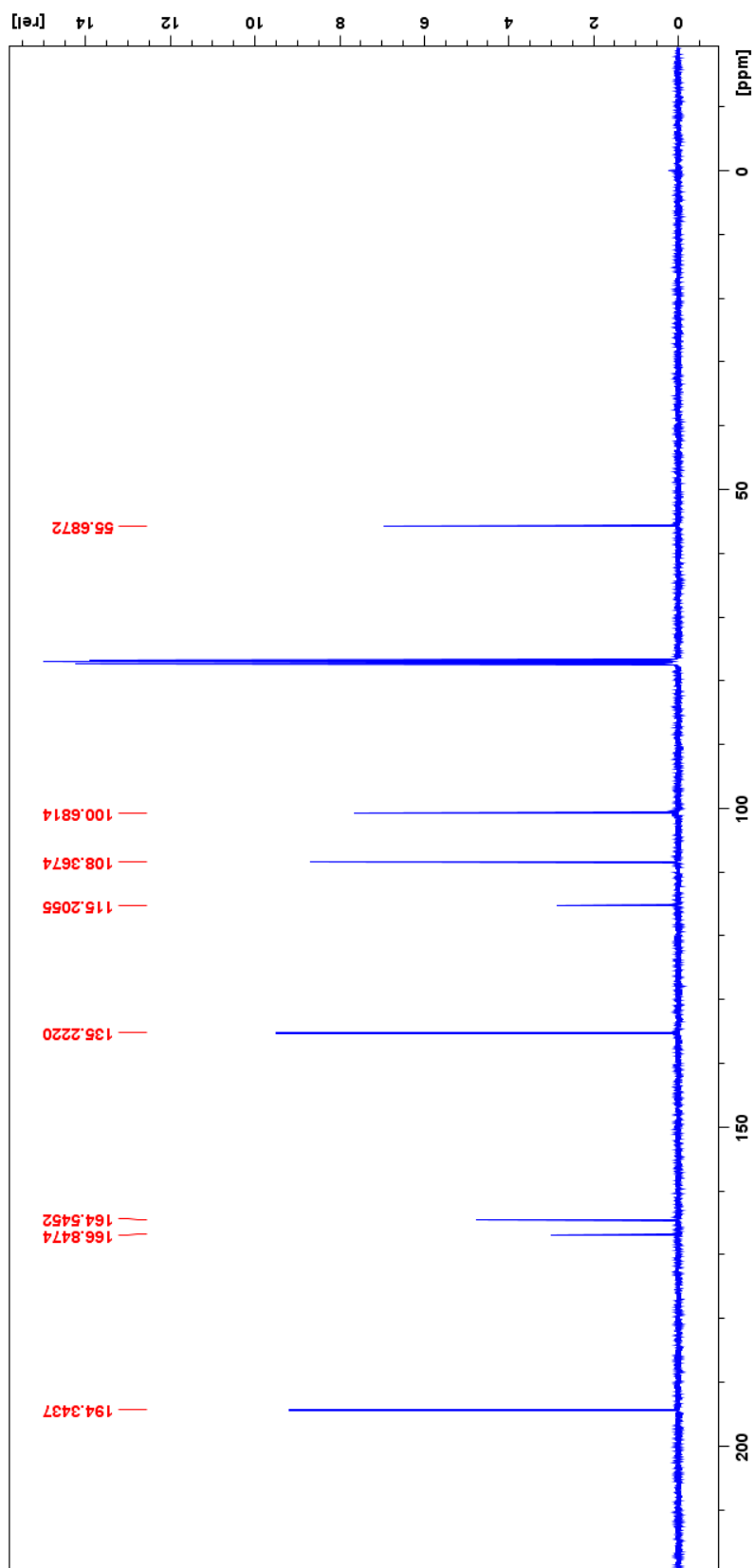


Figure 58. 100 MHz  $^{13}\text{C}$  NMR spectrum of 2-hydroxy-4-methoxybenzaldehyde (8f).

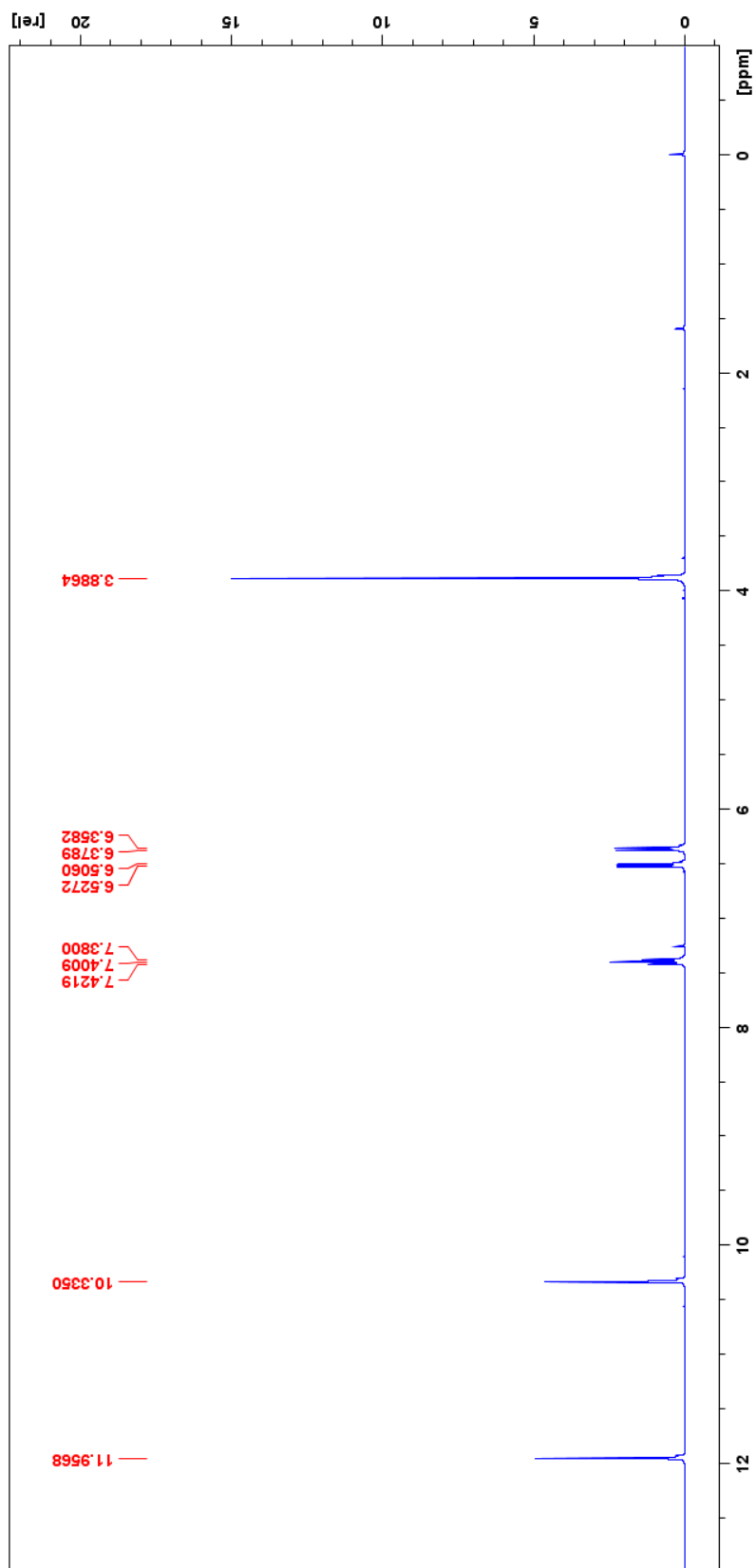
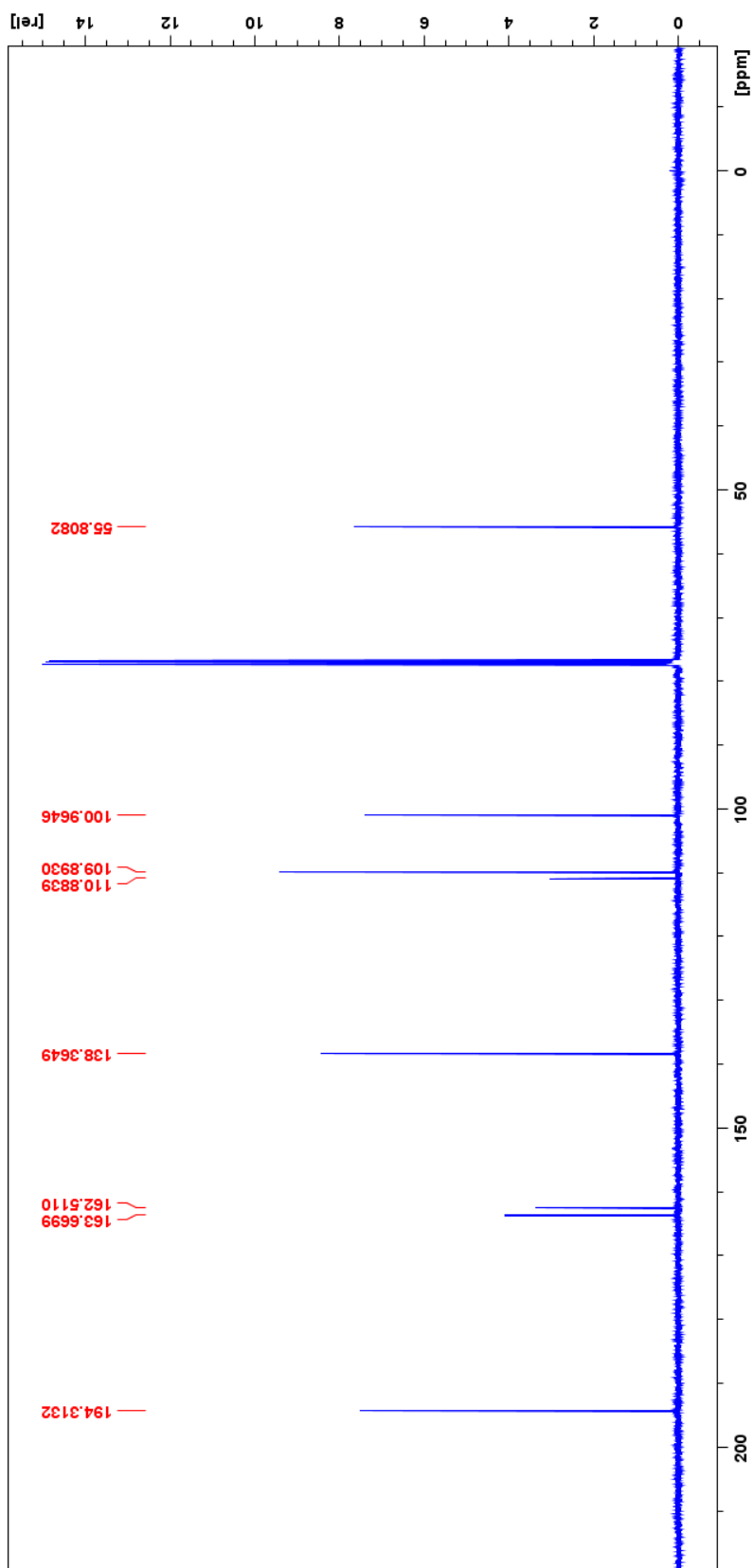


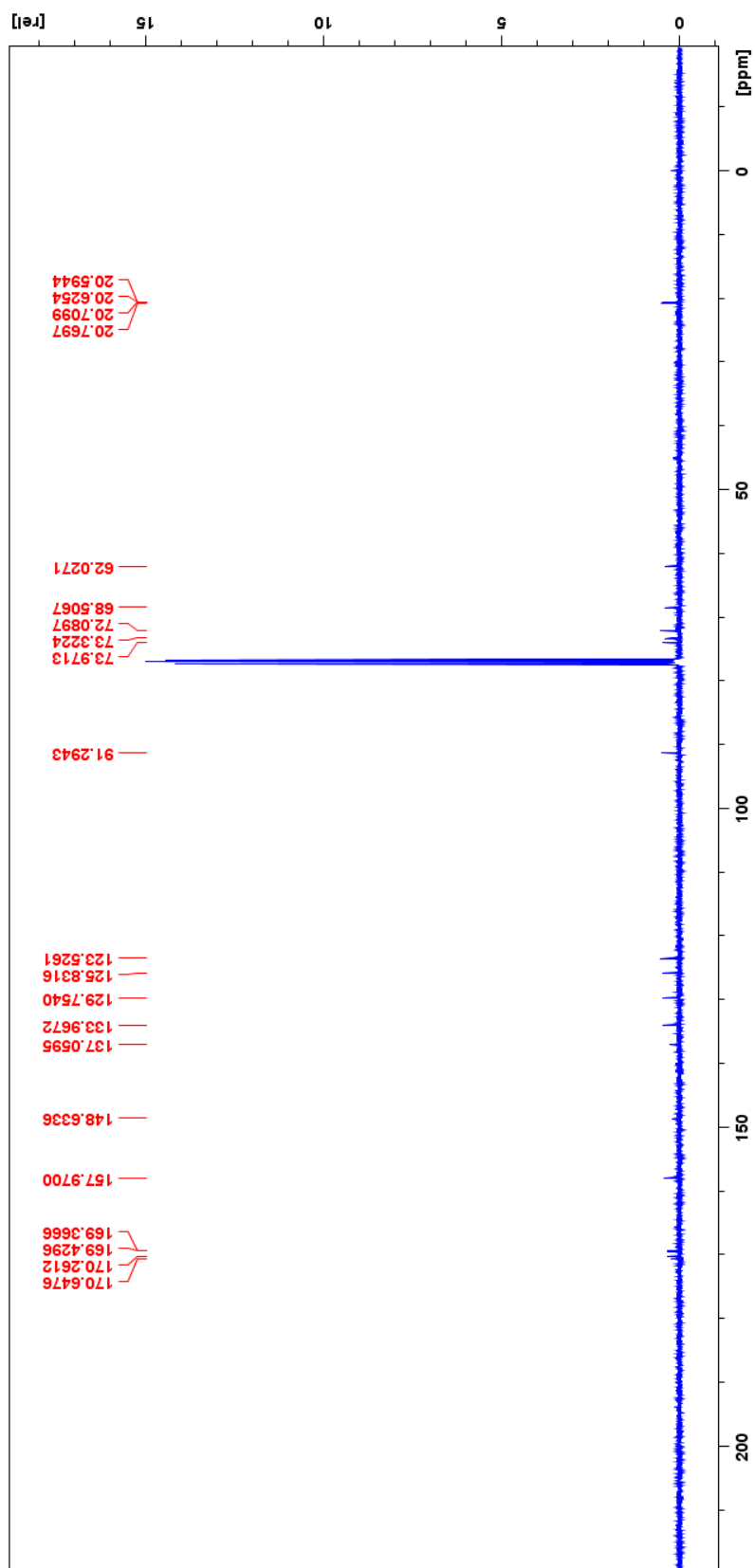
Figure S9. 400 MHz <sup>1</sup>H NMR spectrum of 2-hydroxy-6-methoxybenzaldehyde (8g).



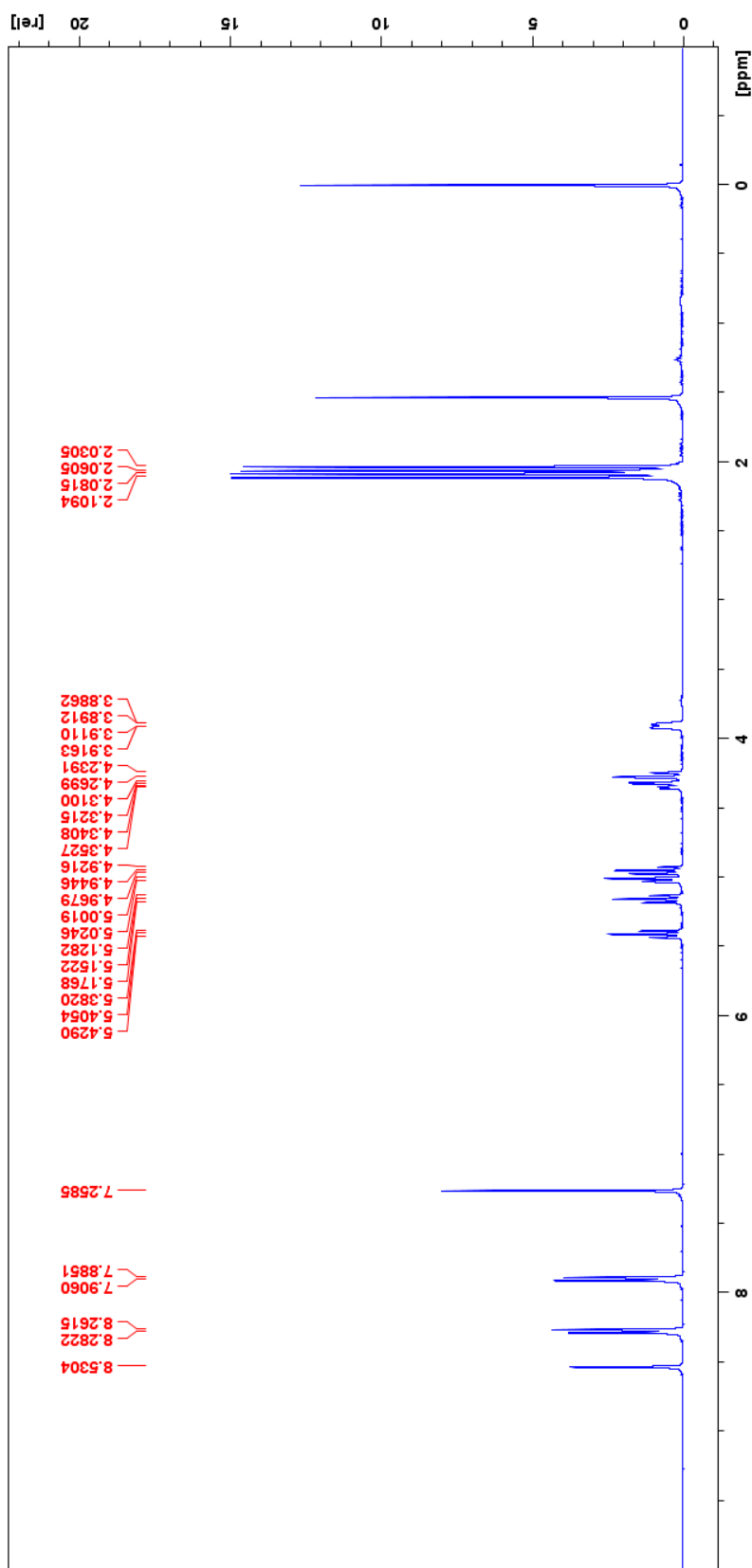


**Figure 60.** 100 MHz  $^{13}\text{C}$  NMR spectrum of 2-hydroxy-6-methoxybenzaldehyde (**8g**).

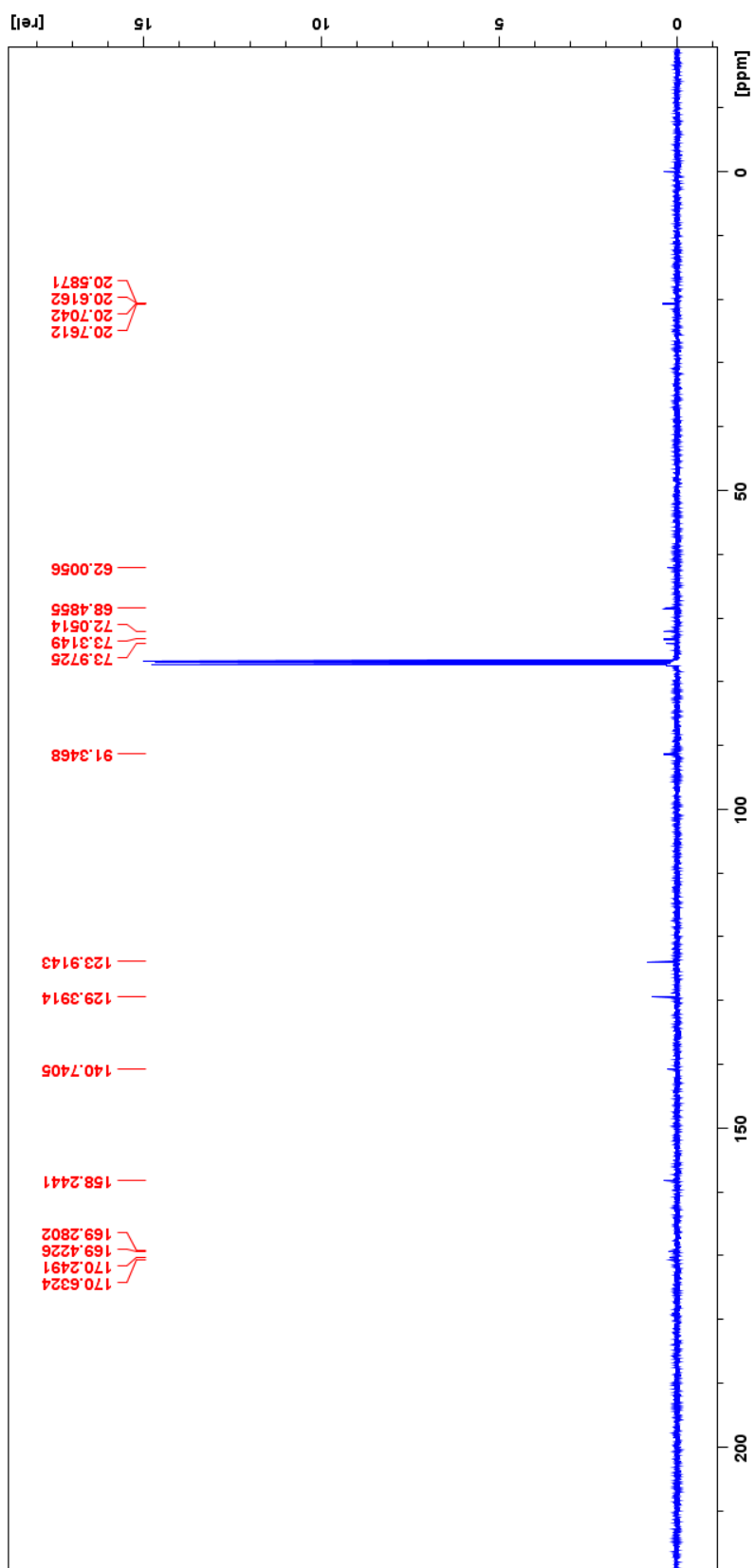




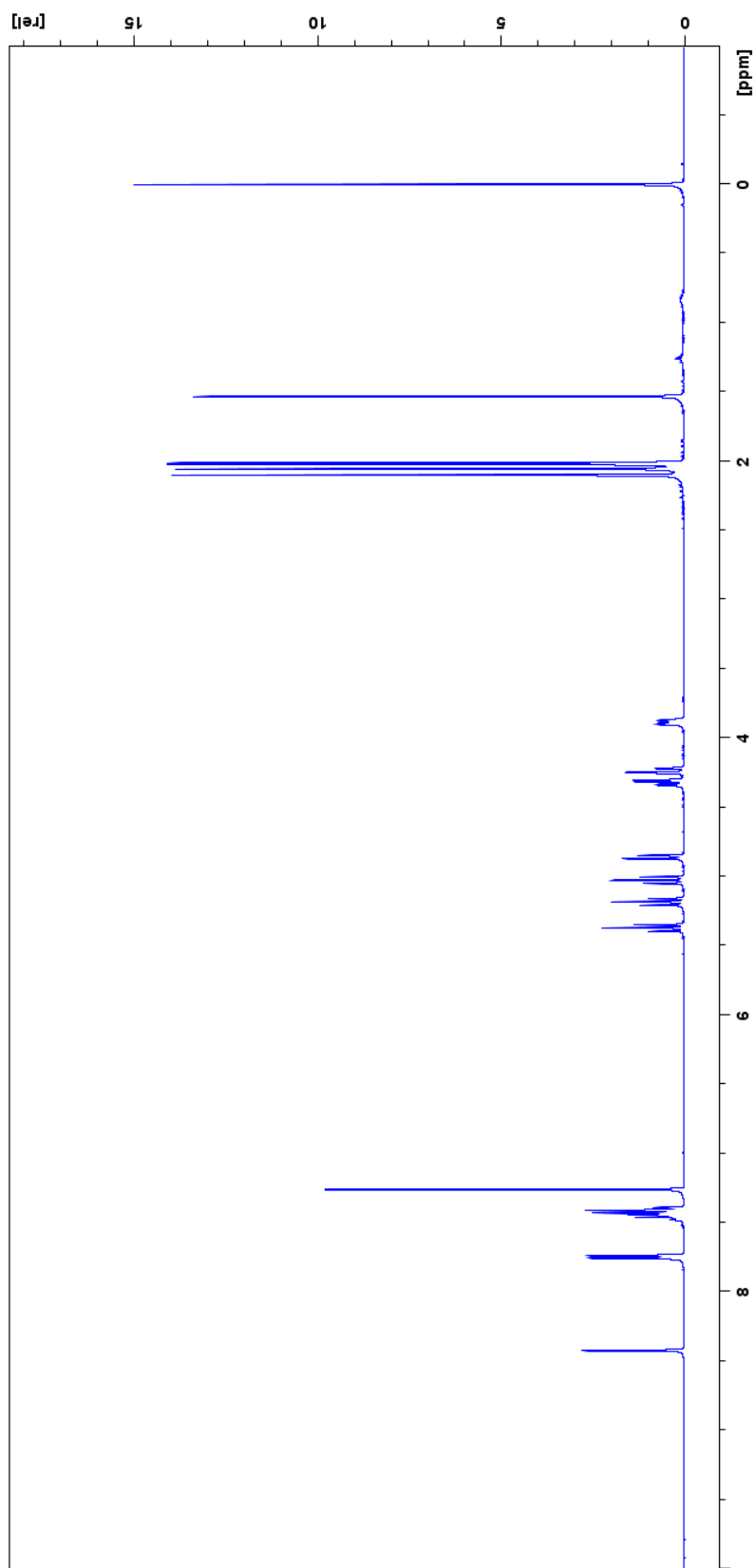
**Figure 62.** 100 MHz  $^{13}\text{C}$  NMR spectrum of *(E)*-(2,3,4,6)-tetra-*O*-acetyl- $\beta$ -D-glucopyranosyl-1-*N*-3-nitrobenzaldimine (**9a**).



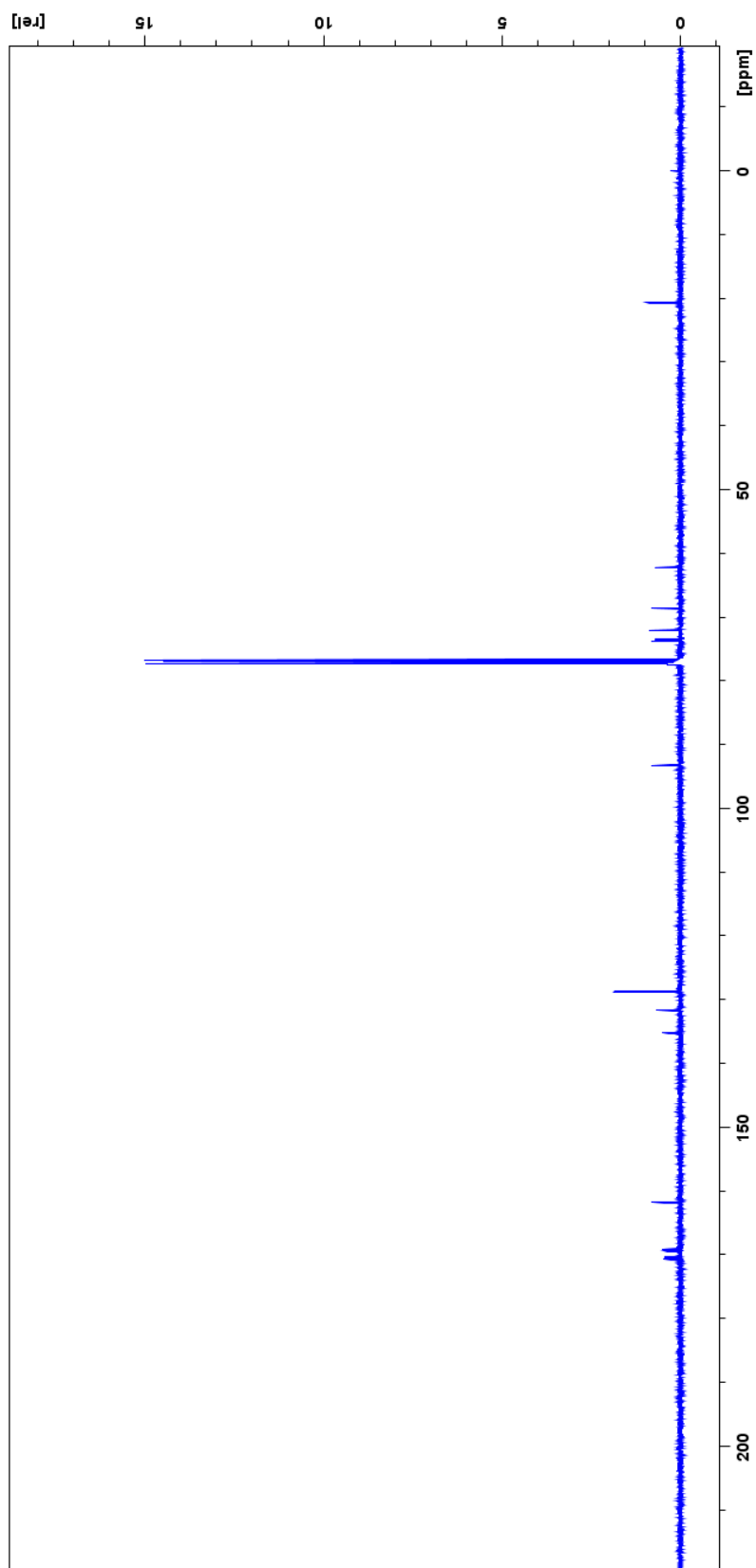
**Figure 63.** 400 MHz <sup>1</sup>H NMR spectrum of (E)-(2,3,4,6)-tetra-O-acetyl-β-D-glucopyranosyl-1-N-4-nitrobenzaldimine (9b).



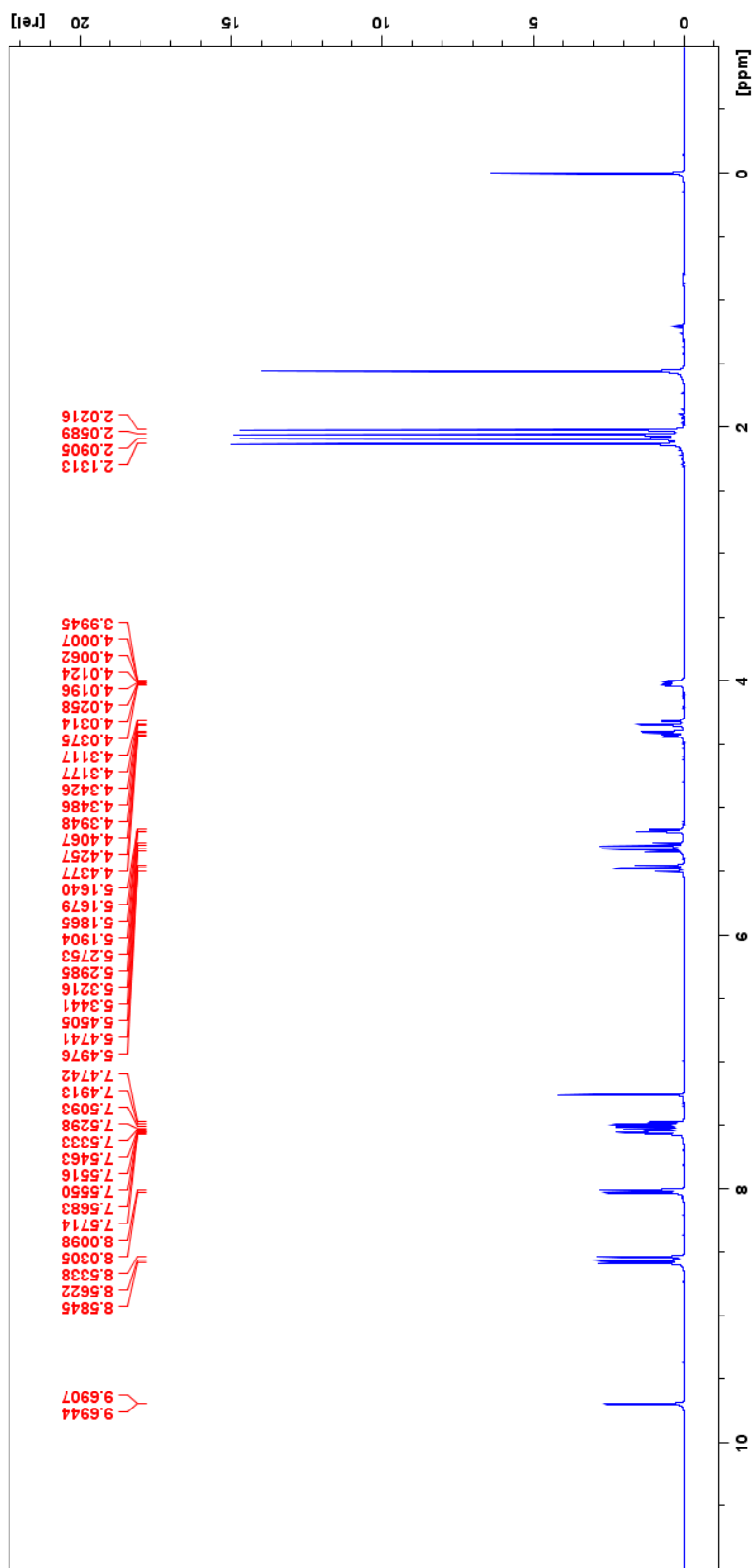
**Figure 64.** 100 MHz  $^{13}\text{C}$  NMR spectrum of  $(E)$ -(2,3,4,6)-tetra-*O*-acetyl- $\beta$ -D-glucopyranosyl-1-*N*-4-nitrobenzaldimine (9b).



**Figure 65.** 400 MHz <sup>1</sup>H NMR spectrum of (E)-(2,3,4,6)-tetra-O-acetyl-β-D-glucopyranosyl-1-N-benzaldimine (**9c**).

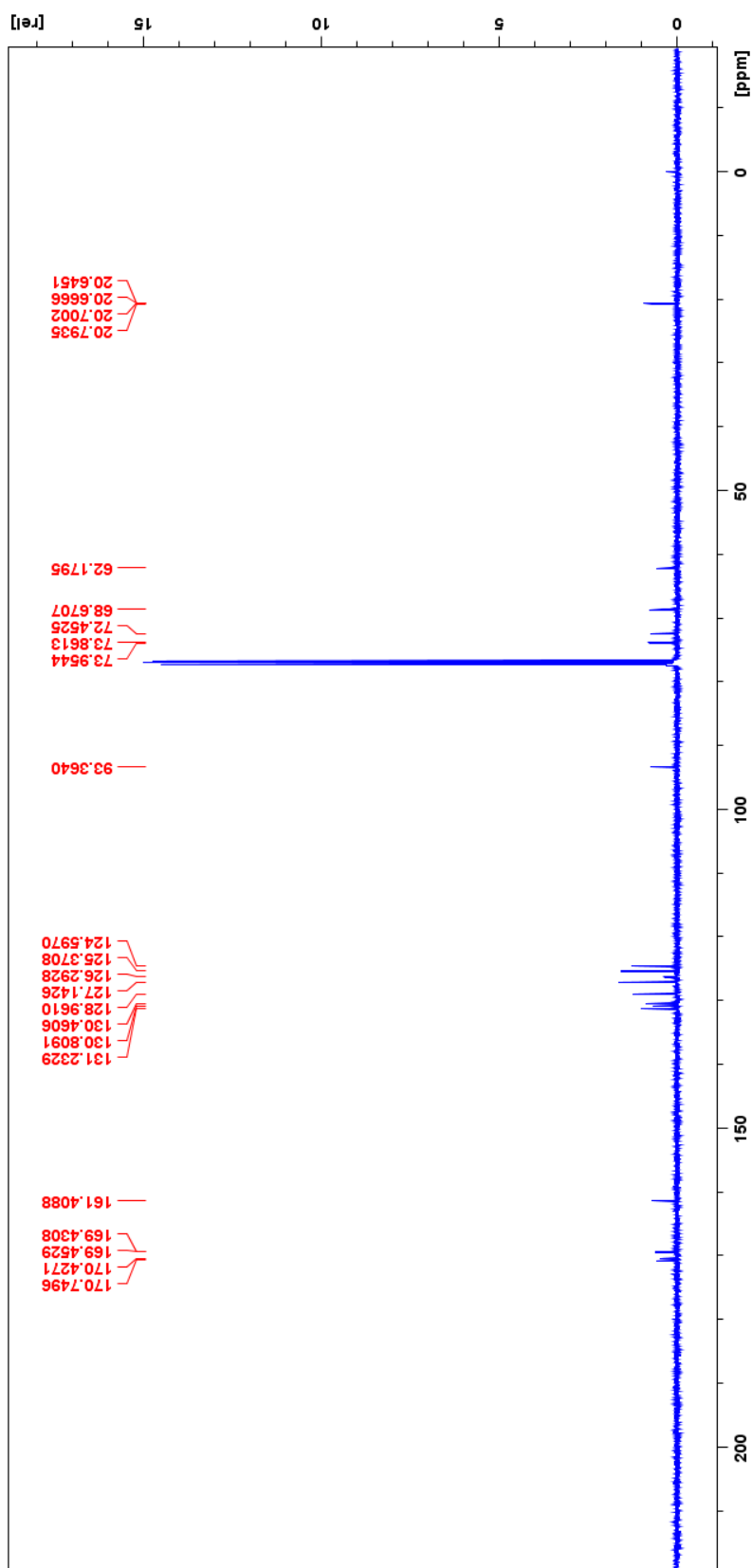


**Figure 66.** 100 MHz  $^{13}\text{C}$  NMR spectrum of  $(E)$ -(2,3,4,6)-tetra-*O*-acetyl- $\beta$ -D-glucopyranosyl-1-*N*-benzaldimine (**9c**).

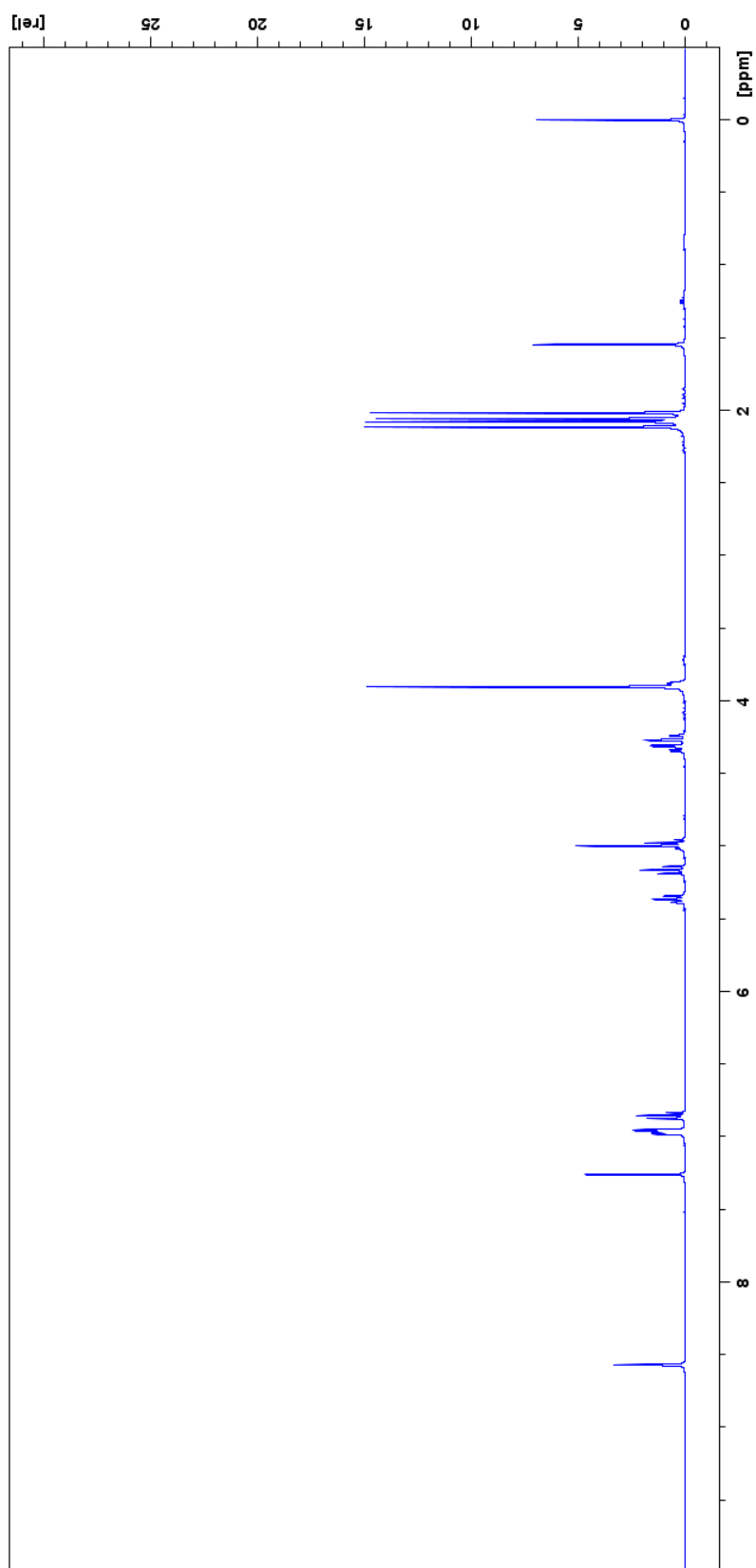


**Figure 67.** 400 MHz  $^1\text{H}$  NMR spectrum of *(E)*-(2,3,4,6)-tetra-*O*-acetyl- $\beta$ -D-alucopyranosyl-1-*N*-9-anthracenecarboxaldimine (**9d**).

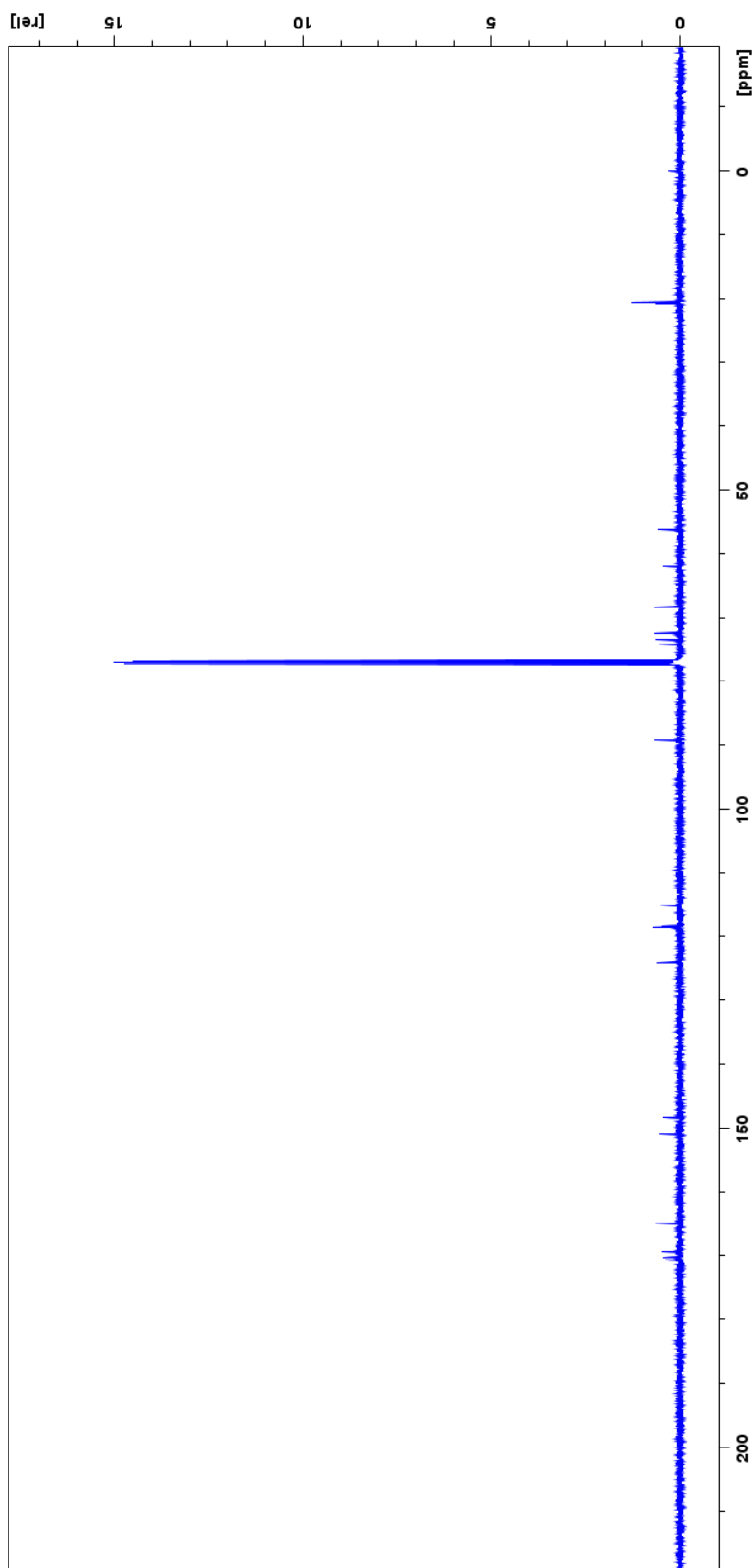




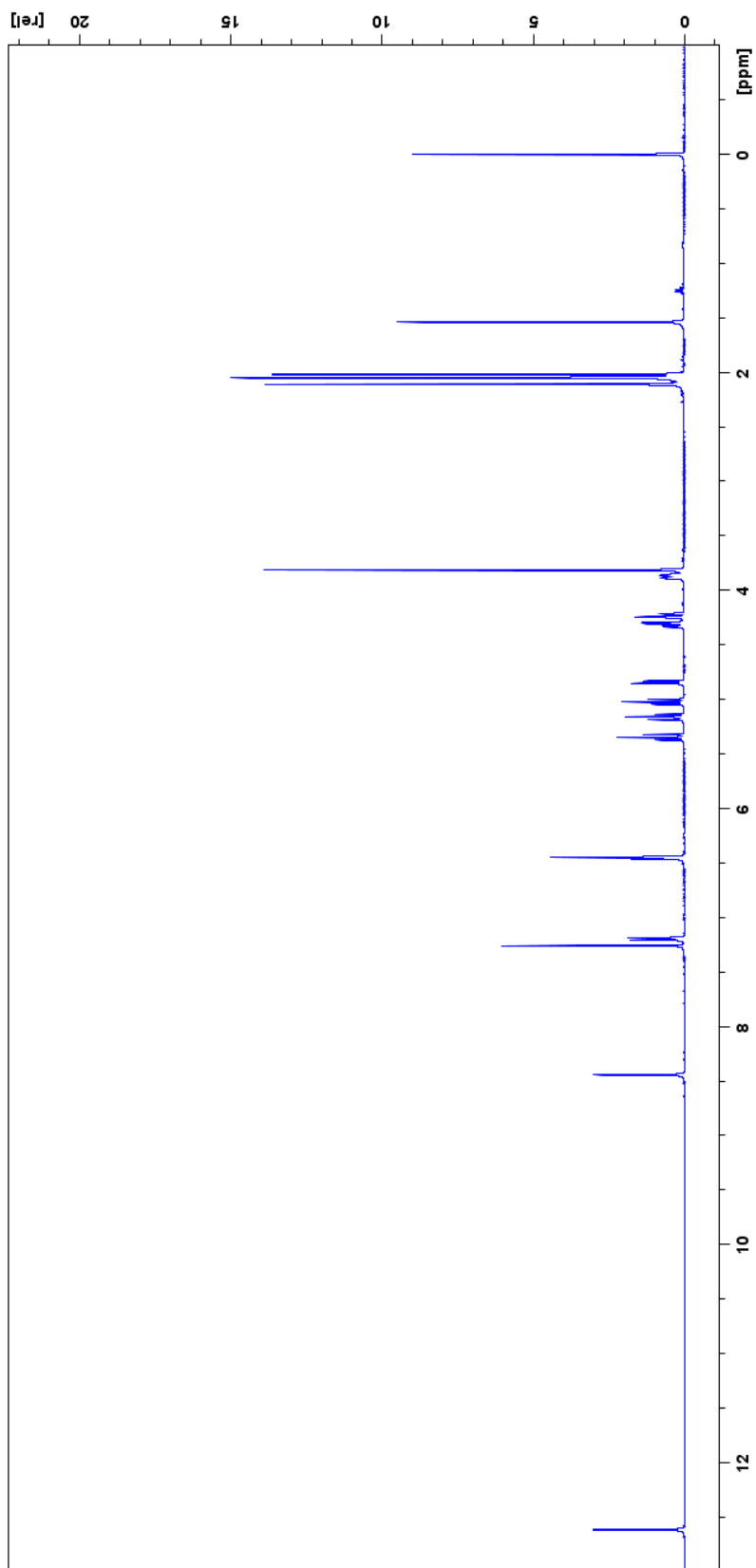
**Figure 68.** 100 MHz  $^{13}\text{C}$  NMR spectrum of  $(E)$ -(2,3,4,6)-tetra-*O*-acetyl- $\beta$ -D-alucopyranosyl-1-*N*-9-anthracenecarboxaldimine (9d).



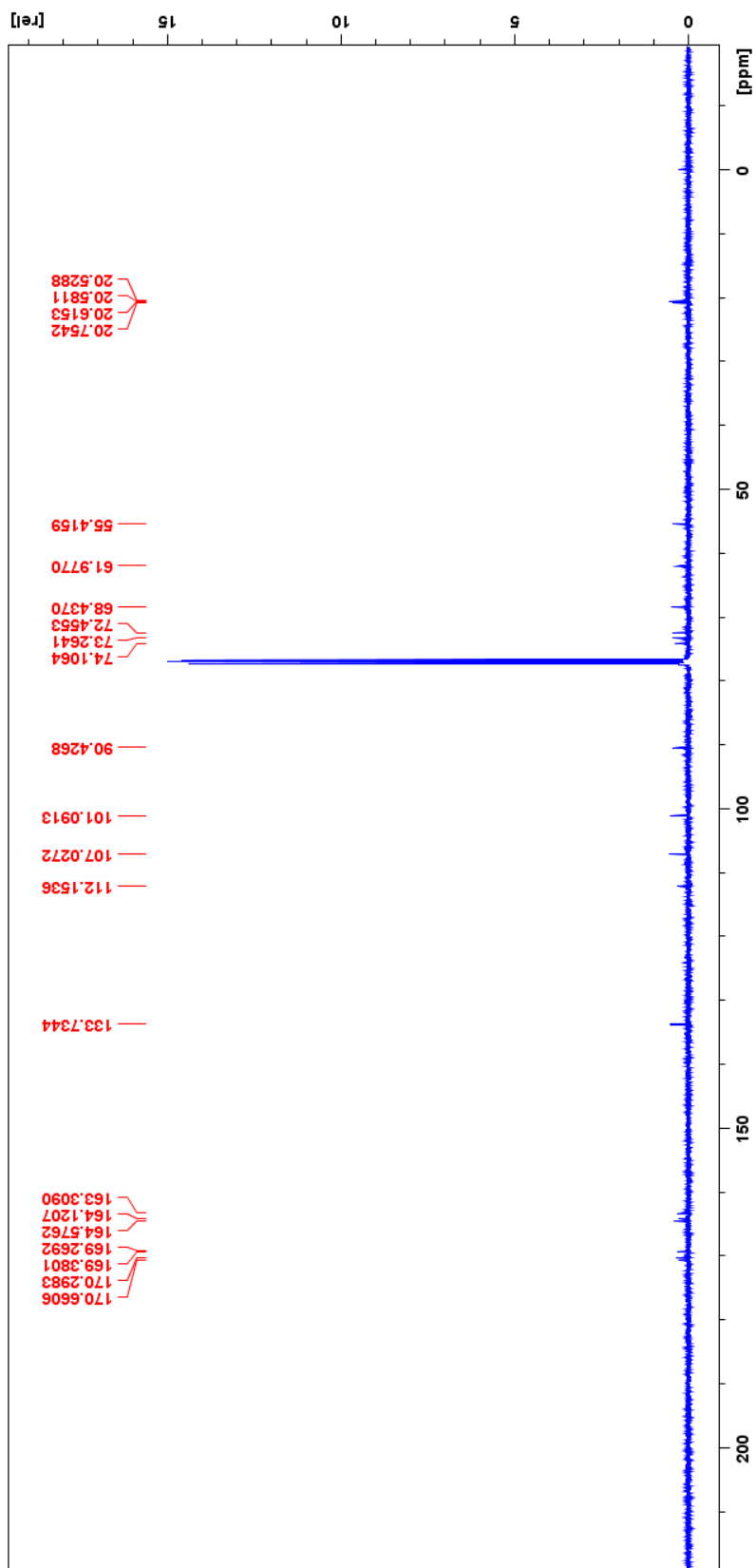
**Figure 69.** 400 MHz <sup>1</sup>H NMR spectrum of (E)-(2,3,4,6)-tetra-O-acetyl-β-D-glucopyranosyl-1-N-2-hydroxy-3-methoxybenzalimine (9e).



**Figure 70.** 100 MHz  $^{13}\text{C}$  NMR spectrum of  $(E)$ -(2,3,4,6)-tetra-*O*-acetyl- $\beta$ -D-glucopyranosyl-1-*N*-2-hydroxy-3-methoxybenzaldimine (**9e**).



**Figure 71.** 400 MHz <sup>1</sup>H NMR spectrum of (E)-(2,3,4,6)-tetra-O-acetyl-β-D-glucopyranosyl-1-N-2-hydroxy-4-methoxybenzalimine (9f).



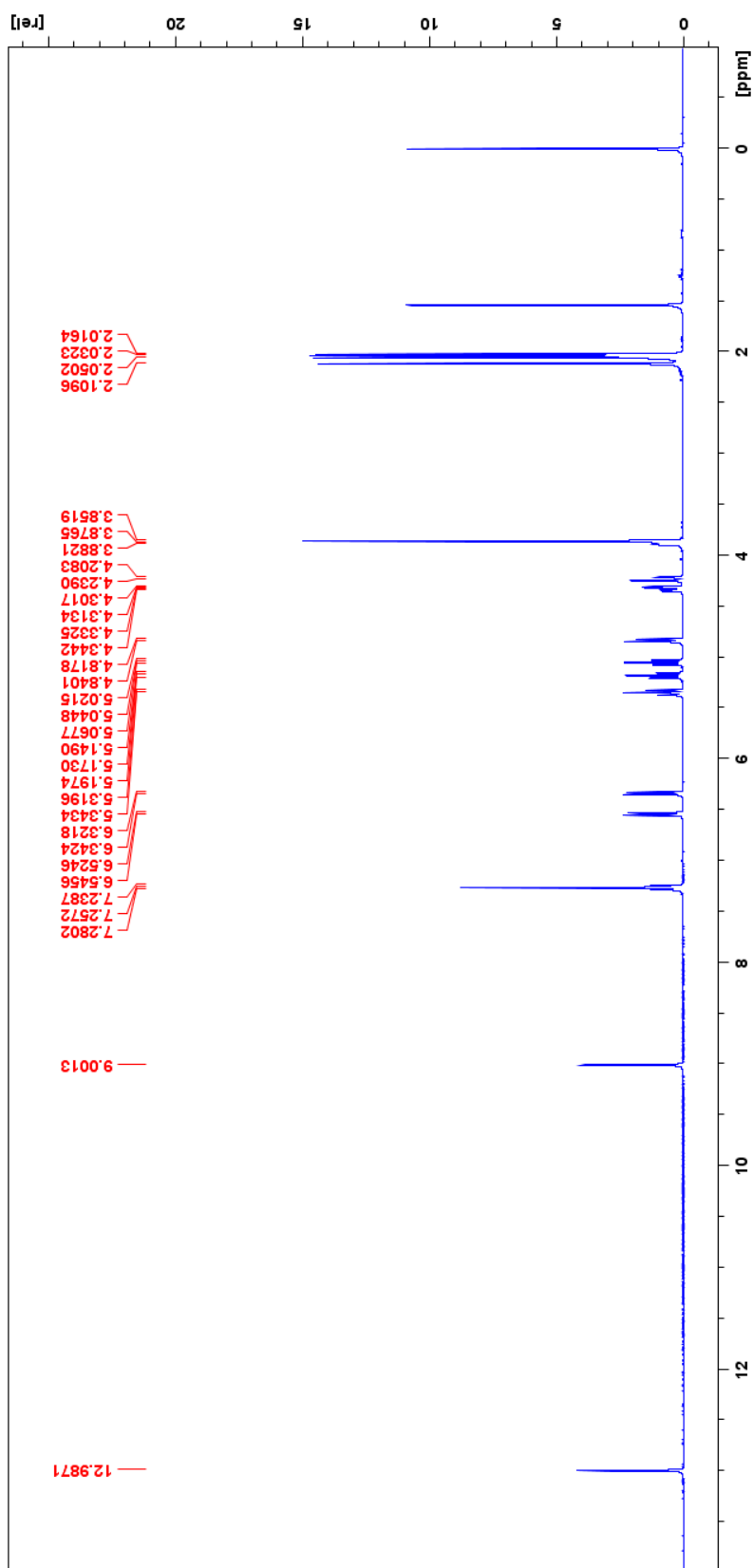


**Figure 73.** 400 MHz <sup>1</sup>H NMR spectrum of (E)-(2,3,4,6)-tetra-O-acetyl-β-D-glucopyranosyl-1-N-2-hydroxy-6-methoxybenzalimine (9g).

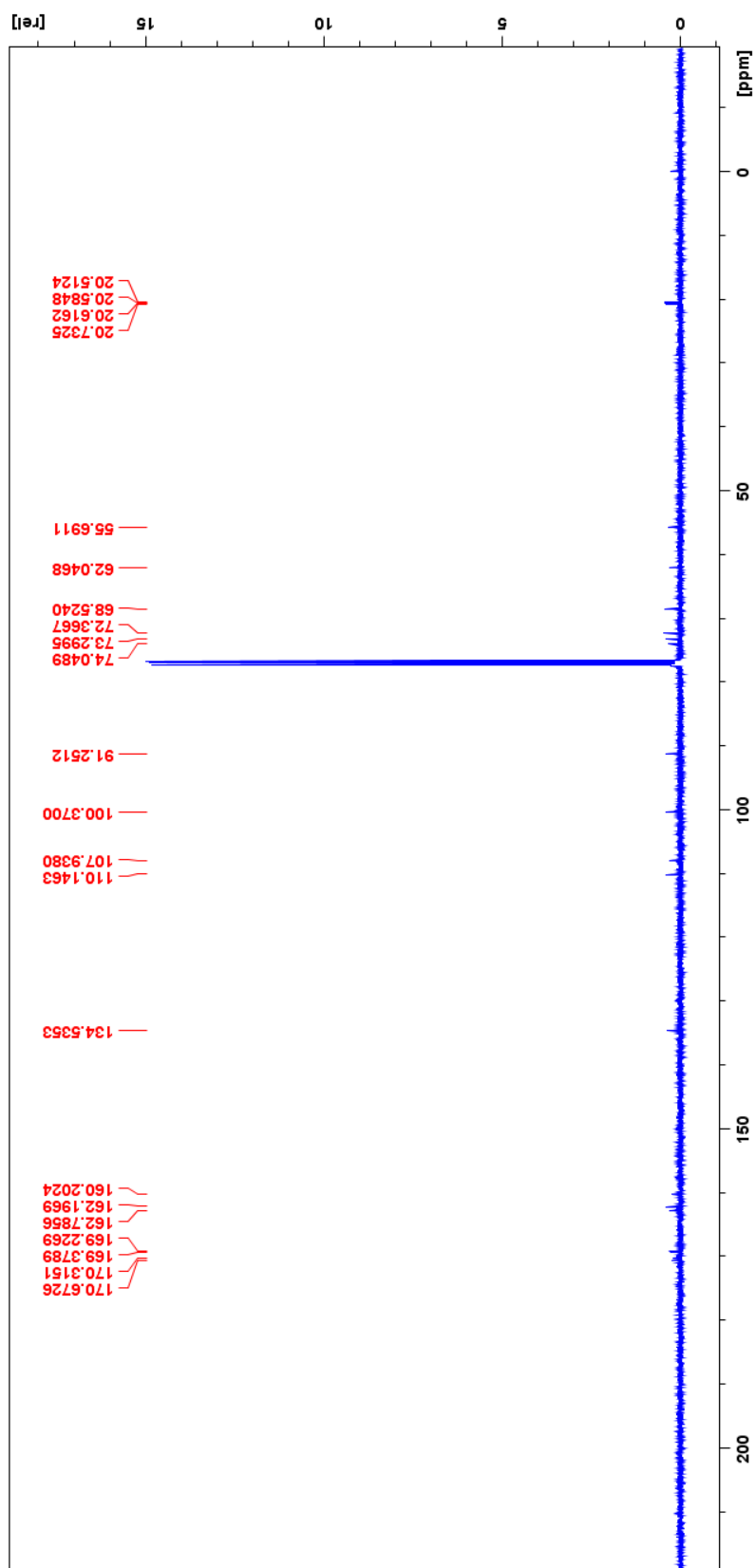


**Figure 74.** 100 MHz  $^{13}\text{C}$  NMR spectrum of  $(E)$ -(2,3,4,6)-tetra-*O*-acetyl- $\beta$ -D-glucopyranosyl-1-*N*-2-hydroxy-6-methoxybenzaldimine (9g).

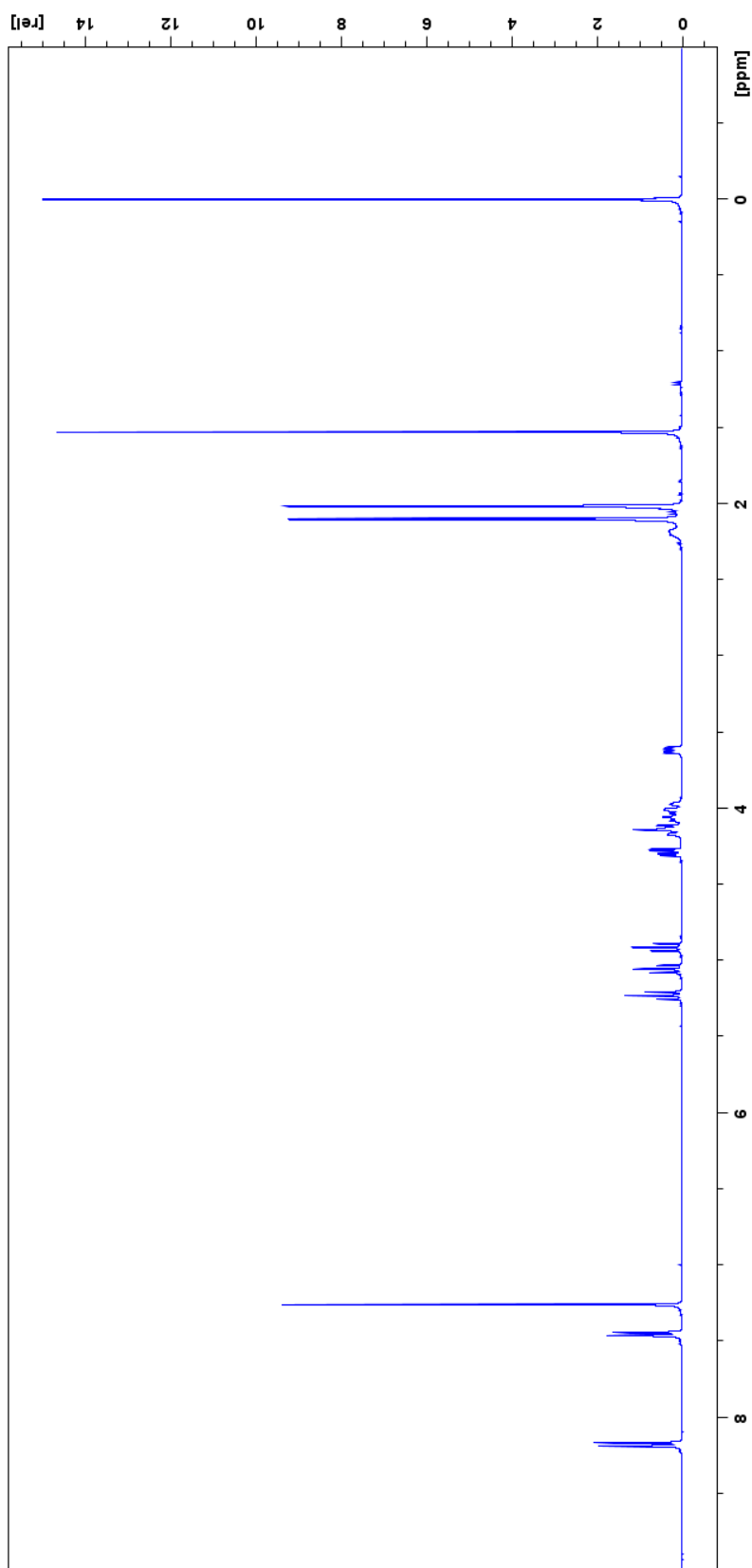


**Figure 75.** 400 MHz <sup>1</sup>H NMR spectrum of (2,3,4,6)-tetra-*O*-acetyl-β-D-glucopyranosyl-1-*N*-4-nitrobenzaldamine (**10b**).



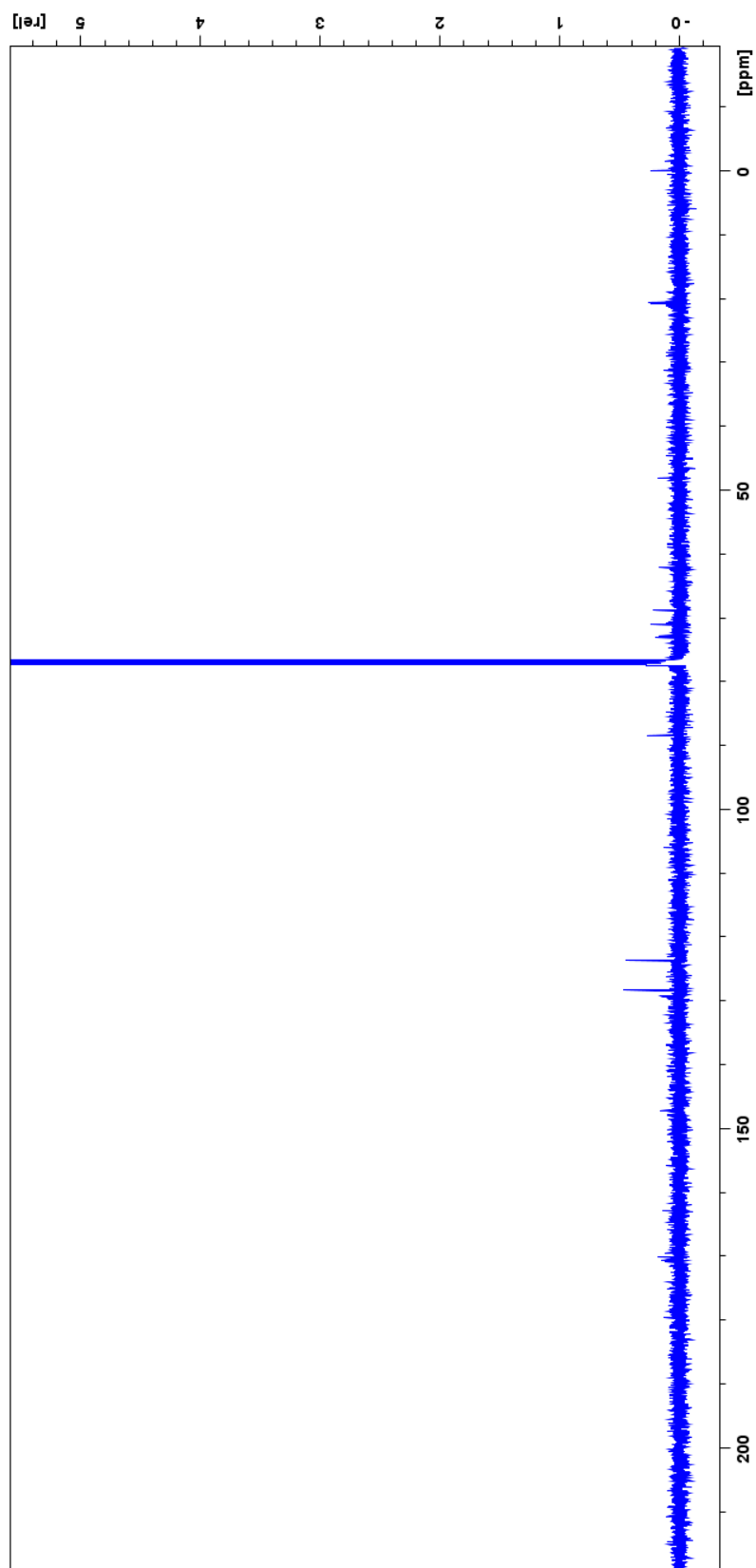


**Figure 76.** 100 MHz  $^{13}\text{C}$  NMR spectrum of (2,3,4,6)-tetra-*O*-acetyl- $\beta$ -D-glucopyranosyl-1-*N*-4-nitrobenzaldamine (**10b**).

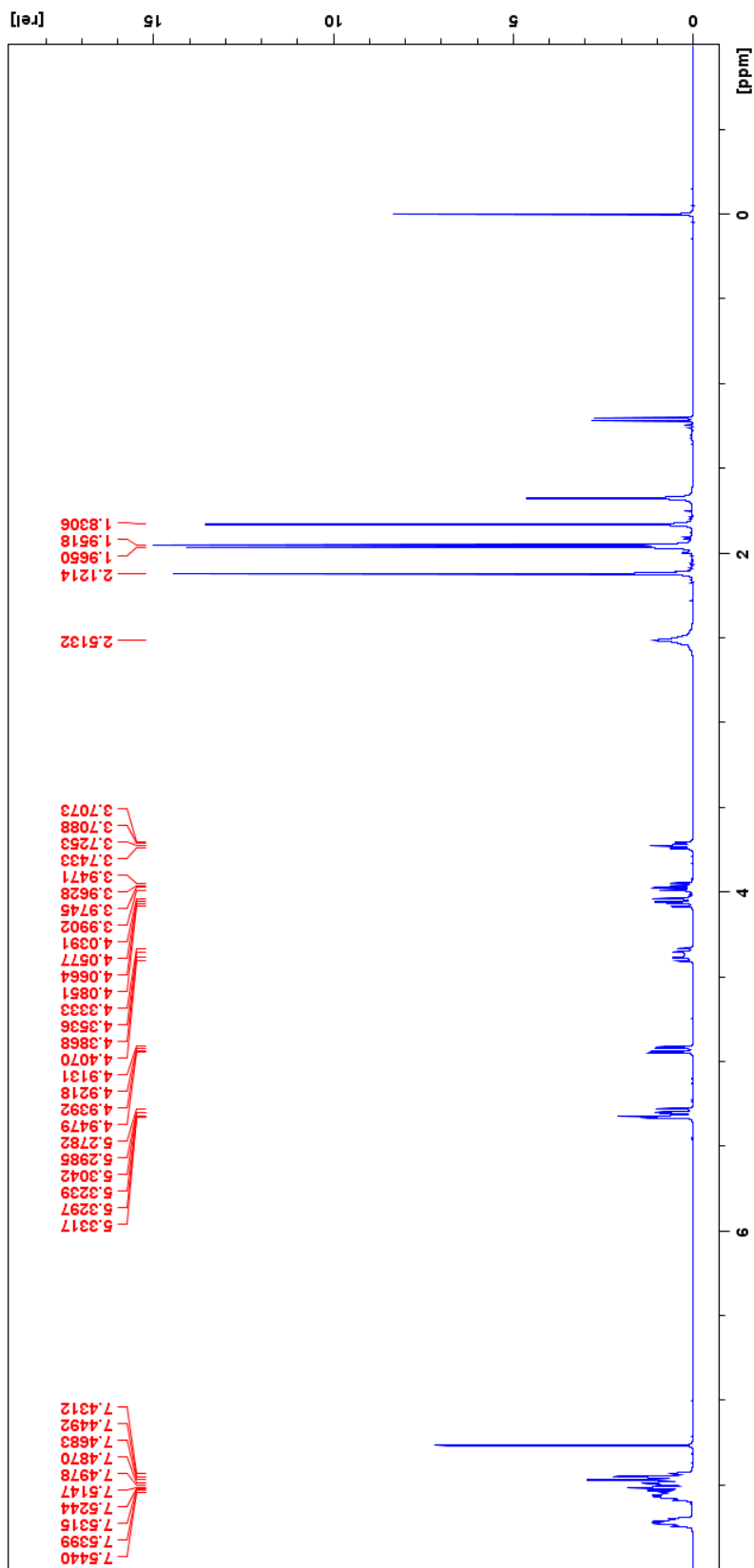


**Figure 77.** 400 MHz <sup>1</sup>H NMR spectrum of 1,2-bis(diphenyl-(2,3,4,6)-tetra-O-acetyl-β-D-galactopyranosyl)-1-N-iminophosphorane) ethane (II) in isopropyl alcohol.

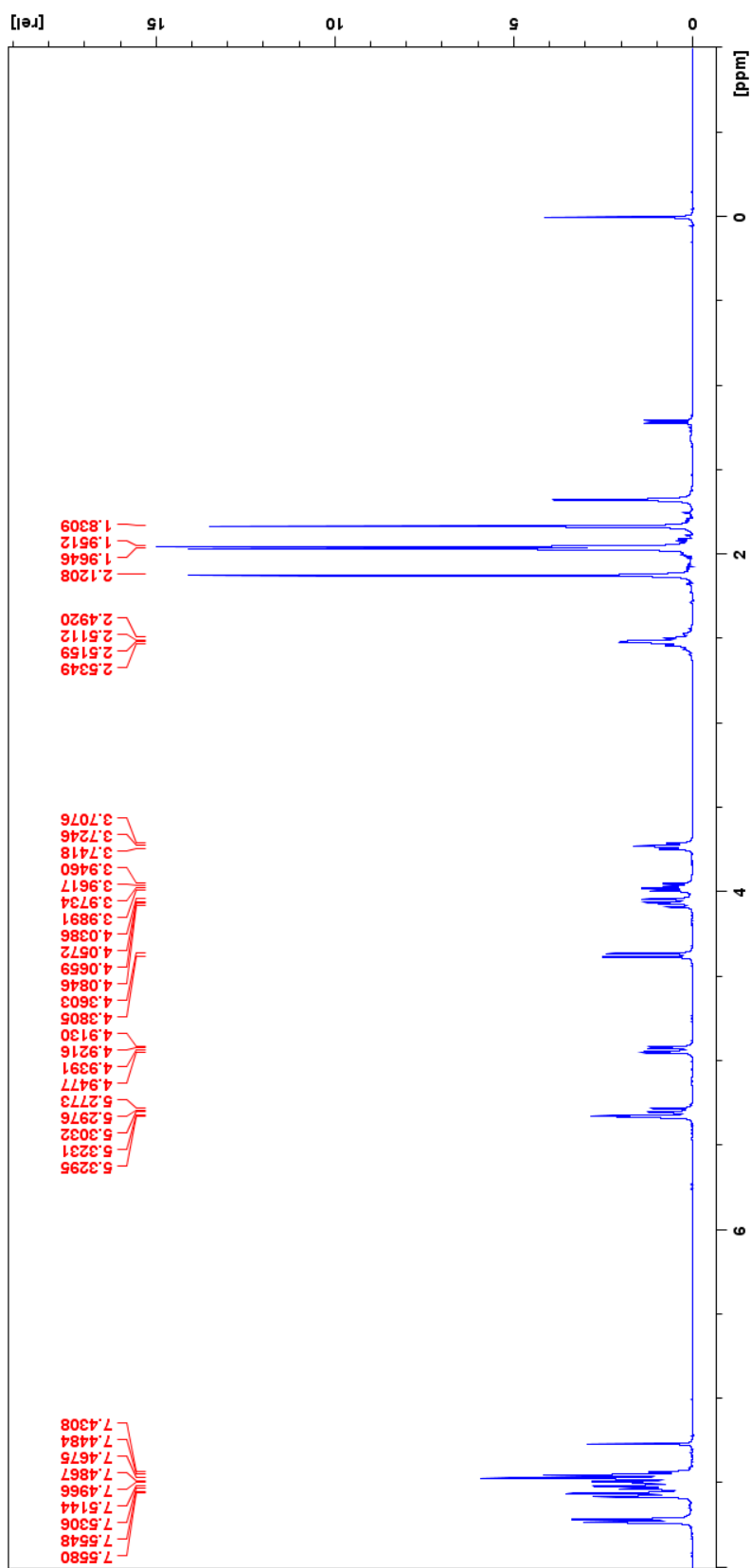


**Figure 78.** 400 MHz <sup>31</sup>P-decoupled <sup>1</sup>H NMR spectrum of 1,2-bis(diphenyl-(2,3,4,6)-tetra-O-acetyl-β-D-galactopyranosyl)-1-N-iminophosphorane) ethane (II) in isopropyl alcohol.

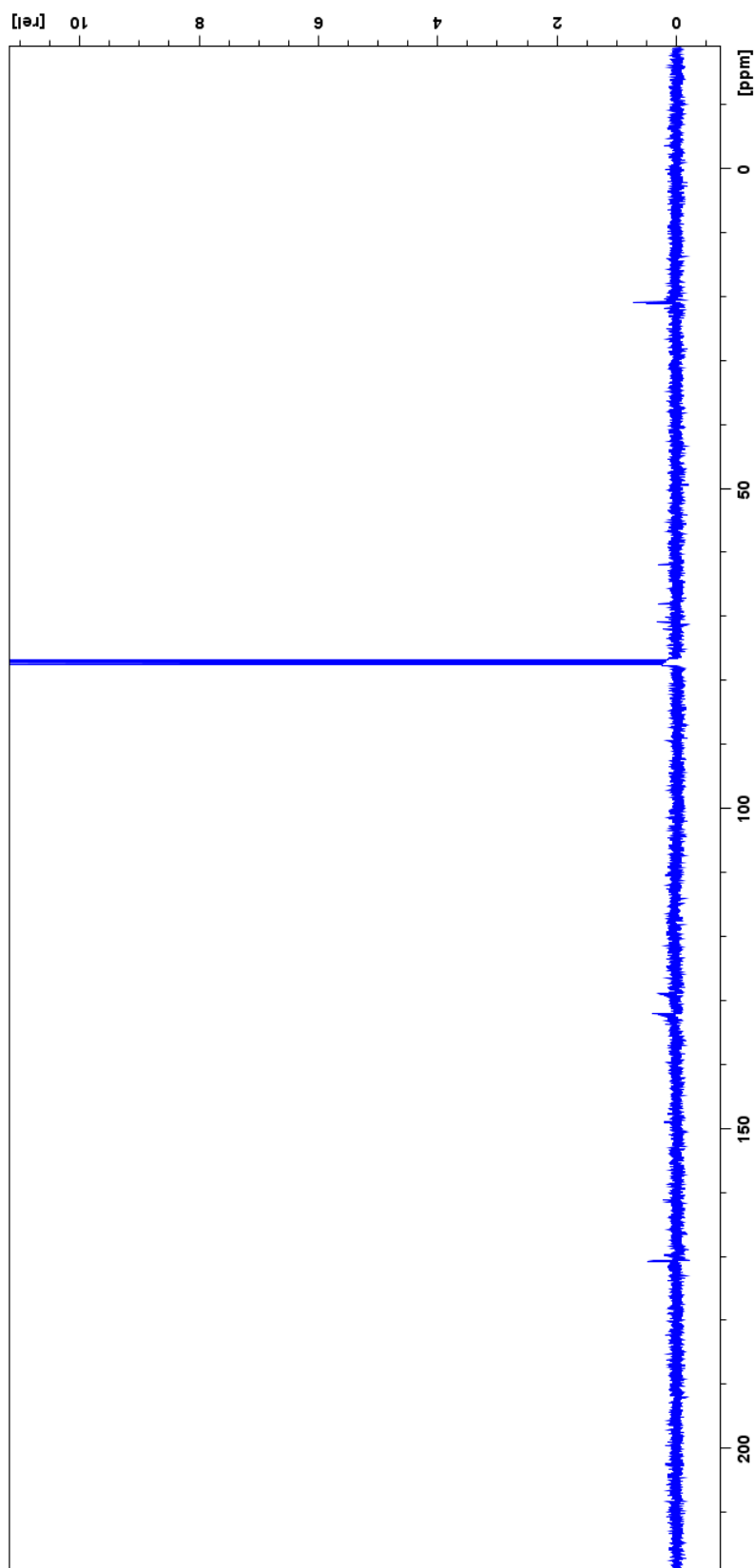


**Figure 79.** 100 MHz  $^{13}\text{C}$  NMR spectrum of 1,2-bis(diphenyl-(2,3,4,6)-tetra-*O*-acetyl- $\beta$ -D-galactopyranosyl-1-*N*-iminophosphorane) ethane (**II**) in isopropyl alcohol.

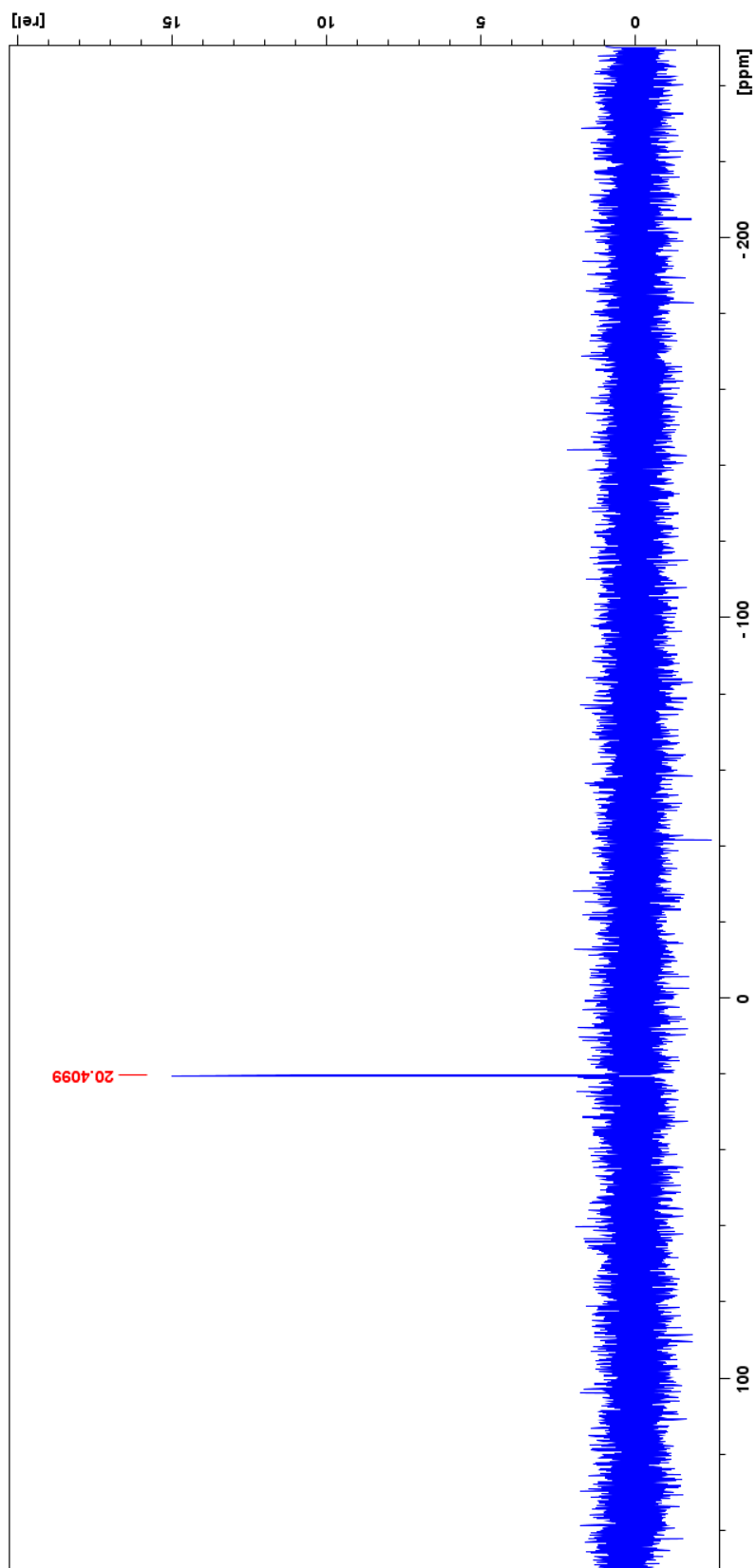


**Figure 80.** 167 MHz  $^{31}\text{P}$  NMR spectrum of 1,2-bis(diphenyl-(2,3,4,6)-tetra-*O*-acetyl- $\beta$ -D-galactopyranosyl)-1-*N*-iminophosphorane) ethane (**II**) in isopropyl alcohol.

## **Appendix B**

X-ray Crystallography Data

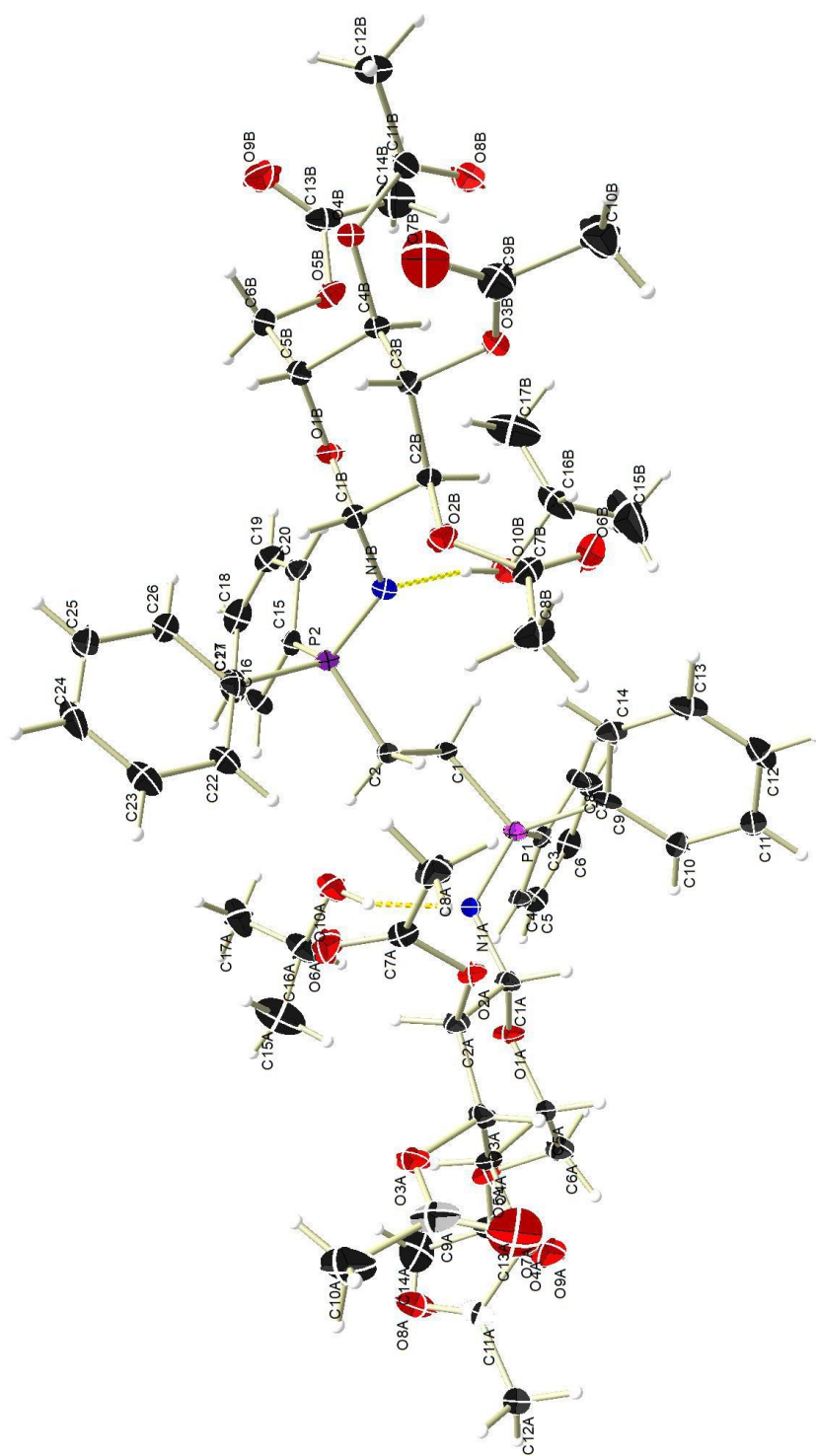


**Table 1.** Experimental data for iminophosphorane **5**.

<b>Crystal data</b>	
Chemical formula	C <sub>54</sub> H <sub>62</sub> N <sub>2</sub> O <sub>18</sub> P <sub>2</sub> ·2(C <sub>3</sub> H <sub>8</sub> O)
<i>M<sub>r</sub></i>	1209.18
Crystal system, space group	Monoclinic, <i>P</i> 2 <sub>1</sub>
Temperature (K)	100
<i>a</i> , <i>b</i> , <i>c</i> (Å)	10.5907 (5), 9.5075 (5), 31.4796 (17)
β (°)	94.9677 (16)
<i>V</i> (Å <sup>3</sup> )	3157.8 (3)
<i>Z</i>	2
Radiation type	Mo <i>K</i> α
μ (mm <sup>-1</sup> )	0.14
Crystal size (mm)	0.50 × 0.30 × 0.10
<b>Data collection</b>	
Diffractometer	Bruker AXS D8 Quest CMOS diffractometer
Absorption correction	Multi-scan <i>SADABS</i> 2014/5: Krause, L., Herbst-Irmer, R., Sheldrick G.M. & Stalke D., <i>J. Appl. Cryst.</i> 48 (2015) 3-10
<i>T<sub>min</sub></i> , <i>T<sub>max</sub></i>	0.686, 0.746
No. of measured, independent and observed [ <i>I</i> > 2σ( <i>I</i> )] reflections	36009, 15426, 13357
<i>R<sub>int</sub></i>	0.032
(sin θ/λ) <sub>max</sub> (Å <sup>-1</sup> )	0.714
<b>Refinement</b>	
<i>R</i> [ <i>F</i> <sup>2</sup> > 2σ( <i>F</i> <sup>2</sup> )], <i>wR</i> ( <i>F</i> <sup>2</sup> ), <i>S</i>	0.039, 0.094, 1.02
No. of reflections	15426
No. of parameters	843
No. of restraints	194
H-atom treatment	H-atom parameters constrained
Δρ <sub>max</sub> , Δρ <sub>min</sub> (e Å <sup>-3</sup> )	0.31, -0.25
Absolute structure	Flack <i>x</i> determined using 5311 quotients [( <i>I</i> <sup>+</sup> )-( <i>I</i> <sup>-</sup> )]/[( <i>I</i> <sup>+</sup> )+( <i>I</i> <sup>-</sup> )] (Parsons, Flack and Wagner, <i>Acta Cryst.</i> B69 (2013) 249-259).
Absolute structure parameter	0.02 (2)

Computer programs: Apex3 v2016.1-0 (Bruker, 2016), *SAINTE* V8.37A (Bruker, 2014), *SHELXS*97 (Sheldrick, 2008), *SHELXL*2016/6 (Sheldrick, 2015, 2016), *SHELXL*E Rev714 (Hübschle *et al.*, 2011).



**Table 2.** Bond lengths (Å) for iminophosphorane **5**.

C1A—N1A	1.424 (3)	C10B—H10D	0.9800
C1A—O1A	1.451 (3)	C10B—H10E	0.9800
C1A—C2A	1.539 (3)	C10B—H10F	0.9800
C1A—H1A	1.0000	C11B—O8B	1.202 (3)
C2A—O2A	1.445 (3)	C11B—O4B	1.353 (3)
C2A—C3A	1.516 (3)	C11B—C12B	1.495 (4)
C2A—H2A	1.0000	C12B—H12D	0.9800
C3A—O3A	1.451 (3)	C12B—H12E	0.9800
C3A—C4A	1.516 (3)	C12B—H12F	0.9800
C3A—H3A	1.0000	C13B—O9B	1.202 (4)
C4A—O4A	1.451 (3)	C13B—O5B	1.347 (3)
C4A—C5A	1.529 (3)	C13B—C14B	1.483 (4)
C4A—H4A	1.0000	C14B—H14D	0.9800
C5A—O1A	1.435 (3)	C14B—H14E	0.9800
C5A—C6A	1.502 (4)	C14B—H14F	0.9800
C5A—H5A	1.0000	O10B—C16B	1.423 (4)
C6A—O5A	1.440 (3)	O10B—H10H	0.8400
C6A—H6AA	0.9900	C15B—C16B	1.485 (5)
C6A—H6AB	0.9900	C15B—H15D	0.9800
C7A—O6A	1.197 (3)	C15B—H15E	0.9800
C7A—O2A	1.342 (3)	C15B—H15F	0.9800
C7A—C8A	1.502 (4)	C16B—C17B	1.484 (6)
C8A—H8AA	0.9800	C16B—H16B	1.0000
C8A—H8AB	0.9800	C17B—H17D	0.9800
C8A—H8AC	0.9800	C17B—H17E	0.9800
C9A—O7A	1.212 (4)	C17B—H17F	0.9800
C9A—O3A	1.344 (4)	O10D—C16D	1.42 (2)
C9A—C10A	1.499 (4)	O10D—H10J	0.8400
C10A—H10A	0.9800	C15D—C16D	1.50 (3)
C10A—H10B	0.9800	C15D—H15J	0.9800
C10A—H10C	0.9800	C15D—H15K	0.9800
C11A—O8A	1.202 (3)	C15D—H15L	0.9800
C11A—O4A	1.350 (3)	C16D—C17D	1.50 (2)
C11A—C12A	1.498 (4)	C16D—H16D	1.0000
C12A—H12A	0.9800	C17D—H17J	0.9800
C12A—H12B	0.9800	C17D—H17K	0.9800
C12A—H12C	0.9800	C17D—H17L	0.9800
C13A—O9A	1.197 (3)	N1B—P2	1.5843 (19)
C13A—O5A	1.342 (3)	C1—C2	1.538 (3)
C13A—C14A	1.491 (4)	C1—P1	1.812 (2)
C14A—H14A	0.9800	C1—H1C	0.9900
C14A—H14B	0.9800	C1—H1D	0.9900
C14A—H14C	0.9800	C2—P2	1.811 (2)
O10A—C16A	1.421 (4)	C2—H2C	0.9900
O10A—H10G	0.8400	C2—H2D	0.9900

C15A—C16A	1.502 (5)	C3—C8	1.398 (3)
C15A—H15A	0.9800	C3—C4	1.399 (3)
C15A—H15B	0.9800	C3—P1	1.814 (2)
C15A—H15C	0.9800	C4—C5	1.397 (4)
C16A—C17A	1.517 (5)	C4—H4	0.9500
C16A—H16A	1.0000	C5—C6	1.390 (4)
C17A—H17A	0.9800	C5—H5	0.9500
C17A—H17B	0.9800	C6—C7	1.385 (4)
C17A—H17C	0.9800	C6—H6	0.9500
O10C—C16C	1.43 (3)	C7—C8	1.387 (4)
O10C—H10I	0.8400	C7—H7	0.9500
C15C—C16C	1.51 (3)	C8—H8	0.9500
C15C—H15G	0.9800	C9—C10	1.395 (3)
C15C—H15H	0.9800	C9—C14	1.400 (3)
C15C—H15I	0.9800	C9—P1	1.815 (2)
C16C—C17C	1.52 (3)	C10—C11	1.383 (4)
C16C—H16C	1.0000	C10—H10	0.9500
C17C—H17G	0.9800	C11—C12	1.388 (4)
C17C—H17H	0.9800	C11—H11	0.9500
C17C—H17I	0.9800	C12—C13	1.381 (4)
N1A—P1	1.5786 (19)	C12—H12	0.9500
C1B—N1B	1.417 (3)	C13—C14	1.393 (4)
C1B—O1B	1.458 (3)	C13—H13	0.9500
C1B—C2B	1.538 (3)	C14—H14	0.9500
C1B—H1B	1.0000	C15—C20	1.393 (3)
O1B—C5B	1.430 (3)	C15—C16	1.398 (3)
C2B—O2B	1.446 (3)	C15—P2	1.814 (3)
C2B—C3B	1.520 (3)	C16—C17	1.390 (4)
C2B—H2B	1.0000	C16—H16	0.9500
C3B—O3B	1.449 (3)	C17—C18	1.386 (4)
C3B—C4B	1.517 (3)	C17—H17	0.9500
C3B—H3B	1.0000	C18—C19	1.387 (4)
C4B—O4B	1.448 (3)	C18—H18	0.9500
C4B—C5B	1.524 (3)	C19—C20	1.393 (4)
C4B—H4B	1.0000	C19—H19	0.9500
C5B—C6B	1.509 (4)	C20—H20	0.9500
C5B—H5B	1.0000	C21—C22	1.394 (3)
C6B—O5B	1.442 (3)	C21—C26	1.398 (3)
C6B—H6BA	0.9900	C21—P2	1.806 (2)
C6B—H6BB	0.9900	C22—C23	1.384 (4)
C7B—O6B	1.206 (3)	C22—H22	0.9500
C7B—O2B	1.346 (3)	C23—C24	1.374 (4)
C7B—C8B	1.501 (4)	C23—H23	0.9500
C8B—H8BA	0.9800	C24—C25	1.385 (4)
C8B—H8BB	0.9800	C24—H24	0.9500
C8B—H8BC	0.9800	C25—C26	1.392 (4)
C9B—O7B	1.203 (4)	C25—H25	0.9500

<b>C9B—O3B</b>	1.342 (3)	<b>C26—H26</b>	0.9500
<b>C9B—C10B</b>	1.510 (4)		

Table 3. Bond angles (degrees) for iminophosphorane 5.

N1A—C1A—O1A	108.63 (19)	O3B—C9B—C10B	110.0 (3)
N1A—C1A—C2A	108.41 (19)	C9B—C10B—H10D	109.5
O1A—C1A—C2A	108.83 (17)	C9B—C10B—H10E	109.5
N1A—C1A—H1A	110.3	H10D—C10B—H10E	109.5
O1A—C1A—H1A	110.3	C9B—C10B—H10F	109.5
C2A—C1A—H1A	110.3	H10D—C10B—H10F	109.5
O2A—C2A—C3A	107.78 (19)	H10E—C10B—H10F	109.5
O2A—C2A—C1A	105.81 (17)	O8B—C11B—O4B	124.0 (2)
C3A—C2A—C1A	112.59 (19)	O8B—C11B—C12B	125.5 (2)
O2A—C2A—H2A	110.2	O4B—C11B—C12B	110.5 (2)
C3A—C2A—H2A	110.2	C11B—C12B—H12D	109.5
C1A—C2A—H2A	110.2	C11B—C12B—H12E	109.5
O3A—C3A—C2A	107.30 (19)	H12D—C12B—H12E	109.5
O3A—C3A—C4A	108.58 (18)	C11B—C12B—H12F	109.5
C2A—C3A—C4A	111.2 (2)	H12D—C12B—H12F	109.5
O3A—C3A—H3A	109.9	H12E—C12B—H12F	109.5
C2A—C3A—H3A	109.9	O9B—C13B—O5B	123.3 (3)
C4A—C3A—H3A	109.9	O9B—C13B—C14B	125.5 (3)
O4A—C4A—C3A	106.9 (2)	O5B—C13B—C14B	111.2 (2)
O4A—C4A—C5A	110.13 (19)	C13B—C14B—H14D	109.5
C3A—C4A—C5A	108.97 (18)	C13B—C14B—H14E	109.5
O4A—C4A—H4A	110.3	H14D—C14B—H14E	109.5
C3A—C4A—H4A	110.3	C13B—C14B—H14F	109.5
C5A—C4A—H4A	110.3	H14D—C14B—H14F	109.5
O1A—C5A—C6A	109.7 (2)	H14E—C14B—H14F	109.5
O1A—C5A—C4A	106.57 (18)	C16B—O10B—H10H	109.5
C6A—C5A—C4A	113.77 (19)	C16B—C15B—H15D	109.5
O1A—C5A—H5A	108.9	C16B—C15B—H15E	109.5
C6A—C5A—H5A	108.9	H15D—C15B—H15E	109.5
C4A—C5A—H5A	108.9	C16B—C15B—H15F	109.5
O5A—C6A—C5A	108.2 (2)	H15D—C15B—H15F	109.5
O5A—C6A—H6AA	110.1	H15E—C15B—H15F	109.5
C5A—C6A—H6AA	110.1	O10B—C16B—C17B	111.4 (4)
O5A—C6A—H6AB	110.1	O10B—C16B—C15B	107.1 (3)
C5A—C6A—H6AB	110.1	C17B—C16B—C15B	113.5 (4)
H6AA—C6A—H6AB	108.4	O10B—C16B—H16B	108.2
O6A—C7A—O2A	124.0 (2)	C17B—C16B—H16B	108.2
O6A—C7A—C8A	125.5 (2)	C15B—C16B—H16B	108.2
O2A—C7A—C8A	110.5 (2)	C16B—C17B—H17D	109.5
C7A—C8A—H8AA	109.5	C16B—C17B—H17E	109.5
C7A—C8A—H8AB	109.5	H17D—C17B—H17E	109.5
H8AA—C8A—H8AB	109.5	C16B—C17B—H17F	109.5
C7A—C8A—H8AC	109.5	H17D—C17B—H17F	109.5
H8AA—C8A—H8AC	109.5	H17E—C17B—H17F	109.5
H8AB—C8A—H8AC	109.5	C16D—O10D—H10J	121.4

O7A—C9A—O3A	123.8 (3)	C16D—C15D—H15J	109.5
O7A—C9A—C10A	125.3 (3)	C16D—C15D—H15K	109.5
O3A—C9A—C10A	110.9 (3)	H15J—C15D—H15K	109.5
C9A—C10A—H10A	109.5	C16D—C15D—H15L	109.5
C9A—C10A—H10B	109.5	H15J—C15D—H15L	109.5
H10A—C10A—H10B	109.5	H15K—C15D—H15L	109.5
C9A—C10A—H10C	109.5	O10D—C16D—C15D	106 (2)
H10A—C10A—H10C	109.5	O10D—C16D—C17D	104 (3)
H10B—C10A—H10C	109.5	C15D—C16D—C17D	109 (3)
O8A—C11A—O4A	124.0 (2)	O10D—C16D—H16D	112.2
O8A—C11A—C12A	125.2 (2)	C15D—C16D—H16D	112.2
O4A—C11A—C12A	110.8 (2)	C17D—C16D—H16D	112.2
C11A—C12A—H12A	109.5	C16D—C17D—H17J	109.5
C11A—C12A—H12B	109.5	C16D—C17D—H17K	109.5
H12A—C12A—H12B	109.5	H17J—C17D—H17K	109.5
C11A—C12A—H12C	109.5	C16D—C17D—H17L	109.5
H12A—C12A—H12C	109.5	H17J—C17D—H17L	109.5
H12B—C12A—H12C	109.5	H17K—C17D—H17L	109.5
O9A—C13A—O5A	123.7 (3)	C7B—O2B—C2B	118.65 (18)
O9A—C13A—C14A	124.6 (3)	C9B—O3B—C3B	118.5 (2)
O5A—C13A—C14A	111.6 (3)	C11B—O4B—C4B	117.64 (19)
C13A—C14A—H14A	109.5	C13B—O5B—C6B	117.1 (2)
C13A—C14A—H14B	109.5	C1B—N1B—P2	124.08 (17)
H14A—C14A—H14B	109.5	C2—C1—P1	111.90 (15)
C13A—C14A—H14C	109.5	C2—C1—H1C	109.2
H14A—C14A—H14C	109.5	P1—C1—H1C	109.2
H14B—C14A—H14C	109.5	C2—C1—H1D	109.2
C16A—O10A—H10G	109.5	P1—C1—H1D	109.2
C16A—C15A—H15A	109.5	H1C—C1—H1D	107.9
C16A—C15A—H15B	109.5	C1—C2—P2	113.89 (15)
H15A—C15A—H15B	109.5	C1—C2—H2C	108.8
C16A—C15A—H15C	109.5	P2—C2—H2C	108.8
H15A—C15A—H15C	109.5	C1—C2—H2D	108.8
H15B—C15A—H15C	109.5	P2—C2—H2D	108.8
O10A—C16A—C15A	110.9 (4)	H2C—C2—H2D	107.7
O10A—C16A—C17A	106.6 (3)	C8—C3—C4	119.9 (2)
C15A—C16A—C17A	112.4 (3)	C8—C3—P1	121.23 (18)
O10A—C16A—H16A	108.9	C4—C3—P1	118.75 (17)
C15A—C16A—H16A	108.9	C5—C4—C3	119.6 (2)
C17A—C16A—H16A	108.9	C5—C4—H4	120.2
C16A—C17A—H17A	109.5	C3—C4—H4	120.2
C16A—C17A—H17B	109.5	C6—C5—C4	120.3 (2)
H17A—C17A—H17B	109.5	C6—C5—H5	119.8
C16A—C17A—H17C	109.5	C4—C5—H5	119.8
H17A—C17A—H17C	109.5	C7—C6—C5	119.6 (2)
H17B—C17A—H17C	109.5	C7—C6—H6	120.2
C16C—O10C—H10I	109.5	C5—C6—H6	120.2

C16C—C15C—H15G	109.5	C6—C7—C8	121.0 (2)
C16C—C15C—H15H	109.5	C6—C7—H7	119.5
H15G—C15C—H15H	109.5	C8—C7—H7	119.5
C16C—C15C—H15I	109.5	C7—C8—C3	119.5 (2)
H15G—C15C—H15I	109.5	C7—C8—H8	120.2
H15H—C15C—H15I	109.5	C3—C8—H8	120.2
O10C—C16C—C15C	107 (3)	C10—C9—C14	119.0 (2)
O10C—C16C—C17C	103 (3)	C10—C9—P1	119.03 (18)
C15C—C16C—C17C	110 (3)	C14—C9—P1	121.97 (19)
O10C—C16C—H16C	112.2	C11—C10—C9	120.7 (2)
C15C—C16C—H16C	112.2	C11—C10—H10	119.6
C17C—C16C—H16C	112.2	C9—C10—H10	119.6
C16C—C17C—H17G	109.5	C10—C11—C12	120.1 (2)
C16C—C17C—H17H	109.5	C10—C11—H11	120.0
H17G—C17C—H17H	109.5	C12—C11—H11	120.0
C16C—C17C—H17I	109.5	C13—C12—C11	119.7 (2)
H17G—C17C—H17I	109.5	C13—C12—H12	120.1
H17H—C17C—H17I	109.5	C11—C12—H12	120.1
C5A—O1A—C1A	111.96 (18)	C12—C13—C14	120.7 (2)
C7A—O2A—C2A	118.51 (19)	C12—C13—H13	119.7
C9A—O3A—C3A	118.4 (2)	C14—C13—H13	119.7
C11A—O4A—C4A	118.2 (2)	C13—C14—C9	119.7 (2)
C13A—O5A—C6A	115.5 (2)	C13—C14—H14	120.1
C1A—N1A—P1	125.34 (16)	C9—C14—H14	120.1
N1B—C1B—O1B	108.7 (2)	C20—C15—C16	119.6 (2)
N1B—C1B—C2B	109.21 (19)	C20—C15—P2	119.85 (19)
O1B—C1B—C2B	108.58 (17)	C16—C15—P2	120.54 (19)
N1B—C1B—H1B	110.1	C17—C16—C15	120.1 (2)
O1B—C1B—H1B	110.1	C17—C16—H16	119.9
C2B—C1B—H1B	110.1	C15—C16—H16	119.9
C5B—O1B—C1B	113.27 (19)	C18—C17—C16	120.0 (3)
O2B—C2B—C3B	107.21 (19)	C18—C17—H17	120.0
O2B—C2B—C1B	106.87 (17)	C16—C17—H17	120.0
C3B—C2B—C1B	113.02 (19)	C17—C18—C19	120.0 (3)
O2B—C2B—H2B	109.9	C17—C18—H18	120.0
C3B—C2B—H2B	109.9	C19—C18—H18	120.0
C1B—C2B—H2B	109.9	C18—C19—C20	120.3 (2)
O3B—C3B—C4B	108.91 (18)	C18—C19—H19	119.8
O3B—C3B—C2B	106.50 (18)	C20—C19—H19	119.8
C4B—C3B—C2B	109.6 (2)	C15—C20—C19	119.8 (2)
O3B—C3B—H3B	110.6	C15—C20—H20	120.1
C4B—C3B—H3B	110.6	C19—C20—H20	120.1
C2B—C3B—H3B	110.6	C22—C21—C26	119.2 (2)
O4B—C4B—C3B	109.1 (2)	C22—C21—P2	122.31 (19)
O4B—C4B—C5B	109.28 (18)	C26—C21—P2	118.50 (19)
C3B—C4B—C5B	108.56 (18)	C23—C22—C21	120.1 (2)
O4B—C4B—H4B	110.0	C23—C22—H22	120.0

<b>C3B—C4B—H4B</b>	110.0	<b>C21—C22—H22</b>	120.0
<b>C5B—C4B—H4B</b>	110.0	<b>C24—C23—C22</b>	120.5 (3)
<b>O1B—C5B—C6B</b>	109.5 (2)	<b>C24—C23—H23</b>	119.7
<b>O1B—C5B—C4B</b>	106.81 (18)	<b>C22—C23—H23</b>	119.7
<b>C6B—C5B—C4B</b>	112.8 (2)	<b>C23—C24—C25</b>	120.3 (2)
<b>O1B—C5B—H5B</b>	109.2	<b>C23—C24—H24</b>	119.8
<b>C6B—C5B—H5B</b>	109.2	<b>C25—C24—H24</b>	119.8
<b>C4B—C5B—H5B</b>	109.2	<b>C24—C25—C26</b>	119.8 (3)
<b>O5B—C6B—C5B</b>	108.1 (2)	<b>C24—C25—H25</b>	120.1
<b>O5B—C6B—H6BA</b>	110.1	<b>C26—C25—H25</b>	120.1
<b>C5B—C6B—H6BA</b>	110.1	<b>C25—C26—C21</b>	120.1 (3)
<b>O5B—C6B—H6BB</b>	110.1	<b>C25—C26—H26</b>	119.9
<b>C5B—C6B—H6BB</b>	110.1	<b>C21—C26—H26</b>	119.9
<b>H6BA—C6B—H6BB</b>	108.4	<b>N1A—P1—C1</b>	106.31 (11)
<b>O6B—C7B—O2B</b>	123.4 (2)	<b>N1A—P1—C3</b>	115.13 (11)
<b>O6B—C7B—C8B</b>	125.4 (2)	<b>C1—P1—C3</b>	104.37 (11)
<b>O2B—C7B—C8B</b>	111.1 (2)	<b>N1A—P1—C9</b>	116.68 (11)
<b>C7B—C8B—H8BA</b>	109.5	<b>C1—P1—C9</b>	108.58 (11)
<b>C7B—C8B—H8BB</b>	109.5	<b>C3—P1—C9</b>	105.00 (11)
<b>H8BA—C8B—H8BB</b>	109.5	<b>N1B—P2—C21</b>	114.84 (11)
<b>C7B—C8B—H8BC</b>	109.5	<b>N1B—P2—C2</b>	108.09 (11)
<b>H8BA—C8B—H8BC</b>	109.5	<b>C21—P2—C2</b>	106.89 (11)
<b>H8BB—C8B—H8BC</b>	109.5	<b>N1B—P2—C15</b>	115.37 (11)
<b>O7B—C9B—O3B</b>	123.9 (3)	<b>C21—P2—C15</b>	104.71 (11)
<b>O7B—C9B—C10B</b>	126.1 (3)	<b>C2—P2—C15</b>	106.33 (12)

**Table 4.** Torsion angles (degrees) for iminophosphorane **5**.

N1A—C1A—C2A—O2A	-74.4 (2)	C14B—C13B—O5B—C6B	175.2 (2)
O1A—C1A—C2A—O2A	167.65 (18)	C5B—C6B—O5B—C13B	-142.6 (2)
N1A—C1A—C2A—C3A	168.14 (19)	O1B—C1B—N1B—P2	-87.2 (2)
O1A—C1A—C2A—C3A	50.2 (3)	C2B—C1B—N1B—P2	154.44 (17)
O2A—C2A—C3A—O3A	76.9 (2)	P1—C1—C2—P2	167.79 (12)
C1A—C2A—C3A—O3A	-166.78 (19)	C8—C3—C4—C5	0.4 (3)
O2A—C2A—C3A—C4A	-164.50 (18)	P1—C3—C4—C5	176.80 (19)
C1A—C2A—C3A—C4A	-48.2 (3)	C3—C4—C5—C6	-1.5 (4)
O3A—C3A—C4A—O4A	-69.0 (2)	C4—C5—C6—C7	1.4 (4)
C2A—C3A—C4A—O4A	173.19 (19)	C5—C6—C7—C8	-0.2 (4)
O3A—C3A—C4A—C5A	172.02 (19)	C6—C7—C8—C3	-0.9 (4)
C2A—C3A—C4A—C5A	54.2 (3)	C4—C3—C8—C7	0.8 (4)
O4A—C4A—C5A—O1A	179.72 (18)	P1—C3—C8—C7	-175.50 (19)
C3A—C4A—C5A—O1A	-63.3 (2)	C14—C9—C10—C11	-1.0 (4)
O4A—C4A—C5A—C6A	58.7 (3)	P1—C9—C10—C11	179.8 (2)
C3A—C4A—C5A—C6A	175.7 (2)	C9—C10—C11—C12	-0.4 (4)
O1A—C5A—C6A—O5A	-72.3 (2)	C10—C11—C12—C13	1.6 (4)
C4A—C5A—C6A—O5A	46.9 (3)	C11—C12—C13—C14	-1.4 (4)
C6A—C5A—O1A—C1A	-167.19 (19)	C12—C13—C14—C9	-0.1 (4)
C4A—C5A—O1A—C1A	69.2 (2)	C10—C9—C14—C13	1.3 (4)
N1A—C1A—O1A—C5A	-179.98 (18)	P1—C9—C14—C13	-179.6 (2)
C2A—C1A—O1A—C5A	-62.1 (2)	C20—C15—C16—C17	-2.0 (4)
O6A—C7A—O2A—C2A	7.3 (4)	P2—C15—C16—C17	176.7 (2)
C8A—C7A—O2A—C2A	-173.4 (2)	C15—C16—C17—C18	0.4 (4)
C3A—C2A—O2A—C7A	-117.6 (2)	C16—C17—C18—C19	0.8 (4)
C1A—C2A—O2A—C7A	121.8 (2)	C17—C18—C19—C20	-0.4 (4)
O7A—C9A—O3A—C3A	0.7 (4)	C16—C15—C20—C19	2.5 (4)
C10A—C9A—O3A—C3A	-177.5 (2)	P2—C15—C20—C19	-176.3 (2)
C2A—C3A—O3A—C9A	-133.0 (2)	C18—C19—C20—C15	-1.3 (4)
C4A—C3A—O3A—C9A	106.7 (2)	C26—C21—C22—C23	0.6 (4)
O8A—C11A—O4A—C4A	8.6 (4)	P2—C21—C22—C23	179.4 (2)
C12A—C11A—O4A—C4A	-170.5 (2)	C21—C22—C23—C24	-0.4 (4)
C3A—C4A—O4A—C11A	119.8 (2)	C22—C23—C24—C25	-0.1 (4)
C5A—C4A—O4A—C11A	-122.0 (2)	C23—C24—C25—C26	0.4 (4)
O9A—C13A—O5A—C6A	-4.7 (4)	C24—C25—C26—C21	-0.3 (4)
C14A—C13A—O5A—C6A	174.9 (2)	C22—C21—C26—C25	-0.2 (4)
C5A—C6A—O5A—C13A	-157.2 (2)	P2—C21—C26—C25	-179.1 (2)
O1A—C1A—N1A—P1	-96.1 (2)	C1A—N1A—P1—C1	-162.6 (2)
C2A—C1A—N1A—P1	145.79 (17)	C1A—N1A—P1—C3	82.3 (2)
N1B—C1B—O1B—C5B	-178.04 (18)	C1A—N1A—P1—C9	-41.4 (2)
C2B—C1B—O1B—C5B	-59.3 (2)	C2—C1—P1—N1A	35.87 (19)
N1B—C1B—C2B—O2B	-74.1 (2)	C2—C1—P1—C3	157.99 (16)
O1B—C1B—C2B—O2B	167.47 (17)	C2—C1—P1—C9	-90.42 (18)
N1B—C1B—C2B—C3B	168.2 (2)	C8—C3—P1—N1A	-179.80 (19)
O1B—C1B—C2B—C3B	49.8 (3)	C4—C3—P1—N1A	3.9 (2)



<b>O2B—C2B—C3B—O3B</b>	74.0 (2)	<b>C8—C3—P1—C1</b>	64.1 (2)
<b>C1B—C2B—C3B—O3B</b>	-168.47 (18)	<b>C4—C3—P1—C1</b>	-112.27 (19)
<b>O2B—C2B—C3B—C4B</b>	-168.30 (17)	<b>C8—C3—P1—C9</b>	-50.1 (2)
<b>C1B—C2B—C3B—C4B</b>	-50.8 (3)	<b>C4—C3—P1—C9</b>	133.58 (19)
<b>O3B—C3B—C4B—O4B</b>	-67.6 (2)	<b>C10—C9—P1—N1A</b>	75.9 (2)
<b>C2B—C3B—C4B—O4B</b>	176.24 (17)	<b>C14—C9—P1—N1A</b>	-103.2 (2)
<b>O3B—C3B—C4B—C5B</b>	173.39 (19)	<b>C10—C9—P1—C1</b>	-164.07 (19)
<b>C2B—C3B—C4B—C5B</b>	57.2 (2)	<b>C14—C9—P1—C1</b>	16.8 (2)
<b>C1B—O1B—C5B—C6B</b>	-170.09 (19)	<b>C10—C9—P1—C3</b>	-52.9 (2)
<b>C1B—O1B—C5B—C4B</b>	67.5 (2)	<b>C14—C9—P1—C3</b>	128.0 (2)
<b>O4B—C4B—C5B—O1B</b>	176.47 (19)	<b>C1B—N1B—P2—C21</b>	-31.0 (2)
<b>C3B—C4B—C5B—O1B</b>	-64.7 (2)	<b>C1B—N1B—P2—C2</b>	-150.2 (2)
<b>O4B—C4B—C5B—C6B</b>	56.2 (3)	<b>C1B—N1B—P2—C15</b>	91.0 (2)
<b>C3B—C4B—C5B—C6B</b>	175.0 (2)	<b>C22—C21—P2—N1B</b>	-104.4 (2)
<b>O1B—C5B—C6B—O5B</b>	-73.2 (2)	<b>C26—C21—P2—N1B</b>	74.5 (2)
<b>C4B—C5B—C6B—O5B</b>	45.6 (3)	<b>C22—C21—P2—C2</b>	15.5 (2)
<b>O6B—C7B—O2B—C2B</b>	-1.4 (4)	<b>C26—C21—P2—C2</b>	-165.67 (19)
<b>C8B—C7B—O2B—C2B</b>	176.8 (2)	<b>C22—C21—P2—C15</b>	128.0 (2)
<b>C3B—C2B—O2B—C7B</b>	-110.1 (2)	<b>C26—C21—P2—C15</b>	-53.1 (2)
<b>C1B—C2B—O2B—C7B</b>	128.4 (2)	<b>C1—C2—P2—N1B</b>	-75.73 (19)
<b>O7B—C9B—O3B—C3B</b>	4.0 (4)	<b>C1—C2—P2—C21</b>	160.15 (17)
<b>C10B—C9B—O3B—C3B</b>	-174.3 (2)	<b>C1—C2—P2—C15</b>	48.71 (19)
<b>C4B—C3B—O3B—C9B</b>	98.3 (3)	<b>C20—C15—P2—N1B</b>	-13.6 (2)
<b>C2B—C3B—O3B—C9B</b>	-143.6 (2)	<b>C16—C15—P2—N1B</b>	167.7 (2)
<b>O8B—C11B—O4B—C4B</b>	5.1 (4)	<b>C20—C15—P2—C21</b>	113.7 (2)
<b>C12B—C11B—O4B—C4B</b>	-174.9 (2)	<b>C16—C15—P2—C21</b>	-65.1 (2)
<b>C3B—C4B—O4B—C11B</b>	108.0 (2)	<b>C20—C15—P2—C2</b>	-133.4 (2)
<b>C5B—C4B—O4B—C11B</b>	-133.4 (2)	<b>C16—C15—P2—C2</b>	47.9 (2)
<b>O9B—C13B—O5B—C6B</b>	-5.4 (4)		

**Table 5.** Hydrogen-bond parameters for iminophosphorane **5**.

<i>D—H</i> ⋯ <i>A</i>	<i>D—H</i> (Å)	<i>H</i> ⋯ <i>A</i> (Å)	<i>D</i> ⋯ <i>A</i> (Å)	<i>D—H</i> ⋯ <i>A</i> (°)
<b>O10A—H10G</b> ⋯ <b>N1A</b>	0.84	2.06	2.866 (5)	162.1
<b>O10C—H10I</b> ⋯ <b>N1A</b>	0.84	2.04	2.73 (6)	138.3
<b>O10B—H10H</b> ⋯ <b>N1B</b>	0.84	1.99	2.822 (4)	169.2
<b>O10D—H10J</b> ⋯ <b>N1B</b>	0.84	2.24	3.04 (3)	159.1

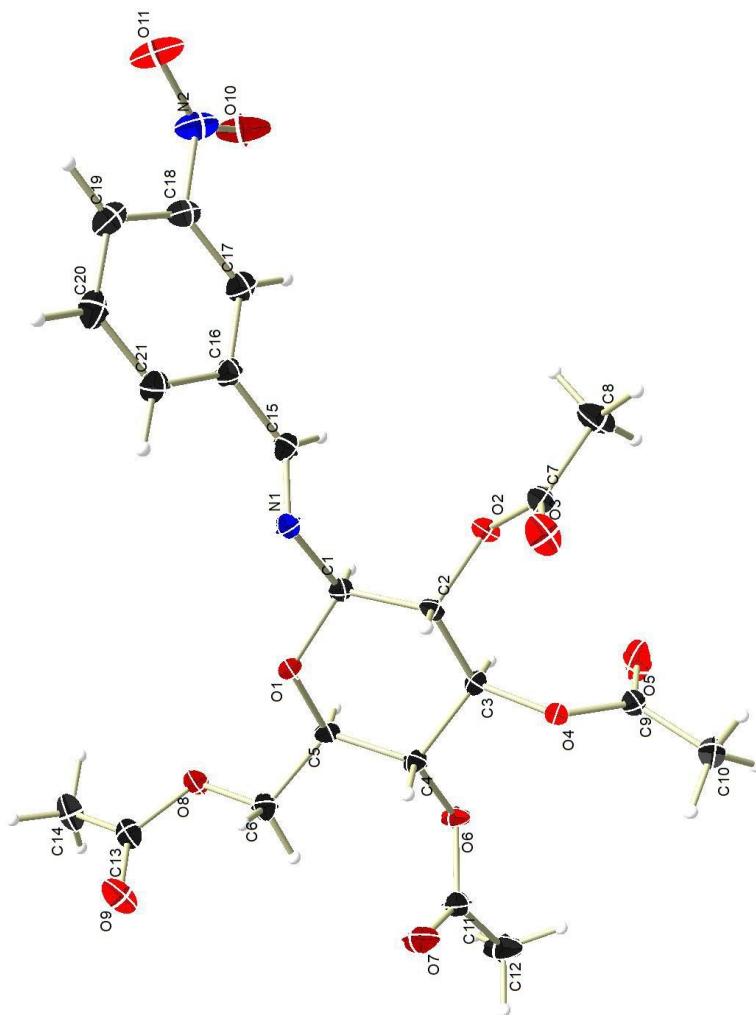


**Figure 82.** X-ray crystal structure of (*E*)-(2,3,4,6)-tetra-*O*-acetyl- $\beta$ -D-glucopyranosyl-1-*N*-3-nitrobenzylidene (**9a**) with 50% probability ellipsoids.

**Table 1.** Experimental data for (*E*)-(2,3,4,6)-tetra-*O*-acetyl- $\beta$ -D-glucopyranosyl-1-*N*-3-nitrobenzaldimine (**9a**).

<b>Crystal data</b>	
Chemical formula	C <sub>21</sub> H <sub>24</sub> N <sub>2</sub> O <sub>11</sub>
$M_r$	480.42
Crystal system, space group	Orthorhombic, $P2_12_12_1$
Temperature (K)	100
$a, b, c$ (Å)	7.0057 (2), 16.4736 (5), 19.5506 (6)
$V$ (Å <sup>3</sup> )	2256.32 (12)
$Z$	4
Radiation type	Cu $K\alpha$
$\mu$ (mm <sup>-1</sup> )	0.99
Crystal size (mm)	0.24 × 0.16 × 0.10
<b>Data collection</b>	
Diffractometer	Bruker AXS X8 Prospector CCD diffractometer
Absorption correction	Multi-scan Apex3 v2016.1-0 (Bruker, 2016)
$T_{\min}, T_{\max}$	0.682, 0.753
No. of measured, independent and observed [ $I > 2\sigma(I)$ ] reflections	28933, 3992, 3977
$R_{\text{int}}$	0.023
$(\sin \theta/\lambda)_{\text{max}}$ (Å <sup>-1</sup> )	0.597
<b>Refinement</b>	
$R[F^2 > 2\sigma(F^2)], wR(F^2), S$	0.022, 0.056, 1.06
No. of reflections	3992
No. of parameters	312
H-atom treatment	H-atom parameters constrained
$\Delta\rho_{\text{max}}, \Delta\rho_{\text{min}}$ (e Å <sup>-3</sup> )	0.18, -0.14
Absolute structure	Flack $x$ determined using 1660 quotients [( <i>I</i> <sup>+</sup> )-( <i>I</i> <sup>-</sup> )]/[( <i>I</i> <sup>+</sup> )+( <i>I</i> <sup>-</sup> )] (Parsons, Flack and Wagner, Acta Cryst. B69 (2013) 249-259).
Absolute structure parameter	-0.01 (2)

Computer programs: Apex3 v2016.1-0 (Bruker, 2016), SAINT V8.37A (Bruker, 2016), SHELXS97 (Sheldrick, 2008), SHELXL2017/1 (Sheldrick, 2017), SHELXLE Rev836 (Hübschle *et al.*, 2011).

**Table 2.** Bond lengths (Å) for (*E*)-(2,3,4,6)-tetra-*O*-acetyl- $\beta$ -D-glucopyranosyl-1-*N*-3-nitrobenzaldimine (**9a**).

O1—C1	1.4222 (18)	C6—H6B	0.9900
O1—C5	1.4293 (18)	C7—C8	1.491 (2)
O2—C7	1.3606 (19)	C8—H8A	0.9800
O2—C2	1.4409 (18)	C8—H8B	0.9800
O3—C7	1.199 (2)	C8—H8C	0.9800
O4—C9	1.3532 (19)	C9—C10	1.492 (2)
O4—C3	1.4425 (19)	C10—H10A	0.9800
O5—C9	1.202 (2)	C10—H10B	0.9800
O6—C11	1.3639 (19)	C10—H10C	0.9800
O6—C4	1.4415 (17)	C11—C12	1.490 (2)
O7—C11	1.203 (2)	C12—H12A	0.9800
O8—C13	1.337 (2)	C12—H12B	0.9800
O8—C6	1.444 (2)	C12—H12C	0.9800
O9—C13	1.205 (2)	C13—C14	1.490 (3)
O10—N2	1.225 (2)	C14—H14A	0.9800
O11—N2	1.224 (2)	C14—H14B	0.9800
N1—C15	1.267 (2)	C14—H14C	0.9800
N1—C1	1.4506 (19)	C15—C16	1.476 (2)
N2—C18	1.472 (2)	C15—H15	0.9500
C1—C2	1.531 (2)	C16—C17	1.392 (2)
C1—H1	1.0000	C16—C21	1.397 (2)
C2—C3	1.524 (2)	C17—C18	1.381 (2)
C2—H2	1.0000	C17—H17	0.9500
C3—C4	1.518 (2)	C18—C19	1.377 (3)
C3—H3	1.0000	C19—C20	1.394 (3)
C4—C5	1.532 (2)	C19—H19	0.9500
C4—H4	1.0000	C20—C21	1.385 (2)
C5—C6	1.510 (2)	C20—H20	0.9500
C5—H5	1.0000	C21—H21	0.9500
C6—H6A	0.9900		

**Table 3.** Bond angles (degrees) for (*E*)-(2,3,4,6)-tetra-*O*-acetyl- $\beta$ -D-glucopyranosyl-1-*N*-3-nitrobenzaldimine (**9a**).

C1—O1—C5	112.77 (11)	C7—C8—H8C	109.5
C7—O2—C2	117.87 (12)	H8A—C8—H8C	109.5
C9—O4—C3	118.79 (12)	H8B—C8—H8C	109.5
C11—O6—C4	116.84 (12)	O5—C9—O4	123.70 (15)
C13—O8—C6	114.67 (13)	O5—C9—C10	125.90 (16)
C15—N1—C1	116.38 (13)	O4—C9—C10	110.39 (14)
O11—N2—O10	123.24 (16)	C9—C10—H10A	109.5
O11—N2—C18	118.33 (16)	C9—C10—H10B	109.5
O10—N2—C18	118.43 (15)	H10A—C10—H10B	109.5
O1—C1—N1	104.47 (12)	C9—C10—H10C	109.5
O1—C1—C2	108.13 (11)	H10A—C10—H10C	109.5
N1—C1—C2	111.43 (13)	H10B—C10—H10C	109.5
O1—C1—H1	110.9	O7—C11—O6	123.14 (15)
N1—C1—H1	110.9	O7—C11—C12	126.05 (15)
C2—C1—H1	110.9	O6—C11—C12	110.80 (14)
O2—C2—C3	107.99 (12)	C11—C12—H12A	109.5
O2—C2—C1	107.66 (11)	C11—C12—H12B	109.5
C3—C2—C1	109.30 (12)	H12A—C12—H12B	109.5
O2—C2—H2	110.6	C11—C12—H12C	109.5
C3—C2—H2	110.6	H12A—C12—H12C	109.5
C1—C2—H2	110.6	H12B—C12—H12C	109.5
O4—C3—C4	106.31 (12)	O9—C13—O8	123.61 (16)
O4—C3—C2	109.26 (12)	O9—C13—C14	123.60 (15)
C4—C3—C2	110.37 (12)	O8—C13—C14	112.69 (14)
O4—C3—H3	110.3	C13—C14—H14A	109.5
C4—C3—H3	110.3	C13—C14—H14B	109.5
C2—C3—H3	110.3	H14A—C14—H14B	109.5
O6—C4—C3	106.89 (12)	C13—C14—H14C	109.5
O6—C4—C5	110.58 (12)	H14A—C14—H14C	109.5
C3—C4—C5	110.68 (12)	H14B—C14—H14C	109.5
O6—C4—H4	109.6	N1—C15—C16	122.16 (15)
C3—C4—H4	109.6	N1—C15—H15	118.9
C5—C4—H4	109.6	C16—C15—H15	118.9
O1—C5—C6	106.29 (12)	C17—C16—C21	119.46 (15)
O1—C5—C4	107.65 (12)	C17—C16—C15	118.38 (15)
C6—C5—C4	110.43 (12)	C21—C16—C15	121.99 (15)
O1—C5—H5	110.8	C18—C17—C16	118.66 (16)
C6—C5—H5	110.8	C18—C17—H17	120.7
C4—C5—H5	110.8	C16—C17—H17	120.7
O8—C6—C5	108.65 (12)	C19—C18—C17	123.19 (16)
O8—C6—H6A	110.0	C19—C18—N2	118.67 (15)

<b>C5—C6—H6A</b>	110.0	<b>C17—C18—N2</b>	118.11 (16)
<b>O8—C6—H6B</b>	110.0	<b>C18—C19—C20</b>	117.59 (15)
<b>C5—C6—H6B</b>	110.0	<b>C18—C19—H19</b>	121.2
<b>H6A—C6—H6B</b>	108.3	<b>C20—C19—H19</b>	121.2
<b>O3—C7—O2</b>	123.54 (14)	<b>C21—C20—C19</b>	120.83 (16)
<b>O3—C7—C8</b>	126.21 (15)	<b>C21—C20—H20</b>	119.6
<b>O2—C7—C8</b>	110.25 (14)	<b>C19—C20—H20</b>	119.6
<b>C7—C8—H8A</b>	109.5	<b>C20—C21—C16</b>	120.22 (16)
<b>C7—C8—H8B</b>	109.5	<b>C20—C21—H21</b>	119.9
<b>H8A—C8—H8B</b>	109.5	<b>C16—C21—H21</b>	119.9

**Table 4.** Torsion angles (degrees) for (*E*)-(2,3,4,6)-tetra-*O*-acetyl- $\beta$ -D-glucopyranosyl-1-*N*-3-nitrobenzaldimine (**9a**).

C5—O1—C1—N1	174.66 (12)	C13—O8—C6—C5	-166.50 (13)
C5—O1—C1—C2	-66.55 (15)	O1—C5—C6—O8	76.55 (15)
C15—N1—C1—O1	-139.46 (14)	C4—C5—C6—O8	-166.96 (12)
C15—N1—C1—C2	104.02 (16)	C2—O2—C7—O3	-3.7 (2)
C7—O2—C2—C3	-106.23 (15)	C2—O2—C7—C8	176.78 (13)
C7—O2—C2—C1	135.85 (13)	C3—O4—C9—O5	8.6 (2)
O1—C1—C2—O2	175.57 (11)	C3—O4—C9—C10	-171.66 (13)
N1—C1—C2—O2	-70.16 (15)	C4—O6—C11—O7	4.5 (2)
O1—C1—C2—C3	58.51 (15)	C4—O6—C11—C12	-176.63 (15)
N1—C1—C2—C3	172.78 (12)	C6—O8—C13—O9	4.5 (2)
C9—O4—C3—C4	123.77 (14)	C6—O8—C13—C14	-172.14 (14)
C9—O4—C3—C2	-117.12 (14)	C1—N1—C15—C16	176.28 (14)
O2—C2—C3—O4	73.13 (14)	N1—C15—C16—C17	170.14 (15)
C1—C2—C3—O4	-170.01 (11)	N1—C15—C16—C21	-14.5 (3)
O2—C2—C3—C4	-170.31 (12)	C21—C16—C17—C18	2.0 (3)
C1—C2—C3—C4	-53.45 (15)	C15—C16—C17—C18	177.45 (15)
C11—O6—C4—C3	134.95 (14)	C16—C17—C18—C19	-0.5 (3)
C11—O6—C4—C5	-104.51 (15)	C16—C17—C18—N2	-178.27 (15)
O4—C3—C4—O6	-68.03 (14)	O11—N2—C18—C19	15.0 (3)
C2—C3—C4—O6	173.59 (12)	O10—N2—C18—C19	-164.39 (17)
O4—C3—C4—C5	171.49 (11)	O11—N2—C18—C17	-167.14 (18)
C2—C3—C4—C5	53.11 (16)	O10—N2—C18—C17	13.5 (3)
C1—O1—C5—C6	-176.58 (12)	C17—C18—C19—C20	-1.2 (3)
C1—O1—C5—C4	65.08 (15)	N2—C18—C19—C20	176.51 (17)
O6—C4—C5—O1	-174.98 (11)	C18—C19—C20—C21	1.5 (3)
C3—C4—C5—O1	-56.73 (15)	C19—C20—C21—C16	0.0 (3)
O6—C4—C5—C6	69.38 (15)	C17—C16—C21—C20	-1.8 (3)
C3—C4—C5—C6	-172.37 (13)	C15—C16—C21—C20	-177.05 (16)